STUDY OF GAS-LIQUID TWO-PHASE FLOW PATTERN TRANSITIONS IN HORIZONTAL PIPE, ANNULUS AND NUCLEAR FUEL TYPE ROD BUNDLE FLOW SYSTEMS

by

© SYLVESTER IFANYI OSAMUSALI
B.Sc. (Ife), M.Eng. (McMaster)

A Thesis
Submitted to the School of Graduate Studies
in Partial Fulfilment of the Requirements
for the Degree
Doctor of Philosophy

McMaster University
July, 1988

STUDY OF GAS-LIQUID-TWO-PHASE FLOW PATTERN TRANSITIONS IN HORIZONTAL PIPE, ANNULUS AND NUCLEAR FUEL TYPE ROD BUNDLE FLOW SYSTEMS

DOCTOR OF PHILOSOPHY (1988)
(Nuclear Engineering)

McMaster University
Hamilton, Ontario

TITLE: Study of Gas-Liquid Two-Phase Flow Pattern Transitions in Horizontal Pipe, Annulus and Nuclear Fuel Type Rod Bundle Flow Systems

AUTHOR: Sylvester Ifanyi Osamusali, B.Sc. (University of Ife, Nigeria)
M.Eng. (McMaster University)

SUPERVISOR: Dr. J. S. Chang

NUMBER OF PAGES: xviii, 189

ABSTRACT

The ability to predict the flow patterns and flow pattern transitions in a two-phase flow process is useful for an accurate prediction of the pressure drop, heat and mass transfer rates, and also for the choice of appropriate two-phase flow design parameters for the system. During a loss of coolant accident (LOCA) in a nuclear reactor, two-phase flow may exist in the primary heat transport loop, and a knowledge of the flow patterns that are occurring at the various flow conditions is needed to accurately model the accident scenario.

Horizontal gas-liquid two-phase flow patterns and flow pattern transitions have been investigated both theoretically and experimentally for a pipe of 5.08 cm i.d., annulus geometries of outer tube diameter 5.08 cm i.d. and inner-to-outer diameter ratios from 0.375 to 0.625, and for a 37-rod nuclear fuel type bundle flow system having an outer tube diameter of 10.16 cm i.d. and rods of diameter, 1.27 cm. The 28-rod bundle flow geometry was also studied theoretically. The flow conditions were at inlet pressures of about 1 to 2 bar and at near room temperature.

In this study, the time averaged void fraction and pressure drop measurements were also successfully obtained. The instantaneous and time averaged void fraction measurements were achieved by the ring type capacitance transducers based on the differences in the dielectric constants of the liquid and gas phases. The various flow patterns occurring in the pipe, annulus and rod bundle flow systems were successfully characterized by direct visual observation through the transparent test sections and also from the signal waveforms of the instantaneous fluctuations in the void fraction, the pressure drop measurements and the ultrasonic transmission waveforms. Flow pattern transitions were determined from both the results of the measured void fraction and direct visual observation.

The experimental results show that the flow pattern structures occurring in horizontal annulus and rod bundle geometries are similar to those observed for the pipe flow case, except the annulus flow system where we characterized two additional flow patterns, namely, "Annulus-Slug" and "Annulus-Plug". These flow patterns are similar to the Slug and Plug flow structures observed for the pipe geometry, but are restricted to the lower annulus channel gap below the annulus rod. These occur at the flow conditions that would otherwise lead to Stratified flow patterns for pipe flow cases.

The results show that the flow pattern transitions for the annulus and rod bundle flow geometries are significantly different from those of the normal pipe flow. The flow pattern transitions for the annulus flow geometries were observed to be significantly influenced by different inner-to-outer diameter ratios, except the Stratified Smooth to Stratified Wavy transition. The Stratified to Intermittent and the Intermittent to Dispersed Bubble transitions occur at lower superficial liquid velocities, while the Intermittent to Annular transition occurs at higher superficial gas velocities for larger inner-to-outer diameter ratios. In the rod bundle geometries, the flow pattern transitions were observed to vary slightly with the particular angle of orientation of the bundle within the enclosing tubeshell. The various influences on the flow pattern transitions observed in the present study are mainly due to the differences in geometries and force distributions.

From direct visual observation results, we also observed that interfacial waves in the rod bundle flow geometry were generated and dissipated at the rod bundle end plates. No significant effect of the rod bundle end plates on the other flow patterns was observed, except a slight effect on the regularity of these intermittent flow patterns, usually becoming more apparent at higher flow rates.

The predicted results for the pipe, annulus and rod bundle geometries agree well with the present experimental observations, and also with the results of the limited previous studies found in the literature.

ACKNOWLEDGEMENT

I wish to express my sincere gratitude to Dr. J.S. Chang for his useful supervision and thorough guidance throughout the course of this work. Further acknowledgement also goes to Dr. M.S. Shoukri and Dr. P.E. Wood for their valuable time and attention to this research.

I wish to extend my gratitude to the members of the McMaster University Thermalhydraulics/Plasma research group for their useful discussions during those weekly group meetings and invaluable assistance in this research project. I would like to especially thank Mr. M. Kiela, the group technician, Mr. T.G. Beuthe, the author of IPLOT who is also one of the members of the group and also my colleague, Mr. J.C. Campeau, with whom I enjoyed discussing the interesting results of this project.

Deep appreciation also goes to the members of the Engineering Word Processing Center for their effort in the final preparation of this thesis and all the publications that formed the core of this work.

And to my Parents, Mr. and Mrs. Gregory Osamusali, and my Brothers and Sisters, all of whom remained with me in constant prayer to God throughout the course of my stay in Canada, and of whom I am always very proud. And to my Fiancee, Lourine, whose constant inspiration stayed on with me to the final completion of this thesis.

Finally I would like to extend my appreciation to the University of Ife, Nigeria, for their financial support, affording me the opportunity to undertake this program. And also to the Department of Engineering Physics, McMaster University for awarding me the Departmental Scholarship without which I may not have completed this program.

TABLE OF CONTENTS

TABLE OF CONTENTS (continued)

TABLE OF CONTENTS (continued)

LIST OF FIGURES

LIST OF FIGURES (continued)

Page

LIST OF FIGURES (continued)

LIST OF FIGURES (continued)

LIST OF FIGURES (continued)

LIST OF TABLES

NOMENCLATURE

A_ℓ, A'_ℓ	= liquid-phase flow areas for pipe and annulus geometries, respectively.	[m^2]
A_g, A'_g	= gas-phase flow areas for pipe and annulus geometries, respectively.	[m^2]
C_ℓ, C_g	= friction factor coefficient for the liquid and gas, respectively.	[–]
d	= diameter of annulus rod.	[m]
D	= inside diameter of tubeshell.	[m]
D_ℓ, D_g	= hydpaulic diameters of liquid and gas-phases, respectively.	[m]
f_i	= interfacial friction factor.	[–]
f_ℓ, f_g	= gas and liquid phase friction factor, respectively.	[–]
F_B	= buoyancy force defined by Eq. (3.15).	[N/m]
F_T	= turbulent force defined by Eq. (3.16).	[N/m]
g	= accleration due to gravity.	[m/s^2]
h_ℓ, h_g	= equilibrium liquid and gas levels, respectively.	[m]
r	= radius coordinate of annulus rod.	[m]
S_ℓ, S'_ℓ	= liquid-phase perimeters for pipe and annulus geometries, respectively.	[m]
S_g, S'_g	= gas-phase perimeter for pipe and annulus geometries, respectively.	[m]
S_i, S'_i	= gas-liquid interface length.	[m]
u_ℓ, u_g	= liquid and gas phase velocities.	[m/s]
$U_{\ell s}$, U_{gs}	= superficial liquid and gas-phase velocities.	[m/s]
x_ℓ, x_g	= liquid and gas phase friction factor exponents.	[–]
k	= wave number.	[m^{-1}]
s	= sheltering coefficient defined in equations (3.1) and (3.2).	[–]

NOMENCLATURE (continued)

Greek Letters

θ	= angle.	[rad]
γ	= function defined by Eq. (2.12).	[–]
β	= function defined by Eq. (2.23).	[–]
μ	= viscosity.	[Ns/m^2]
α_g	= void fraction.	[–]
ε	= dielectric constant.	[F/m]
τ	= shear stress.	[N/m^2]
η	= wave amplitude.	[m]
σ	= surface tension.	[N/m]
ρ	= density.	[Kg/m^3]

ABBREVIATIONS

A	Annular
DB	Dispersed Bubble
EB	Elongated Bubble
PA	Periodic Annular
PL	Plug
SL	Slug
SS	Stratified Smooth
SW	Stratified Wavy
WA	Wavy Annular

CHAPTER 1

INTRODUCTION

1.1 Background

Two-phase flow applications refer to various chemical processes and power plants. Typical examples include gas-oil two-phase flow transportation in pipelines, evaporation of liquid to high pressure steam in steam generators, turbines and pressurizers. Two-phase flow also occurs during loss-of-coolant accidents (LOCA) due to blowdown of pressure pipes in nuclear power plant primary heat transport loops. During the past two decades, the need to satisfy safety requirements of nuclear power plant operations has led to numerous research activities on gas-liquid two-phase flows.

The study of gas-liquid two-phase flow is mostly complicated by the existence of one or more deformable and moving interfaces. A mixture of gas and liquid flowing in a pipe, annulus or nuclear rod bundle can assume a variety of interfacial configurations known as FLOW PATTERNS or FLOW REGIMES in two-phase flow. Detailed definitions of the various flow patterns occurring in horizontal two-phase flow systems are given in Section 1.4. Flow patterns significantly affect and can be affected by heat, mass and momentum transfers between the two phases and the solid boundaries presented by the flow tube geometry. In engineering designs requiring the application of gas-liquid two-phase flow, it is important to be able to predict the particular flow patterns and flow pattern transitions occurring at a given flow condition, to enable appropriate choice of design parameters for each flow pattern. For example, under loss-of-coolant accident (LOCA) in the nuclear power plant primary heat transport system, we can accurately model for the two-phase flow parameters if the particular flow patterns occurring can be predicted at the given conditions. However, in spite of various investigations, prediction of the flow patterns for gas-liquid two-phase flow systems has remained a central unresolved problem.

The occurrence of a particular flow pattern depends on conditions of the flow, pressure, heat flux, densities and viscosities of the phases, surface tension, system geometry and inclination to the horizontal, flow direction (upward, downward, cocurrent or counter-current), entrance length and the method of forming the two-phase flow. A simple presentation of the results of flow pattern studies is usually in the form of flow pattern maps [1] where the various flow patterns are represented as areas on a graph. Due to the various conditions affecting flow patterns, it is impossible to represent every parameter influencing the flow patterns on a two-dimensional map while still keeping it simple to use. Flow pattern maps give an indication of the particular flow pattern that would occur at given system flow conditions. One of the earliest maps proposed was due to Baker [2]. A host of others have since been presented by Govier and Omer [3], Hubbard and Dukler [4], White and Huttington [5], Al Sheikh et al. [6], Mandhane et al. [7], Taitel and Dukler [8], Weisman et al. [9] and Aly [10] to mention a few. Mandhane et al. [7] presented a gas-liquid two-phase flow pattern map based on the superficial velocities of the phases, using a large bank of data covering a wide range of pipe diameters. This map has a convenient form and has been widely used due to the large amount of data and the range of pipe diameters represented.

In this work, studies of flow pattern transitions for the annulus and rod bundle geometries have been conducted and the results compared with those of pipes, since these geometries are also of practical importance in the various chemical processes, coal fire, oil fire, and nuclear power plants, and have not been widely investigated.

1.2 Review of Previous Work

In the study of two-phase flow patterns as revealed in the published literature, it has not been well established whether the results for the pipe flow geometry can be applied to more complex flow systems, like the annulus and rod bundle flow geometries. Physical mechanistic models and experimental investigations [8,9] have revealed a significant dependence of flow patterns on pipe diameters. This pipe diameter influence is due mainly to channel-wall-frictional interactions resulting from differences in the flow geometrical parameters. The flow geometrical parameters for the annulus and rod bundle flow systems are compared with the pipe flow cases in Section 2. The annulus and rod bundle flow cases represent much more complex profiles and differ quite significantly in order of magnitude from the pipe flow cases [11]. Very few investigations on flow pattern transitions have been directed at the annulus and rod bundle flow geometries. Earlier investigations include Chang et al. [12], Nicholson et al. [13] and Becker et al. [14] for flow pattern transitions in annulus flow systems. Vertical rod bundle flow pattern transition studies have been conducted by Bergles [15] and Venkateswararao et al. [16]. Aly [10] experimentally investigated the case for a horizontal air-water flow, studying an interior subchannel of a 37-rod bundle flow geometry using a needle contact probe. In this case, probes can cause more flow obstructions and can only be used in the outer subchannels due to the great difficulty of introducing measuring devices in the restricted spaces between the rods. Krishnan and Kowalski [17] investigated the Stratified to Slug flow transition in a horizontal pipe containing a 7-rod bundle. And in a recent study, they extended their work to cover other flow patterns for the 7-rod bundle geometry. These tests were carried out for both air-water and Freon gas-water flows. The flow patterns were characterized by direct visual observations and also by conductivity probes. Minato et al. [18] also investigated the Stratified to Slug flow transitions for a horizontal air-water 37-rod bundle flow system by direct visual observation. Various predictive models have also been proposed for the rod bundle flow systems [17,18]. These are mostly derived from the classical work of Taitel and Dukler [8] for the pipe geometry without fully accounting for the differences in geometrical parameters. The geometrical parameters (e.g. interfacial areas) needed to close the two-fluid model formulations have mainly been obtained from empirical correlations. As will be shown later in Section 2, the interfacial area for rod bundle flow systems, for example, varies nonmonotonically with the stratified equilibrium liquid level. The typical case for the 37-rod bundle flow system is observed to be quite complex due to the large number of rods present [11]. Hence it may not be possible to accurately represent this parameter from empirical correlations, for large number rod bundle two-phase flow systems.

1.3 Objectives

The objectives of this study are to determine flow patterns occurring in horizontal annulus and rod bundle geometries, and compare the flow pattern transitions for these geometries with the pipe flow results.. In this work, experimental and theoretical investigations have been conducted to predict two-phase flow pattern transitions for a 5.08 cm i.d. pipe, annuli with outer diameter, 5.08 cm and inner diameter from 1.905 cm to 3.175 cm, and a 37-rod bundle flow geometry with rods of diameter, 1.27 cm. The physical mechanistic approach of Taitel and Dukler [8] for horizontal pipe flow systems is modified and extended to modelling the horizontal annulus and rod bundle flow systems. In the Taitel and Dukler model [8], the geometric parameters are central to the transition criteria, and is more suitable for modelling the annulus and rod bundle flow cases than the alternative approach of computing the void fraction directly from Lockhart-Martinelli correlations or other schemes. Since these correlations originally developed for pipes may not be suitable for the annulus and rod bundle geometries. The predictive flow pattern transitions are investigated for different inner-to-outer diameter ratios for the annulus geometries, and for different rotation angles from 0° to 45° for 28 and 37-rod nuclear fuel type bundles, used in the CANDU nuclear reactors. A detailed experimental investigation has been conducted to carefully map the flow patterns occurring in the pipe, annulus, and 37-rod bundle geometries for air-water two-phase flow at room temperature and near atmospheric pressure. The flow patterns have been characterized by direct visual observations, and by waveform signals of the pressure, ultrasonic and capacitance transducers used for measuring the system pressure drop, liquid level and void fractions, respectively. A detailed description of the experimental techniques are presented in Section 6.

1.4 Horizontal Two-Phase Flow Patterns

Gas-liquid two-phase flow can assume a variety of interfacial configurations, namely, flow patterns, at different gas and liquid flow rates for a given system. This is due mainly to the compressibility of the gas phase and the deformable interfaces presented by the two phases flowing together in a pipe or other flow geometries. Horizontal gas-liquid two-phase flows have been observed to exhibit the following flow patterns, namely, Stratified Smooth, Stratified Wavy, Slug, Plug, Annular, Wavy-Annular and Dispersed Bubbly flow patterns. Schematics of these flow structures are shown in figure 1.1. The flow pattern analysis will be based on the definitions given below, as have been experimentally observed for the pipe, annulus and rod bundle geometries, in this study.

The Stratified Smooth (SS) flow occurs when the liquid is flowing at the bottom of the pipe and the gas flows along the top due to buoyancy, and the gas-liquid interface is smooth. The Stratified Wavy (SW) flow is similar in description to the Stratified Smooth flow, however, the gas-liquid interface is wavy. Both the Plug (PL) flow, sometimes designated as Elongated Bubbles (EB) at high liquid flow rate, and Slug (SL) flow are what Taitel and

Dukler [8] refer to as Intermittent (I) flow, and are characterized by the liquid bridging the gap between the gas-liquid interface and the top of the pipe. The difference between Plug and Slug flow regimes depends on the degree of agitation of the liquid bridge. Plug flow is considered to be the limiting case of Slug flow with no entrained bubbles existing in the liquid bridge. Annular (A) flow occurs when the pipe walls are wetted by a thin liquid film while the gas, at high velocity, flows through the center of the pipe. Liquid droplets are usually entrained in this gas core. When the upper pipe wall is periodically wetted by highly aerated large amplitude waves, the flow is neither Slug which requires a complete liquid bridge, nor Annular which is characterized by a stable liquid film. Taitel and Dukler[8] designated this flow pattern as the Wavy-Annular (WA) flow. However this regime was not recognized by Mandhane et al. [7], and was considered to be Slug flow. The Dispersed Bubble (DB) or Bubbly flow regime is characterized by small gas bubbles distributed throughout the liquid phase which otherwise fills the pipe. The transition to this flow pattern is considered to occur when the elongated gas bubbles lose contact with the top of the tube. Initially the bubbles are near the top of the pipe, but at higher liquid flow rates, become uniformly distributed throughout the bulk of the liquid filling the system.

In the annulus flow geometry, we observed and defined some new flow patterns, namely, "Annulus-Plug" and "Annulus-Slug" flow patterns. The Annulus-Slug flow pattern occurs when the liquid tends to bridge the gap between the gas-liquid interface and the lower surface of the annulus rod. This occurs over a small range of low liquid flow rates for high gas rates and may be due to capillary surface tension force as was proposed in the transition between Stratified and Intermittent flow patterns for small diameter capillary tubes [19]. At lower gas flow rates, we also characterized the Annulus-Plug flow. This is similar in description to the Annulus-Slug flow pattern with little or no bubbles entrained in the liquid bridge. The range of gas flow rates over which these new flow patterns were observed to occur represent the Stratified flow region, and have been classified as such in the present study.

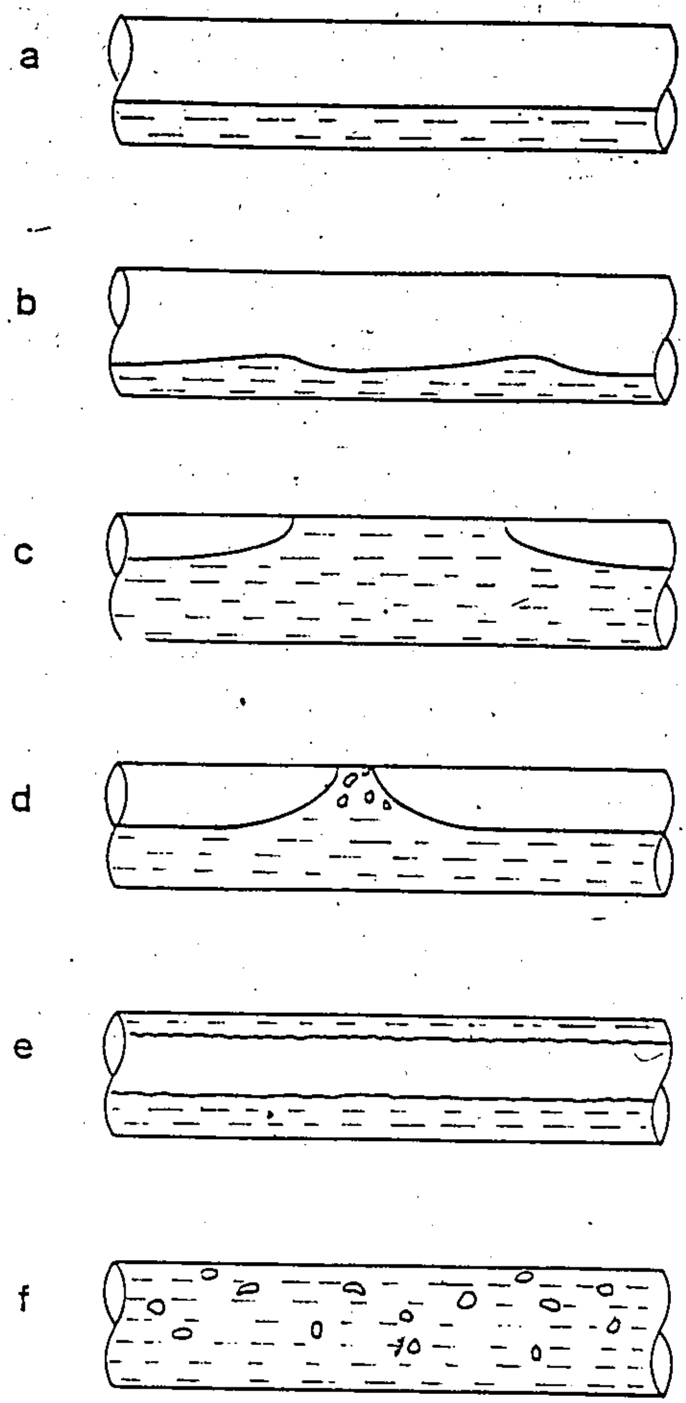

Figure 1.1 Horizontal Pipe Two-Phase Flow Pattern Structures:
(a) Stratified Smooth (SS)
(b) Stratified Wavy (SW)
(c) Plug (PL)
(d) Slug (SL)
(e) Annular (A)
(f) Dispersed Bubbly (DB)

CHAPTER 2

HORIZONTAL FLOW PATTERN TRANSITION MODEL

In this model the mechanistic approach of Taitel and Dukler [8] for horizontal pipe two-phase flow is followed. This model provides a means of including the effects of fluid properties, pipe sizes and flow geometries. The Helmholtz instability model proposed by Taitel and Dukler [8] for transition from Stratified to Intermittent flow patterns is modified here to include the effect of interfacial surface tension force, since this may oppose wave growth at the interface by acting to flatten out any curved surfaces. This is extended to modelling horizontal annulus and rod bundle flow geometries where the geometric effect of each individual rod present is fully accounted for. Thus, in order to describe the flow pattern structures which result in these flow systems it is first necessary to describe the mechanisms which arise in a fully developed pipe flow system.

2.1 One-Dimensional Equilibrium Stratified Flow

In analyzing two-phase flow, the basic equations governing the conservation of mass, momentum and energy already well established for single-phase flow are solved based on some idealized models and simplifying assumptions. The models generally used include:

(i) The Homogeneous Equilibrium Model (HEM), which assumes the phases to be represented by a single fluid flowing in the whole system, with fluid properties given by appropriately weighted properties of the individual phases.

(ii) The Separated Flow or Two-Fluid Model, which assumes the two phases to be flowing on separate layers and the basic conservation equations written separately for each phase.

(iii) The Flow Pattern Model assumes the two phases to form a given flow distribution represented by some idealized geometry and the conservation equations solved within this geometrical framework.

The Homogeneous and Separated flow models have been widely applied in a variety of engineering systems involving two-phase flow design calculations. The general conservation equations for two-phase flow have been derived by several authors [20,21].

In the model presented in this study, the process of analyzing the transitions between the various flow patterns starts from the condition of stratified flow and the mechanisms whereby a change can be expected to take place is imposed on the system [8]. A steady state one-dimensional stratified two-phase flow is therefore assumed. Further simplifying assumptions include:

(i) Each phase has a mean velocity across a given plane normal to the flow.

(ii) The pressure across any plane normal to the tube axis is uniform.

(iii) The flow is non accelerating and the gas-liquid interface is stratified smooth.

(iv) The total cross-sectional area occupied by the gas and liquid in any plane normal to the tube axis is equal to the sum of the areas occupied by individual phases.

Any information that may be lost in view of these assumptions are therefore supplied by an appropriate choice of constitutive relationships.

The situation assumed in this analysis is shown in figure 2.1, where subscripts g and ℓ represent the gas and liquid phases, respectively. Here the approach of Taitel and Dukler [8] is used to analyze the flow. A simple momentum balance on each phase assuming no pressure differential across the gas-liquid interface yields,

$$-\frac{dP}{dz} - \tau_\ell \frac{S_\ell}{A_\ell} + \tau_i \frac{S_i}{A_\ell} = 0 \qquad (2.1)$$

for the liquid phase, and

$$-\frac{dP}{dz} - \tau_g \frac{S_g}{A_g} - \tau_i \frac{S_i}{A_g} = 0 \tag{2.2}$$

for the gas phase, where P represents the pressure, S_g and S_ℓ represent the wetted perimeters by the gas and liquid phases, respectively, S_i represents the interfacial perimeter, A_g and A_ℓ represent the cross-sectional area occupied by the gas and liquid, respectively, and τ_i, τ_g and τ_ℓ represent the interfacial , and the gas and liquid shear stresses, respectively.

In the above equations, the interfacial shear stress has opposite signs for each phase in accordance with Newton's third law. For cocurrent flow the positive sign is given to the heavier fluid which tends to have a lower velocity. Combining these two equations yields:

$$-\tau_\ell \frac{S_\ell}{A_\ell} + \tau_g \frac{S_g}{A_g} + \tau_i S_i\left(\frac{1}{A_\ell} + \frac{1}{A_g}\right) = 0 \tag{2.3}$$

2.2 Constitutive Relations

The shear stresses are evaluated in the conventional manner using the form suggested by Blasius [22],

$$\tau_\ell = f_\ell \rho_\ell \frac{u_\ell^2}{2}; \quad \tau_g = f_g \rho_g \frac{u_g^2}{2}; \quad \tau_i = f_i \rho_g \frac{(u_g - u_i)^2}{2} \tag{2.4}$$

with the friction factors evaluated from

$$f_\ell = C_\ell\left(\rho_\ell \frac{D_\ell u_\ell}{\mu_\ell}\right)^{-x_\ell}; \qquad f_g = C_g\left(\rho_g \frac{D_g u_g}{\mu_g}\right)^{-x_g} \tag{2.5}$$

The hydraulic diameters in the above equations are evaluated in the usual manner as four times the fluid flow area, divided by the wetted perimeter. However, in this case, the method of Taitel and Dukler [8] and Agrawal et al. [23] are followed where it is assumed that the wall resistance is similar to that of open channel flow for the liquid and closed channel flow for the gas. Analysis indicates, however, that changes in this assumption have little effect on the results. Thus the resulting expressions for the hydraulic diameters are,

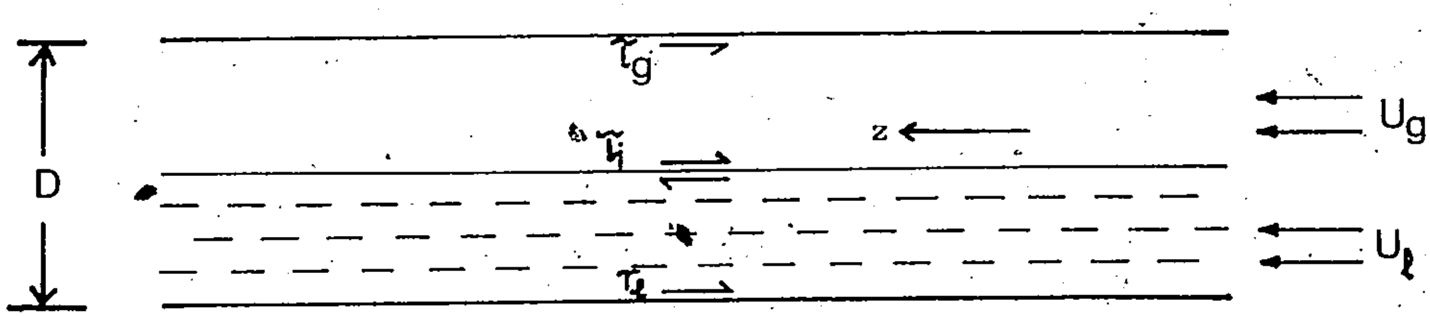

Figure 2.1 Equilibrium Stratified Horizontal Two-Phase Pipe Flow.

$$D_\ell = 4\,\frac{A_\ell}{S_\ell}\,; \qquad D_g = \frac{4A_g}{S_g+S_i} \tag{2.6}$$

To determine the expression for interfacial friction factor, f_i, we assume $f_i=f_g$ in accordance with the results of Taitel and Dukler [8] and Gazely [24] for a stratified smooth interface as assumed in this analysis. Hence we can evaluate the interfacial shear stress with the same relationship as the gas-wall shear stress if we assume $u_g>>u_i$. The condition of $u_g>>u_i$ can be attained at flow conditions leading to the transitions observed. Generally, the interfacial friction factor, f_i, can be significantly larger than the gas-wall friction factor, f_g, for wavy interfaces due to increased interfacial roughness from the gas flow induced surface waves. It may therefore be necessary to apply more sophisticated relationships for the interfacial friction factor. Numerous empirical relationships have been suggested for f_i (Cheremissinoff and Davis [25], Kowalski [26], Andrittos and Hanratty [27], Andreussi and Persen [28] and Lin and Hanratty [29]). Lin and Hanratty [29], for example, used $f_i=2f_g$ to obtain a good agreement with their experimental results. In this work, the choice of a relationship for the interfacial friction factor, f_i, is verified a posteriori by direct comparison with experimental data.

In the evaluation of the constants in the Blasius equation it is assumed that the results from single-phase analysis may be applied directly [8]. For the case of steady laminar flow the variables C and x are 16.0 and 1.0, respectively, corresponding to the Poiseuille flow. For steady turbulent flow, these parameters have values of 0.046 and 0.2, respectively, which corresponds to the well known Blasius equation for smooth pipe flow. In this analysis, the transition to turbulent motion is assumed to occur in a given phase when its Reynolds number, given by the terms in brackets in equation (2.5) exceeds 2000 [8,38].

2.3 Flow Geometric Parameter

2.3.1 Pipe Flow

Equations (2.3) to (2.6) fully describe the two-phase stratified flow once the expressions for the geometric parameters of the system are obtained. Simple analysis of figure 2.2 yields the following expressions for the pipe flow geometry:

$$A_\ell = \frac{D^2}{4}\left[\pi - \arccos(\gamma) + \gamma\sqrt{1-\gamma^2}\right] \tag{2.7}$$

$$A_g = \frac{\pi D^2}{4} - A_\ell \tag{2.8}$$

$$S_\ell = D[\pi - \arccos(\gamma)] \tag{2.9}$$

$$S_g = \pi D - S_\ell \tag{2.10}$$

$$S_i = D\sqrt{1-\gamma^2} \tag{2.11}$$

where

$$\gamma = 2h_\ell/D - 1 \tag{2.12}$$

2.3.2 Annulus Flow

For the general case of the eccentric annulus geometry where the annulus rod is located at coordinate R(r,θ), the following expressions for the geometric parameters are obtained for three regions of the equilibrium liquid level, h_ℓ, as shown in figure 2.3.

(i)

$$h_\ell \leq \left[\frac{1}{2}(D-d) + r\,\mathrm{Sin}\theta\right]$$

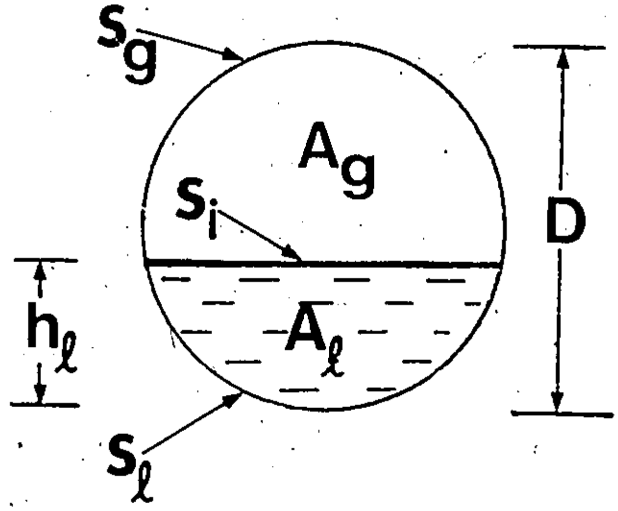

Figure 2.2 Pipe Flow Cross-Section.

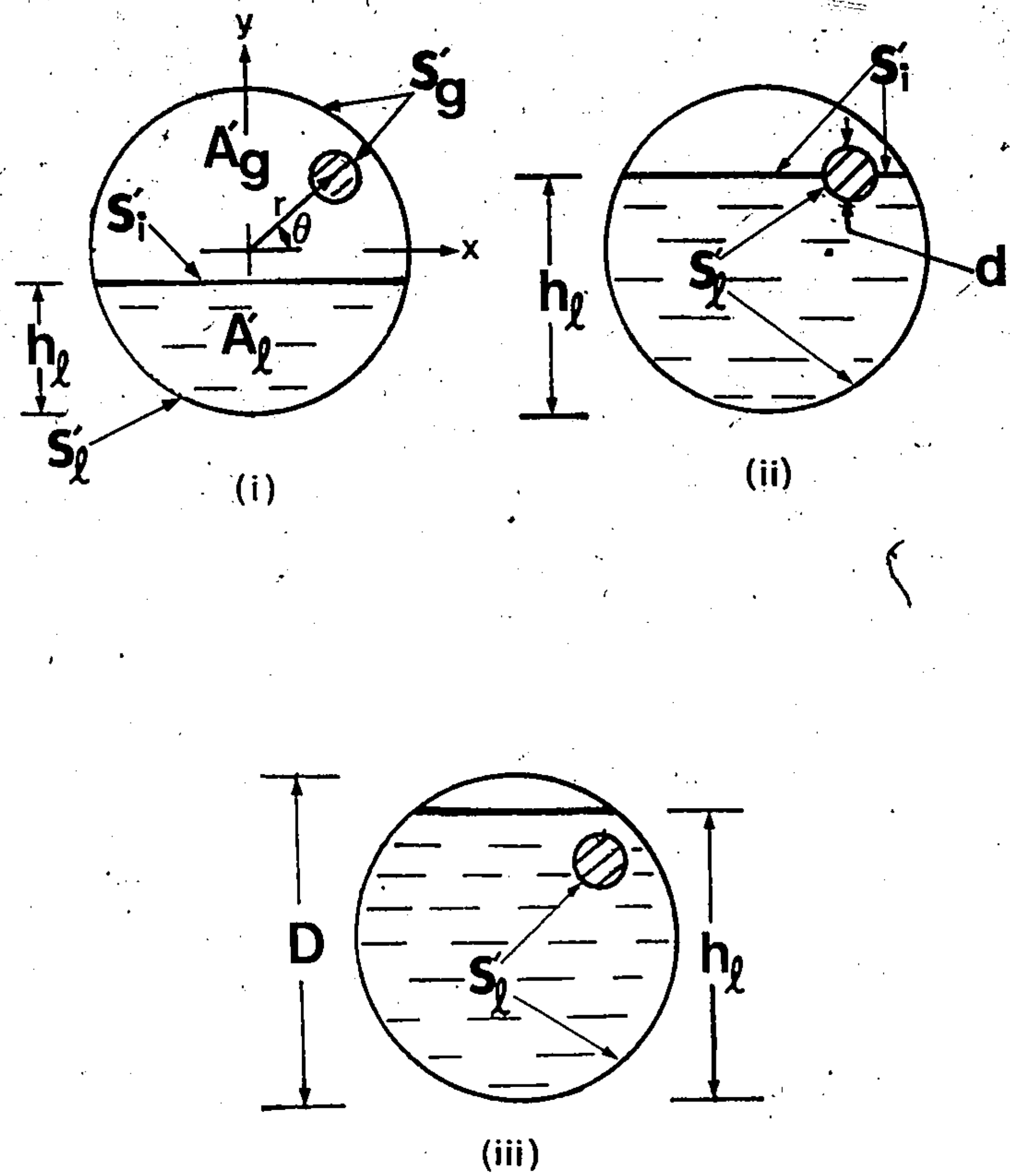

Figure 2.3 Annulus Flow Cross-Section.

$$A'_\ell = A_\ell \tag{2.13}$$

$$A'_g = A_g - \frac{\pi d^2}{4} \tag{2.14}$$

$$S'_\ell = S_\ell \tag{2.15}$$

$$S'_g = S_g + \pi d \tag{2.16}$$

$$S'_i = S_i \tag{2.17}$$

(ii)

$$\left[\frac{1}{2}(D-d) + r\,\mathrm{Sin}\theta\right] < h_\ell < \left[\frac{1}{2}(D+d) + r\,\mathrm{Sin}\theta\right]$$

$$A'_\ell = A_\ell - \frac{d^2}{4}\left[\pi - \arccos(\beta) + \beta\sqrt{1-\beta^2}\right] \tag{2.18}$$

$$A'_g = \frac{\pi}{4}(D^2 - d^2) - A'_\ell \tag{2.19}$$

$$S'_\ell = S_\ell + d\left[\pi - \arccos(\beta)\right] \tag{2.20}$$

$$S'_g = \pi(D+d) - S'_\ell \tag{2.21}$$

$$S'_i = S_i - d\sqrt{1-\beta^2} \tag{2.22}$$

where

$$\beta = (2h_\ell - D - 2r\,\mathrm{Sin}\theta)/d \tag{2.23}$$

(iii)

$$h_\ell \geq \left[\frac{1}{2}(D+d) + r\,\mathrm{Sin}\theta\right]$$

$$A_\ell' = A_\ell - \frac{\pi d^2}{4} \tag{2.24}$$

$$A_g' = A_g \tag{2.25}$$

$$S_\ell' = S_\ell + \pi d \tag{2.26}$$

$$S_g' = S_g \tag{2.27}$$

$$S_i' = S_i \tag{2.28}$$

The special case of concentric annular flow geometry corresponds to the rod being located at coordinate R(0,0). In the above expressions for the annulus geometry, we have simply subtracted the contributions to A_ℓ, A_g, and S_i, due to the presence of the annulus rod, from the pipe flow results given by equations (2.7), (2.8) and (2.11), and added together the contributions to S_ℓ and S_g due to the annulus rod with those given by equations (2.9) and (2.10) for the pipe.

2.3.3 Rod Bundle Flow

The geometric parameters for the rod bundle flow case as shown in figure 2.4 are obtained by computing the above annulus flow expressions for every rod in the system located at coordinate $R_i(r_i,\theta_i)$.

Typical calculations of the geometric parameters for the 37-rod bundle flow case are shown in figures 2.5 and 2.6, where the geometric parameters for the pipe flow case are also compared. Figures 2.5 and 2.6 show that parameters such as S_g, S_ℓ, and S_i are significantly influenced by the existence of rod bundles in the two-phase flow section, while little influence is observed for A_g and A_ℓ as shown in figure 2.7. Figure 2.6 also shows that the interfacial area becomes nonmonotonic with equilibrium liquid level in the rod bundle flow cases with order of magnitude small compared with the pipe flow cases.

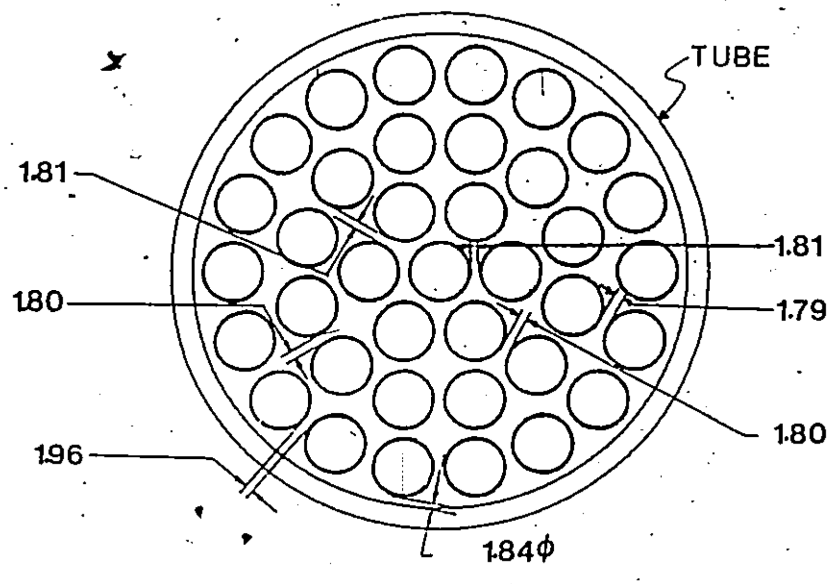

Figure 2.4 37-Rod Bundle Flow Cross-Section

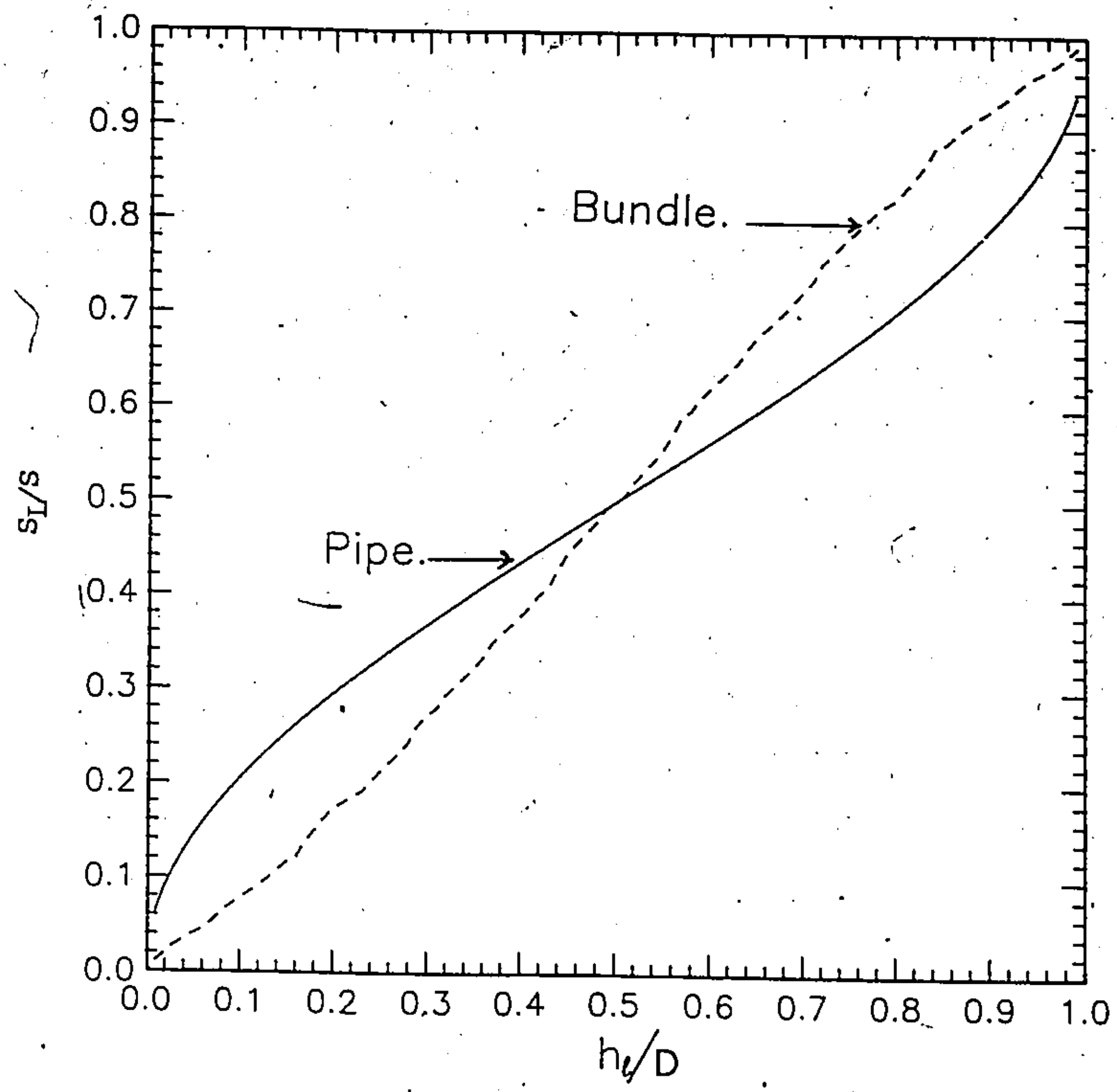

Figure 2.5 Wetted Perimeter for a Stratified 37-Rod Bundle Flow

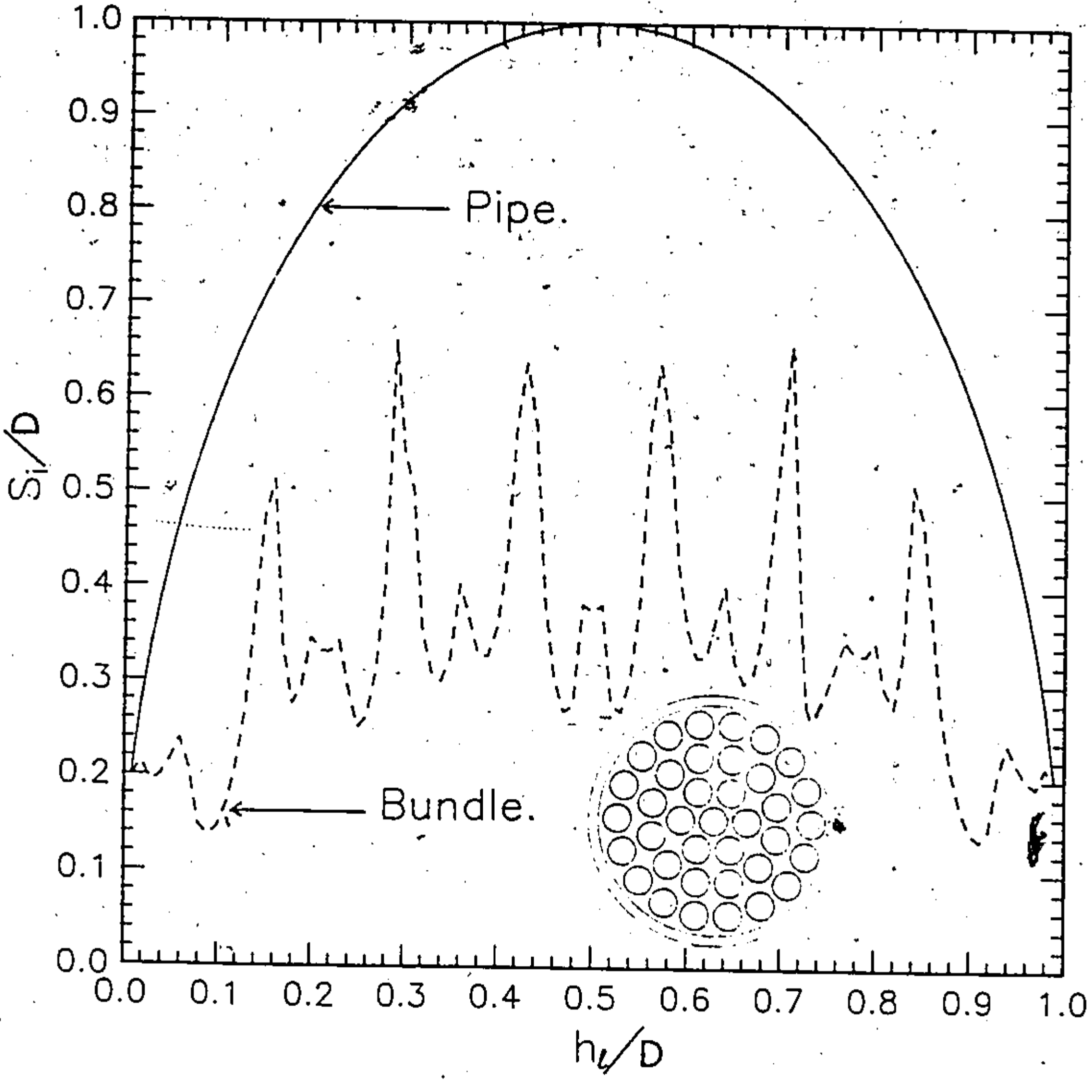

Figure 2.6 Interfacial Length for a Stratified 37-Rod Bundle Flow at the Reference Orientation Angle Shown.

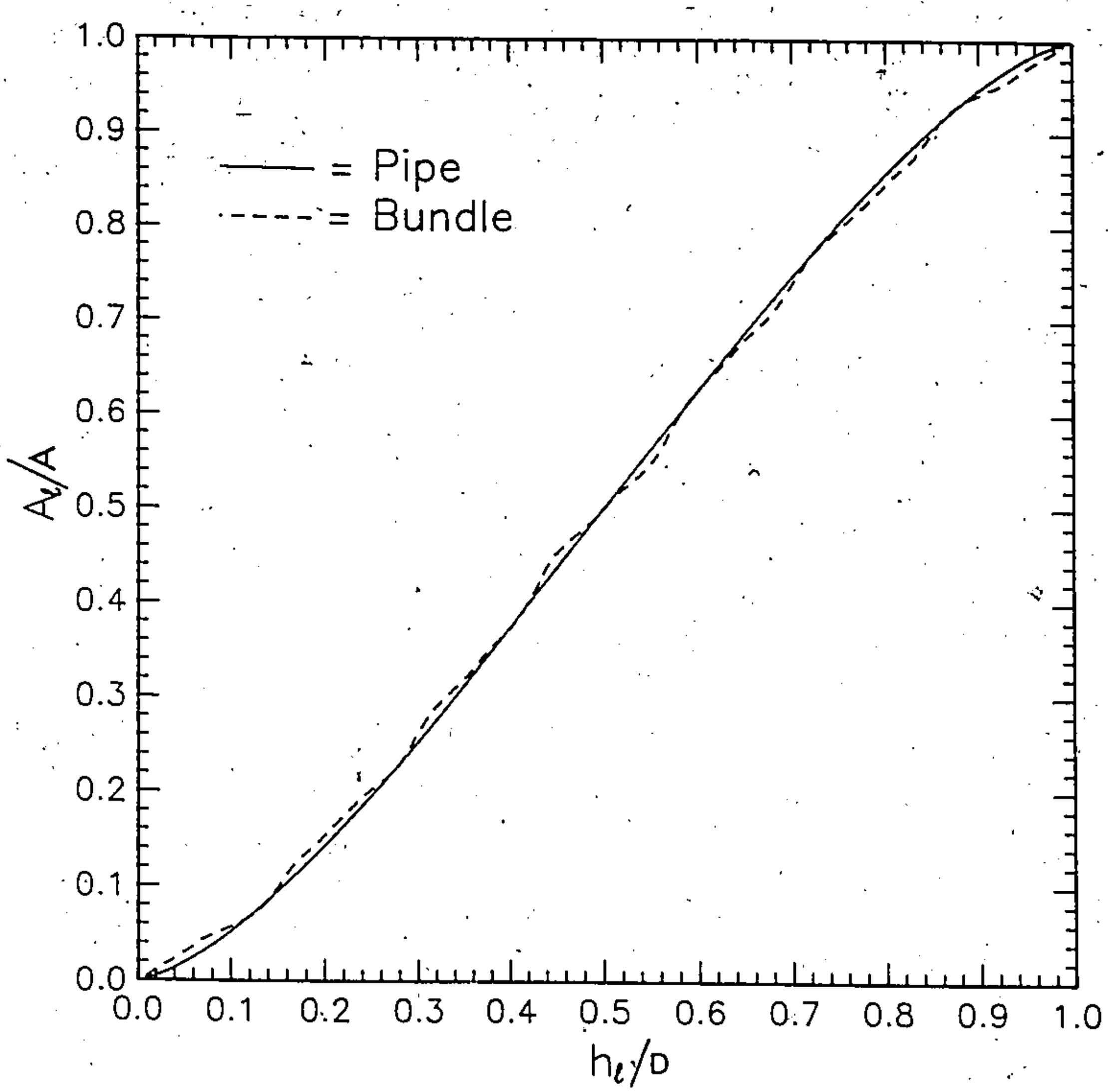

Figure 2.7 Liquid Holdup for a Stratified 37-Rod Bundle Flow

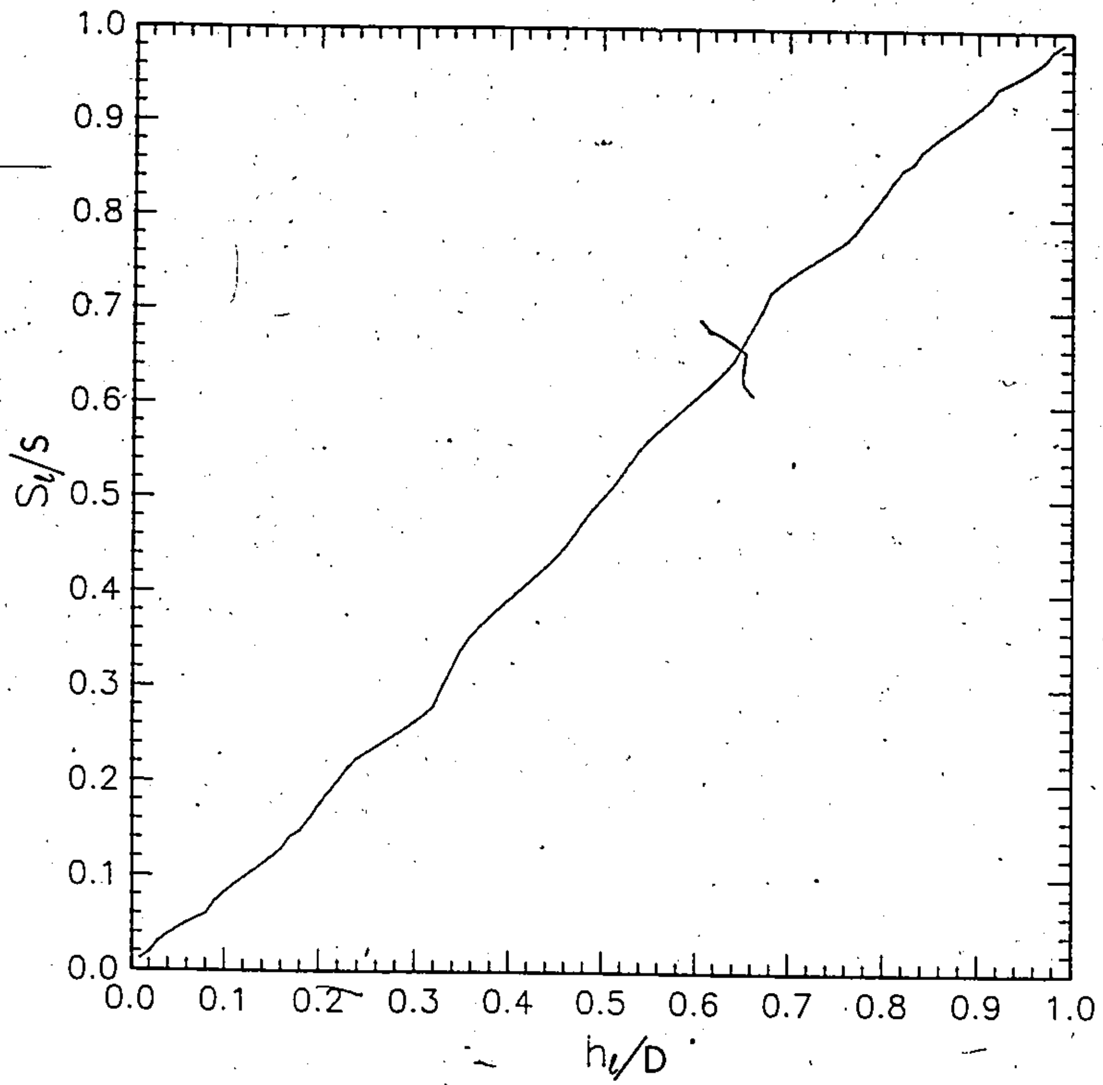

Figure 2.8 Wetted Perimeter for a Stratified 28-Rod Bundle Flow

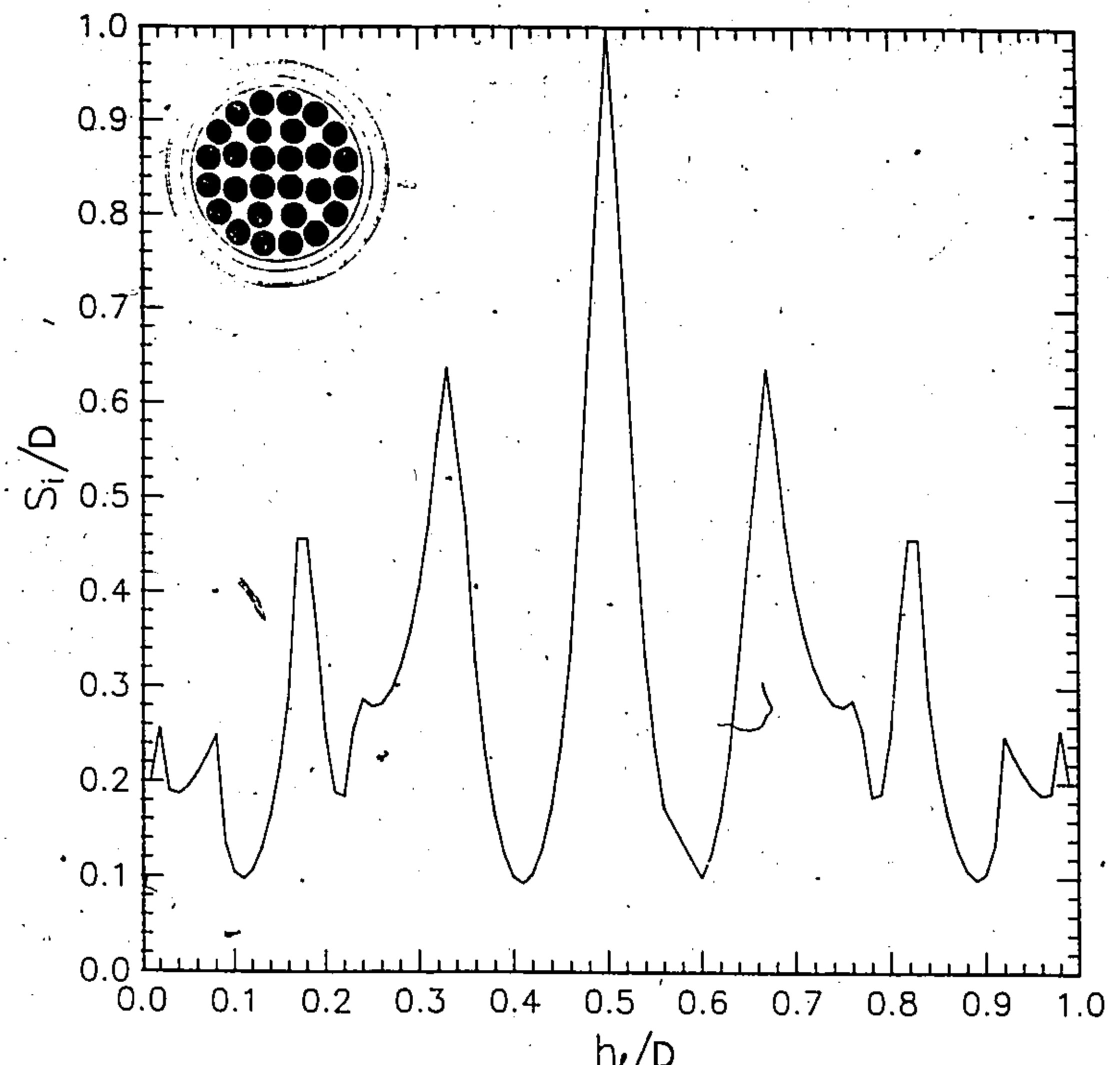

Figure 2.9 Interfacial Length for a Stratified 28-Rod Bundle Flow at the Reference Orientation Angle Shown.

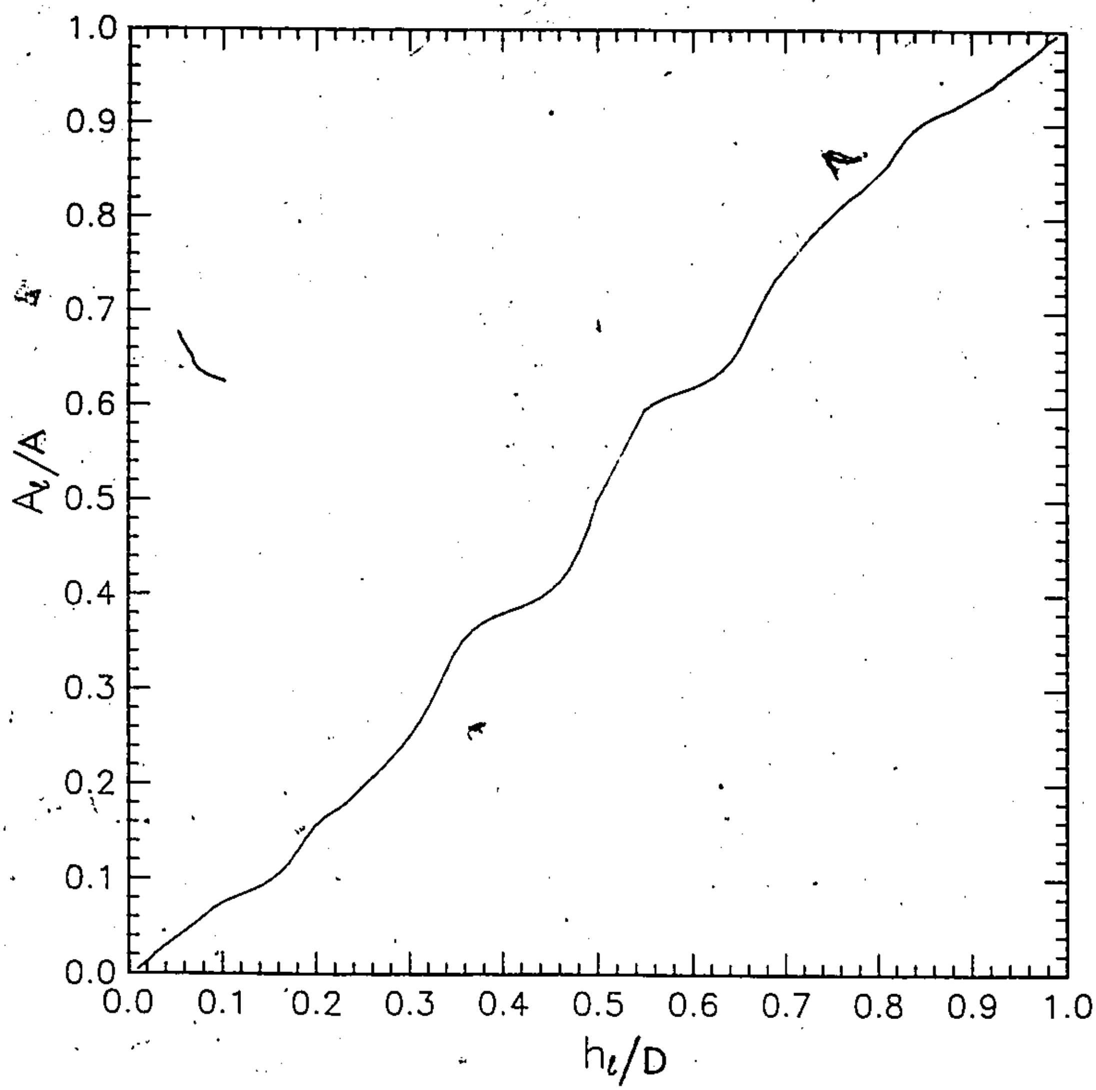

Figure 2.10 Liquid Holdup for a Stratified 28-Rod Bundle Flow

Similar results were also obtained for the 28-rod bundle flow geometry as shown in figures 2.8 to 2.10. Again, we observe significant influences on S_g, S_ℓ and S_i due to the presence of rod bundles. And the interfacial width, S_i, is observed to vary nonmonotonically with equilibrium liquid level, h_ℓ, with order of magnitude small compared with the pipe flow geometry.

However, effects of surface tenison have been neglected in the interfacial length and area calculations. This could affect the results for rod bundles, where the sharp peaks in the interfacial length calculations may become less pronounced.

CHAPTER 3

FLOW PATTERN TRANSITION MECHANISM

3.1 Stratified Smooth to Stratified Wavy Transition

In a steady state two-phase flow, the formation of a stratified wavy structure is associated with the situation where the gas velocity is sufficiently high to cause waves to form through interfacial shear. For a non-accelerating flow, Jeffreys [30] postulated the following criteria for wave generation:

$$c(u_g - c)^2 > \frac{4\mu_\ell g(\rho_\ell - \rho_g)}{\rho_\ell \rho_g s} \tag{3.1}$$

In the above inequality, ρ_ℓ, ρ_g, μ_ℓ, g and s are the liquid density, gas density, liquid viscosity, gravity and a sheltering coefficient, respectively. Jeffreys [30] suggested a value of $s=0.3$ for the sheltering coefficient, while other researchers [8,31] have recommended much smaller values of the order of $s=0.01$. Apparently, the value of s depends on how one defines a wave. A variety of different wave structures on two-phase stratified surfaces have been described [32]. They may be listed in three main groups, namely, ripple waves, two-dimensional waves and three-dimensional waves. In this study, the value of $s=0.01$, based on comparison of predicted and experimental results has been used throughout for the sheltering coefficient.

The constant c which appears in equation (3.1) represents the speed of the waves. For most practical cases, it is assumed that $u_g > c$ [8]. And previous theories and experimental results [8,33,34,35] indicate that the ratio of wave velocity to mean liquid film velocity decreases with increasing Reynolds number. For turbulent flow, this ratio approaches unity [8]. Thus for simplicity, the relation, $u_\ell = c$, has been used in this study, following Taitel and Dukler [8].

Substituting the above approximations into equation (3.1) yields the criterion for transition from Stratified Smooth to Stratified Wavy flow as,

$$u_g \geq \left[\frac{4g\mu_\ell(\rho_\ell - \rho_g)}{s\rho_\ell \rho_g u_\ell} \right]^{1/2} \tag{3.2}$$

3.2 Stratified To Intermittent or Annular Flow Transitions

The essential mechanism for transition from Stratified to Intermittent (Slug and Plug) or Annular flow patterns is the unconfined growth of a surface wave instability. For a critical set of flow conditions, a wave travelling on a stratified surface will grow until it blocks the flow of the gas phase. At low gas flow rates, the blockage forms a complete bridge (though possibly agitated) and Plug or Slug flow results. At higher gas flow rates, there may be insufficient liquid flowing to properly sustain the bridge. Hence the liquid in the wave is swept up around the inner wall of the pipe resulting in Annular flow [8]. The growth of a wave may occur due to the action of the gas flowing over it, or to the action of a capillary surface tension force acting to pull the gas liquid interface up to form the complete bridge.

For the first case; consider a finite solitary wave flowing over an otherwise stratified smooth liquid in a pipe of diameter, D, as shown in figure 3.1. The wave has a peak height, h'_ℓ, and the equilibrium stratified liquid height is h_ℓ. As the gas accelerates over the wave the pressure, P', in that region decreases due to the Bernoulli effect causing the wave to grow. At the same time, the force of gravity and the interfacial surface tension force acting to flatten out the wave tends to make it decay. Thus, neglecting the motion of the fluids, the condition for wave growth on the gas-liquid interface may be written as,

$$P - P' > (h'_\ell - h_\ell)(\rho_\ell - \rho_g)\,g + \sigma \frac{d^2\eta}{dx^2} \tag{3.3}$$

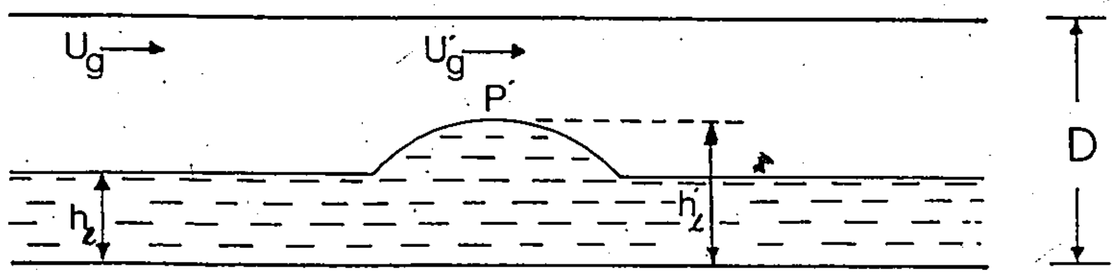

Figure 3.1 Kelvin-Helmholtz Instability Mechanism for Stratified to Intermittent Transition.

where the average mean curvature of the solitary wave is denoted by $d^2\eta/dx^2$. Therefore, for the case where the liquid surface tension becomes significant, the wave will grow when

$$P - P' > (h_\ell' - h_\ell)(\rho_\ell - \rho_g)\, g + \sigma k^2 (h_\ell' - h_\ell) \tag{3.4}$$

The pressure distribution is given from inviscid analysis as follows,

$$P - P' = \frac{1}{2}\rho_g(u_g'^2 - u_g^2) \tag{3.5}$$

Combining these two equations, and noting from continuity that $A_g u_g = A'_g u'_g$ assuming the gas phase to be incompressible, the criterion for wave growth becomes,

$$u_g > \left[\frac{2\{g(\rho_\ell - \rho_g) + \sigma k^2\}(h_\ell' - h_\ell)}{\rho_g} \, \frac{A_g'^2}{(A_g^2 - A_g'^2)} \right]^{1/2} \tag{3.6}$$

For small finite disturbances, A_g, may be expanded in terms of h_ℓ in a Taylor series;

$$A_g' = A_g - \frac{dA_g}{dh_\ell}(h_\ell - h_\ell') + O(h_\ell - h_\ell')^2 \tag{3.7}$$

Ignoring terms of order $(\Delta h_\ell)^2$ and higher in this analysis, the criterion for wave growth becomes,

$$u_g = B\left[\frac{\{g(\rho_\ell - \rho_g) + \sigma k^2\} A_g}{\rho_g \dfrac{dA_\ell}{dh_\ell}} \right]^{1/2} \tag{3.8}$$

where $B = A'_g/A_g$.

The coefficient B is dependent on A'_g and therefore cannot be determined directly. Taitel and Dukler [8] used the following reasoning to construct an alternative expression for B. When the equilibrium stratified liquid level approaches the top of the pipe, A'_g is small and any wave of finite amplitude will cause B to approach zero. However, when the stratified liquid level is small, the appearance of a small amplitude wave will have little effect on the size of the gas gap. A simple function that fits these extremes and is only dependent on known parameters is [8],

$$B = 1 - \frac{h_\ell}{D} \tag{3.9}$$

The above expression for B corresponds closely to the results obtained from previous analysis of the same problem by Wallis and Dobson [36] and Kordyban and Ranov [37]. These analyses, like the model of Taitel and Dukler [8], propose that the transition to intermittent flow depends on the value of B. In this study, a criterion of $B=0.5$ is taken as the condition which distinguishes Intermittent from Annular or Wavy Annular flows. For $B>0.5$, the flow is considered Annular or Wavy Annular, and for $B<0.5$, the flow is Intermittent (i.e. Slug or Plug). The constant, k represents the critical wave number at the point of transition, where the wave tends to grow indefinitely, and is given from the Kelvin-Helmholtz instability consideration of an equilibrium stratified two-phase flow system as shown in figure 3.1 by,

$$k^2 = \frac{g(\rho_\ell - \rho_g)}{\sigma} \tag{3.10}$$

The criterion for wave growth with the effect of interfacial surface tension force accounted for in the Kelvin-Helmholtz instability analysis of finite amplitude waves becomes,

$$u_g > 1.414\, B \left[\frac{g(\rho_\ell - \rho_g) A_g}{\rho_g \dfrac{dA_\ell}{dh_\ell}} \right]^{1/2} \tag{3.11}$$

The term dA_ℓ/dh_ℓ appearing in equations (3.8) and (3.11) may be determined directly from differentiation of equation (2.7) for the pipe, and equations (2.13), (2.18) and (2.24) for the annulus and rod bundle flow geometries.

For small diameter capillary tubes, the lower channel gap of annuli or subchannels of rod bundles, capillary surface tension forces may have important effects on the flow pattern structure. A wetting liquid has a tendency to climb the inner tube wall due to a capillary force and forms a complete bridge leading to intermittent flow [38].

The transition to Plug flow at low gas and liquid flow rates is modelled by comparing the gravity and capillary surface tension forces [38]. It is assumed that initially

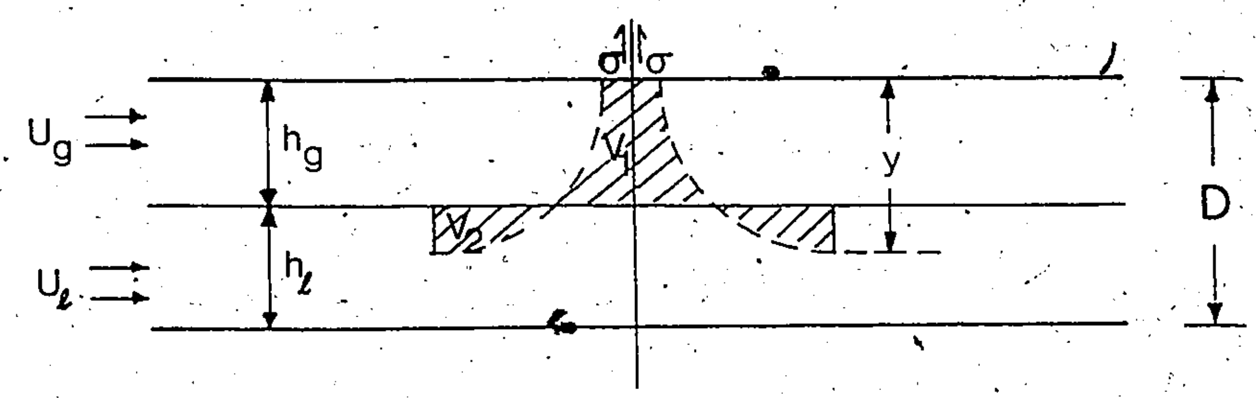

Figure 3.2 Capillary Surface Tension Consideration for Stratified to Intermittent Transition in Small Tubes.

the flow is stratified at an arbitrary liquid level as shown in figure 3.2 by the solid interface. Due to capillarity, the liquid climbs to the upper level reducing the liquid level in the vicinity of the newly formed Plug, indicated by the dotted line. The transfer of liquid requires that $V_1 = V_2$. Furthermore, in order for this process to be stable, the capillary surface tension forces must overcome the gravitational forces, ignoring the motion of the fluids.

In this simplified analysis, the flow is treated as two-dimensional and the Plug is assumed to have a circular shape of radius, y. Under these conditions, we can equate $V_1 = V_2$ for mass balance and this yields,

$$y = \frac{4}{\pi} h_g \tag{3.12}$$

where h_g is the equilibrium gas level. A static force balance on the system yields

$$\sigma = \rho_\ell g\left(y^2 - \frac{\pi}{4} y^2\right) \tag{3.13}$$

or

$$h_g \leq \frac{\pi}{4}\left[\frac{\sigma}{\rho_\ell g\left(1 - \frac{\pi}{4}\right)}\right]^{1/2} \tag{3.14}$$

as the transition criteria for pipe sizes smaller than a certain maximum. In these cases, transition will take place whenever the liquid level is high enough to satisfy mass balance given by equation (3.12). For adiabatic air/water flow at near atmospheric pressure, intermittent flow occurs when the equilibrium gas level is less than 4.6 mm.

3.3 Intermittent to Dispersed Bubble Flow Transition

During Intermittent (Slug and Plug) flow, the elongated bubbles formed are observed to flow on top of the liquid due to buoyancy effects. However, at higher liquid flow rates than those encountered in intermittent flow, the gas phase tends to mix with the fast flowing liquid leading to dispersed gas bubbles existing in the liquid phase. This occurs when turbulent fluctuations in the liquid overcomes the buoyancy forces tending to keep the bubbles on top of the pipe [8]. The buoyancy force per unit length of the gas region is given by [8],

$$F_B = g(\rho_\ell - \rho_g)A_g \tag{3.15}$$

and the liquid turbulent force acting upon the gas is given by

$$F_T = \frac{1}{2}\rho_\ell \overline{u'^2}\, S_i \tag{3.16}$$

where u', is the velocity fluctuation in the radial direction, and the root-mean-square of the fluctuation is taken equal to the friction velocity, and we obtain:

$$\sqrt{\overline{u'^2}} = u_\ell \left(\frac{f_\ell}{2}\right)^{1/2} \tag{3.17}$$

hence,

$$F_T = \frac{1}{4} S_i \rho_\ell f_\ell u_\ell^2 \tag{3.18}$$

Therefore, the criterion for transition from Intermittent to Dispersed Bubble flow pattern becomes,

$$u_\ell \geq \left[\frac{4\, g(\rho_\ell - \rho_g)A_g}{f_\ell \rho_\ell S_i}\right]^{1/2} \tag{3.19}$$

For transitions in the annulus and rod bundle flow geometries, the above criterion derived from Taitel and Dukler's work [8] for the pipe flow case have been used together with substituting the respective expressions for the geometrical parameters, which have been fully derived for the pipe, annulus and rod bundle flow geometries in Section 2.3.

CHAPTER 4

NUMERICAL PROCEDURE

The flow pattern transitions discussed in Section 3 are calculated numerically by REGIME-3 [38] and REGIME-4 [11] codes. The general procedure used for these codes are as shown in the flowchart of figure 4.1. And detailed procedure is enumerated below:

(1) Given the pipe diameter and flow conditions, the physical properties of the fluids are specified. Specify the diameter of the rods and their coordinates in the annulus and rod bundle flow geometries. Also specify the rod bundle orientation within the enclosing tube for the rod bundle flow case.

(2) Calculate the total cross-sectional area, A, and the total wetted perimeter of the flow section, S. Calculate the angular coordinates for the case of the rod bundle geometry. Then choose a suitable increment for the equilibrium liquid level.

(3) Determine the Stratified Smooth to Stratified Wavy transition location from the criteria given by equation (3.2).

(i) Choose a value for the sheltering coefficient, s. In this work, a value of $s=0.01$ was used throughout for the sheltering coefficient.

(ii) Initialize the equilibrium liquid level, h_ℓ, and calculate the geometrical parameters, A_g, A_ℓ, S_g, S ,and S_i from equations (2.7) to (2.27) for the pipe, annulus and rod bundle geometries using subroutine SHAPE, as shown in figure 4.2.

(iii) Initialize the liquid velocity, and calculate the gas velocity from the transition criteria given by equation (3.2). Calculate for the liquid velocity from the momentum equation (2.3) and iterate until convergence according to the criterion,

$$\left| \frac{u_\ell^i - u_\ell^{i-1}}{u_\ell^i} \right| < \varepsilon \qquad (4.1)$$

where ε was assigned a value of 10^{-4} in this study.

Then calculate the superficial gas and liquid velocities.

(4) Using the same procedure as above, determine the Stratified to Intermittent transition from the transition criteria given by equation (3.11). For capillary tubes of diameter less than a certain maximum, this transition criteria is given by equation (3.14).

(5) Determine the Intermittent to Dispersed Bubble flow transition from the criteria given by equation (3.19). The same procedure as described in (3) above is used here. However, in this case we iterate for the gas phase velocity from the momentum equation (2.3), since the liquid velocity is given from the transition criteria, equation (3.19). The subroutine SPEEDG is used to achieve this, and the convergence criterion given by equation (4.1) is used for the gas phase velocity, u_g.

(6) Determine the Intermittent to Annular or Wavy Annular flow transition.

  (i) Specify the equilibrium liquid level to a value, one-half the inside diameter of the pipe.

  (ii) Initialize the gas velocity to a suitable value.

  (iii) Proceed as in (3) above to obtain converged values of the liquid phase velocity, and consequently the superficial velocities.

Computer printouts employing the procedure described in this section for the pipe, annulus and rod bundle flow geometries are listed in Appendix III.

The numerical results obtained in this study have been analyzed in the form of flow pattern maps based on the superficial gas and liquid velocities. The REGIME-3 code

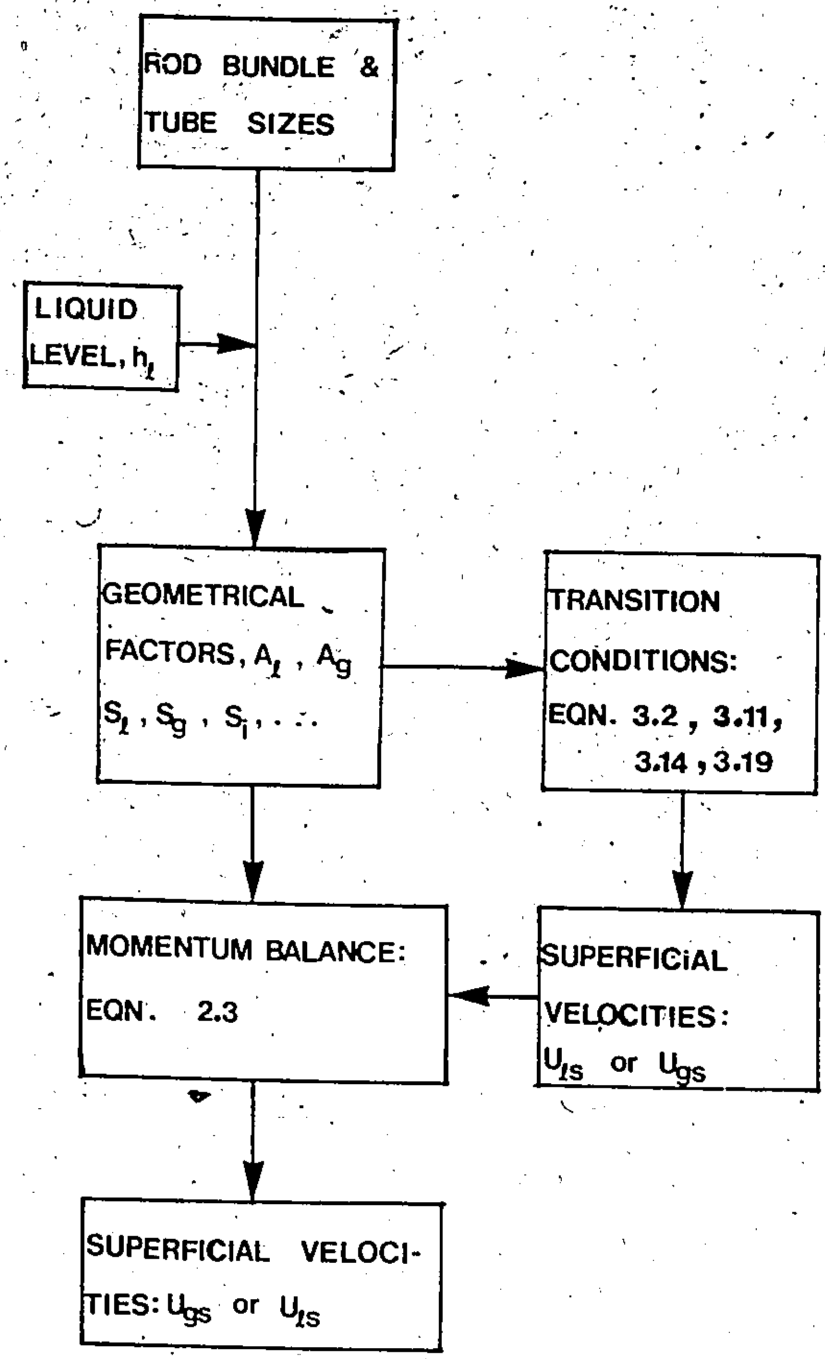

Figure 4.1 Schematic Flowchart of REGIME-4 Code.

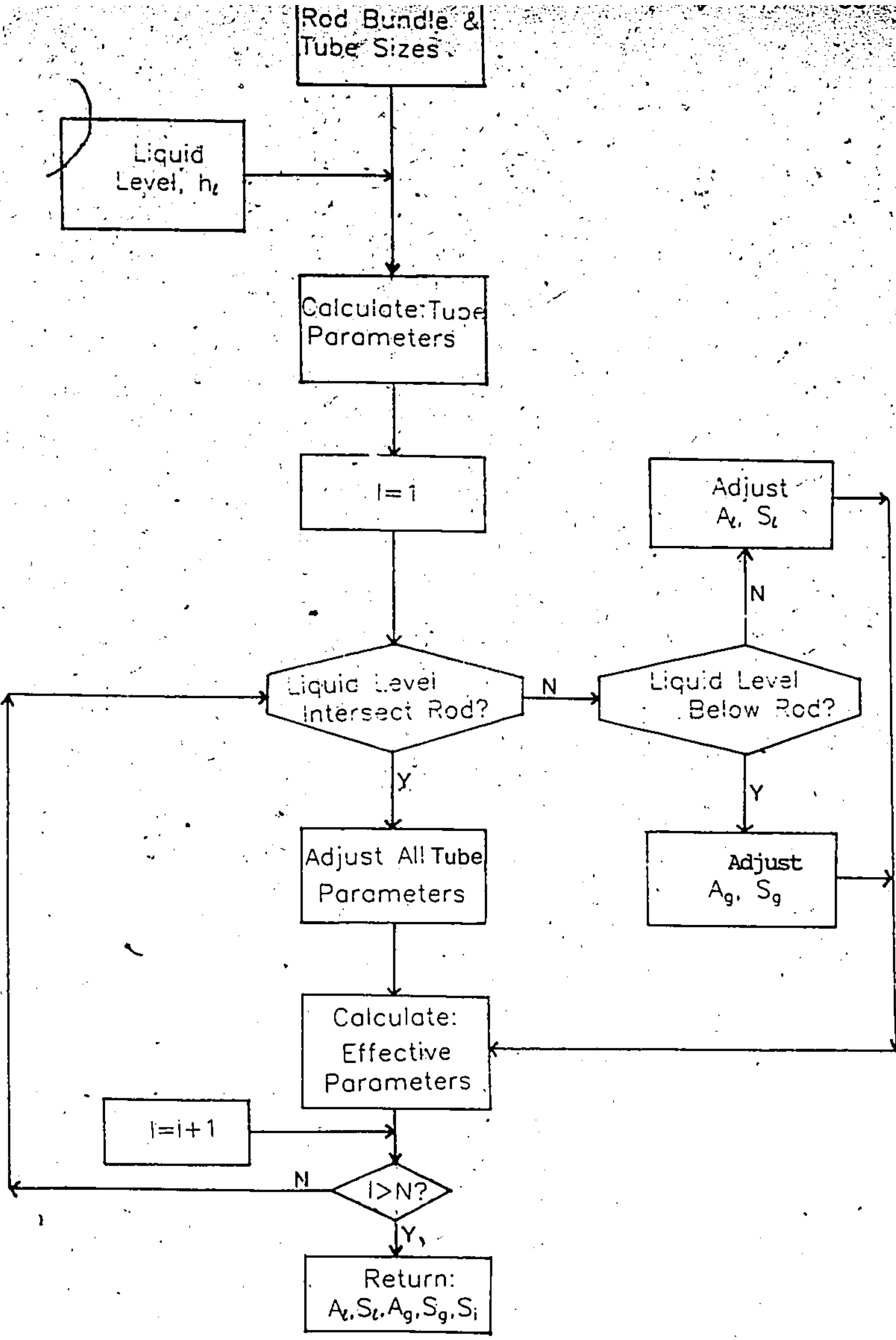

Figure 4.2 Schematic Flowchart of Subroutine SHAPE.

calculates two-phase flow pattern transitions in horizontal gas-liquid flow in pipes with branches. Typical flow pattern transitions for different pipe branches and angles are given in Appendix II. The REGIME-4 code calculates two-phase flow pattern transitions in annulus and rod bundle geometries. The numerical procedure presented here is also capable of calculating liquid holdup for horizontal equilibrium stratified flow in pipes, annulus and rod bundle geometries.

CHAPTER 5

NUMERICAL RESULTS AND DISCUSSIONS

5.1 Pipe Flow

Figure 5.1 shows the numerical results of the flow transitions for a horizontal air-water two-phase flow at room temperature and near atmospheric pressure, in a 5.08 cm i.d. pipe. The solid lines represent the numerical results of the model presented in this study for pipe flow. In this model the effect of interfacial surface tension force which acts to oppose the growth of waves at the gas-liquid interface is included in the Stratified to Intermittent transition criteria. The dashed lines represent the results of the model by Taitel and Dukler [8] which does not consider interfacial surface tension effect for this transition.

The results of the model presented in this work predict the Stratified to Intermittent or Annular flow transition to occur at higher superficial velocities than the Taitel and Dukler model [8]. The small kinks observed in the Stratified to Intermittent transition at low superficial gas velocities represent the transition from laminar to turbulent flow in the gas phase. The laminar to turbulent flow transition for the liquid phase occurs at superficial flow velocities less than that presented here. The interfacial surface tension effect may not be very significant, in general, since this transition is observed to occur at superficial velocities of the same order of magnitude, but, the influence of pipe diameters on the Stratified to Intermittent flow pattern transition may be enhanced when the interfacial surface tension effect is considered.

Figure 5.2 shows the results of horizontal flow transitions for different pipe sizes from 1.0 cm to 20.0 cm i.d. The results indicate that there is a significant influence of pipe diameters on the flow pattern transitions. The Stratified to Intermittent or Annular trans-

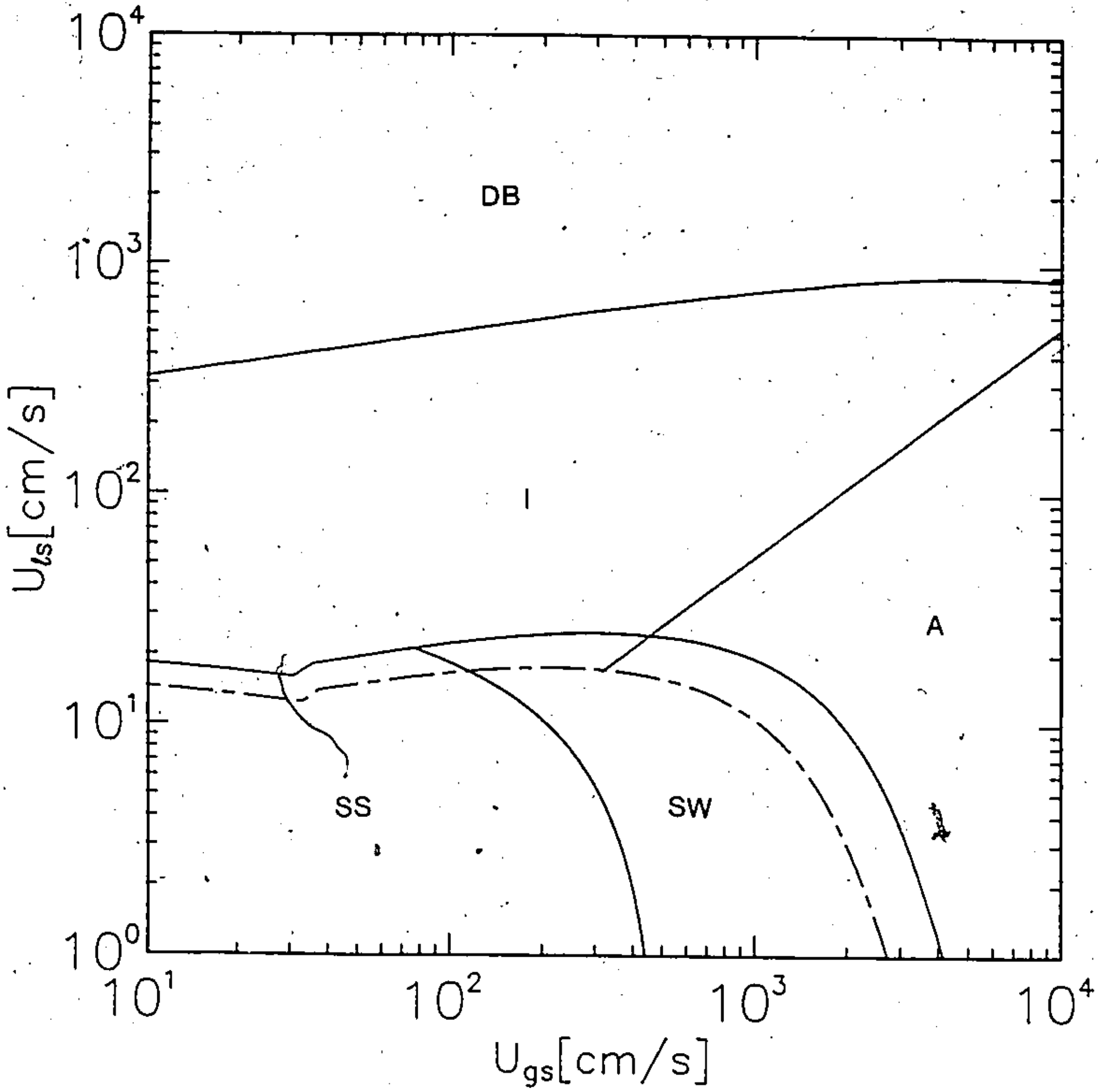

Figure 5.1 Predicted Flow Pattern Transitions for 5.08 cm i.d. Pipe Flow.

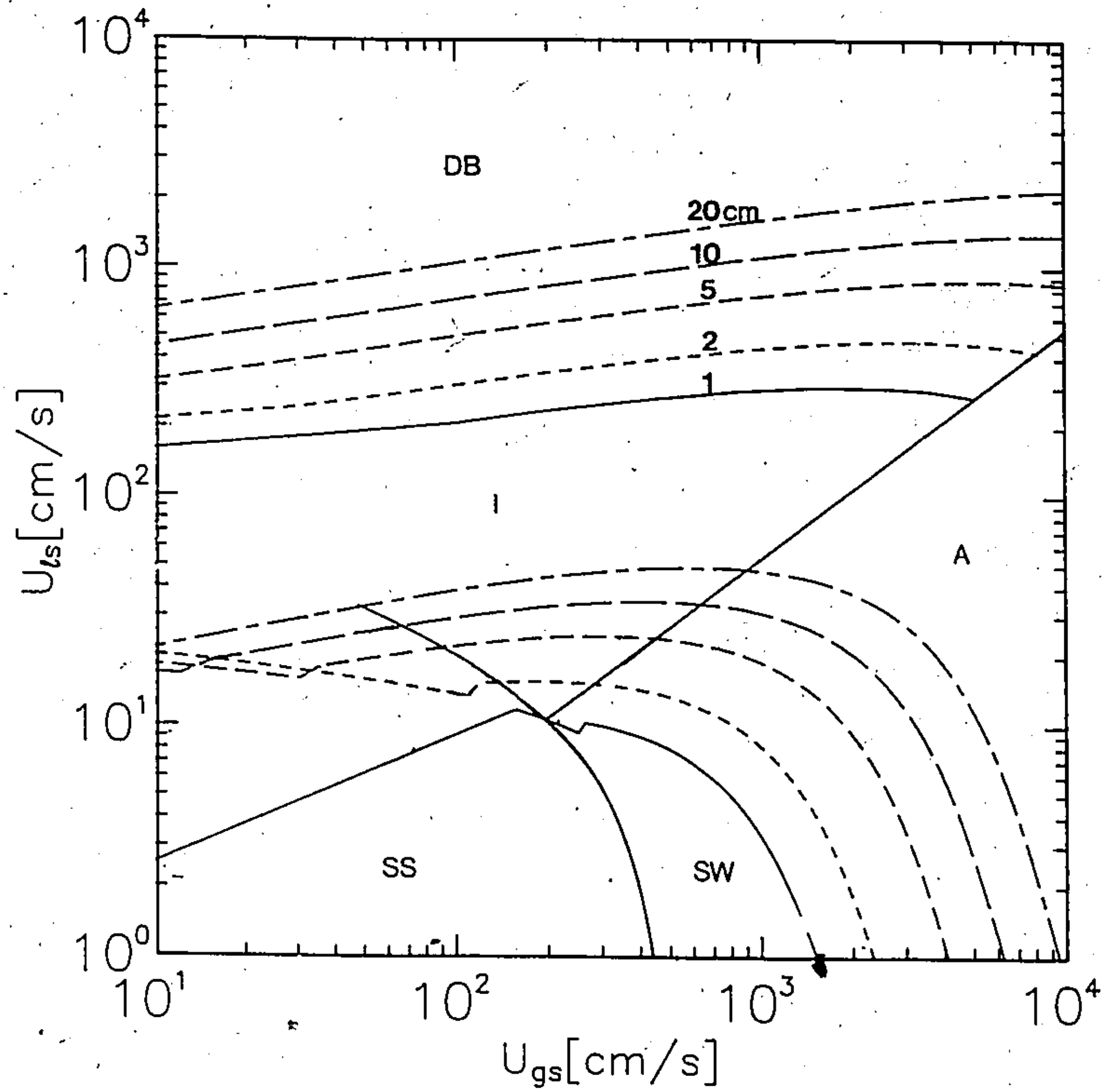

Figure 5.2 Predicted Effect of Pipe Diameter on Flow Pattern Transitions.

ition is predicted to occur at higher superficial gas and liquid velocities for larger pipe sizes. The Intermittent to Dispersed Bubble transition is also seen to be significantly affected. The Dispersed Bubble flow patterns are predicted to occur at lower superficial liquid velocities for smaller pipe sizes. The Stratified Smooth to Stratified Wavy and the Intermittent to Annular or Wavy-Annular flow transitions are observed to be rather insensitive to pipe diameters. For larger pipe sizes, the influence of pipe diameters on flow pattern transitions seems to become decreased.

The Stratified to Plug flow transitions occur at much lower superficial liquid velocities for small diameter tubes, $D < 1.0$ cm i.d., as shown from the results of the 1.0 cm i.d. pipe. In this case, the transition mechanism is mostly governed by the capillary surface tension force which tends to pull the gas-liquid interface, against the stabilizing force of gravity, up to the upper wall of the tube.

5.2 Annulus Flow

Figure 5.3 shows the results of horizontal two-phase flow transitions in annulus geometries having pipe diameter of 5.08 cm i.d. and rod diameters from 1.905 cm to 3.175 cm, and hence, inner-to-outer diameter ratios from 0.375 to 0.625. The results show that the flow pattern transitions are significantly influenced by the inner-to-outer diameter ratios of annulus geometries. Figure 5.3 also shows the flow pattern transitions for a horizontal 5.08 cm i.d. pipe which corresponds to an annulus geometry of inner-to-outer diameter ratio, 0.00. The flow pattern transitions for annuli are observed to be different from those of pipes, and the Stratified to Intermittent flow transitions are the most significantly influenced. This transition is predicted to occur at lower superficial liquid velocities in annuli with larger inner-to-outer diameter ratios. The pipe flow case is observed to occur at higher superficial liquid velocities than for annulus geometries.

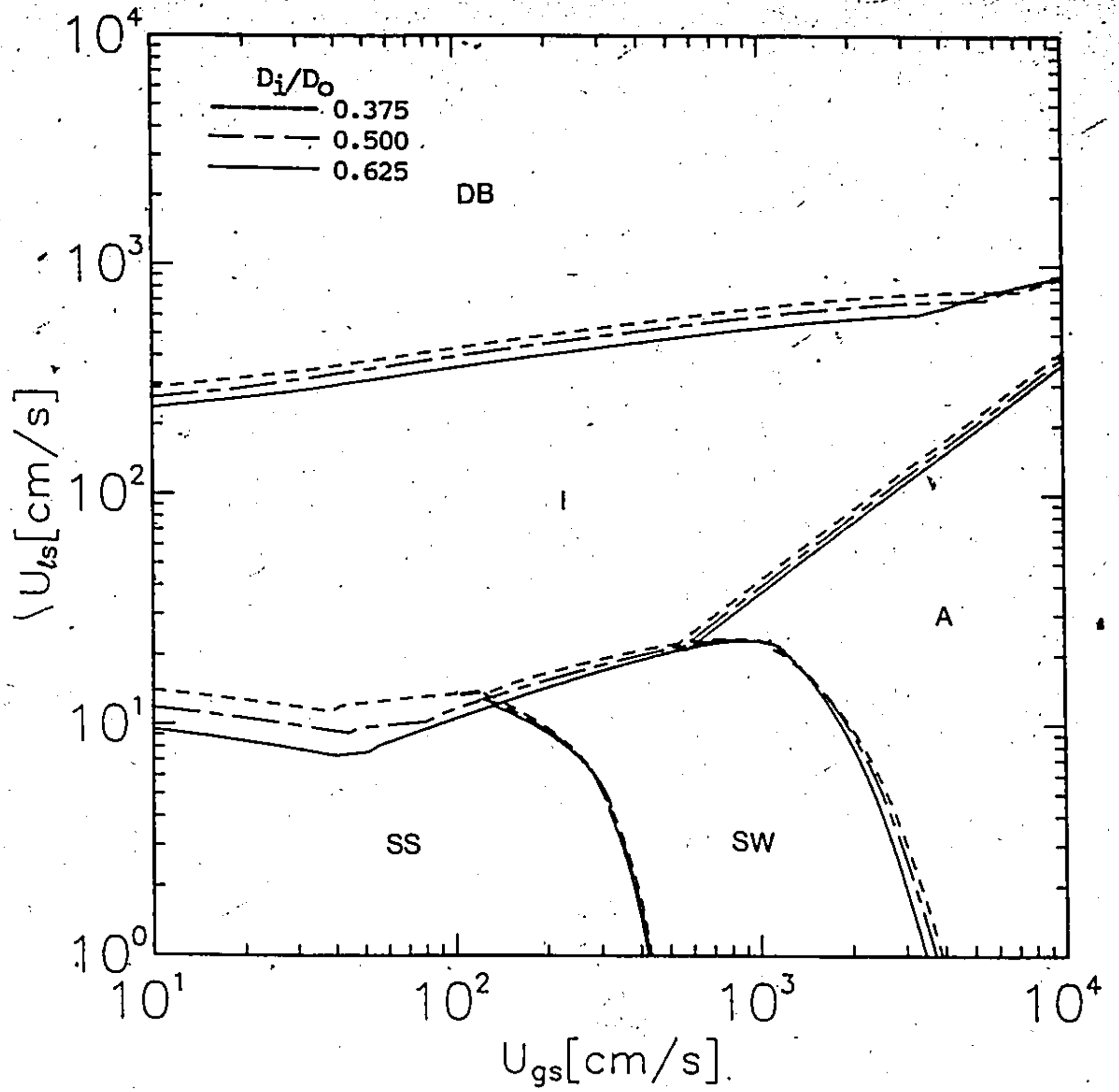

Figure 5.3 Effect of Inner-to-Outer Diameter Ratios on Two-Phase Flow Pattern Transitions in Annulus Geometry from Theoretical Predictions.

The Stratified to Annular or Wavy-Annular flow transition is not significantly affected by different inner-to-outer diameter ratios, and very little influence is predicted for the Intermittent to Annular or Wavy-Annular and the Intermittent to Dispersed Bubble flow transitions.

The Intermittent to Annular or Wavy-Annular flow transition occurs at lower superficial gas velocities for annuli with smaller inner-to-outer diameter ratio. The pipe flow case which corresponds to an annulus of diameter ratio, 0.00, is seen to occur earlier than the annulus results due to flow acceleration in the annulus geometry. A similar trend observed for the Stratified to Intermittent transition is predicted for the Intermittent to Dispersed Bubble flow transition. This transition occurs at higher superficial liquid velocities for smaller inner-to-outer diameter ratios. For pipe flow cases, this transition is observed to occur at higher superficial liquid velocities than for annuli.

Figure 5.3 shows that the Stratified Smooth to Stratified Wavy flow transition is insensitive to different inner-to-outer diameter ratios.

5.3 Rod Bundle Flow

The numerical results of the flow pattern transitions occurring in the horizontal 28 and 37-rod bundle flow geometries is as shown in figures 5.4 to 5.5, respectively, and the predicted flow pattern transitions of a 10.16 cm i.d. pipe is also shown here. The flow pattern transitions for the pipe is shown to be remarkably different from those of rod bundles. This may be due principally to significant differences in the pipe and rod bundle flow geometries.

Large effect of geometry is observed for the Stratified to Intermittent and the Intermittent to Dispersed Bubble flow transitions. The rod bundle flow results show irregular transition locations occurring at high gas flow rates. This is observed for both the Stratified to Intermittent and the Intermittent to Dispersed Bubble flow patterns, and may be due to the

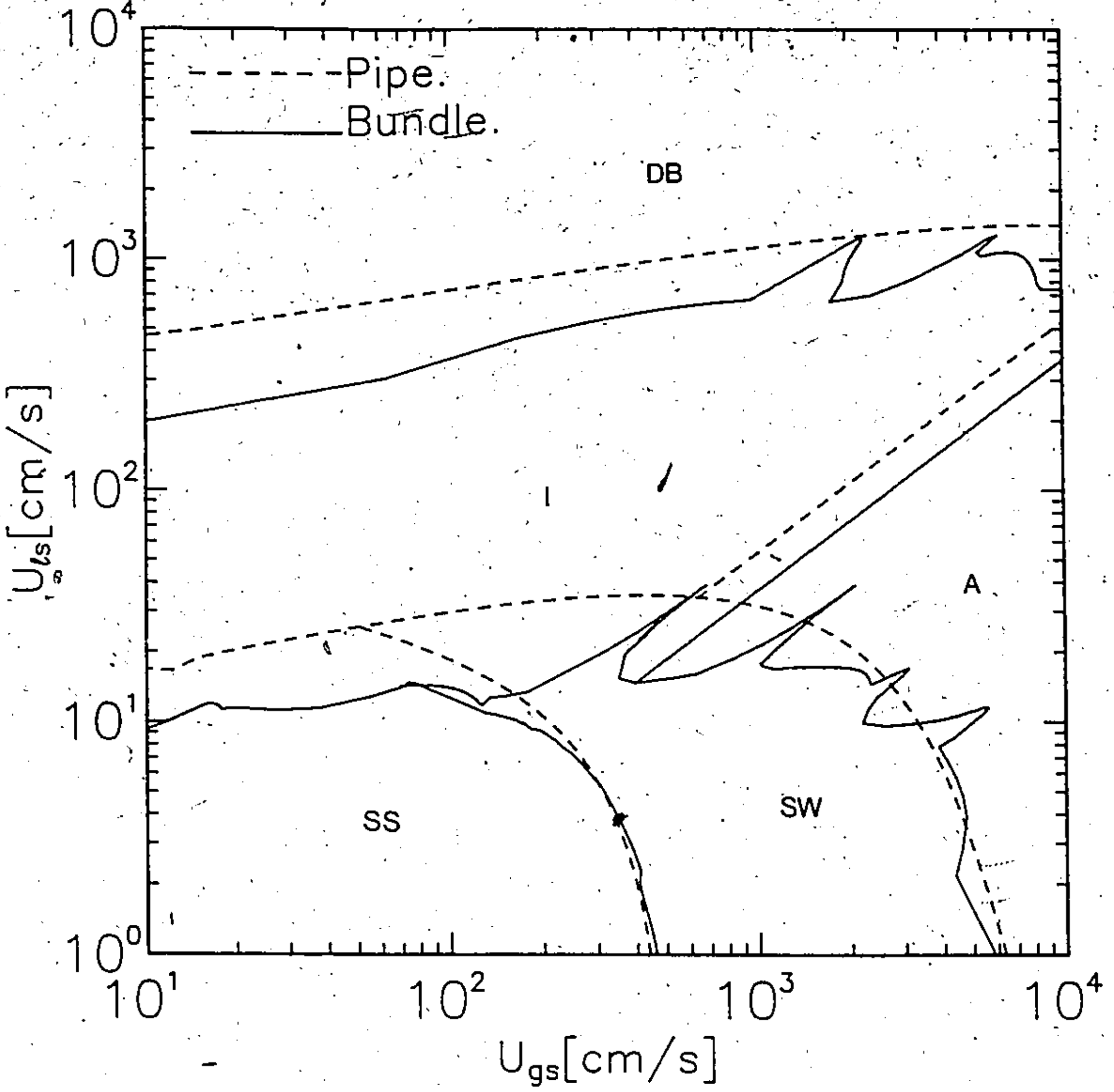

Figure 5.4 **Predicted Flow Pattern Transitions for 28-Rod Bundle Flow.**

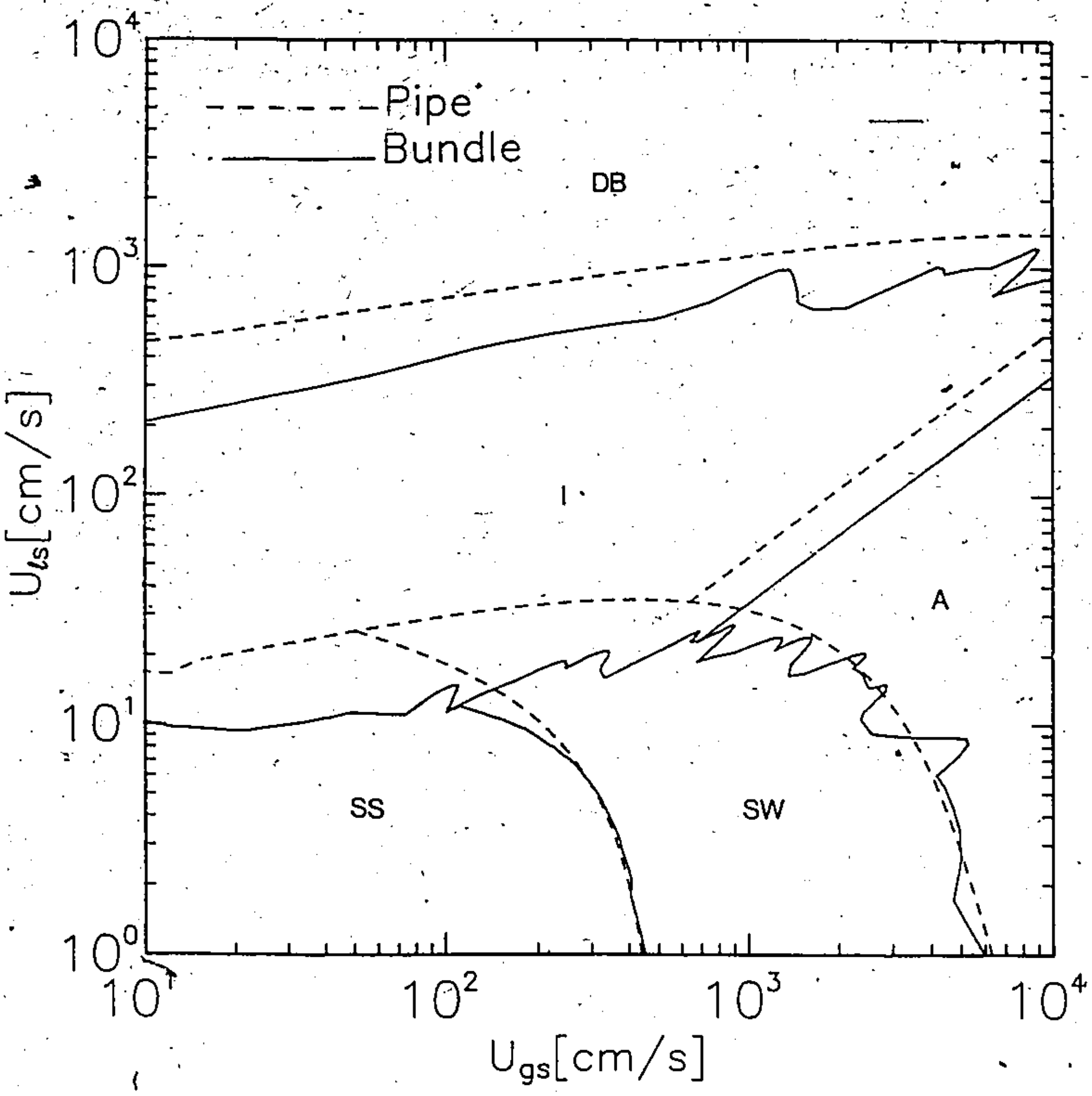

Figure 5.5 Predicted Flow Pattern Transitions for 37-Rod Bundle Flow.

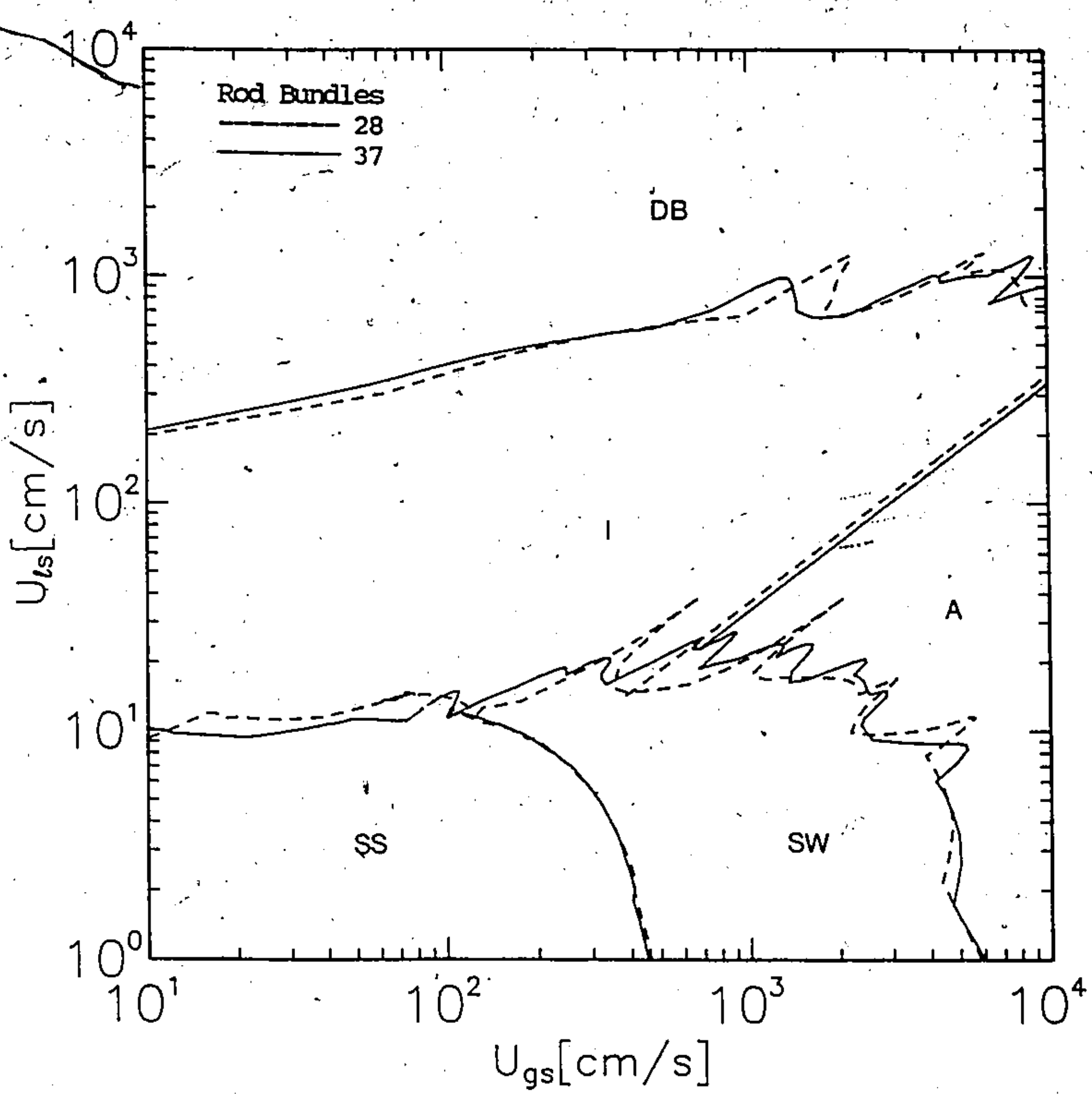

Figure 5.6 Comparison of 28 and 37-Rod Bundle Flow Pattern Transitions.

nonmonotonic variations observed for the rod bundle interfacial areas (Section 2). This shape for the interfacial areas leads to fluctuations in the critical gas velocities as determined from the Stratified to Intermittent transition criteria. The Stratified to Intermittent and the Intermittent to Dispersed Bubble flow transitions are predicted to occur at lower superficial liquid velocities than for the pipe geometry.

The Intermittent to Annular flow transitions are also affected by the complex flow geometries presented by rod bundles. This transition is predicted to occur at higher superficial gas velocities for rod bundle systems, and may be due to increase in gas velocity resulting from the significant reduction in the flow area.

The Stratified Smooth to Stratified Wavy and the Stratified Wavy to Annular flow transitions are observed to be insensitive to the presence of rod bundles in the tube.

Figure 5.6 shows a comparison between the 28 and 37-rod bundle flow pattern transitions, and little influence on the transitions are observed from the results. However, significant differences in the results may exist between rod bundles having large geometrical variations. Figure 5.6 shows that the Intermittent to Dispersed Bubble flow regime occurs at lower superficial liquid velocities for the 37-rod bundle flow geometry.

The rod bundle flow pattern maps of figures 5.4 to 5.6 are for a 0° orientation as defined in figure 5.8. Figure 5.7 represents the numerical flow pattern transitions for the 37-rod bundle geometry at various possible orientations from 0° to 45°. The Stratified to Intermittent and the Intermittent to Dispersed Bubble flow pattern transitions are seen to be influenced by the rod bundle orientations. Thus, they have been represented as transition bands rather than lines to account for any uncertainties due to arbitrary orientation of the rod bundle within the enclosing tube, since in a practical situation the orientation of the rod bundles within the tube may not be known specifically.

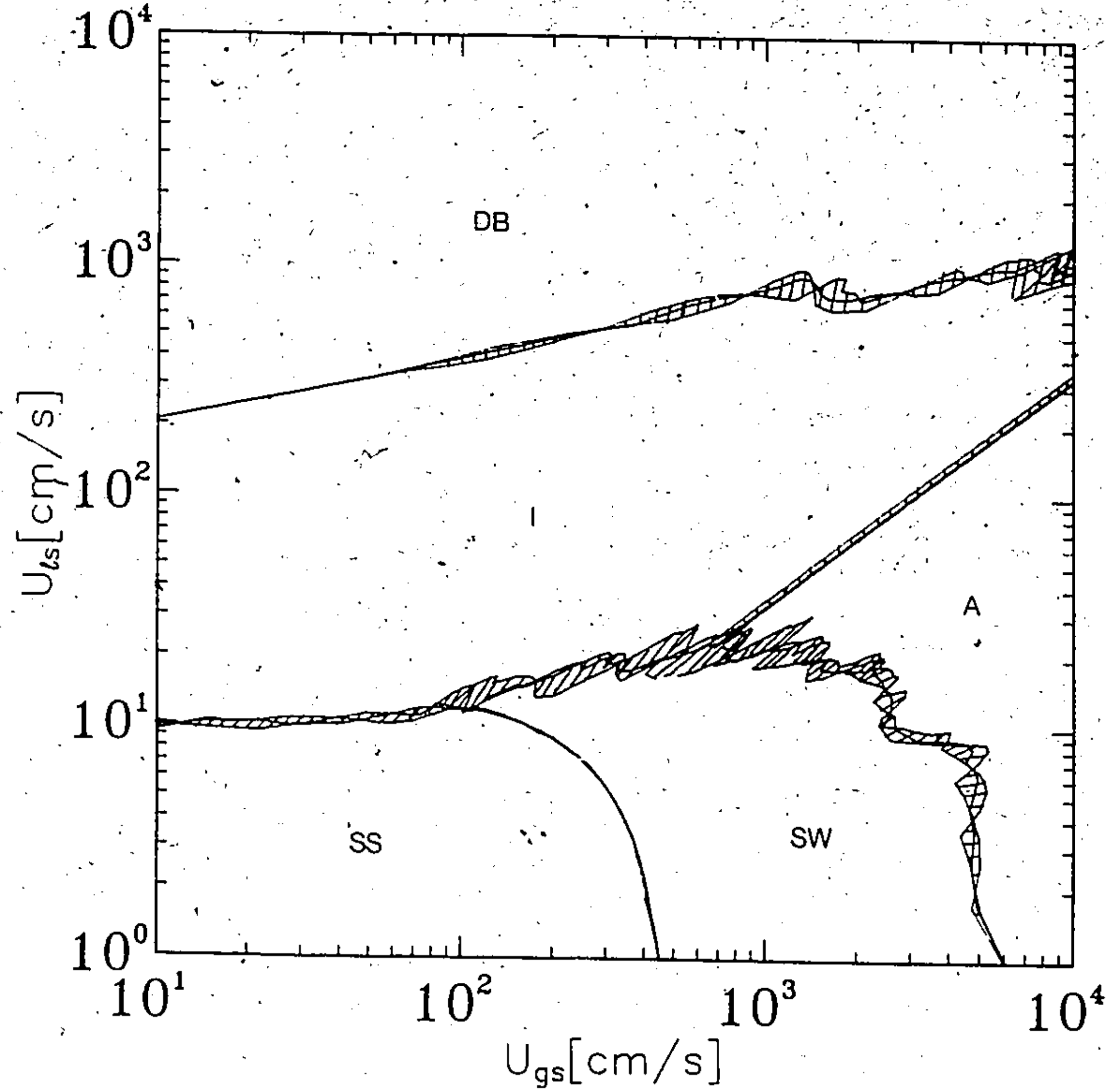

Figure 5.7 Predicted Flow Pattern Transition for 37-Rod Bundle Flow Including the Effect of Orientation Angles.

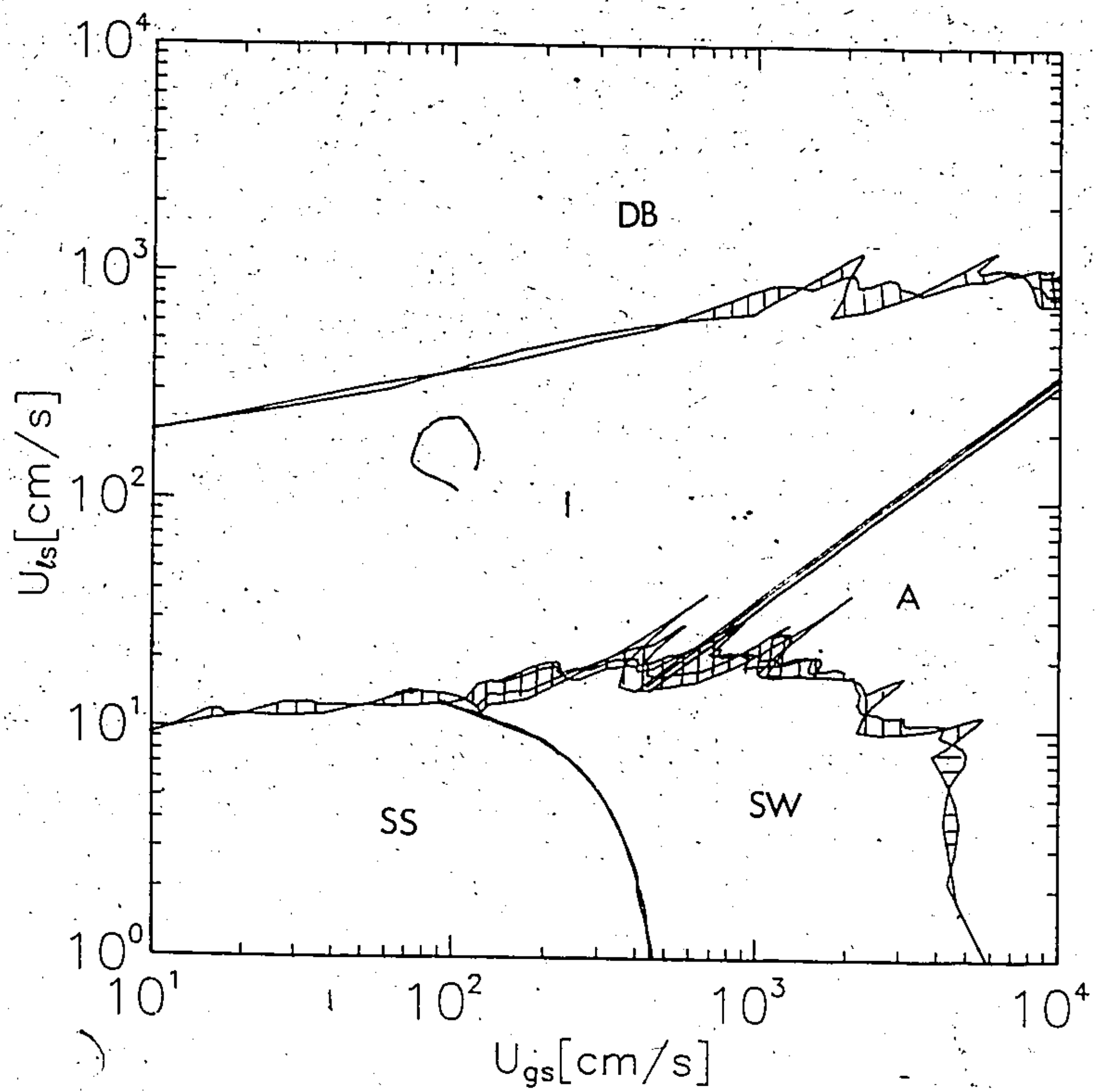

Figure 5.8 Predicted Flow Pattern Transitions for 28-Rod Bundle Flow Including the Effect of Orientation Angles.

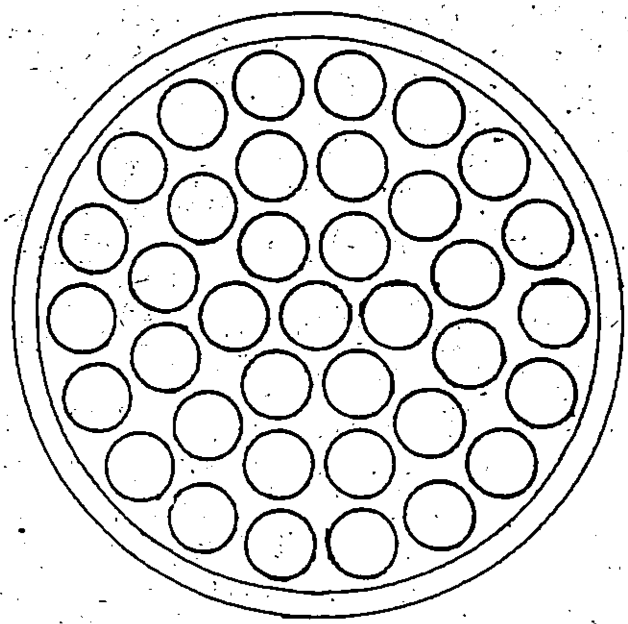

37

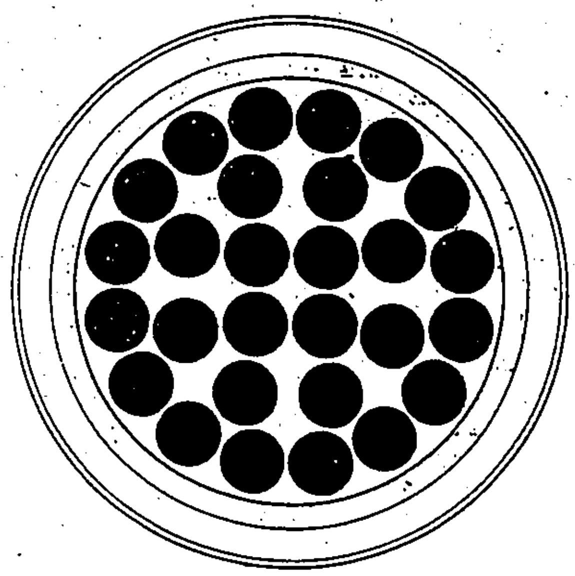

28

Figure 5.9 28 and 37-Rod Bundle Flow Cross-Sections at Zero Degree Orientation Angle.

CHAPTER 6

EXPERIMENTAL

6.1 Loop Description and Experimental Procedure

6.1.1 Pipe and Annulus Experiment

A schematic diagram of the experimental loop used in this study is as shown in figure 6.1. The set-up is a recirculating air-water two-phase flow system having a transparent test section made of acrylic tubing, 5.08 cm i.d. and 365.7 cm long. The set-up for the annulus experiment is as shown in this figure. This is constructed by placing an aluminum rod along the central axis of the tube. The annulus rod consists of two tube sections press fitted together and supported at both ends and about 1.5m from the upstream end. Water is pumped from a large separator tank through a Fischer and Porter rotameter calibrated to a maximum liquid flow rate of 1.11 ℓ/s. The water remains essentially at room temperature since it sits in the separator tank long enough to reach thermal equilibrium with the surrounding. And air from the laboratory supply is flowed past a pressure regulator, an air filter and through a Brooks Instrument rotameter, Model No. 1110-10H3A1D, calibrated up to a maximum air flow rate of 11.33 ℓ/s.

The air and water flow through a separated type mixing section and into the test section. This is a 'Wye' branch with the air introduced in the upper branch and water in the lower branch. Most of the mixing sections used for air-water two-phase flow are made of pipe 'Tees' with the air introduced in the branch and water in the run. Lin and Hanratty [29] reported similar results for flow transitions when water is introduced in the branch and air in the run, except at the Stratified to Slug transition for low superficial gas velocities, but Weisman et al. [9] found no effect of different entry sections on flow transitions.

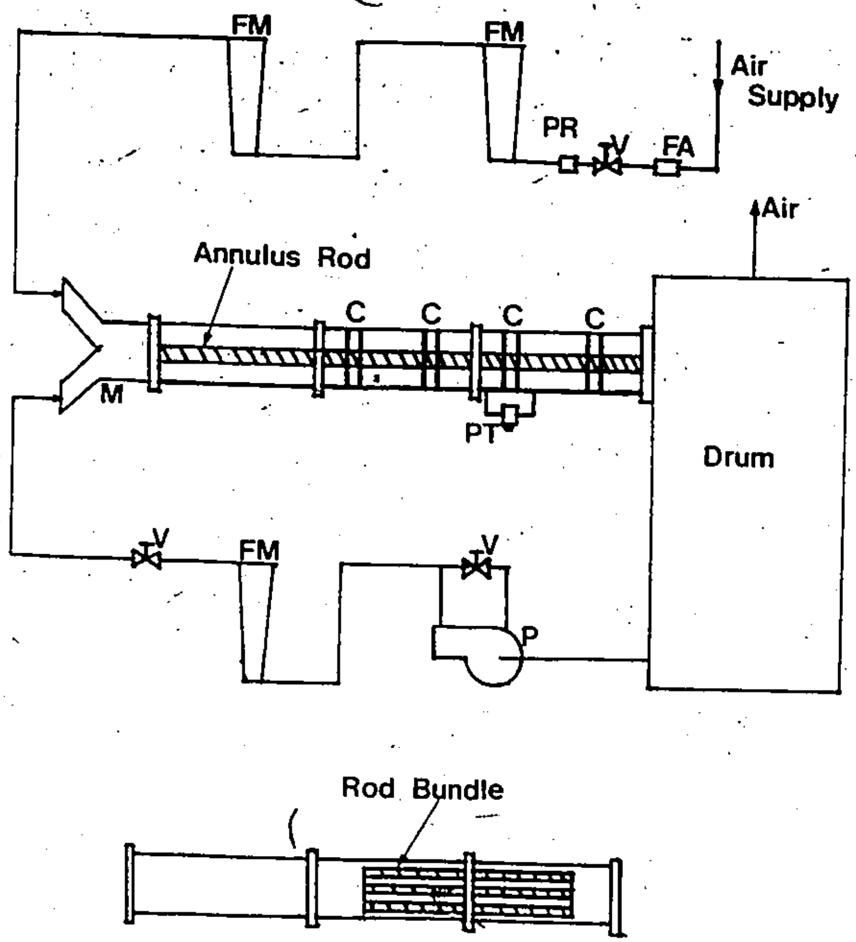

C	Capacitance Transducer
FM	Flow Meter
M	Mixer
P	Pump
PR	Pressure Regulator
PT	" Transducer

Figure 6.1 Schematics of Experimental Loop.

The redistribution of the two phases within the test section for different flow rates of air and water are monitored from the analog output signals of the ring-type capacitance transducer [39] via a Booton capacitance meter, Model No. 72B, operated at 1 MHz. In order to characterize certain flow patterns occurring in the annulus gap location below the axial rod, the ultrasonic transmission technique [40] was modified and used. Pressure drop measurements in the annulus flow system was achieved with the Validyne DP15 differential type pressure transducer. A 1.38 kPa pressure transducer diaphragm was selected for use. This gave a good sensitivity and remained stable throughout the range of flow conditions studied.

6.1.2 Rod Bundle Flow Experiment

This present loop was slightly modified to accommodate two 37-rod bundles with rods of diameter, 1.27 cm and length, 100 cm. These were placed next to each other in the downstream of the test section. The rod bundles were enclosed in a 10.16 cm i.d. tube section. The tube section was constructed of two 150 cm long clear anodized aluminum materials. A 150 cm long transparent section made of acrylic tubing was used in place of one of the aluminum tube sections in the downstream part to enable direct visual observation of the flow patterns occurring in the system. The experiment was performed at room temperature and at atmospheric pressure.

A homogeneous type mixing section was used in this case with the air introduced in the branch and water in the run. And the two-phase flow patterns occurring in the system characterized by direct visual observation and from the analog output signals of the ring-type capacitance transducer. Pressure measurements was accomplished with the Validyne DP15 differential pressure transducers enclosing an 8.62 kPa pressure transducer diaphragm. A larger pressure diaphragm has been used in this case since there is increased pressure drop in the system due to contributions from the rod bundles present. Also, good sensitivity and high stability was obtained throughout the range of flow conditions studied by using this diaphragm size.

6.2 Measurement Techniques

Pressure drop and void fraction are of primary importance in the design of two-phase flow systems. The void fraction represents the fraction of the two-phase flow section occupied by the gas phase. Knowledge of this parameter is useful for the estimation of neutron absorption by the liquid phase in the design of boiling water nuclear reactors, and also for determining the system pressure drop. The pressure drop essentially governs the pumping power requirements of the system.

6.2.1 Pressure Drop Measurement

The pressure drop measurements were achieved by the pressure transducer technique. Validyne DP15 differential pressure transducers (response time of 2 microseconds) enclosing diaphragms of sensitivities 1.38 kPa and 8.62 kPa, were used for the annulus and rod bundle flow experiments, respectively. The output is analog voltage via a homemade carrier demodulator. The pressure transducers were calibrated versus a water manometer. The maximum change in the water column was adjusted to match the maximum sensitivity of the pressure diaphragm, and the span of the demodulator adjusted to a selected voltage. The zero of the carrier demodulator was adjusted to correspond to 0 Volts. The calibration procedure involves lowering the water column stepwisely from its maximum and the corresponding output voltage noted. Typical pressure calibration curves are given in Appendix I.

Horizontal gas-liquid two-phase flow is characterized by asymmetry in the flow distribution due to the influence of gravity, where the liquid tends to flow at the bottom of the pipe and the gas phase flows on top. The pressure tapping lines were therefore made at the bottom of the pipe to reduce any electrical noise that could be caused by the presence of gas bubbles within the tapping lines. The pressure transducers were also purged of any air in the tapping lines before the experimental runs, and the zero adjustment checked to ensure that the measurements were within calibration limits.

The analog voltage output of the pressure transducer for various flow conditions studied were analyzed using the Apple IIe computer via the Analog to Digital Converter (ADC) for time averaged pressure drops. The fluctuations of the pressure drop signals were also recorded with the Goertz chart recorder, and used for monitoring the various flow patterns occurring in the system. The signal waveforms were observed to be distinct for different flow patterns, and were used to supplement flow pattern identification by direct visual observation.

6.2.2 Void Fraction Measurement

The void fraction measurements were achieved by the capacitance transducer technique [39]. This is based on the large differences in the dielectric constants of the liquid, gas and tube materials. Detailed description of the method is given by Chang et al. [39].

From theoretical considerations, the electric field and potential profiles of the two ring electrodes of figure 6.2 can be schematically represented as shown in figure 6.3 for an ideal condition, neglecting the radial component of the electric field. The problem can therefore be analyzed by a simple equivalent capacitance circuit method, assuming the axial electric field is constant along the axial direction. Different phase distributions can be analyzed in the form of series or parallel connections between parallel plate electrodes as shown in figure 6.4. The output capacitance can thus be calculated as a function of void fraction for various flow patterns. Typical calculations for the Annular, Stratified and Slug

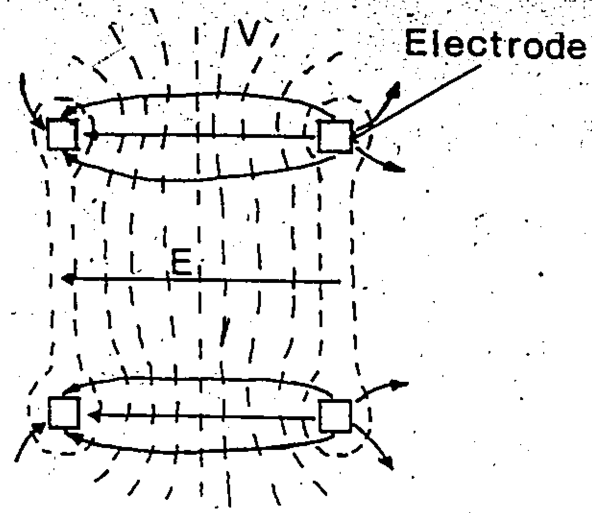

Figure 6.2 Electric Field and Potential Profiles for Ring-Type Capacitance Transducers.

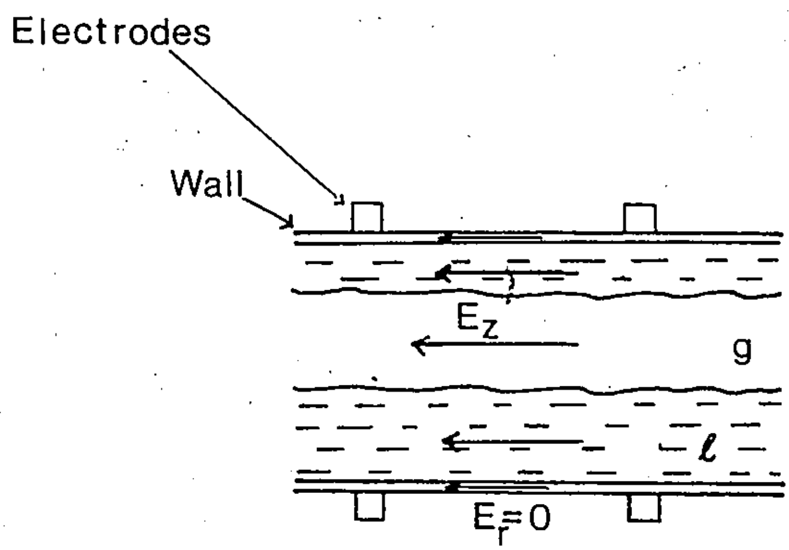

Figure 6.3 Schematic Representation of Ring-Type Capacitance Transducer in a Two-Phase Flow Section.

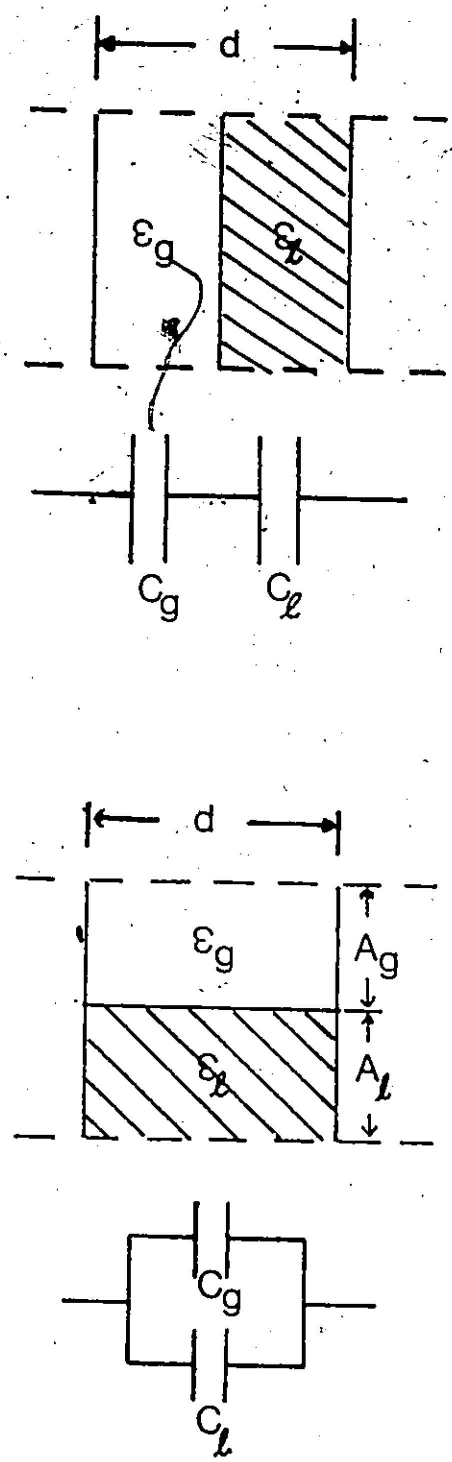

Figure 6.4 **Equivalent Capacitance Circuits for Ring-Type Capacitance Transducer.**

flow patterns are given below. Idealized representations of these flow patterns are as shown in figure 6.5.

(i) Annular and Stratified Flow Patterns:

From the flow pattern representations as shown in figure 6.5, the equivalent circuits for the Annular and Stratified flow patterns are similar and of parallel connections. In this case, the total capacitance reduces to,

$$C_T = C_g + C_\ell + C_w \tag{6.1}$$

and we note that any metallic material, like the rod bundle or the annulus rod, that may be enclosed within the two-phase flow zone does not contribute to the total capacitance, since electric field cannot penetrate metals, in general (i.e. the dielectric constant for metals is infinite). Since we are only interested in the changing parameters, namely, the gas and liquid content of the two-phase flow section, the wall capacitance which remains constant can therefore be combined with the total capacitance to yield,

$$C_p = (C_T - C_w) = C_g + C_\ell \tag{6.2}$$

Substituting the expression for parallel plate capacitance we obtain,

$$C_p = \frac{\varepsilon_o A}{d} [\varepsilon_{\ell s} - (\varepsilon_{\ell s} - 1)\alpha_g] \tag{6.3}$$

where α_g, represents the void fraction, and ε_{ls}, ε_0, A, C_p are the liquid specific dielectric constants, permittivity of free space, total flow cross-sectional area and the two-phase flow capacitance, respectively. The specific dielectric constant of unity was substituted for the gas-phase.

(ii) Slug Flow Pattern:

Again, from the idealized representations as shown in figure 6.5, we observe that the equivalent circuit for the slug flow pattern is a combination of both parallel and series

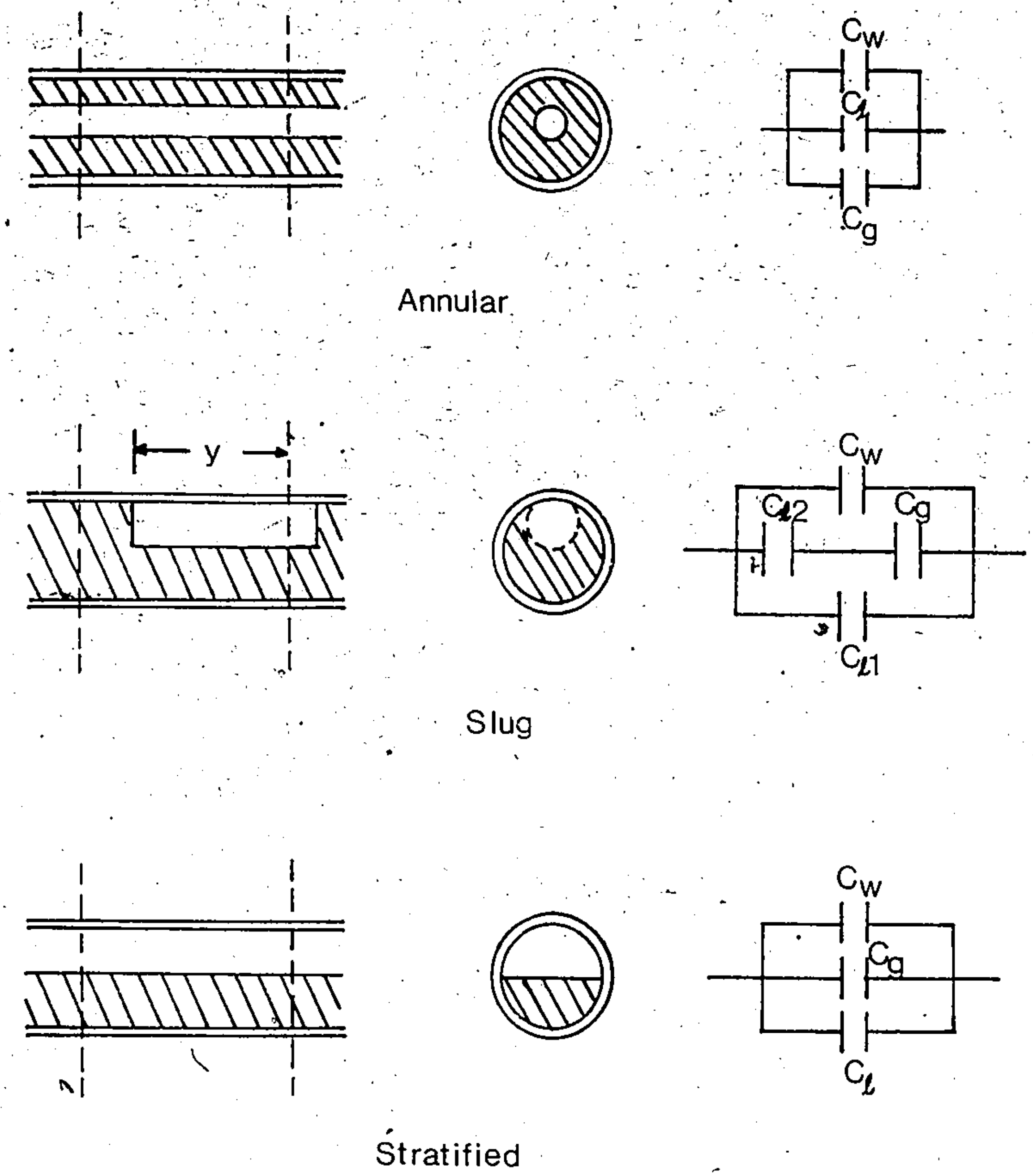

Figure 6.5 Equivalent Capacitance Circuits for Different Two-Phase Flow Patterns.

connections. In this case, the two-phase capacitance reduces to,

$$C_p = C_{\ell 1} + \frac{C_{\ell 2} C_g}{C_{\ell 2} + C_g} \tag{6.4}$$

Substituting the expression for capacitance between two parallel plates, we obtain.

$$C_p = \frac{\varepsilon_o A}{y\, d} \left[\varepsilon_{\ell s}(y - d\alpha_g) + \frac{d^2 \alpha_g\, \varepsilon_{\ell s}}{y\, \varepsilon_{\ell s} + (d - y)} \right] \tag{6.5}$$

where

$$A_\ell = A - A_g \,; \qquad \alpha_g = \frac{y\, A_g}{A\, d}$$

have been substituted to obtain the above equation. d and y are as defined in figure 6.5. Equation (6.5) can be further simplified to give

$$C_p = \frac{\varepsilon_o A}{d} \left[\varepsilon_{\ell s} - \frac{(\varepsilon_{\ell s} - 1)\, \alpha_g}{\left(\frac{y}{d}\right) + \frac{1}{\varepsilon_{\ell s}} \left(1 - \frac{y}{d}\right)} \right] \tag{6.6}$$

For the special case where y=d, the two-phase capacitance for Slug flow pattern given by equation (6.6) simply reduces to the expression for Stratified and Annular flow patterns given by equation (6.3). Figure 6.6 shows a plot of the theoretical output capacitances as a function of the volume averaged void fraction for various flow patterns occurring in a horizontal air-water two-phase flow system ($\varepsilon_{gs} = 1$, $\varepsilon_{ls} = 80$) for any tube size and pipe flow geometry. Different cases of the Slug flow pattern for various values of y/d, from y/d = 0.5 to y/d = 1.0 are also shown. No significant flow pattern dependence on the capacitance-void fraction relationship as shown in figure 6.6 is observed. In fact, for area averaged void fractions, the capacitance output for Stratified, Annular and Slug flows can be represented by the same curve. Chang et al. [39] also observed no significant effect of the capacitance-void fraction relationships on flow patterns, experimentally and theoretically for a 2.0 cm i.d. pipe in a vertical air-water two-phase flow.

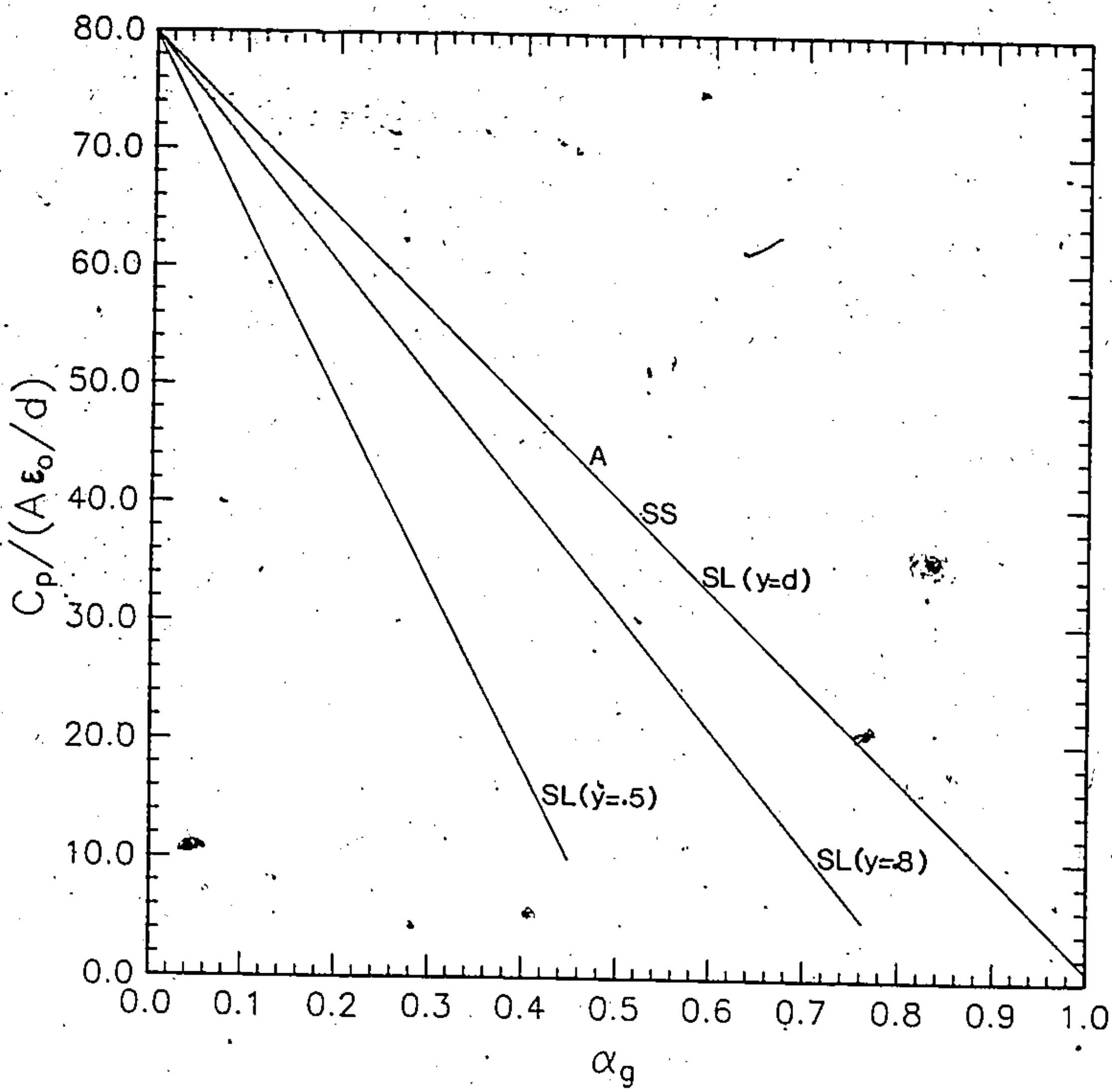

Figure 6.6 Predicted Output Capacitance as a Function of Void Fraction for Different Flow Patterns.

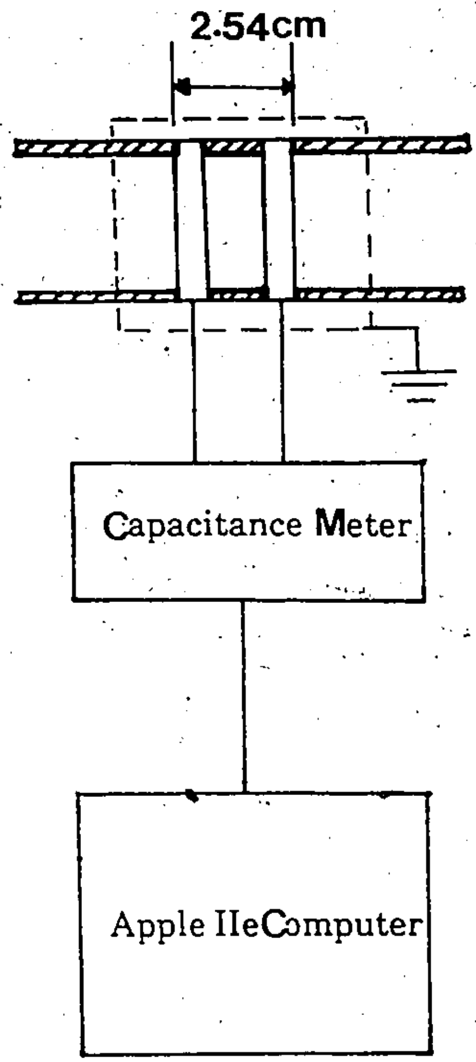

Figure 6.7 Schematics of Ring-Type Capacitance Transducer.

Figure 6.7, shows the schematics of the ring-type capacitance transducer set-up used in the present study. The electrodes consist of two brass strips, 1.27 cm wide placed 1.27 cm apart around the outside of the acrylic tube, downstream of the two-phase flow test section. The electrodes are electrically insulated and also electrostatically shielded with copper foil. The whole set-up is grounded as shown in figure 6.7. The output capacitance becomes analog voltage via the capacitance meter. In the rod bundle experiment, the computer terminal in the neighbouring room was observed to interfere with the output signals when in use. This may be due to the 37-rod bundles acting as a radio-frequency antenna, since the bundles were not electrically grounded to avoid further flow disturbances. However, the rod bundle experiments were conducted only when the computer terminal was not being used to avoid any interference with the void fraction signal output.

The capacitance transducer was calibrated versus the pulse-echo ultrasonic technique for liquid level detection in the pipe experiment. In the annulus experiment, the liquid level was measured directly with a level meter, since the annulus rod interferes with the pulse-echo ultrasonic technique. However, for the rod bundle experiment, the capacitance transducer was calibrated versus the pulse-echo ultrasonic technique. The ultrasonic transducer was placed downstream of the rod bundle in the region where there is no interference of the rods with ultrasonic signals as shown in figure 6.8. And the equilibrium liquid level was also measured directly by a meter rule placed at the end flange as shown in figure 6.8.

Figure 6.9 shows a comparison between the equilibrium liquid levels obtained by both the pulse-echo ultrasonic technique and direct measurement with meter rule. Figure 6.10 shows the void fraction calibration curve obtained for the 37-rod bundle flow system. The void fraction for a given equilibrium liquid level is obtained from calculations of geometrical parameters for the 37-rod bundle flow as discussed in Section 2.3. The void fraction calibration curves for the pipe and annulus flow systems are given in Appendix I.

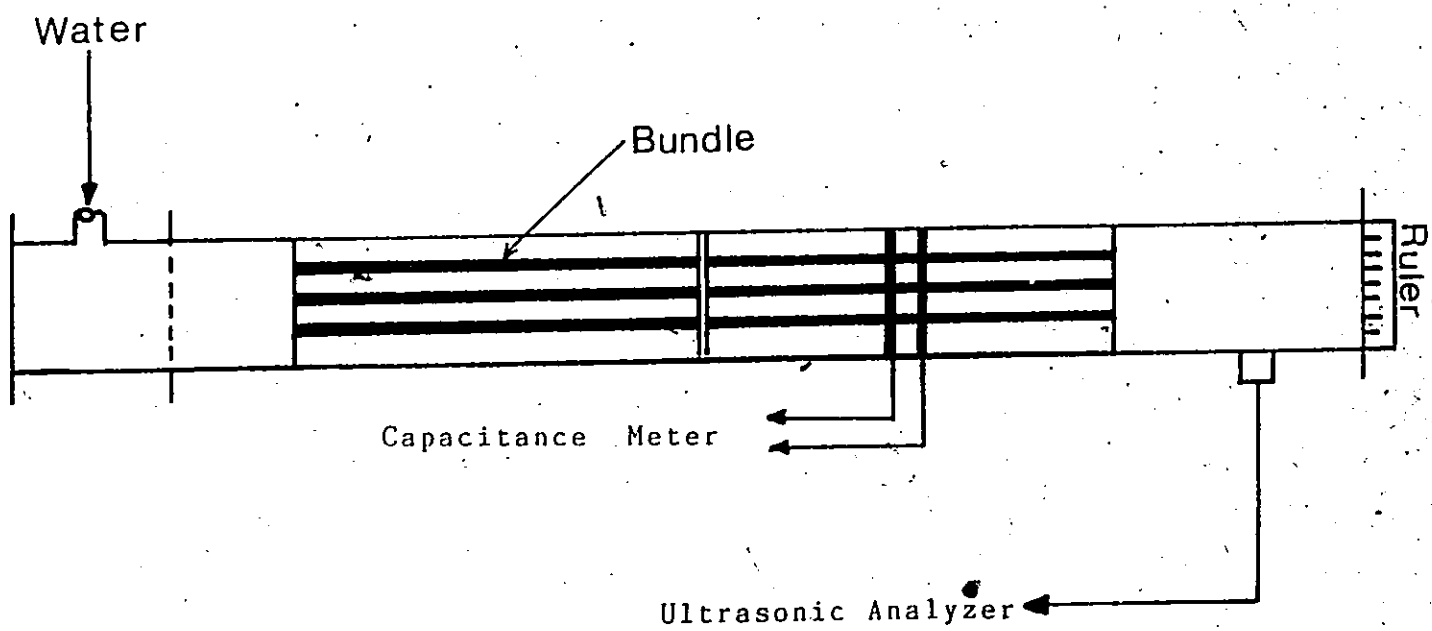

Figure 6.8 Void Fraction Calibration Set Up for 37-Rod Bundle Flow.

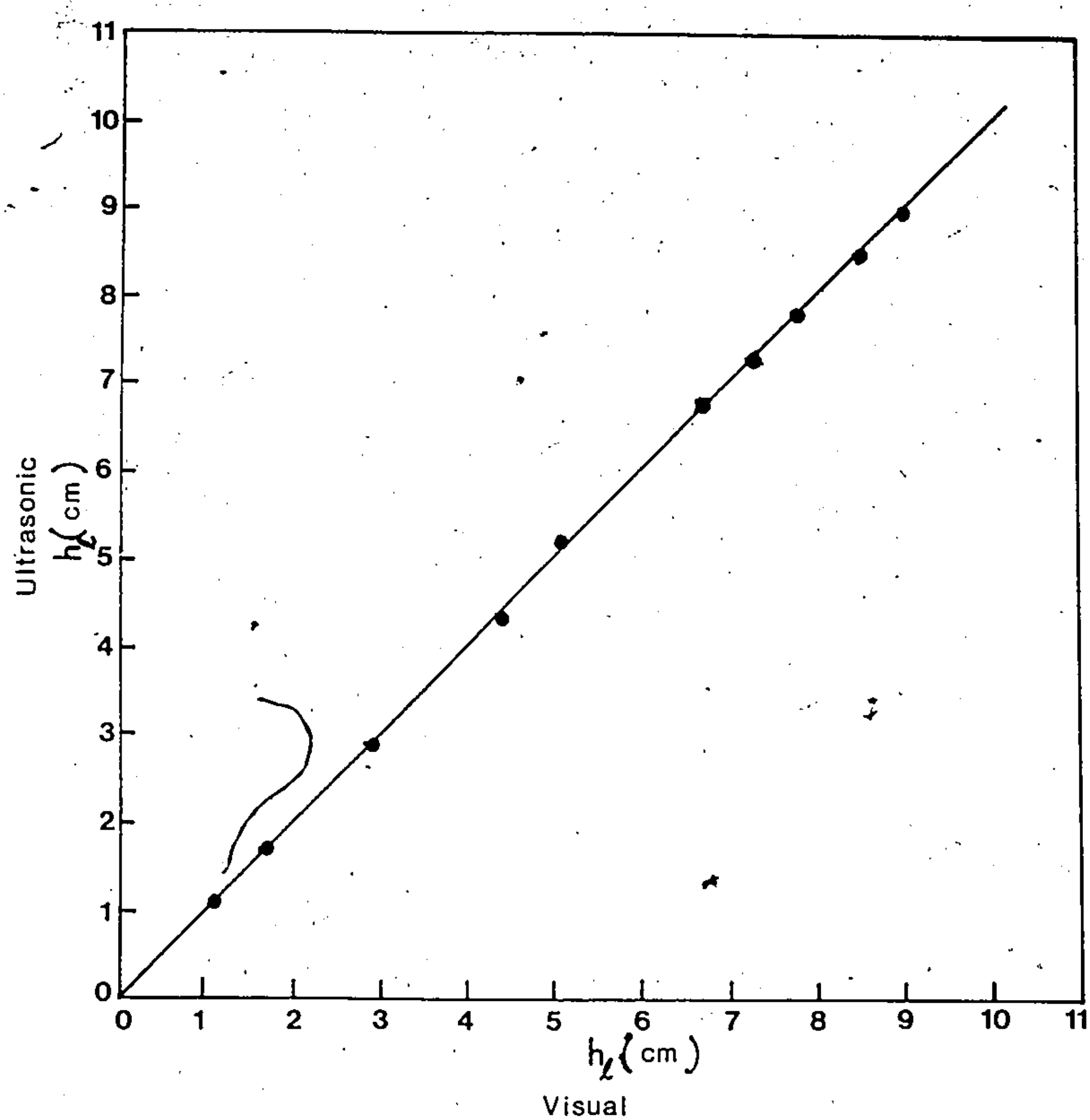

Figure 6.9 Equilibrium Stratified Liquid Level for 37-Rod Bundle Flow

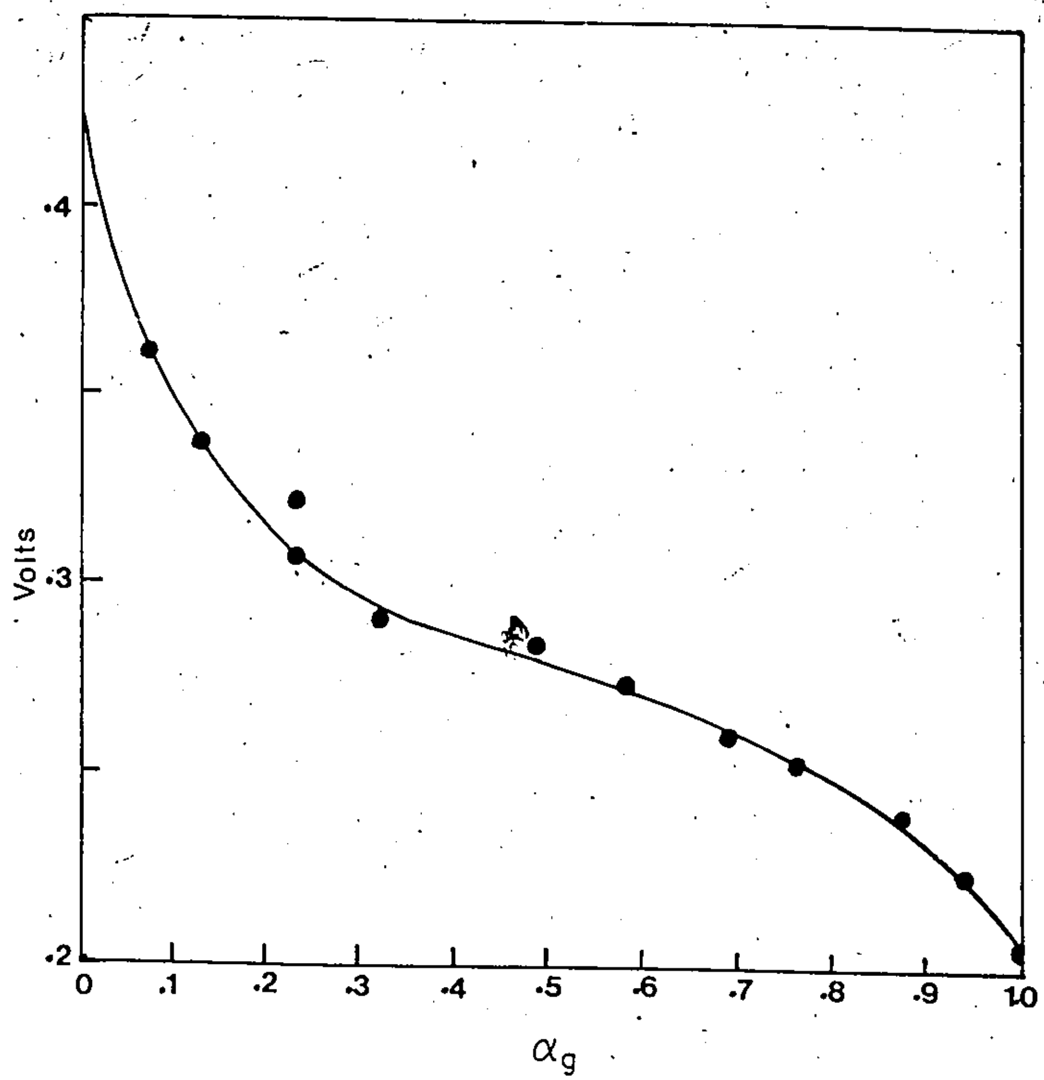

Figure 6.10 Void Fraction Calibration Curve for 37-Rod Bundle Flow.

The analog voltage output of the capacitance transducer for different flow conditions were analyzed using the Apple IIe computer via the ADC for time averaged void fractions. Fluctuations of the void fraction signals was recorded using the Goertz chart recorder and were observed to be distinct for different flow patterns. These were therefore used to supplement flow pattern identification by direct visual observations.

CHAPTER 7

FLOW PATTERN CHARACTERIZATION

The characterization of flow patterns is important in the development of better models for two-phase flow systems. Of all the techniques available for characterizing the flow patterns occurring in a two-phase flow system, the direct visual observation method seems to have been the most widely used at low flow rates, and the high speed photography technique at high flow rates, for clear transparent test sections.

However, it may not be possible to observe the structure of the two-phase flow clearly with these techniques due to multiple reflection and refraction of light at the gas-liquid interfaces. Real time X-radiography [41] and neutron radiography [42] techniques may be used to overcome these problems, and are also applicable to characterizing flow patterns in small tube diameter pipe flow opaque sections constructed from materials having low radiation attenuation. However, the large amount of uncertainties associated with photographic methods have led to the development of other techniques, namely, conductance probes, capacitance probes and impedance probes. The flow patterns occurring in a two-phase flow system may be characterized from the signal waveforms of the probes. These electrical probe methods have the advantage of being quite economical, but often interfere with the flow and change the two-phase flow phenomena. Conductivity probes are also restricted to electrically conducting fluids, and are significantly influenced by the presence of a space charge in the environment. In rod bundle flow systems, it is impossible to insert measuring devices in the restricted spaces of the closely packed rods beyond the outer subchannels.

Recently, techniques using fluctuations of instantaneous measurements of pressure drops [43], and void fractions [44] have been used for identifying flow patterns. Void measurement techniques are reviewed by Hewitt [45] and Banerjee and Lahey [46]. Among these techniques, the conductivity probes and the gamma-ray densitometer methods seem to be the most widely used. The neutron and ultrasonic beams seem to be the most promising, since they can be applied to flows in high pressure metallic pipes and high temperature liquid metal systems where intrusive techniques based on electrical or optical principles cannot be used. The ultrasonic technique is also useful for large diameter pipes or vessels. The electrical probes are applicable in the measurements of fast transient phenomena, and in contrast, radiation techniques are restricted to thin pipes and require a strong source to observe fast transient phenomena, but also require a large amount of radiation shielding for safety.

Most capacitance techniques have been used for liquid level diagnostics, void fraction or liquid film thickness measurement by immersing a single or twin needle probe, or parallel strip or twin electrodes. In this study, the value of the capacitance measurement rather than changes in it is used to determine void fraction in horizontal flow systems, and fluctuations in the instantaneous measurements are used to characterize the flow patterns. The ring-type capacitance transducer technique [39] is used here. This is based on the dielectric constants of the liquid, gas and tube materials. Capacitance transducers are most economical, offer simple installation, applicable to fast transients up to a few microseconds and are basically non-intrusive devices. The ring type capacitance transducer is made of two longitudinally attached parallel ring electrodes on the outside of the pipes. The capacitance was measured by a Boonton Electronics 72B capacitance meter operated at 1 MHz. The analog voltage output was analyzed using the Apple IIe computer via the ADC to obtain the time averaged void fraction. The Goertz chart recorder was used to record the signal waveforms for monitoring the various flow patterns occurring in the system.

Typical pressure drop and void fraction waveforms observed by pressure and capacitance transducers are shown in figures 7.1 to 7.3, for the pipe, annulus and 37-rod

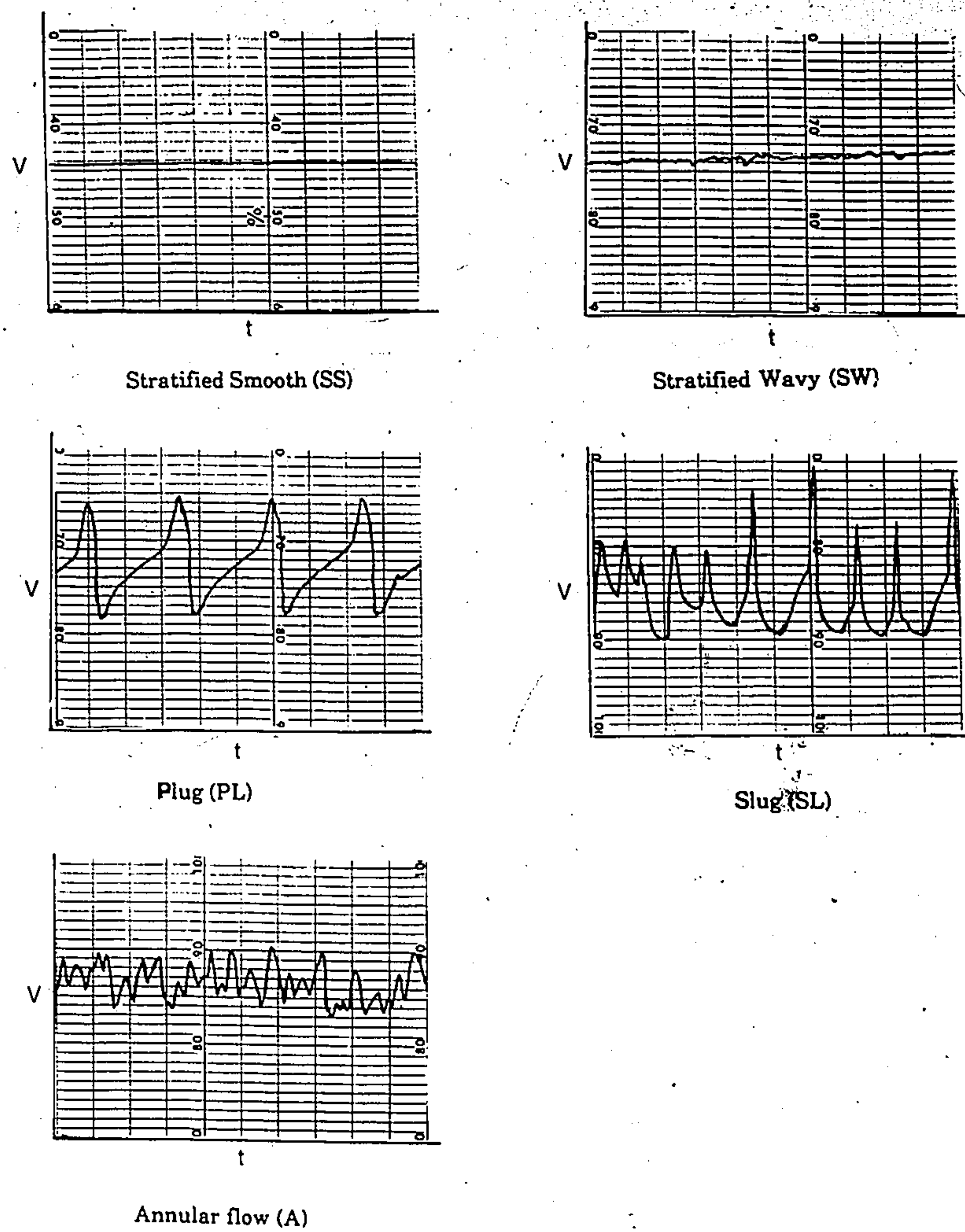

Figure 7.1 Typical Void Fraction Waveforms for 5.08 cm i.d. Pipe Flow.

bundle flow geometries, respectively. As can be seen from these figures, the void fraction waveforms seem to be more sensitive to the flow patterns, and consequently used for characterizing flow patterns in the present study. Also shown in figures 7.1 through 7.3 are the corresponding flow pattern structures from experimental observations. The Stratified Smooth flow pattern is represented by steady and smooth waveforms of the pressure drop and void fraction signals, while the Stratified Wavy flow pattern corresponds to small amplitude wavy fluctuations in the signals. The Plug and Slug flow patterns are observed to be represented by intermittent large amplitude fluctuations of the pressure drop and void fraction signals. The Slug flow signal fluctuations are observed to occur more frequently than the case for Plug flow pattern. The pipe flow waveforms for the Plug and Slug flow patterns are observed to be nearly periodic in occurrence, while a deviation from this periodicity in the signal fluctuations is observed for the Slug flow pattern in the annulus and rod bundle flow systems.

The waveforms of figure 7.2 represent the Elongated Bubble flow observed at lower gas flow rates for high liquid flow rates, and grouped among Plug flow patterns in this work. The Annular and Wavy Annular flow pattern representations are observed to be non-monotonic fluctuations of the pressure drop and void fraction nearly continuous in time. However, the waveforms obtained in the present study correspond mainly to the Wavy-Annular flow pattern or the transition region from Slug to fully developed Annular flow patterns. This is characterized as the situation where the flow is neither Slug, since a complete liquid bridge is not present, nor Annular flow , since the liquid film observed around the tube periphery is not continuous at the upper section. In the 37-rod bundle flow system and under the present experimental conditions, we observed only a few cases of the Wavy-Annular flow pattern at high gas flow rates, where the liquid film is observed to be flowing on the wall of the enclosing tube and around the rods at the upper section of the bundle. The rods

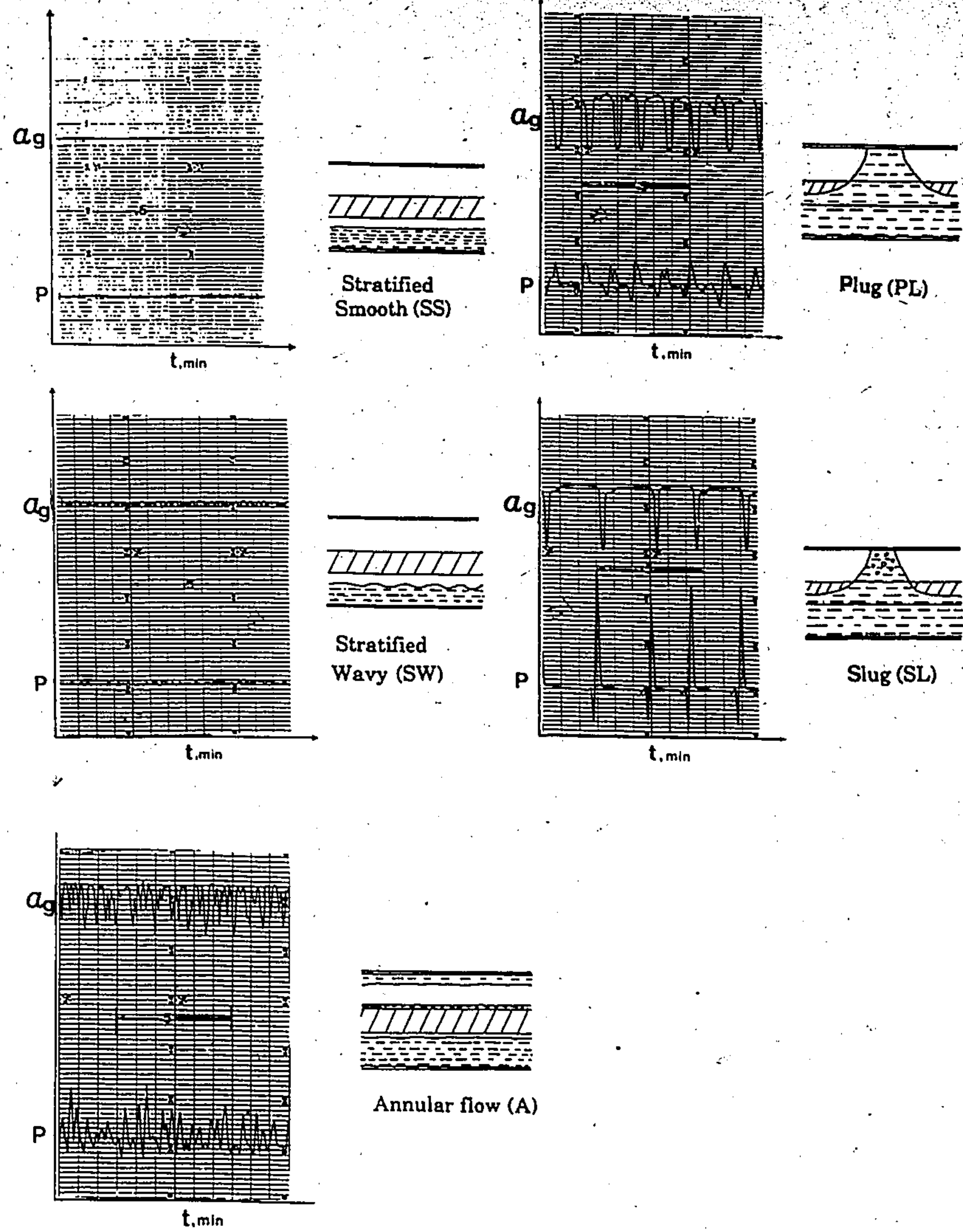

Figure 7.2 Typical Pressure Drop and Void Fraction Waveforms for Annulus Flow.

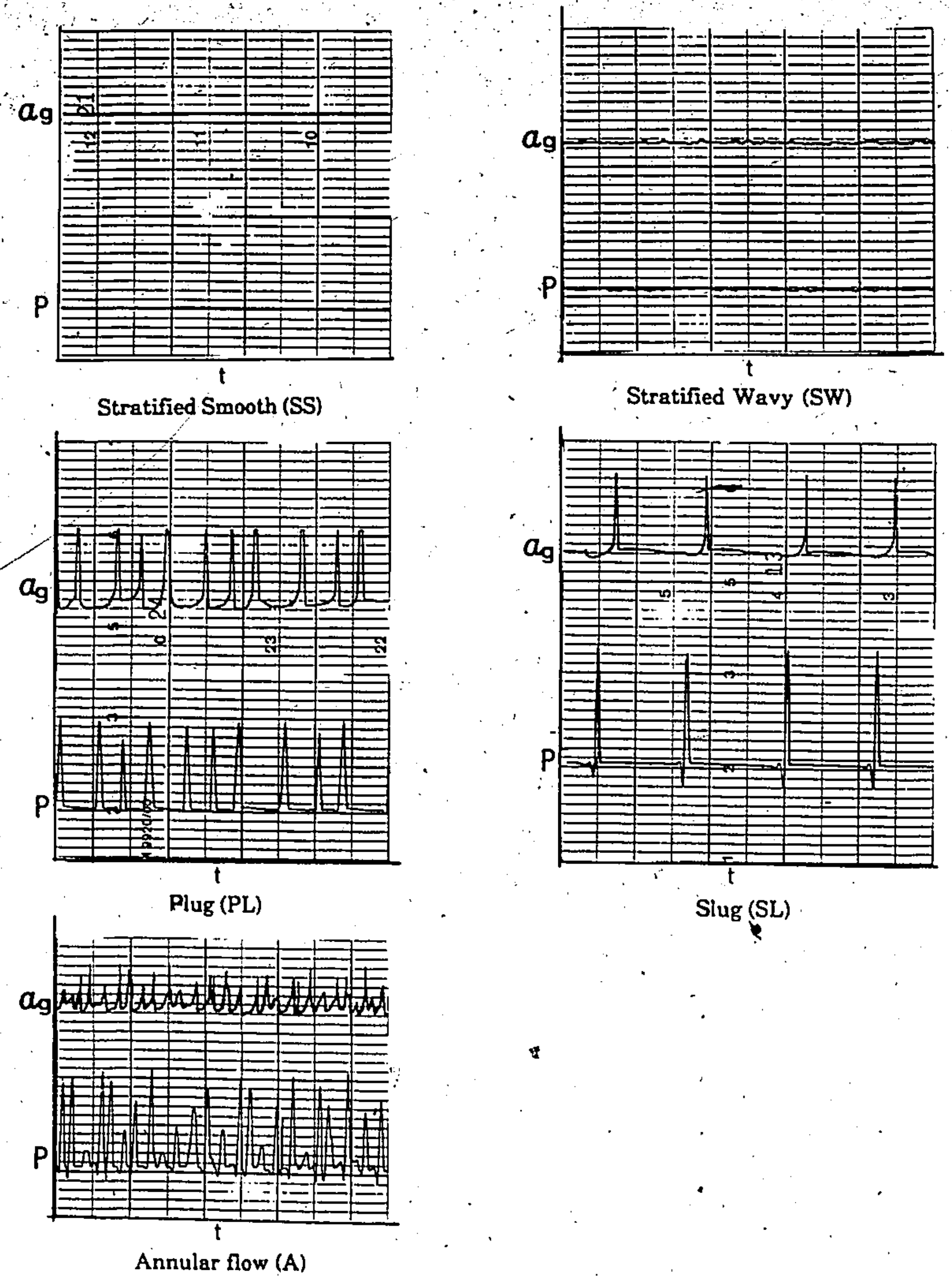

Figure 7.3 Typical Pressure Drop and Void Fraction Waveforms for 37-Rod Bundle Flow.

were observed to also be wetted by very thin liquid films which immediately disappeared after the passage of the wave. The typical waveforms are as shown in figure 7.3, where we observe the remarkable difference from the Slug flow pattern waveforms.

We also characterized the Annulus-Slug and Annulus-Plug flow patterns for the annuli. From the visual observation results and pressure drop and void fraction waveforms of figure 7.2, the Annulus-Slug and Annulus-Plug flow patterns were not clearly identified. This is because the liquid bridge associated with these flow patterns may not always touch the annulus rod and could be mistaken for large amplitude Stratified Wavy flow pattern. The ultrasonic transmission technique [40] was therefore modified for use in this case.

The Annulus-Slug flow pattern occurs when the liquid tends to bridge the gap between the gas-liquid interface and the lower surface of the annulus rod. At lower gas flow rates, the Annulus-Plug flow pattern may exist. This is similar in description to the Annulus-Slug flow pattern with little or no gas bubbles present in the liquid bridge. However, the range of gas superficial velocities over which these flow patterns occur represent the Stratified flow region, hence we have chosen to classify these flow patterns under Stratified flow patterns in the present study.

In order to characterize flow patterns more accurately in the annulus geometry, the ultrasonic transmission method was used [40]. Two Panametrics contact probe ultrasonic transducers, 6.35 mm in diameter, operating at a frequency of 2.25 MHz, were placed face to face from each other in the flow channel as shown in figure 7.4. One of the ultrasonic transducers was placed inside the annulus rod and the other was placed on the outside of the tube. The whole set up is completely external to the flow, and hence does not cause any flow disturbances during measurements. The ultrasonic signals transmitted by one transducer are received by the other via a Panametrics ultrasonic analyzer. Since the annulus channel gap and the propagation velocity of sound in the liquid are known, only the received signal

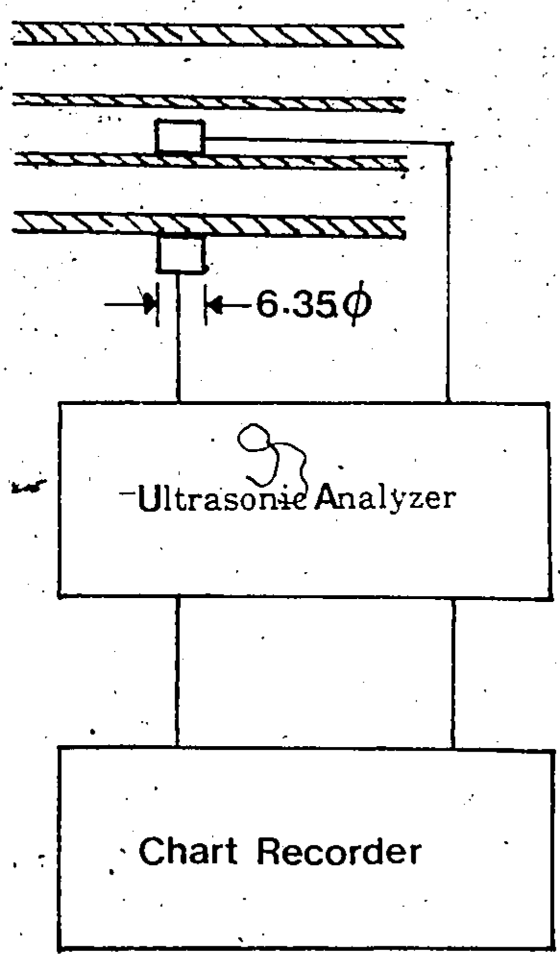

Figure 7.4 Schematics of Ultrasonic Transmission Technique.

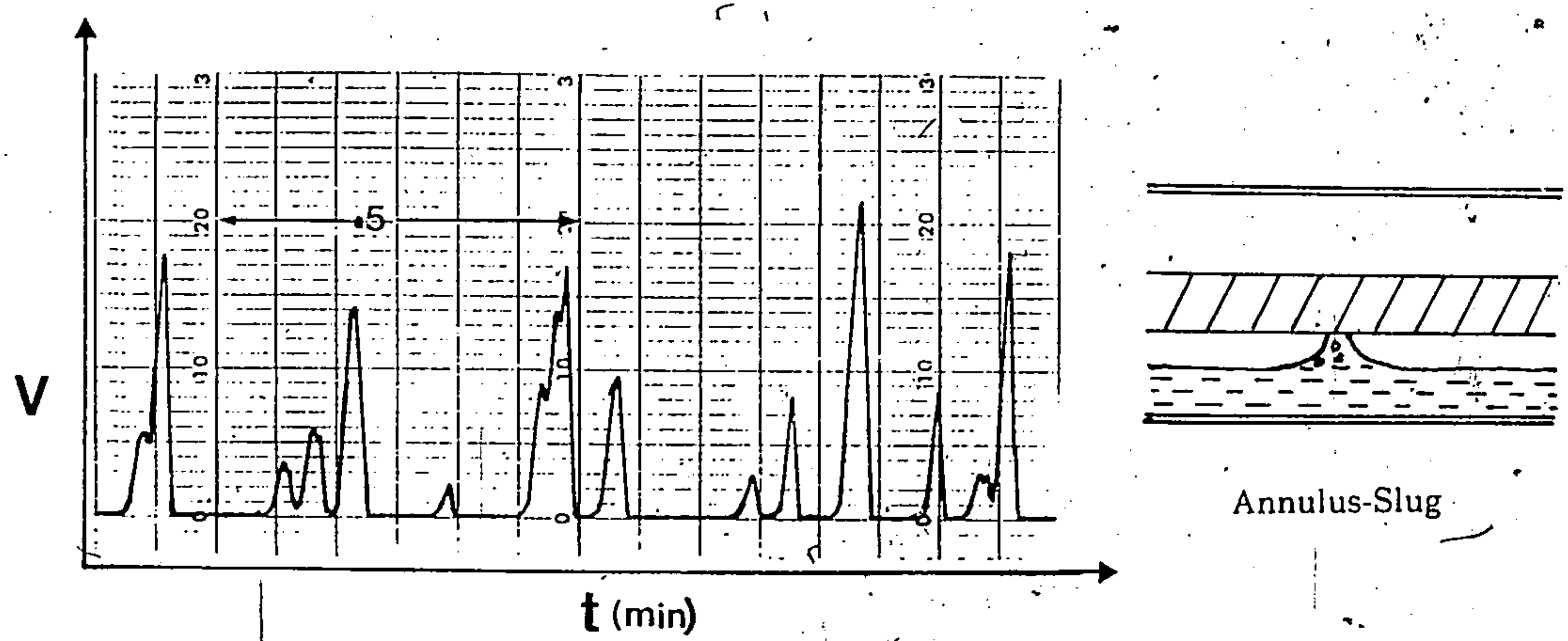

Figure 7.5 Typical Ultrasonic Transmission Waveforms for Annulus Flow.

intensities occurring whenever the annulus channel gap is flooded are recorded by the Goertz chart recorder via the ultrasonic analyzer. Here we must note that the ultrasonic signal cannot pass through the gas-liquid interface due to acoustic mismatch between the two phases [40].

Typical ultrasonic transmission waveforms are shown in figure 7.5. It is clearly seen from here that the ultrasonic wave signals are only transmitted when the entire channel between the central annulus rod and the lower inner tube wall is flooded with water. It is important to note that the wave height will be reduced by the existence of small bubbles in the liquid bridge, or the physical geometry of the Slug and the air-water interfacial geometries. Figure 7.5 shows that the Annulus-Slug and Annulus-Plug flow patterns can be identified with the present method, and also the presence of bubbles in this liquid bridge.

Figures 7.1 through 7.5 show that the methods used in this study are quite objective and successful for flow pattern characterization, and can be used along with direct visual observation technique, especially for high gas flow rates, and also for complex pipe geometries like the annuli and rod bundles where it is impossible to objectively identify the particular flow patterns occurring by relying only on direct visual observation.

CHAPTER 8

EXPERIMENTAL RESULTS AND DISCUSSIONS

8.1 Pipe Flow Results

8.1.1 Flow Patterns

The Stratified Smooth, Stratified Wavy, Plug, Slug and Wavy-Annular flow patterns were experimentally observed for the 5.08 cm i.d.pipe. These are presented on flow pattern maps based on superficial velocities in figure 8.1. Figure 8.1 also shows the predicted results of REGIME-4 code and the results of the model due to Taitel and Dukler [8]. The results show that the REGIME-4 code which accounts for the effect of interfacial surface tension in the Stratified to Intermittent (Slug and Plug) flow transition criteria agrees better with the experimental results presented here than the Taitel and Dukler [8] model. And at low gas flow rates, the theoretical results deviate significantly from experiment.

The models have considered a balance between lifting forces due to Bernoulli effect for the fast flowing gas phase, and the stabilizing effects of gravity and interfacial surface tension forces. This physical mechanism is assumed by these models to be valid for both the fast and slow ranges of the gas flow rate. However, better agreement with experiment has been obtained at high gas flow rates, where the gas velocity is high enough for Bernoulli effect to dominate other lifting forces that may be acting. At low gas flow rates, a different approach has been suggested where stability mechanisms involving the growth of small disturbances should be considered [29].

For modelling the Stratified to Intermittent flow transition, other models have been proposed where a balance between the stabilizing forces of gravity and capillary surface tension forces for small capillary tubes [19], or the lifting force corresponding to the kinematic

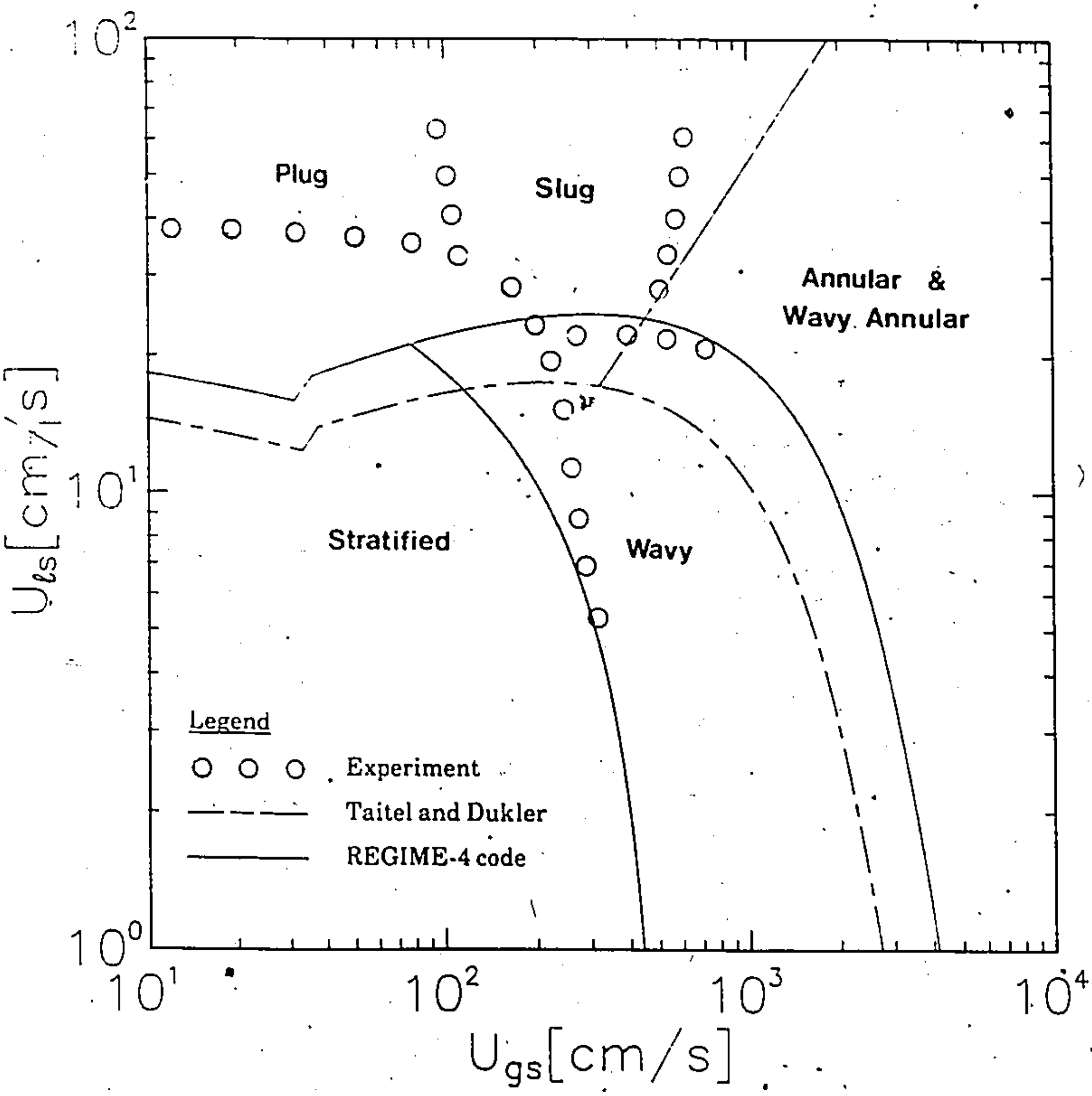

Figure 8.1 Comparison of Experimental and Predicted Flow Pattern Transitions for 5.08 cm i.d. Pipe Flow.

energy surplus of liquid in the idealized wave region [18] is sought. From experimental observations, the Stratified to Plug flow transition occurs in the range of gas flow rate where the gas phase velocity is too low to cause the generation of waves at the gas-liquid interface. In this range of flow rate, liquid turbulent fluctuations may dominate the lifting forces resulting from Bernoulli effect, and may be considered to be the mechanism governing the Stratified Smooth to Plug flow transition, occurring at low gas flow rates. In fact, the velocity of a gravity wave in liquid of depth z is $\sqrt{gz}$. For 50% voidage in a 5.08 cm i.d. tube, this velocity is 49.9 cm/s which is of the same order as the Stratified Smooth to Plug flow transition velocity at low gas flow rates.

8.1.2 Void Fraction

Figure 8.2 shows the time averaged void fraction as a function of the superficial gas velocity for various superficial liquid velocities in a 5.08 cm i.d. pipe under horizontal two-phase flow. The results show that the void fraction generally increases with the superficial gas velocity. It also increases with decreasing superficial liquid velocity at low gas flow rates, at the flow conditions where Stratified flow patterns are expected to occur. It is observed to vary rather nonmonotonically with the superficial liquid velocity at high gas flow rates.

Except at the Stratified Smooth to Stratified Wavy transition, we observe sharp changes in the void fraction at the various transition locations as indicated in figure 8.2. If we try to re-plot figure 8.2 in the form of a contour map as shown in figure 8.3, it becomes obvious that the void fraction changes suddenly at the flow pattern transition boundaries. This was also observed by Lightstone et al. [47] in a 1.91 cm i.d. horizontal two-phase pipe flow, and in gas-solid two-phase pipe flow [48]. Accurate location of experimental flow pattern transitions may thus be aided by information from full analysis of the time averaged void fraction.

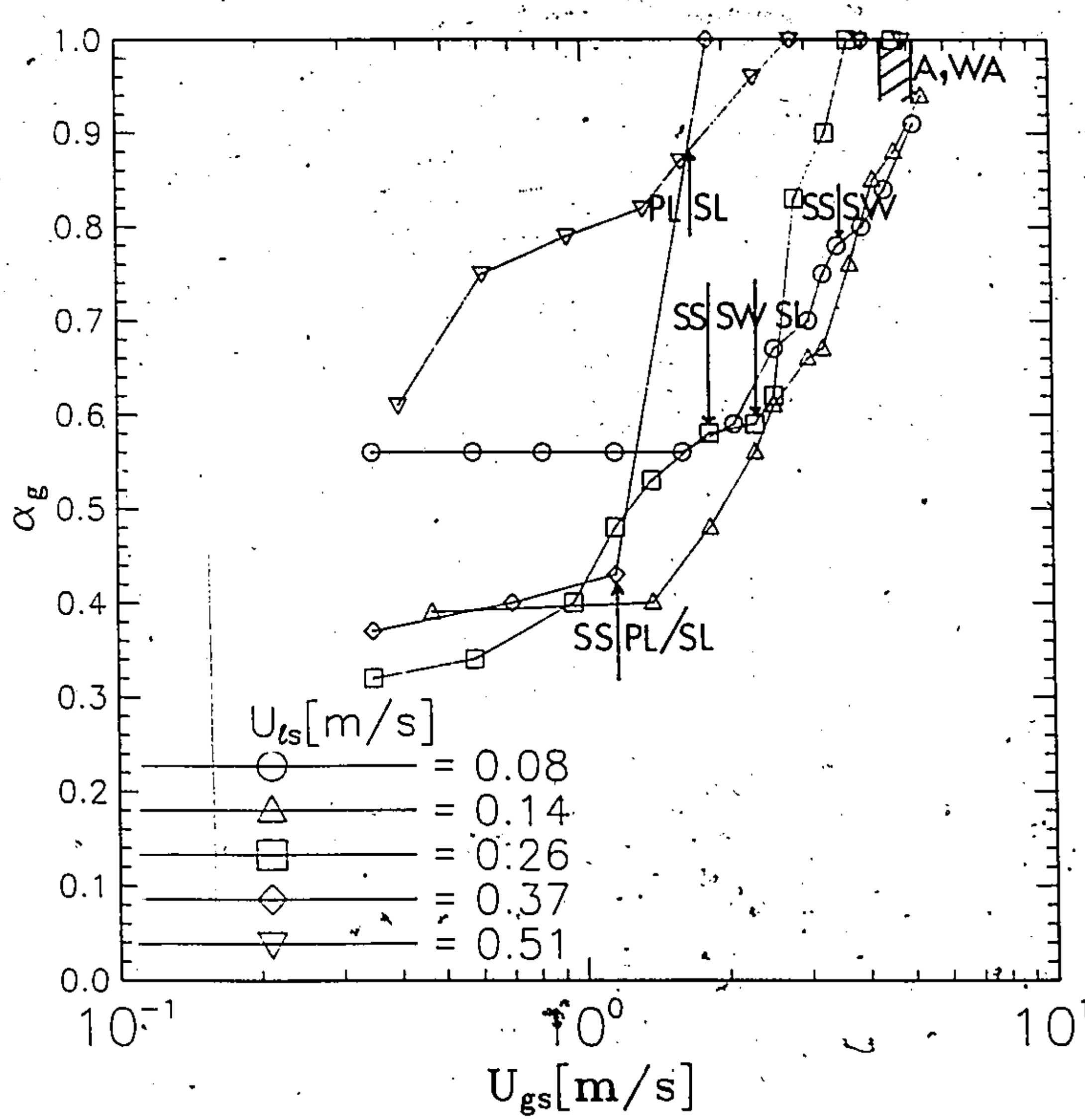

Figure 8.2 Time Averaged Void Fraction as a Function of Superficial Velocities for 5.08 cm i.d. Pipe Flow

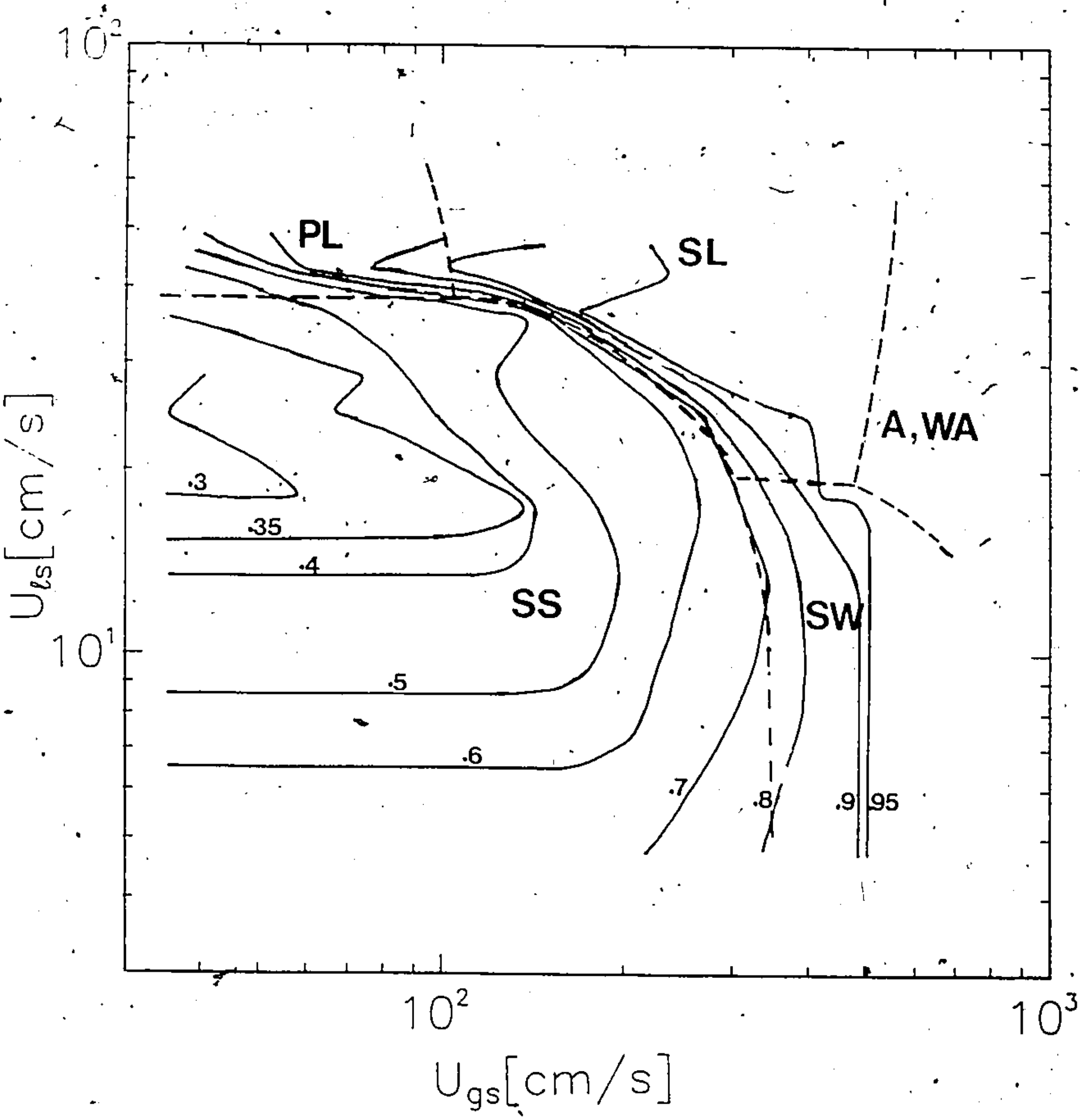

Figure 8.3 Void Fraction Contour Map for 5.08 cm i.d. Pipe Flow

Further analysis of the void fraction results in terms of the local phase velocities is given in Appendix II.

8.2 Annulus Flow Results

8.2.1 Flow Patterns

The experimental flow pattern transition for annulus geometries of outer tube diameter, 5.08 cm i.d. and axial rod diameters from 1.905 cm to 3.175 cm, are represented in figure 8.4 as a function of the inner-to-outer diameter ratios ranging from 0.375 to 0.625. The Stratified Smooth, Stratified Wavy, Plug, Slug and Wavy-Annular flow patterns were successfully characterized in the present study. The results show that flow pattern transitions are significantly influenced by different inner-to-outer diameter ratios. This effect was also predicted by the numerical model discussed in Section 4.

Figure 8.4 shows that the Stratified to Intermittent (Slug and Plug) flow transition occurs at lower superficial liquid velocities for larger inner-to-outer diameter ratios. A similar trend was also predicted by the REGIME-4 numerical code. The Plug to Slug and Slug to Wavy-Annular flow transitions are also influenced by different diameter ratios. And are observed to occur at higher superficial gas velocities for larger inner-to-outer diameter ratios. The case for Slug to Wavy-Annular flow transition is again as predicted by the numerical results discussed in Section 4. Annuli with larger inner-to-outer diameter ratios provide narrower passages for the fluids leading to flow acceleration, and consequently a higher superficial gas velocity at which this transition takes place. Similarly, the Stratified to Intermittent flow transitions occurring earlier in annuli with larger diameter ratios may be due to a combination of two effects. Flow acceleration of the phases and frictional forces from the axial rods tending to damp the interfacial waves are larger for these annulus geometries.

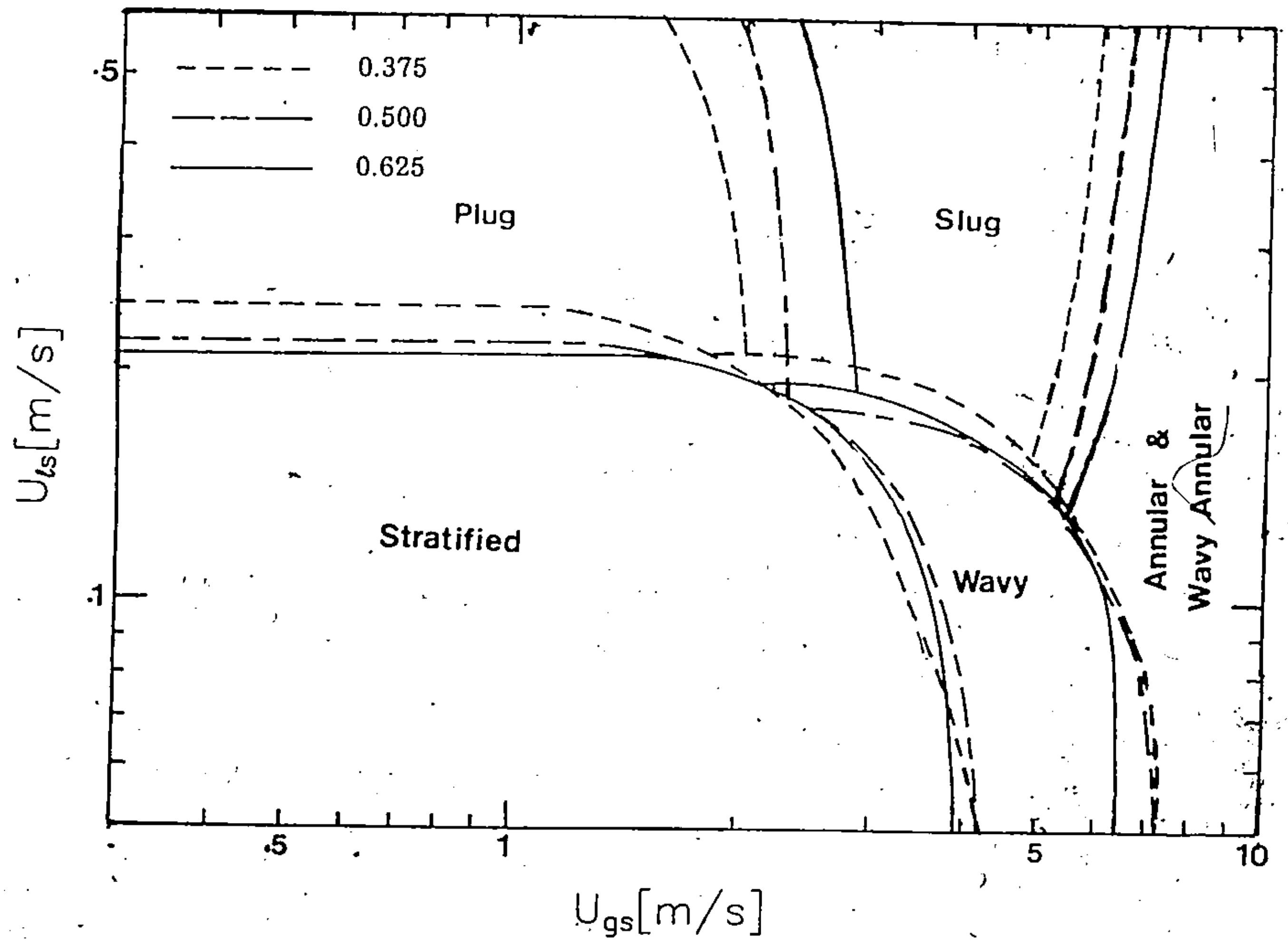

Figure 8.4 Experimental Flow Pattern Transitions for Annulus Flow as a Function of Inner-to-Outer Diameter Ratios.

The Stratified Smooth to Stratified Wavy and Stratified Wavy to Annular transitions are observed to be quite insensitive to differences in the inner-to-outer diameter ratios. However, the gas flows at which these transitions occur are very fast, and may lead to some uncertainties in accurately locating the transition boundaries.

Figure 8.5 shows the experimental flow pattern transitions of an annulus geometry of diameter ratio 0.50 as compared with the predicted results. Figure 8.5 also shows the experimental results of a 5.08 cm i.d. pipe. The Stratified to Plug and Slug flow transitions occur at lower superficial velocities than the pipe case due to differences in force distribution and flow acceleration in the annulus geometry. The Plug to Slug and Slug to Wavy-Annular flow transitions are observed to occur at higher superficial gas velocities than the pipe case, due mainly to flow acceleration in the annulus geometry.

The wide discrepancy observed for the Stratified to Intermittent transition may be due to two reasons. The frictional damping forces that may be acting on the interfacial waves which eventually grow to form Slugs have not been considered in the mechanism for this transition. At low gas flow rates, the Stratified to Plug flow transition is observed to be nearly independent of the superficial gas velocity. At the liquid phase velocities where this transition is expected to occur, turbulent fluctuations in the liquid may dominate Bernoulli effects in the physical mechanism governing this transition. In the numerical model presented, the lifting force due to Bernoulli effect was assumed to be valid throughout the full range of gas flow rate studied.

Due to differences in flow geometry between the pipe and annulus flow systems, the Intermittent region is observed to be enhanced for the annulus geometry. Also waves that would otherwise grow to form Slugs and Plugs in the pipe flow case are observed to be damped on encountering the annulus rod. This damping effect was also observed by earlier investigators for gas-oil two-phase flow in annulus geometries [13].

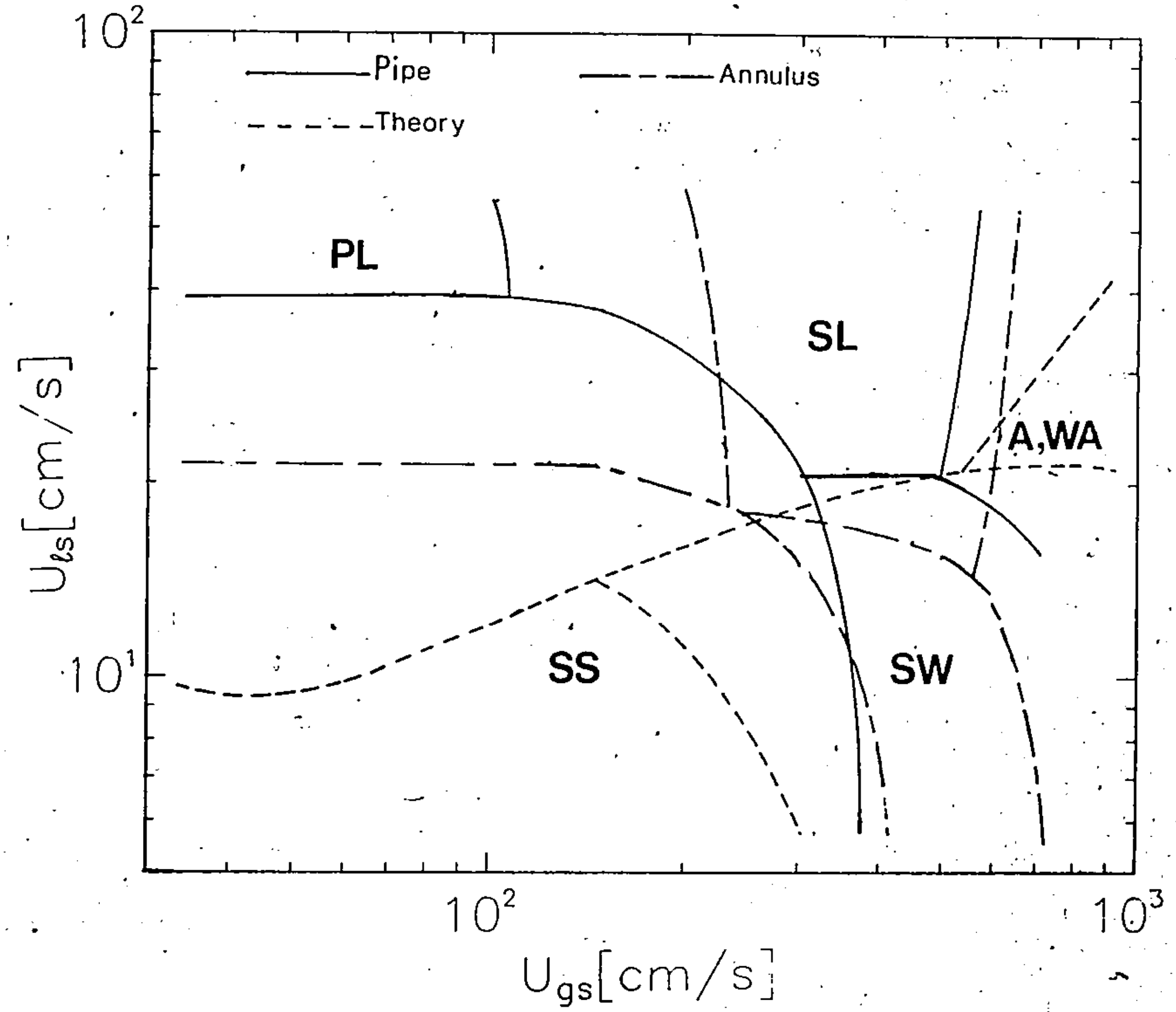

Figure 8.5 Comparison of Experimental and Predicted Flow Pattern Transitions for Annulus of Inner-to-Outer Diameter Ratio, 0.500

8.2.2 Pressure Drop

The time averaged pressure drop for annulus geometries of inner-to-outer diameter ratios, 0.375, 0.500 and 0.625, as a function of the superficial gas velocity for various superficial liquid velocities, from 5.4 cm/s to 58.4 cm/s, are shown in figures 8.6, 8.7 and 8.8, respectively. Also shown on these figures are the respective flow pattern transitions observed for the annulus flow geometries. At low superficial gas velocities, $u_{gs} < 100$ cm/s, the pressure drop is observed to increase with the liquid flow rate, except for the Stratified Smooth flow patterns where the pressure drop is practically flat. At higher superficial gas velocities, the pressure drop also increases with liquid flow rates for Stratified flow, but varies nonmonotonically with superficial liquid velocities for the Plug, Slug and Wavy-Annular flow patterns.

Generally, the pressure drop is observed to increase with superficial gas velocities except for Stratified flow at low liquid and gas flow rates, where it is observed to be nearly independent of the superficial gas velocity. At high liquid flow rates, it decreases with the superficial gas velocity due probably to slight differences in the Plug flow pattern occurring here, which may be described as a series of elongated bubbles flowing at the upper region of the channel. The flow pattern transitions do not seem to significantly affect the observed time averaged pressure drop.

Larger pressure drops were observed for annulus geometries with larger inner-to-outer diameter ratios. A time averaged pressure drop of about 0.20 KPa and 0.40 KPa were observed for inner-to-outer diameter ratios, 0.375 and 0.500, respectively. The observed increase in pressure drop with larger inner-to-outer diameter ratio is may be due to increased fluid-wall frictional interaction.

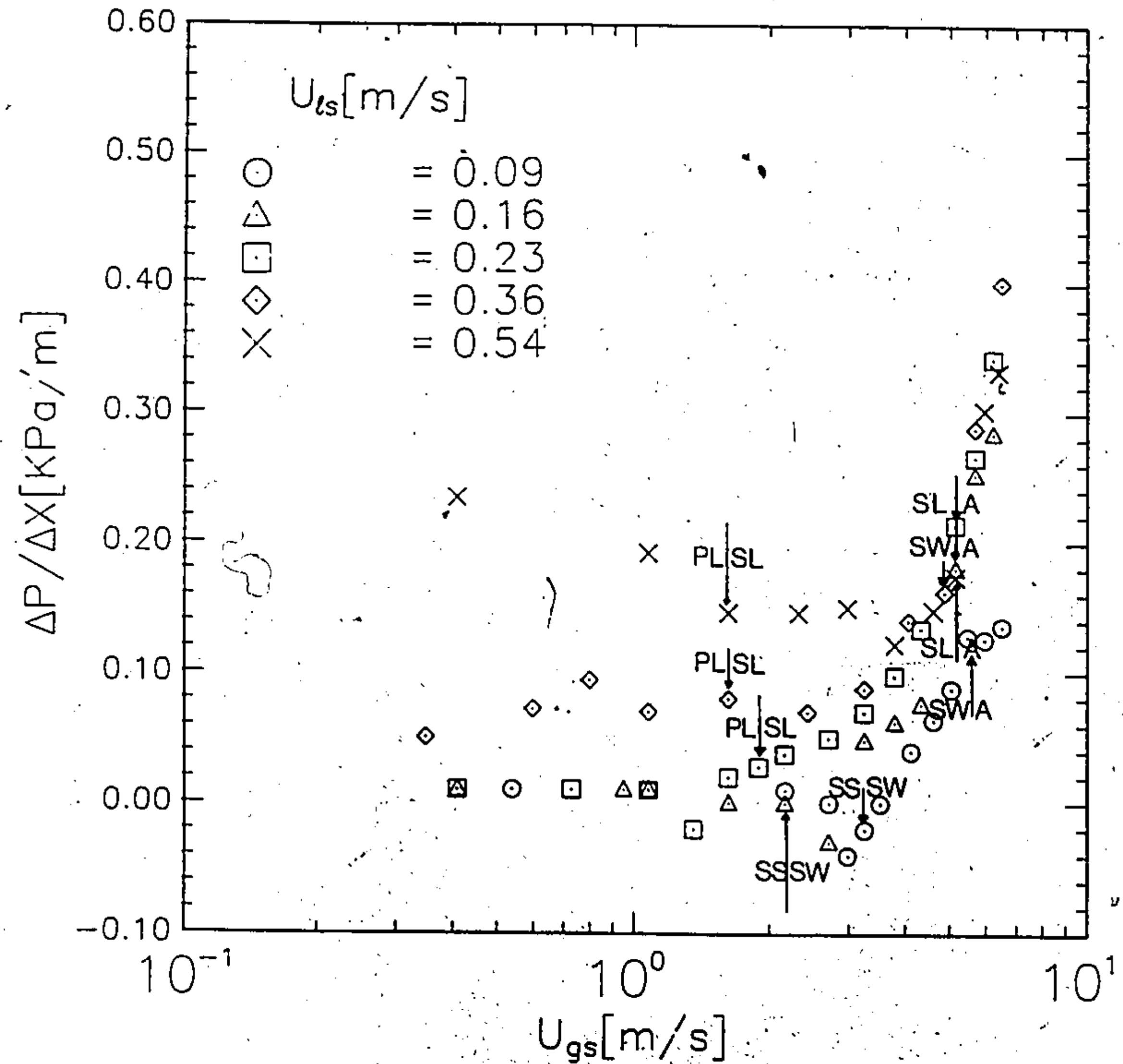

Figure 8.6 **Pressure Drop as a Function of Superficial Velocities for Annulus of Inner-to-Outer Diameter Ratio, 0.375.**

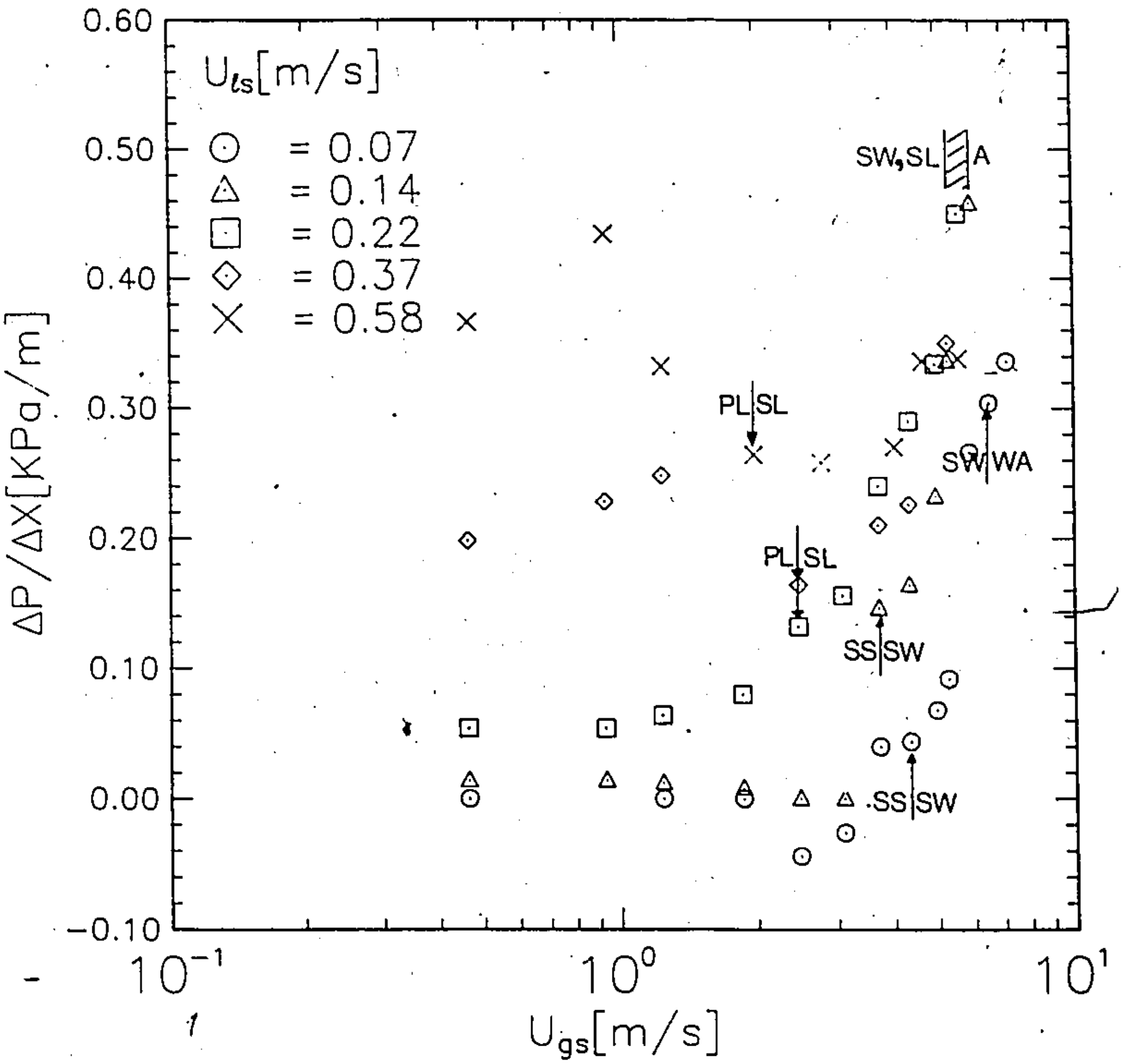

Figure 8.7 Pressure Drop as a Function of Superficial Velocities for Annulus of Inner-to-Outer Diameter Ratio, 0.500.

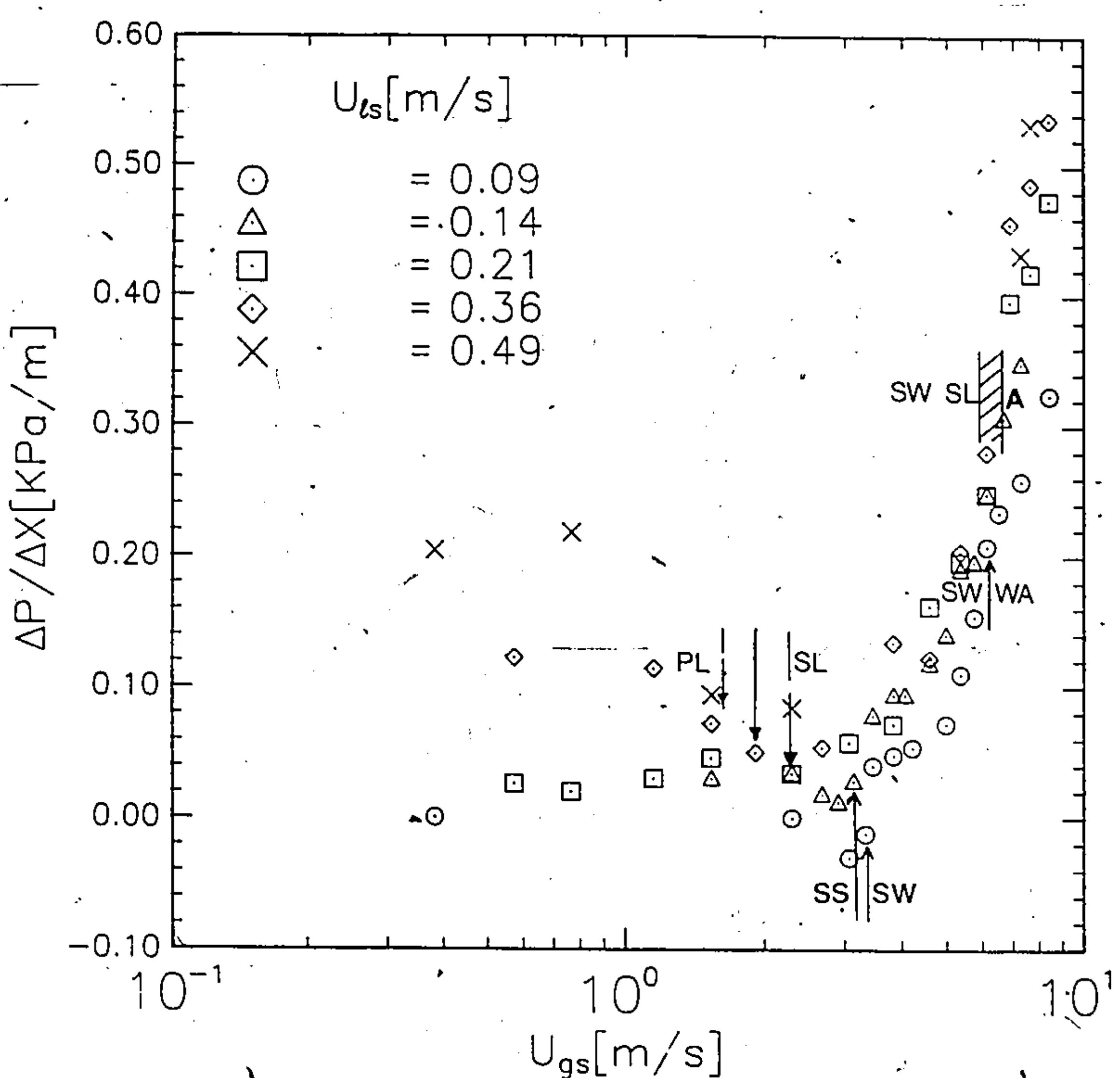

Figure 8.8 Pressure Drop as a Function of Superficial Velocities for Annulus of Inner-to-Outer Diameter Ratio, 0.625.

Negative pressure drops are observed for Stratified flow at low superficial liquid velocities, and for superficial gas velocities ranging from 100 cm/s to 400 cm/s. This may be due to a hydraulic jump observed in the equilibrium liquid level near the pressure transducer location, caused by capillary forces tending to lift the gas-liquid interface, and thus bridging the gap between the interface and the central annulus rod. This results in the formation of additional flow patterns observed for the present geometry, namely, the Annulus-Slug and Annulus-Plug flow patterns.

8.2.3 Void Fraction

Figures 8.9 to 8.11 show the time averaged void fraction for annulus geometries of inner-to-outer diameter ratios, 0.375, 0.500 and 0.625, respectively, as a function of the superficial gas velocity for various superficial liquid velocities, from 9.0 cm/s to 49.4 cm/s. Also shown in these figures are the various flow pattern transitions observed for the annulus geometries.

The flow pattern transitions are quite sharply distinguishable from the void fraction profiles, except the Stratified Wavy and Slug to Wavy-Annular transitions, which are represented as bands. This represents the uncertainty in accurately locating this transition boundary.

The void fraction profile is observed to be nearly independent of the superficial gas velocity for the Stratified Smooth flow pattern, and increases sharply at the transition to Stratified Wavy pattern for low superficial liquid velocity. At higher superficial liquid velocities, the Plug, Slug and Wavy-Annular flow patterns were also characterized. And the void fraction is observed to increase gradually for Plug flows, but sharply for Slugs. The void fraction almost approaches unity at the transition to Wavy-Annular flow. The time averaged void fraction observed for the annulus geometries are observed to vary more sharply with the

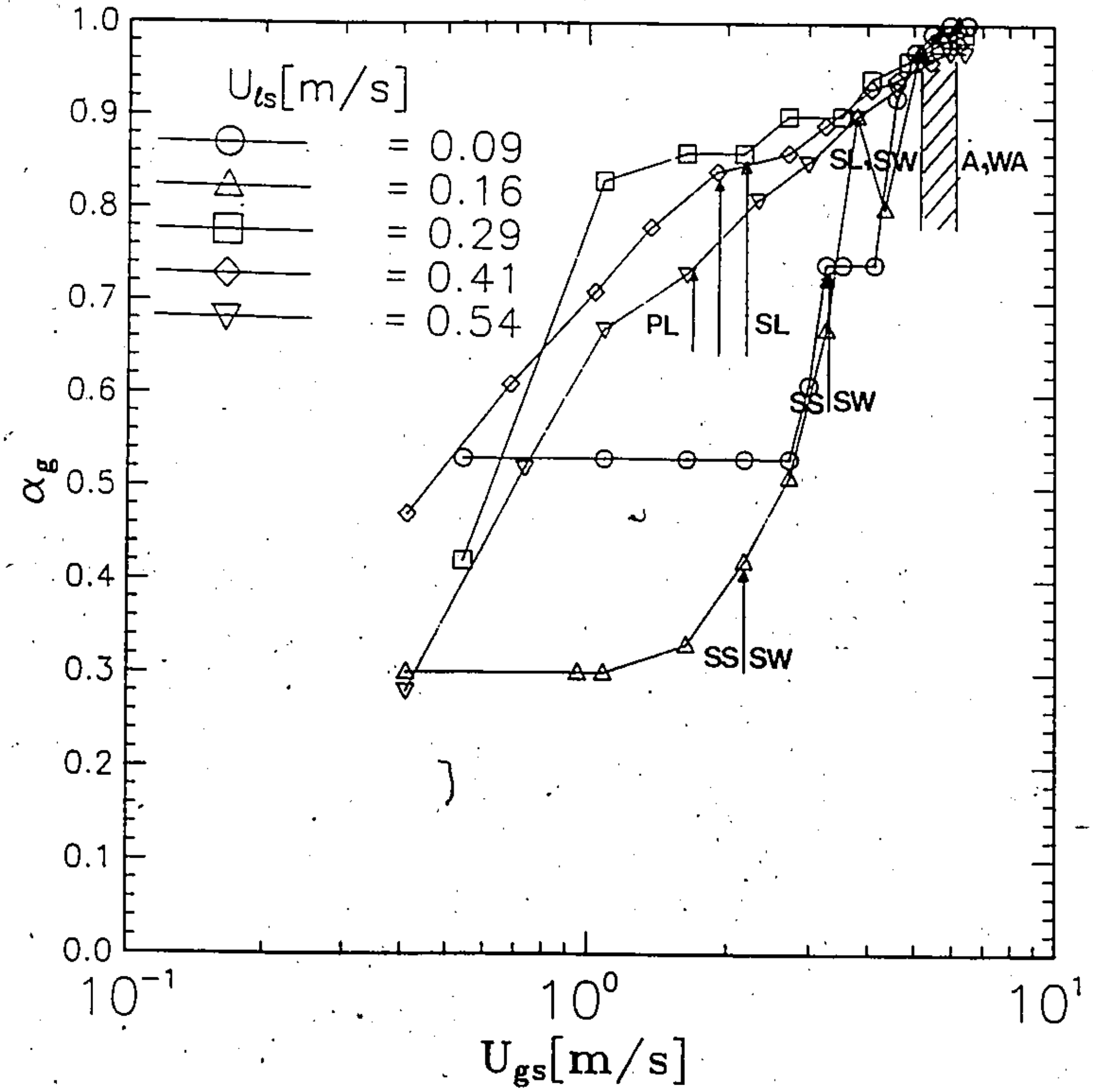

Figure 8.9 Time Averaged Void Fraction as a Function of Superficial Velocities for Annulus of Inner-to-Outer Diameter Ratio, 0.375.

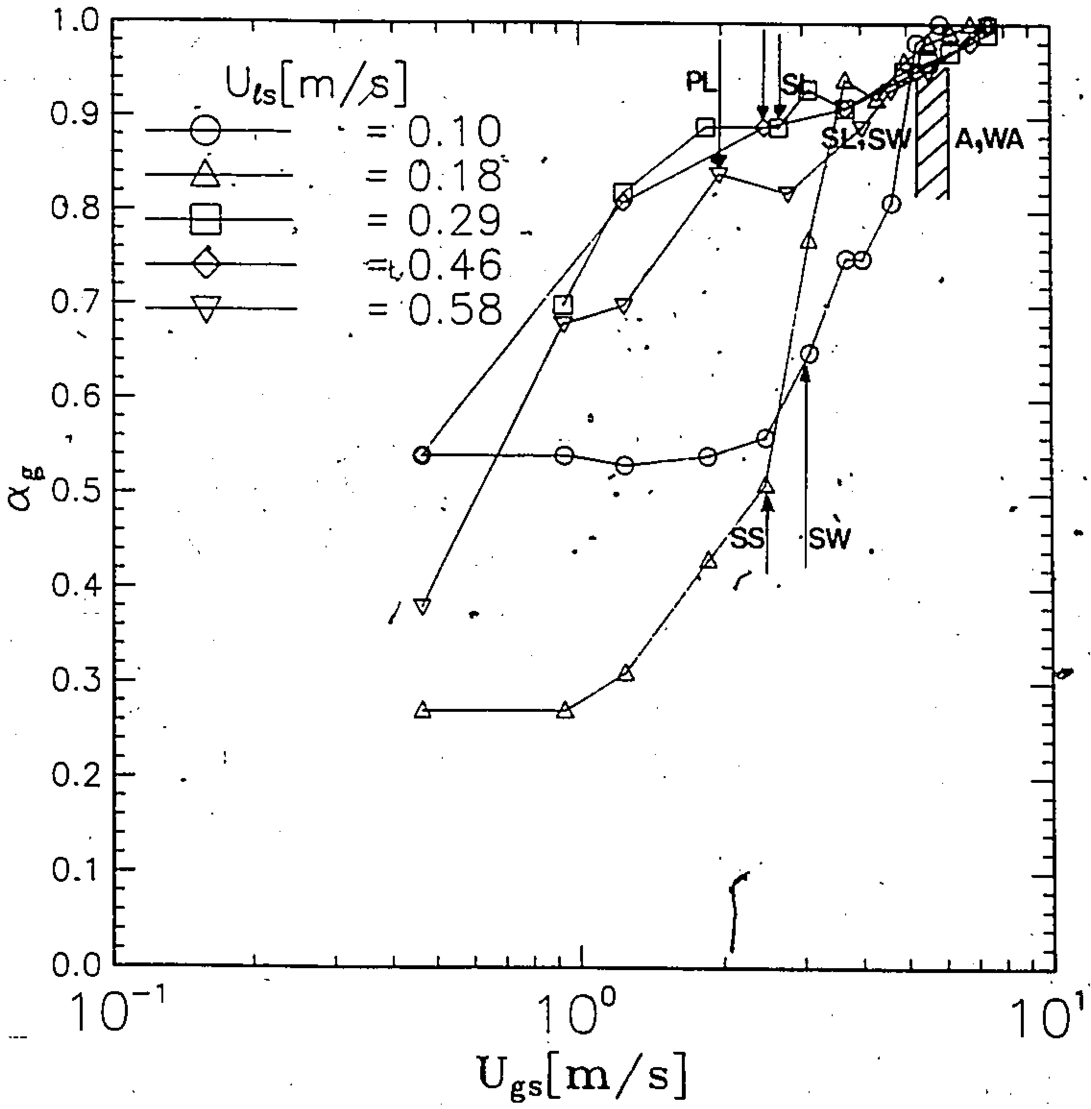

Figure 8.10 Time Averaged Void Fraction as a Function of Superficial Velocities for Annulus of Inner-to-Outer Diameter Ratio, 0.500.

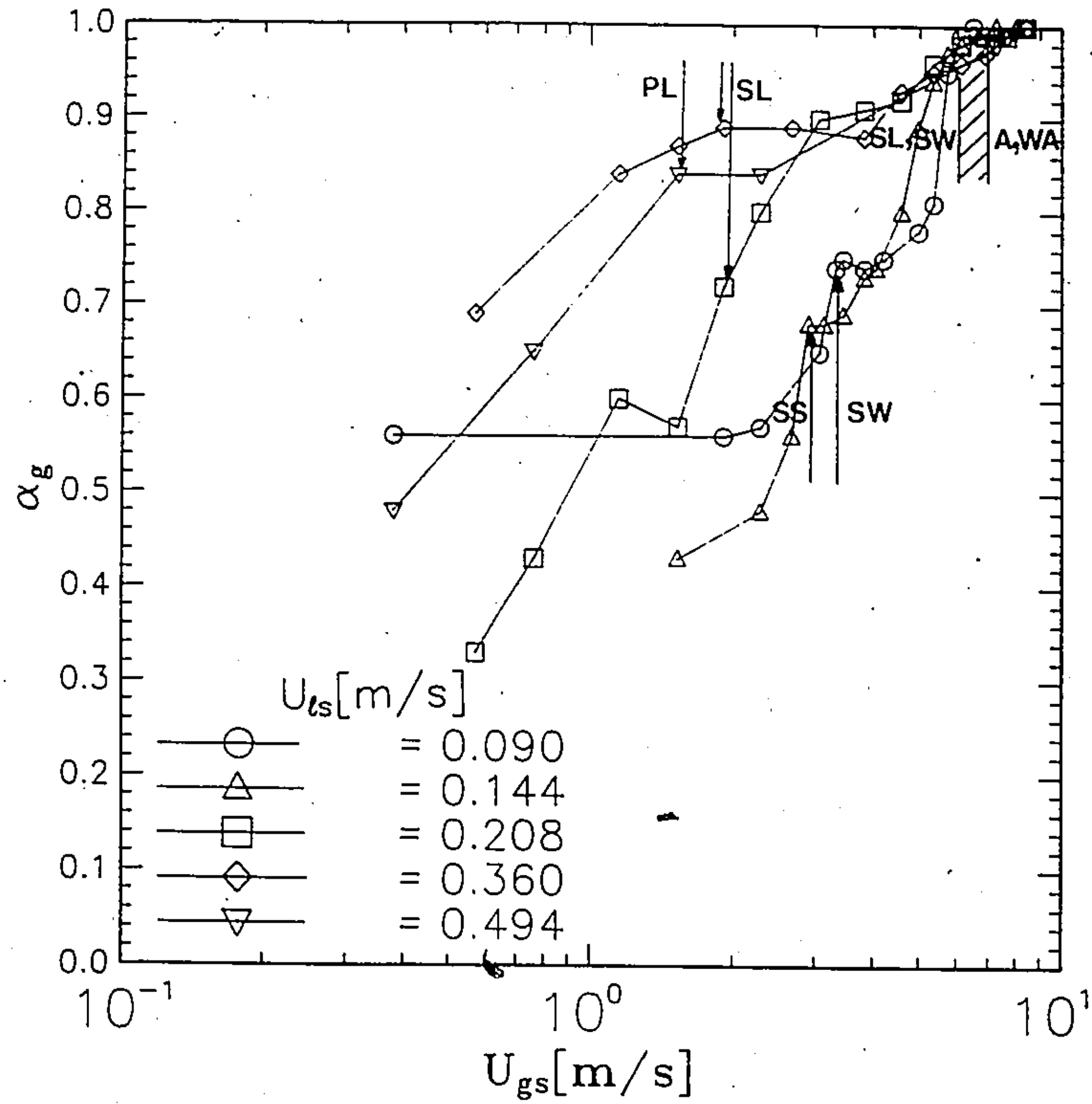

Figure 8.11 Time Averaged Void Fraction as a Function of Superficial Velocities for Annulus of Inner-to-Outer Diameter Ratio, 0.625.

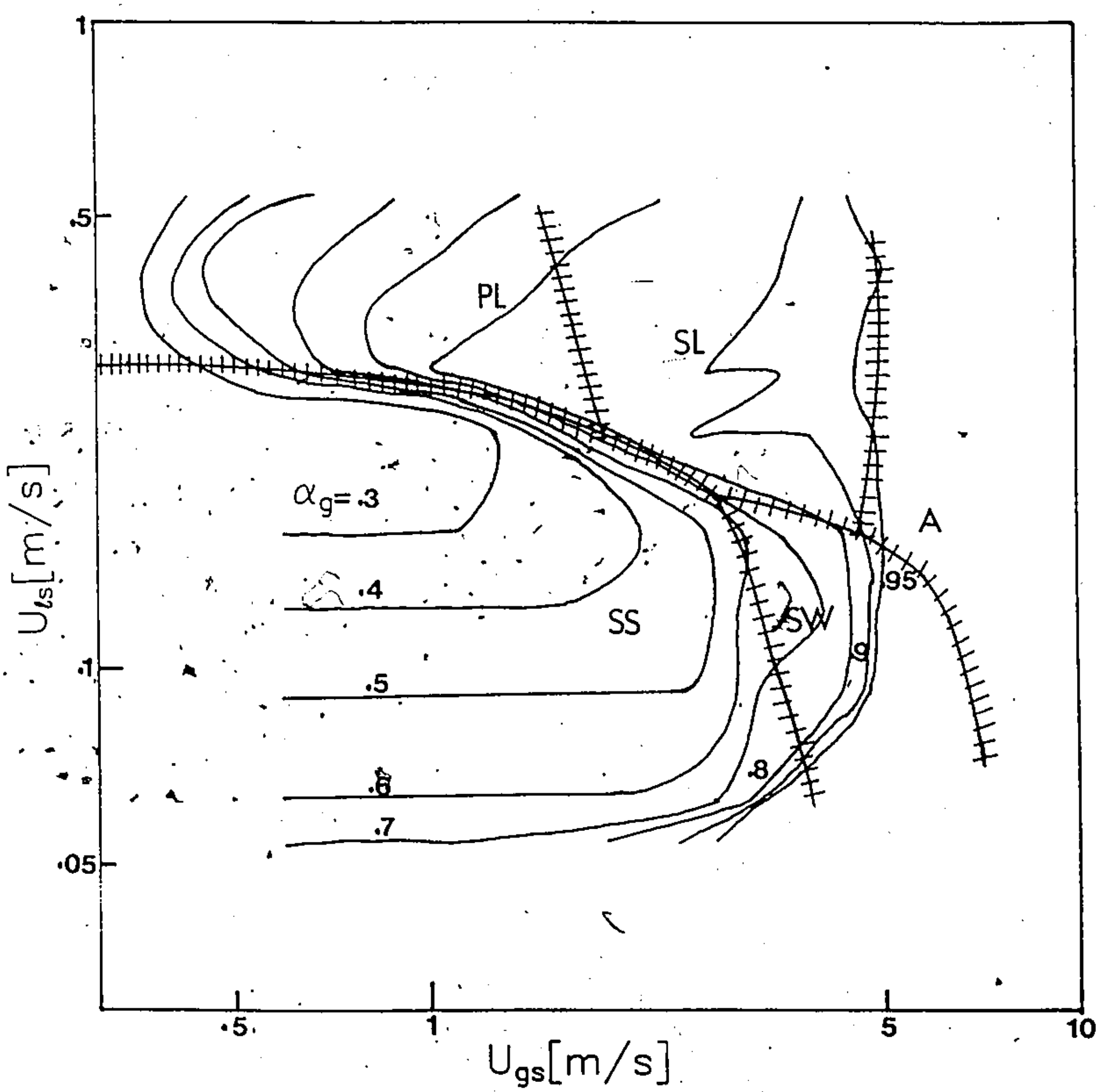

Figure 8.12 **Void Fraction Contour Map for Annulus of Inner-to-Outer Diameter Ratio, 0.375.**

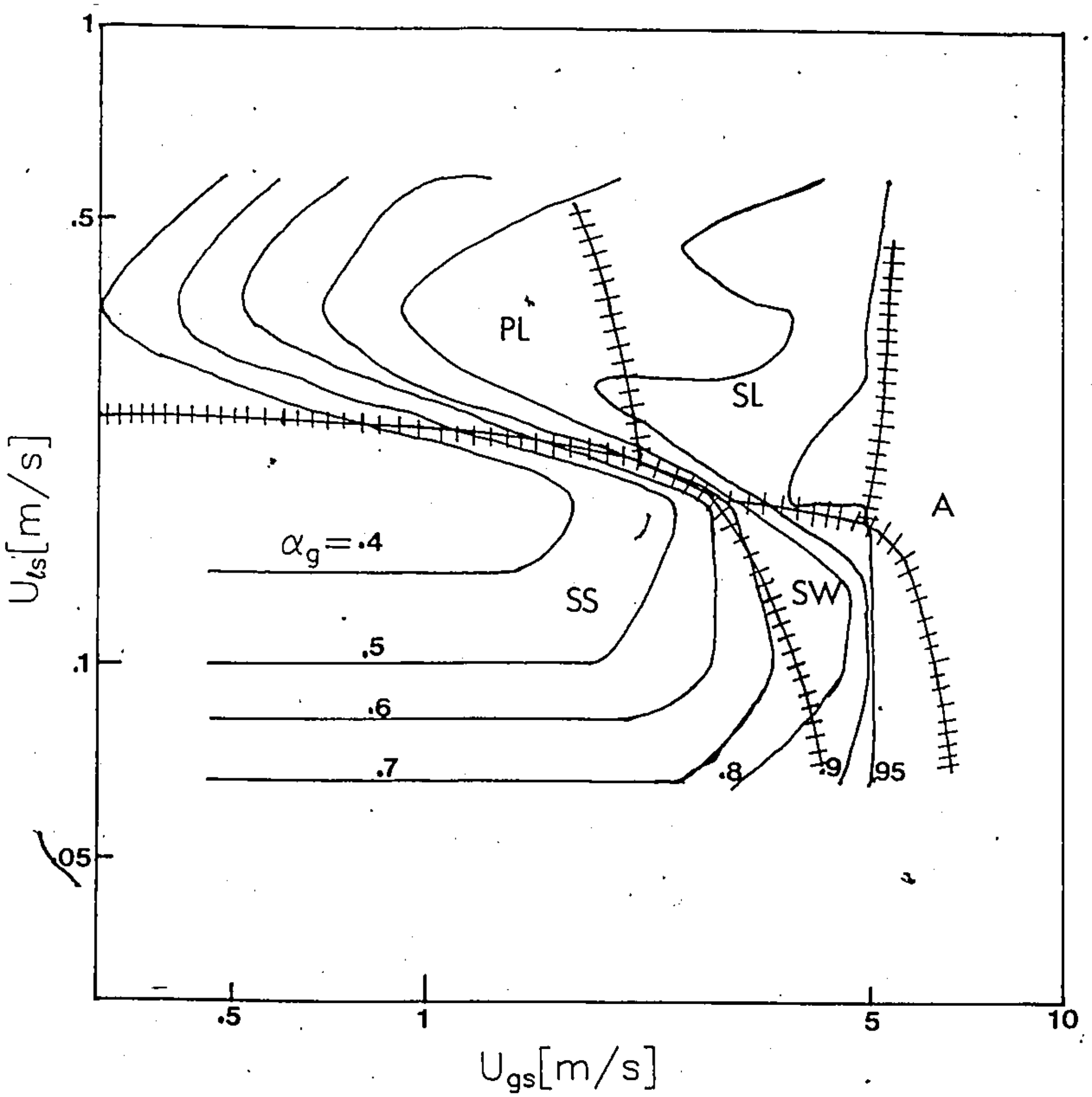

Figure 8.13 Void Fraction Contour Map for Annulus of Inner-to-Outer Diameter Ratio, 0.500.

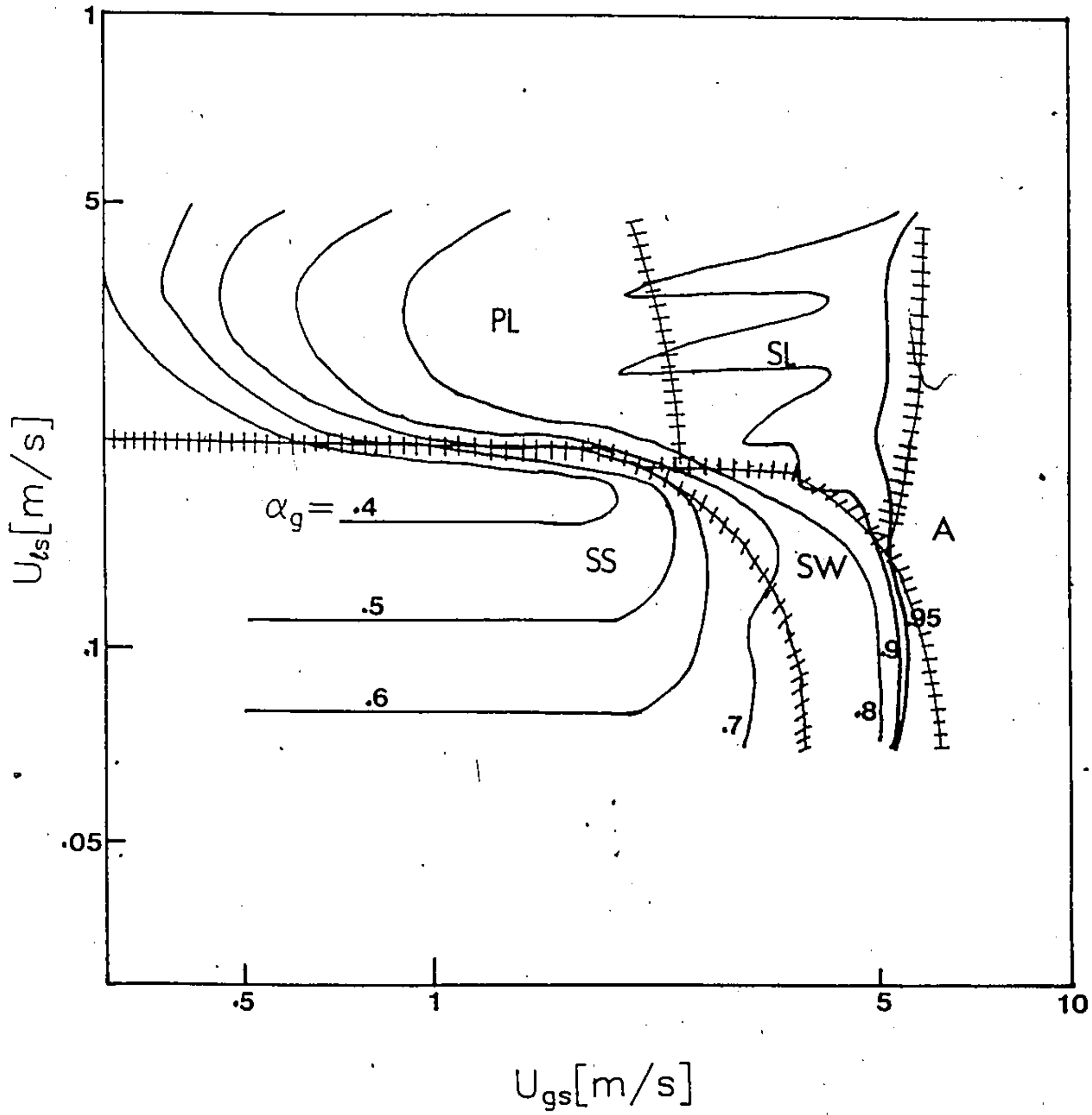

Figure 8.14 Void Fraction Contour Map for Annulus of Inner-to-Outer Diameter Ratio, 0.625.

superficial gas velocity for the pipe and for smaller inner-to-outer diameter annulus flow systems.

Generally, the void fraction is observed to vary nonmonotonically with the superficial liquid velocity as was observed earlier for pipe flow, but shows a more complex dependence for annulus geometries. This is probably due to the additional flow patterns, namely, Annulus-Plug and Annulus-Slug, observed for annulus geometries. If we re-plot the void fraction profiles in the form of contour maps as shown in figures 8.12, 8.13 and 8.14, for annulus geometries of diameter ratios, 0.375, 0.500 and 0.625, respectively, we observe that at the flow pattern transitions, the void fraction changes sharply with superficial gas velocities. This features more prominently for the Stratified to Intermittent (Slug and Plug) or Wavy-Annular transitions. At the Stratified to Intermittent transition, the void fraction contours show an inflexion at high superficial liquid velocities. The Stratified to Wavy-Annular transition represents the range of liquid velocity where the void fraction approaches unity, and nearly independent of the superficial gas velocity.

Thus at high superficial liquid velocity for low superficial gas velocities, where the time averaged void fraction was observed to be small and increasing with the superficial gas velocity, the time averaged pressure drop is large but decreasing with superficial gas velocity. Larger pressure drop is observed at higher superficial gas velocities where the time averaged void fraction approaches unity. Highly aerated Slug and Wavy-Annular flow patterns are observed to be occurring in the annulus geometries at these flow conditions.

Further analysis of the void fraction results in terms of the local phase velocities is given in Appendix II.

8.3 Rod Bundle Flow Results

8.3.1 Flow Pattern

Figures 8.15 and 8.16 show the experimental flow pattern transitions of a horizontal 37-rod bundle flow system for both bubbly and separated entrance conditions, respectively. The bubbly entrance condition refers to the case where the rod bundles are placed just next to the exit of the mixing section, while the separated entrance condition is the case where the rod bundle is placed some distance downstream from the mixing section. The flow pattern transition results were the same for both entrance conditions, except at low gas flow rate where the Stratified to Intermittent transition occurred earlier for the separated entrance condition.

At flow conditions where transition from Stratified to Plug flow pattern occurs, the whole body of the liquid phase was observed to oscillate resembling sinusoidal waves. These eventually died out and Stratified flow pattern existed as the gas phase flow rate was increased. An increase in the liquid flow rate caused the oscillating gas-liquid interface to touch the top of the fluid, leading to the formation of liquid bridge, and consequently Plug flow pattern. This phenomenon featured more prominently for the bubbly entrance condition. Hence the discrepancy in the Stratified to Plug flow transition at low gas flow rates, observed between the bubbly and separated entrance conditions may represent a transition region.

The Plug and Slug flow patterns observed in the rod bundle geometry were observed to be similar in description to the typical pipe flow cases. But no periodic behaviour was observed for the Slug flow pattern as in the case for pipes. This is probably due to flow obstruction by the rod bundle end plates. At low gas flow rates, liquid flowing in the liquid bridge ensues from every subchannel during Plug flow. At high gas flow rates, the liquid bridge is observed to be flushed downstream, with most of the phenomenon confined to the upper section of the rod bundle system, with a continuous liquid film flowing at the bottom of

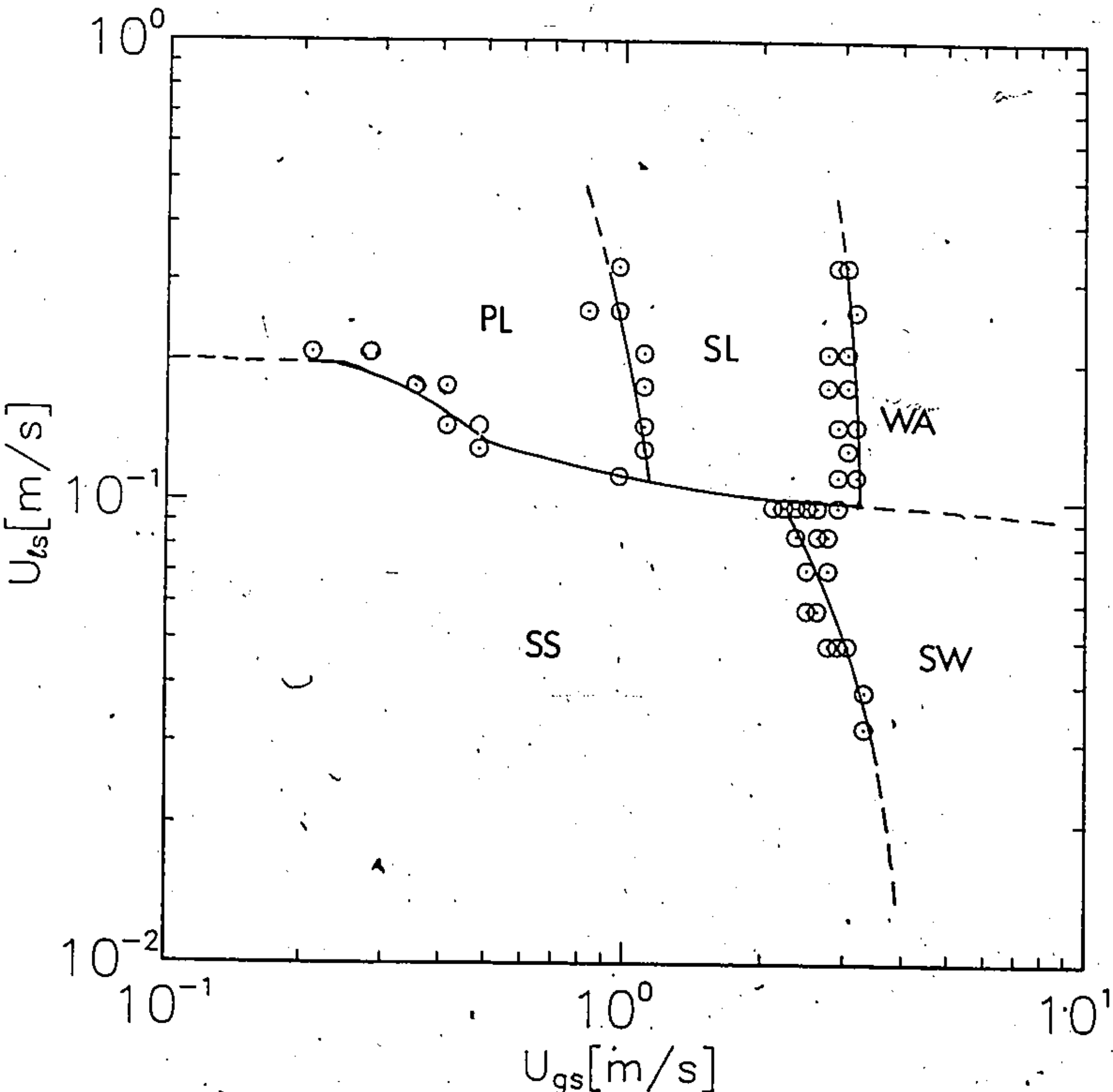

Figure 8.15 Experimental Flow Pattern Transitions of 37-Rod Bundle Flow for Bubbly Entrance Condition.

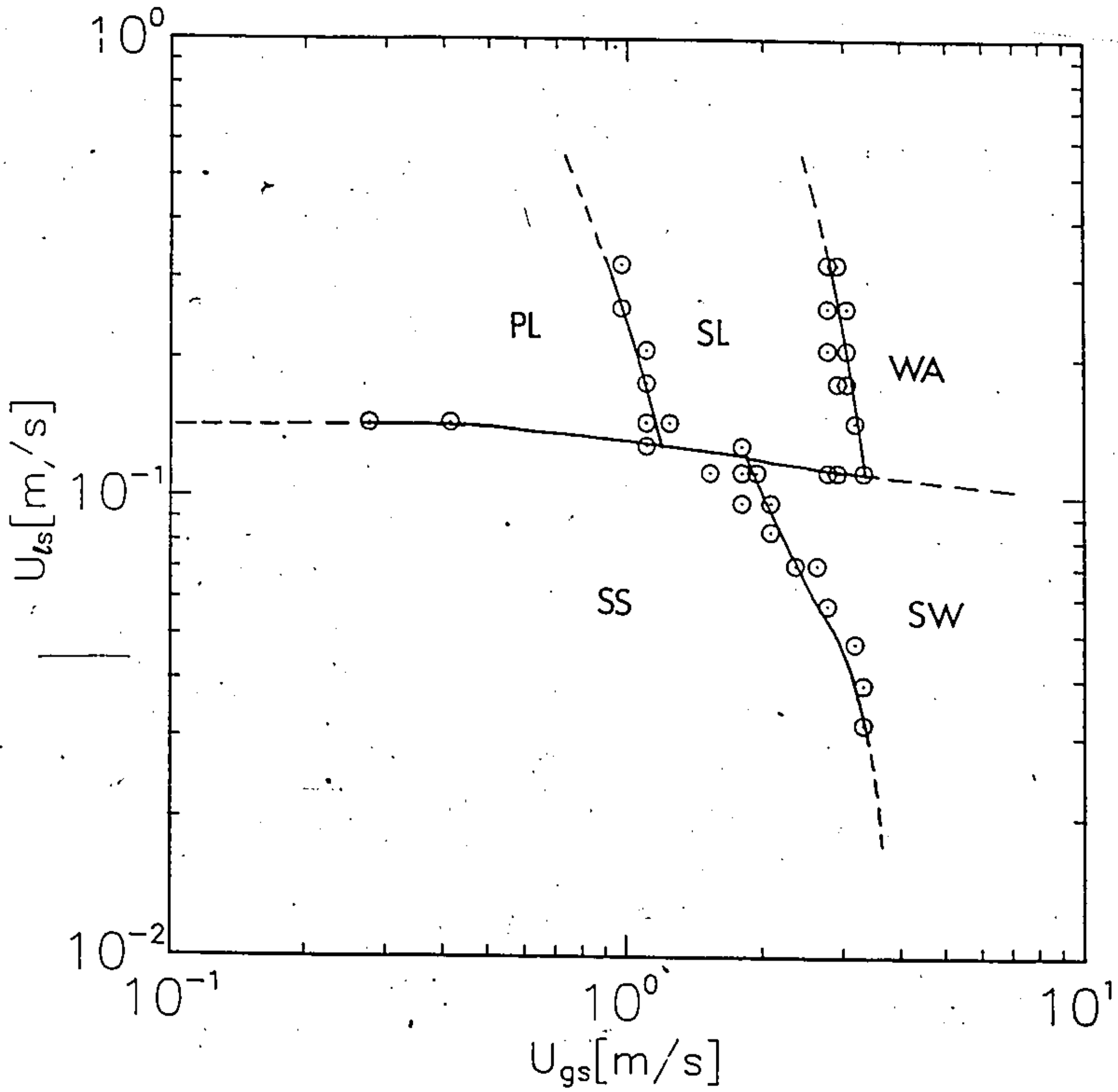

Figure 8.16 Experimental Flow Pattern Transitions of 37-Rod Bundle Flow for Separated Entrance Condition.

the rod bundle channel. This corresponds to the Wavy-Annular flow pattern, where frequently flowing intermittent and highly aerated slugs exist with significant trails of liquid film observed on the enclosing tube walls. Very thin liquid films were also observed to flow on the exposed rods in the upper section of the bundle, but were observed to drain off almost immediately.

The Stratified Wavy flow pattern was sometimes observed to be generated at the rod bundle end plates. The existence of the interfacial waves can be identified by direct visual observation only when the equilibrium liquid level does not intersect a rod in the bundle. However, the Stratified Wavy flow pattern was successfully characterized for every case of the equilibrium liquid level from the pressure drop and void fraction waveforms, via the pressure and capacitance transducers, respectively. The interfacial waves were of small amplitudes, and observed to touch the upper rod when confined in the space between the rods. Isolated and sometimes elongated bubbles were observed in the space between the outer rod and the wall of the enclosing tube, near the gas-liquid interface. These eventually collapse or swept downstream in some cases. This phenomenon occurred only at conditions where Stratified Wavy flow was observed in the system.

At flow conditions where Plug, Slug or Wavy-Annular flow were observed to occur, bundle misalignment did not have any significant effect on the flow transitions. This may be due to the rather violent nature of the Slug and Wavy-Annular flow, and the stratified/full pipe single-phase nature characterizing the Plug flow. However, interfacial waves occupying one bundle sometimes dissipated on entering a misaligned bundle with the liquid in the wave spilled onto rods in the next upper row. Bundle misalignment also led to wave generation observed at different flow rates from the conditions leading to wave dissipation. For misaligned bundles, waves were observed to be generated in the downstream rod bundle when the equilibrium liquid level does not intersect a row of rods. On the other hand, waves.

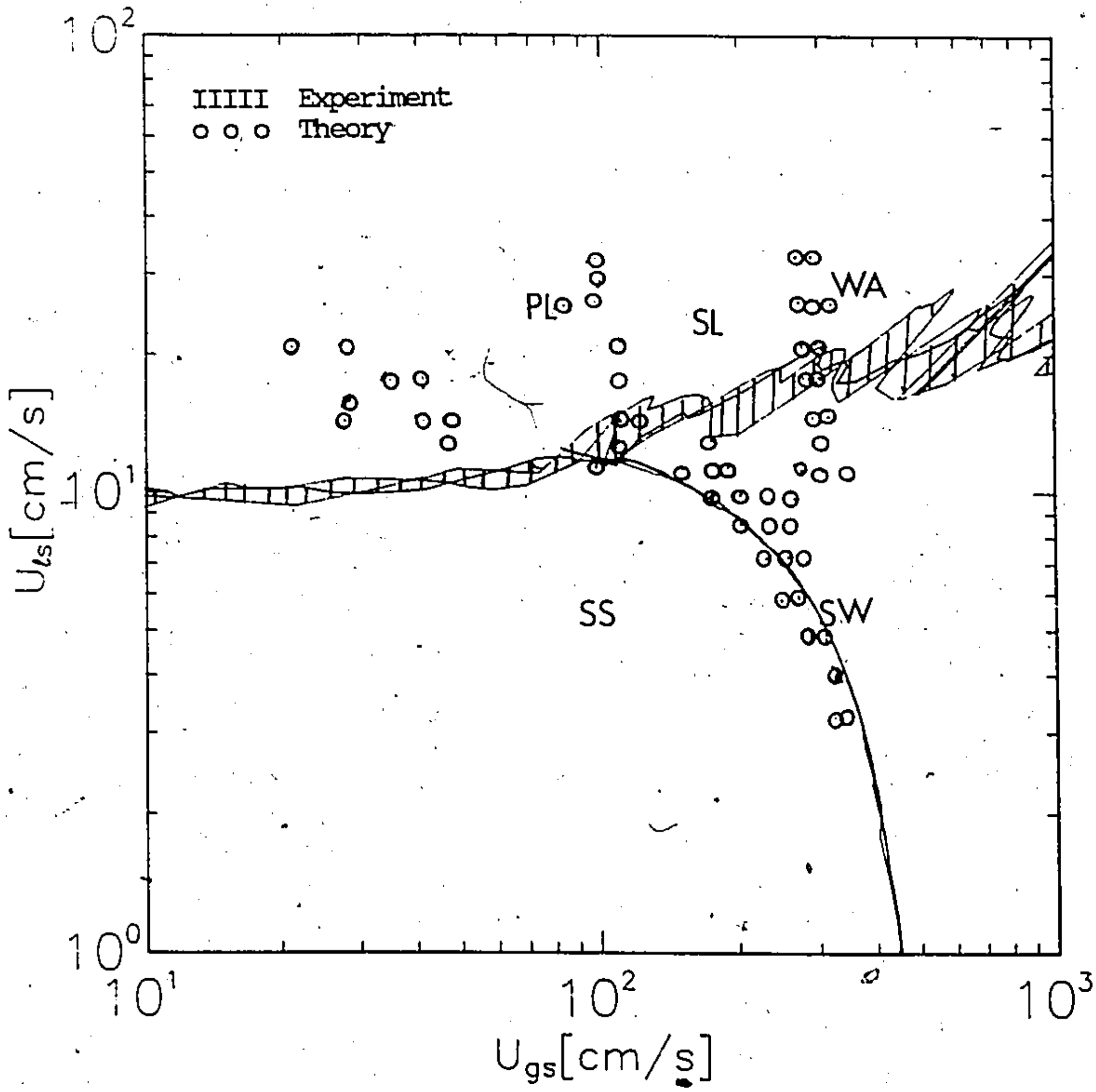

Figure 8.17 Comparison of Experimental and Predicted Flow Pattern Transitions for 37-Rod Bundle Flow.

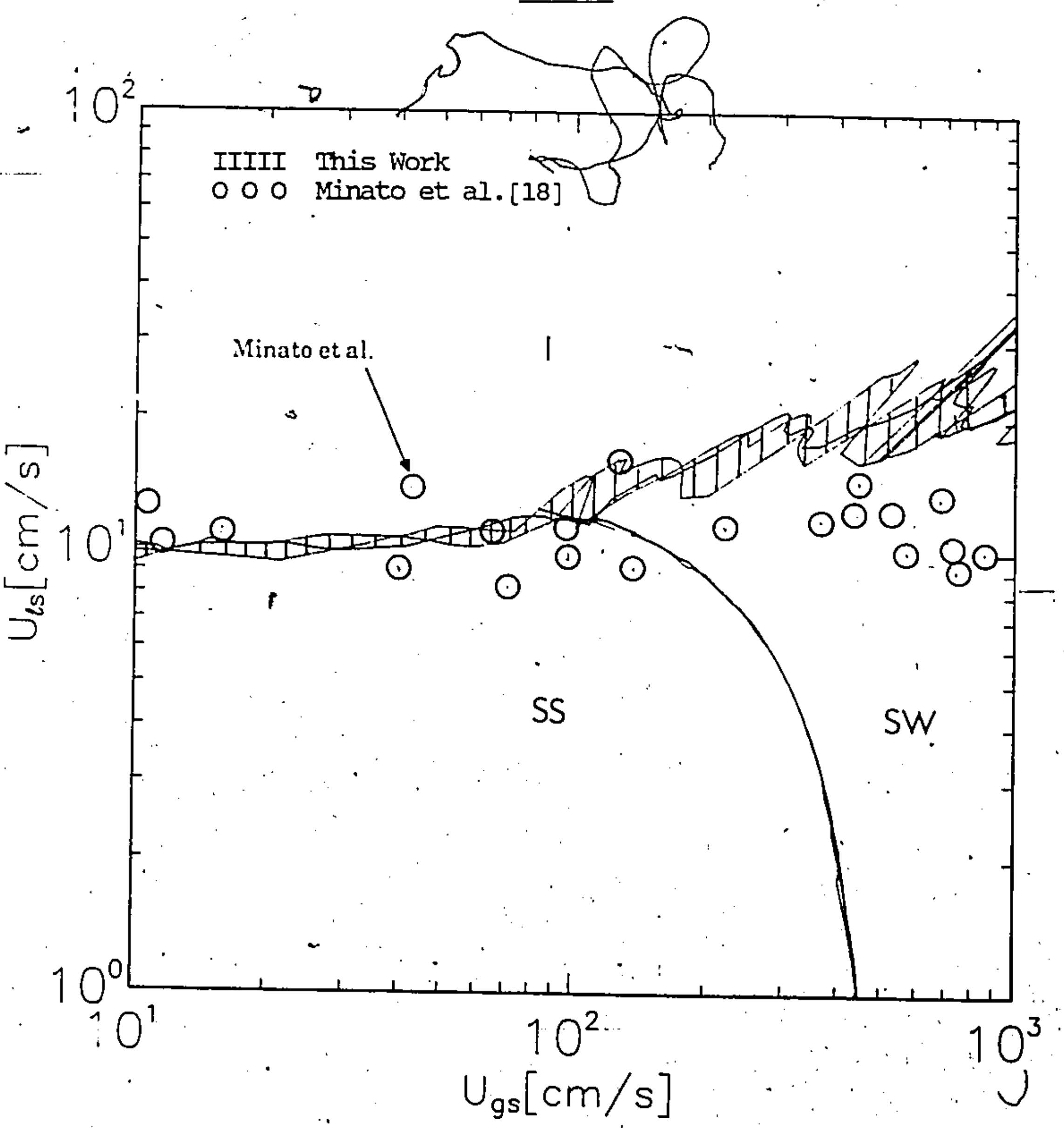

Figure 8.18 Comparison of Predicted Flow Pattern Transitions with Experimental Results of Minato et al.[18] for 37-Rod Bundle Flow

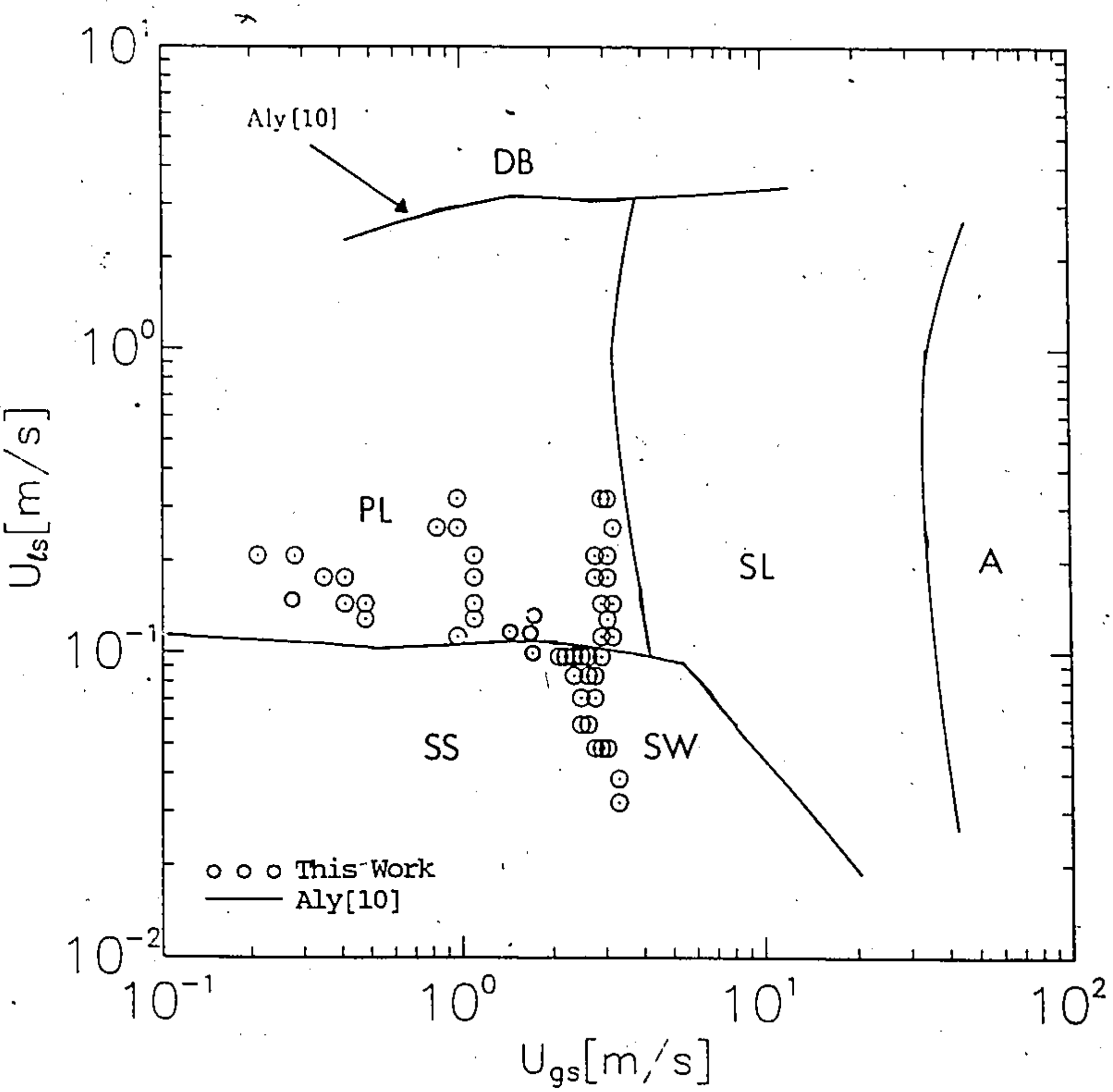

Figure 8.19 Comparison of Present Experimental Results with those of Aly [10] for 37-Rod Bundle Flow

existing in the upstream bundle dissipated on encountering the next bundle when the stratified equilibrium liquid level intersects a row of rods.

Figure 8.17 represents the calculated and experimental results of the 37-rod bundle horizontal two-phase flow studied here. We observe that the REGIME-4 numerical code is in good agreement with the experimental results within the limits of experimental and theoretical errors. The uncertainty in the theoretical results is due to an arbitrary orientation of the 37-rod bundle within the enclosing tube as may obtain in a practical situation. The present results are compared with those of Minato et al. [18] obtained by direct visual observation only, in figure 8.18. And the results are in good agreement for the Stratified to Intermittent flow transitions. Figure 8.19 also compares the results of the present experiment with the work of Aly [10], obtained indirectly from interpretations of the waveforms of a conductivity probe placed in an outer subchannel of a 37-rod bundle. The results of figure 8.19 are generally in good agreement, except the Slug to Annular flow transition. In this case, we characterized the Wavy-Annular flow pattern as represented by very frequent and highly aerated Slug flowing with significant trails of liquid films on both the rods and the tube walls in the upper section of the bundle. This may be considered to be the Slug/Annular transition region, whereas fully developed Annular flow was observed by Aly [10] at gas flow rates, an order of magnitude higher than the onset of Slug/Annular region or the Slug to Wavy-Annular transition observed in the present study.

8.3.2 Pressure Drop

Figure 8.20 shows the time averaged pressure drop as a function of the superficial gas velocity for various superficial liquid velocities, ranging from 6.0 cm/s to 32.0 cm/s. Sudden increase is observed for the pressure gradient at a superficial liquid velocity of 10.0 cm/s. This may be due to increased wall friction from the rod bundles which contribute signi-

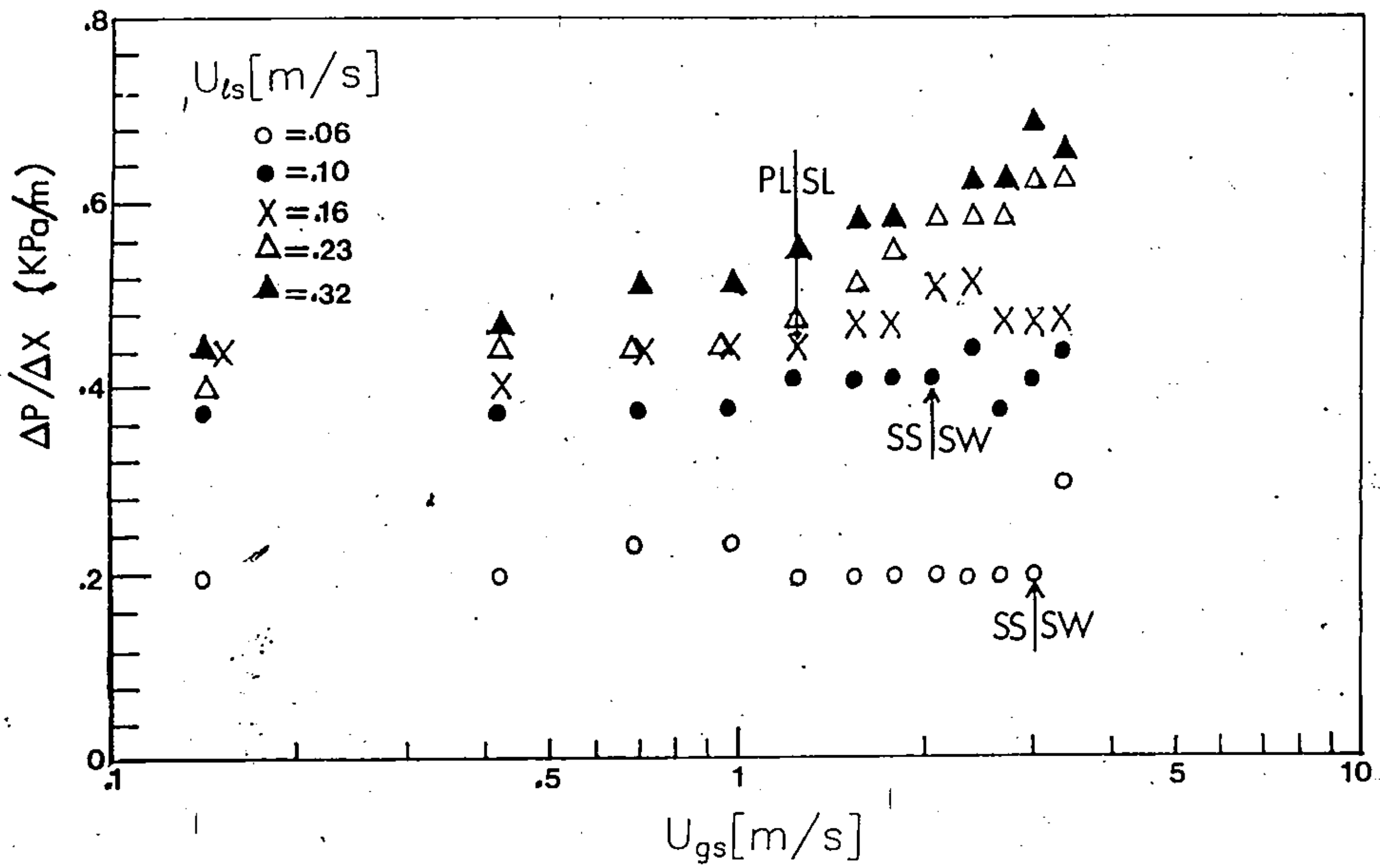

Figure 8.20 Pressure Drop as a Function of Superficial Velocities for 37-Rod Bundle Flow.

ficantly to the pressure drop as the superficial liquid velocity is increased to this value. Generally, the time averaged pressure drop is observed to increase with increasing superficial liquid velocity, and remains nearly insensitive to the superficial gas velocity at low gas flow rates. The pressure drop increases quite sharply, and is slightly non-monotonic with the superficial gas velocity at high gas flow rates due to large fluctuations observed for the pressure drop at these flow conditions.

Figure 8.20 also shows the flow pattern transitions observed for the 37-rod bundle flow geometry. Transitions between the various flow patterns can not be clearly located from the pressure drop profiles. For Stratified Smooth flows, the time averaged pressure drop is almost independent of the superficial gas velocity, but increases suddenly at the transition to Stratified Wavy flows. The time averaged pressure drop is observed to increase very gradually with superficial gas velocities for Plug flows, and quite sharply but unsteady at the transition to Slug flow. Increasing the liquid flow rate results in an increase in the pressure drop for Intermittent flows. In the presentation given here, the Wavy-Annular flow results have been grouped along with Slug flows, since we only observed a few patterns at the flow conditions studied.

8.3.3 Void Fraction

The time averaged void fractions measured for the 37-rod bundle flow geometry are shown in figure 8.21 as a function of the superficial gas velocity, for different superficial liquid velocities, from 3.0 cm/s to 32.0 cm/s. The various flow pattern transitions observed are also indicated in this figure. These are observed to occur at points where the time averaged void fraction changes suddenly. The Stratified Smooth to Plug flow transition indicated at the superficial liquid velocity of 13.0 cm/s, for time averaged void fraction of 0.54 represents the liquid rate where the first Plug flow was experimentally observed in the present system.

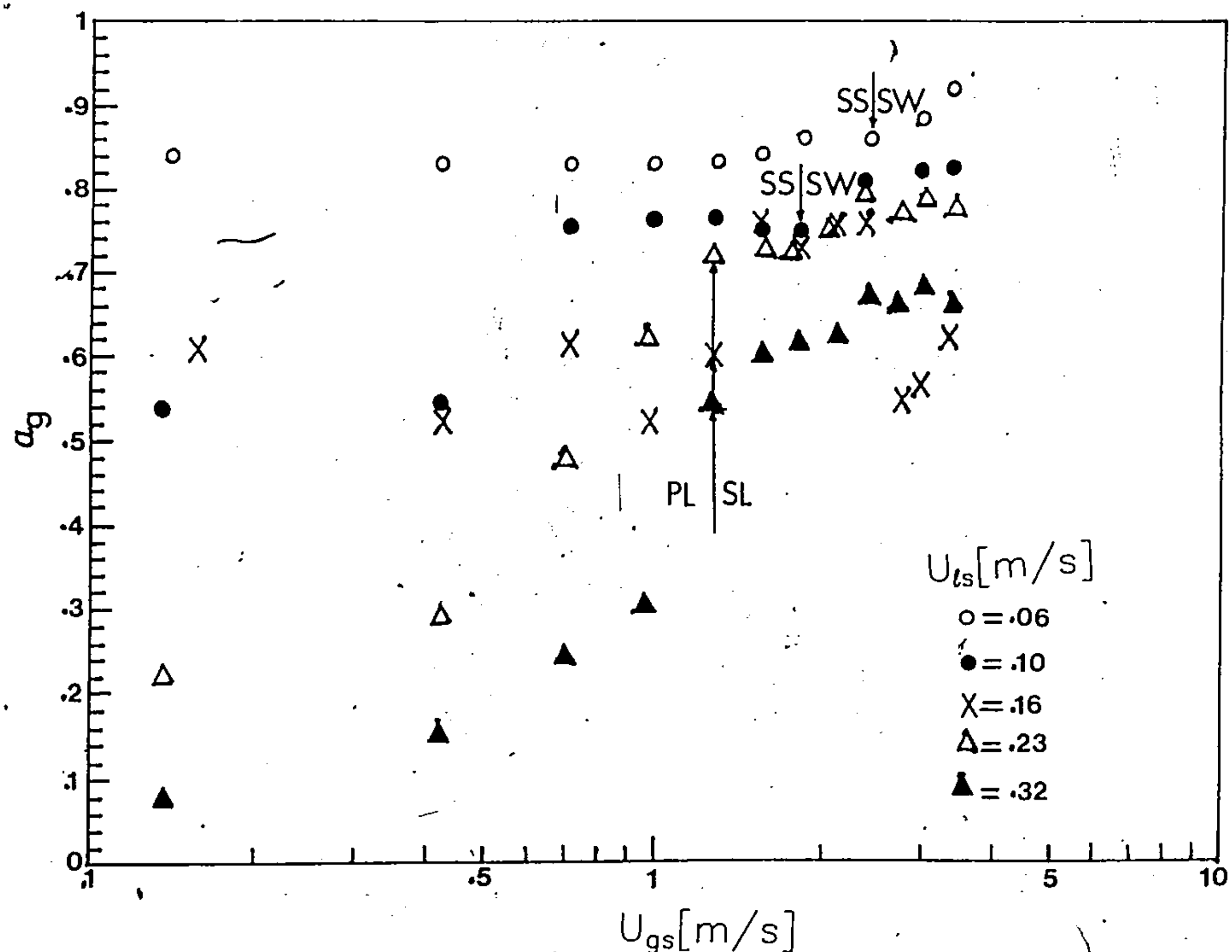

Figure 8.21 Void Fraction as a Function of Superficial Velocities for 37-Rod Bundle Flow.

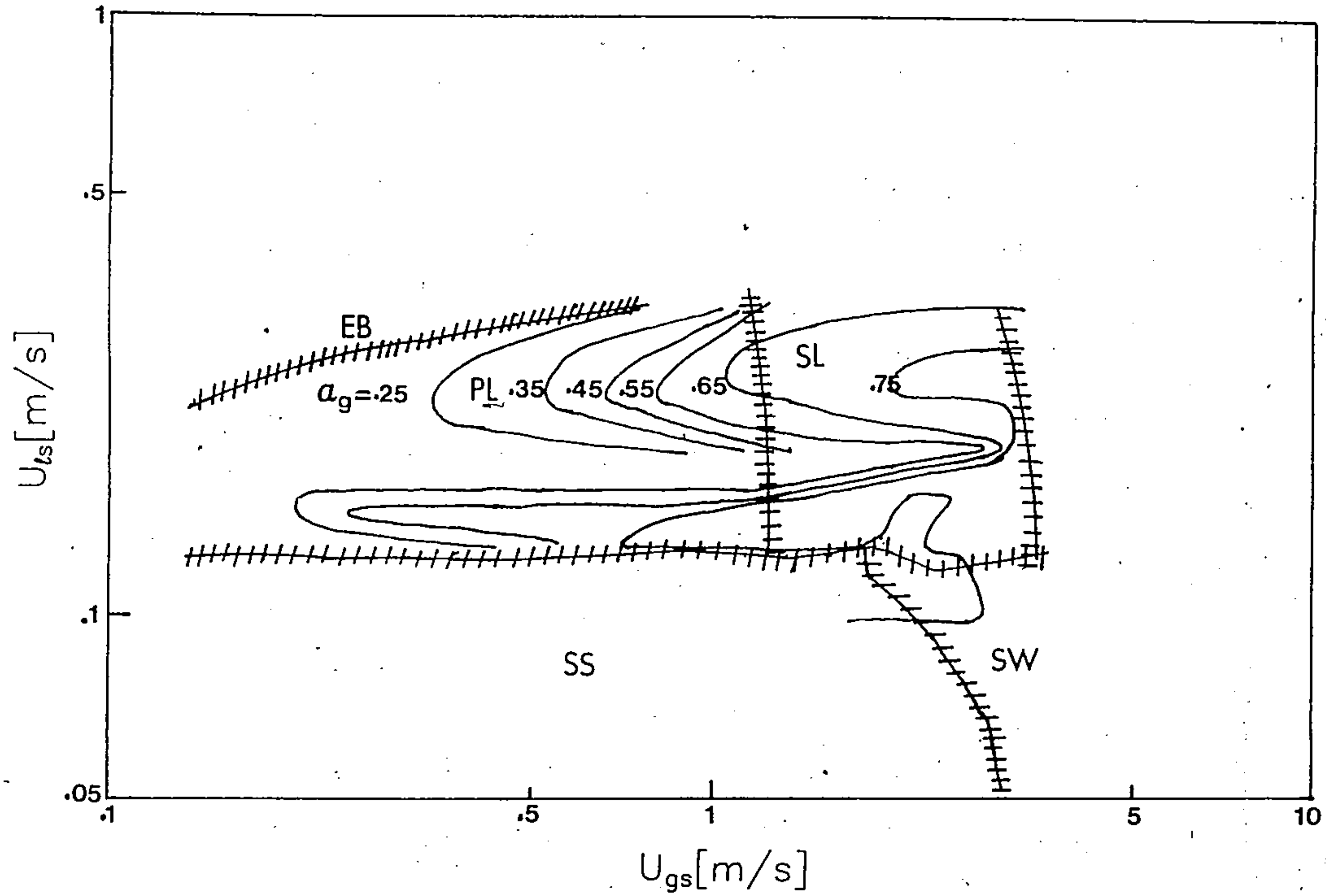

Figure 8.22 Void Fraction Contour Map for 37-Rod Bundle.

The time averaged void fraction is generally observed to decrease with increasing superficial liquid velocities and nearly independent of the superficial gas velocity at up to 40 cm/s. At higher superficial gas velocities, the time averaged void fraction is observed to increase with gas flow rate, and slightly non-monotonic with both the gas and liquid superficial velocities. At a superficial liquid velocity of 16.0 cm/s, the void fraction was observed to vary even more non-monotonically with the gas flow rate, fluctuating between 0.54 and 0.76, with only Intermittent flow patterns occurring at this flow condition.

In Stratified flow, the time averaged void fraction are nearly independent of the superficial gas velocity, except at the transition to Stratified Wavy flow patterns where sudden changes in the void fraction are observed to occur. The void fraction is observed to increase with increasing superficial gas velocity for the Elongated Bubble, Plug and Slug flow patterns, with sudden jump observed at transition locations.

Re-plotting the time averaged void fraction profiles of figure 8.21 in the form of void fraction contour maps in figure 8.22, we observe clearly that the flow pattern transitions are characterized by sudden increases in the void fraction. This is seen to feature more prominently for the Stratified to Plug flow transition, as was also observed for the pipe and annulus flow geometries. Accurate location of the various flow pattern transitions may therefore be achieved from full analysis of the time averaged void fraction as is evident from the present discussions.

Further analysis of the void fraction results in terms of the local phase velocities is given in Appendix II.

CHAPTER 9

CONCLUDING REMARKS

The 5.08 cm i.d. pipe, annuli of inner-to-outer diameter ratios, 0.375, 0.500 and 0.625, and 37-rod bundle flow geometries have been investigated for horizontal two-phase flow pattern distributions. The study involved detailed experimental and theoretical investigations of the flow patterns and flow pattern transitions for these flow geometries. Measurements of the void fraction and pressure drop for the different geometries were also conducted. The pipe flow results were compared with those of the annulus and rod bundle flow geometries, and the following conclusions have been obtained based on the present studies:

(1) The various flow patterns observed for the horizontal annulus and rod bundle flow geometries are similar in description to those usually observed for the normal pipe flow, namely, Stratified Smooth, Stratified Wavy, Slug, Plug, Annular and Wavy-Annular flow patterns. However, in the annular flow geometry, additional flow patterns, namely, Annulus-Slug and Annulus-Plug, were also characterized. These are similar to the Plug and Slug flow patterns observed for the pipe flow, except that they are occurring only within the lower annulus channel gap.

(2) The flow pattern characterization for the pipe, annulus and 37-rod bundle flow geometries were achieved independently by direct visual observation and by the ring type capacitance transducer placed completely external to the flow. The signal waveforms of the capacitance transducer were observed to be distinct for the different flow patterns.

(3) The ring type capacitance transducer placed external to the flow to avoid any flow disturbances were successfully used for the measurement of void fraction in the pipe, annulus and rod bundle flow systems.

(4) The Slug flow patterns are characterized by large pressure drop fluctuations, especially in the 37-rod bundle flow geometry. Sudden changes in the time averaged void fractions were observed at the various flow pattern transitions for the different geometries. This observation supplements the direct visual observation results for accurately locating the flow pattern transitions.

(5) In these flow geometries, a significant range of transition between the Stratified Smooth to Plug flow patterns was observed, and is nearly independent of the gas flow rate. The Slug to Wavy-Annular flow transition is observed to be nearly independent of the liquid flow rate. The Wavy-Annular flow pattern essentially represents the transition region between the Slug and the fully developed Annular flow patterns, and may exist up to an order of magnitude of the superficial gas velocity.

(6) The flow pattern transitions are significantly different between the pipe, annulus and rod bundle flow geometries. The Stratified to Intermittent and the Intermittent to Dispersed Bubble flow transitions are observed to occur at lower superficial liquid velocities, while the Intermittent to Annular flow transition occurs at higher superficial gas velocities for the annulus and rod bundle flow geometries than the pipe flow cases.

(7) The flow pattern transitions for the annulus flow geometries vary with different inner-to-outer diameter ratios, where the Stratified to Intermittent and Intermittent to Dispersed Bubble flow transitions occur at lower superficial liquid

velocities, and the Intermittent to Annular flow transition occurs at higher superficial gas velocities for larger inner-to-outer diameter ratios.

(8) The 28 and 37-rod bundle flow pattern transitions are predicted to vary slightly with the angle of orientation of the rod bundles within the enclosing tubeshell. The flow pattern transitions in this case have been represented by bands to account for any uncertainties due to arbitrary orientation of the rod bundle within the tubeshell, in a practical situation. Also the predicted flow pattern transitions differ slightly between the 28 and 37-rod bundle flow geometries.

(9) The flow pattern transitions for the 37-rod bundle flow geometry were observed to be insensitive to different entrance conditions, except the Stratified to Intermittent transition at low gas flow rate observed to occur at lower superficial liquid velocity for the stratified entrance condition.

(10) Small amplitude interfacial waves were observed to be generated and dissipated at the rod bundle end plates, depending on the flow rates, while little effect of the end plates on the regularity of the Plug, Slug and Wavy-Annular flow patterns was observed.

(11) Large discrepancies between experimental and theoretical predictions were observed for the Stratified Smooth to Plug flow transitions for these flow geometries. The mechanism, the Bernoulli effect, which assumes the existence of interfacial waves may not be suitable for modelling this transition between the Stratified Smooth and Plug flow patterns. Since fully developed turbulent flow conditions already exist in the liquid phase, liquid turbulent fluctuations may dominate Bernoulli effect as the lifting force opposing gravity in the mechanism leading to this transition. The actual mechanism governing this transition may depend on a range of sizes for the pipe section, since for small capillary pipes of

diameter, $D < 1.0$ cm i.d., and for larger pipe sizes of diameter, $D > 5.0$ cm i.d., additional transition mechanisms apart from Bernoulli effect need to be considered.

CHAPTER 10

RECOMMENDATIONS FOR FUTURE STUDY

The following points should be recommended as a future program to extend the knowledge of flow patterns in pipes, annulus and rod bundles:

(1) Experimental two-phase flow pattern be conducted for diabatic systems to understand the full effect of heat addition. Steam-water two-phase flow experiments could be used to simulate these conditions. In order to characterize the flow patterns occurring in this case, the ring type capacitance transducer may be used. A section of the system may be made from pyrex/lucite piece, where the capacitance transducer may be mounted, to monitor void fraction fluctuations, and consequently the flow patterns occurring in the system.

(2) The theoretical model should consider additional forces in the mechanisms governing the various flow pattern transitions. In particular, the Stratified Smooth to Plug and the Slug to Annular flow transitions which were observed to deviate significantly from experimental results. In the annulus and rod bundle flow geometries, frictional forces due to the presence of the rods may be significant in the mechanism for Stratified to Intermittent flow transition.

(3) From the results of the present investigation, it is recommended that analyses of the time averaged void fraction measurements be extended to locating the transition boundaries between the various flow patterns, since sudden changes in void fractions are observed to occur at transition locations.

(4) Objective flow pattern characterization may be achieved by an indirect interpretation of the signal waveforms of void fraction measurements, distinct for the

different flow patterns, together with the results of direct visual observations. The capacitance transducer technique based on differences in the dielectric constants of the respective phases, and placed external to the flow to avoid any flow obstructions, as has been successfully applied in this study is recommended.

REFERENCES

1. COLLIER, J.G., Convective Boiling and Condensation, McGraw Hill Book Co., Maidenhead, 1972.

2. BAKER, O., "Simultaneous Flow of Oil and Gas", Oil Gas J., Vol. 53, No. 7, pp 185-195, 1954.

3. GOVIER, G.W. and M.M. OMER, "The Horizontal Pipeline Flow of Air-Water Mixtures", Can. J. Chem. Eng., Vol. 40, pp 93-104, 1962.

4. HUBBARD, M.G. and A.E. DUKLER, "The Characterization of Flow Regimes for Horizontal Two-Phase Flow", Proc. 1966 Heat Trans. and Fluid Mech. Inst., Stanford Univ. Press, pp 100-121, 1966.

5. WHITE, P.D. and R.L. HUNTINGTON, "Horizontal Co-Current Two-Phase Flow of Fluids in Pipe Lines", Petrol. Eng., Vol. 27, No. 9, D40, 1955.

6. AL-SHEIKH, J.N., D.E. SAUNDERS and R.S. BRODKEY, "Prediction of Flow Patterns in Horizontal Two-Phase Pipe Flow", ibid, Vol. 48, No. 21, 1970.

7. MANDHANE, J.M., G.A. GREGORY and K. AZIZ, "A Flow Pattern Map for Gas-Liquid Flow in Horizontal Pipes", Int. J. Multiphase Flow, Vol. 1, pp 537-553, 1974.

8. TAITEL, Y. and A.E. DUKLER, "A Model for Predicting Flow Regime Transitions in Horizontal and Near Horizontal Gas-Liquid Flow", AIChE Journal, Vol. 22, No. 1, pp 47-55, 1976.

9. WEISMAN, J.D., D. DUNCAN, J. GIBSON and T. CRAWFORD, "Effects of Fluid Properties and Pipe Diameters on Two-Phase Flow Patterns in Horizontal Lines", Int. J. Multiphase Flow, Vol. 5, pp 437-462, 1979.

10. ALY, A.M.M., "Flow Regime Boundaries for an Interior Subchannel of a Horizontal 37-Element Bundle", Can. J. Chem. Eng., Vol. 59, No. 2, pp 158-163, 1981.

11. OSAMUSALI, S.I. and J.S. CHANG, "REGIME-4 Code for Prediction of Flow Regime Transitions in a Horizontal Pipe, Annulus and Rod Bundle Flow Under Gas-Liquid Two-Phase Flow", Proc. 8th Annual Can. Nuclear Soc. Conf., Saint John, N.B., 1987.

12. CHANG, J.S., S.T. REVANKAR, R. RAMAN and F.B.P. TRAN, "Application of an EHD Technique to a Nuclear Power Plant Emergency Core Cooling System", IEEE Trans. Industrial Applications, Vol. IA-21, No. 4, pp 712-723, 1985.

13. NICHOLSON, M.K., J.R. NICKERSON, K.AZIZ and G.A. GREGORY, "A Comparison of Flow Regime and Pressure Drop in Adiabatic and Diabatic Two-Phase

Simulations", Proc. 7th Int. Conf. Heat Tran., Munich, Paper No. TF11, pp 6-10, 1982.

14. BECKER, K.M., A. LETZTER, O. NYLUND and B. SCHOLIN, "An Experimental Study of the Effect of the Axial Heat Flux Distribution on the Dryout Conditions in a 3650-mm Long Annulus", Int. J. Multiphase Flow, Vol. 7, No. 1, pp 47-61, 1981.

15. BERGLES, A.E., "Two-Phase Flow Structure Observations for High Pressure Water in a Rod Bundle", Two-Phase Flow and Heat Transfer in Rod Bundles, Schrock, V.E. Ed., ASME Press, pp 47-55, 1969.

16. VENKATESWARARAO, P., R. SEMIAT and A. E. DUKLER, "Flow Pattern Transition for Gas-Liquid Flow in a Vertical Rod Bundle", Int. J. Multiphase Flow, Vol. 8, No. 5, pp 509- 524, 1982.

17. KRISHNAN, V.S. and J.E. KOWALSKI, "A Study of the Stratified to Slug Flow Transition in a Horizontal Pipe Containing a Rod Bundle", AIChE Symp. Series, Vol. 80, No. 236, pp 282-289, 1984.

18. MINATO, A., T. IKEDA and M. NAITOH, "Mechanistic Model of Slugging Onset in Horizontal Circular Tubes", J. Nucl. Sci. and Tech., Vol. 23, No. 9, pp 761-768, 1986.

19. BARNEA, D., Y. LUNINSKI and Y. TAITEL, "Flow Patterns in Horizontal and Vertical Two-Phase Flow in Small Diameter Pipes", Can. J. Chem. Eng., Vol. 61, pp 617-720, 1983.

20. ISHII, M., Thermo-Fluid Dynamic Theory of Two-Phase Flow, Eyrolles, 1975.

21. DELHAYE, J.M., "Basic Equations for Two-Phase Flow Modelling", Two-Phase Flow and Heat Transfer in the Power and Process Industries, Bergles, A.E., J.G. Collier, J.M. Delhaye, G.F. Hewitt, and F. Mayinger, Eds., Hemisphere Pub. Co., New York, 1981.

22. BLASIUS, H. Forschg. Arb. Ing.-Wes., No. 134, 1913.

23. AGRAWAL, S.S., G.A. GREGORY and G.W. GOVIER, "An Analysis of Horizontal Stratified Two-Phase Flow in Pipes", Can. J. Chem. Eng., Vol. 51, pp 280-286, 1973.

24. GAZELY, C., "Interfacial Shear and Stability in Two-Phase Flow", Ph.D. Thesis, Univ. of Delaware, Newark, 1949.

25. CHEREMISSINOFF, N.P. and E.J. DAVIS, "Stratified Turbulent-Turbulent Gas-Liquid Flow", AIChE Journal, Vol. 25, No. 1 pp 48-56, 1979.

26. KOWALSKI, J.E., "Wall and Interfacial Shear Stress in Stratified Flow in a Horizontal Pipe", AIChE Journal, Vol. 33, No. 2, pp 274-281, 1987.

27. ANDRITTOS, N.A. and T.J. HANRATTY, "Influence of Interfacial Waves in Stratified Gas-Liquid Flows", AIChE Journal, Vol. 33, No. 3, pp 444-454, 1987.

28. ANDREUSSI, P. and L.N. PERSEN, "Stratified Gas-Liquid Flow in Downwardly Inclined Pipes", Int. J. Multiphase Flow, Vol. 13, No. 4, pp 565-575, 1987.

29. LIN, P.Y. and T.J. HANRATTY, "Effect of Pipe Diameter on Flow Patterns for Air-Water Flow in Horizontal Pipes", Int. J. Multiphase Flow, Vol. 13, No. 4, pp 549-563, 1987.

30. JEFFREYS, H., "On the Formation of Water Waves by Wind", Proc. Royal Soc., A107, 189, 1925.

31. BENJAMIN, T.B., "Shearing Flow Over a Wavy Boundary", J. Fluid Mech., Vol. 6, pp 161-205, 1959.

32. HANRATTY, T.J. and J.M. ENGEN, "Interaction Between a Turbulent Air Stream and a Moving Water Surface", AIChE Journal, Vol. 3, pp 299-304, 1957.

33. CHU, K.T., "Statistical Characteristics and Modelling of Wavy Liquid Films in Vertical Two-Phase Flow", Ph.D. Thesis, Univ. of Houston, Texas, 1973.

34. BROCK, R.R., "Periodic Permanent Roll Waves", Proc. ASCE, Vol.90, HYD 12, pp 2565-2580, 1970.

35. FULFORD, G.D., "The Flow of Liquids in Thin Films", Adv. Chem. Eng., Vol. 5, pp 151-236, 1964.

36. WALLIS, G.B. and J.E. DOBSON, "The Onset of Slugging in Horizontal Stratified Air-Water Flow", Int. J. Multiphase Flow, Vol. 1, pp 173-193, 1973.

37. KORDYBAN, E.S. and T. RANOV, "Mechanism of Slug Formation in Horizontal Two-Phase Flow", Trans. ASME, J. Basic Eng., Vol. 92, Ser. D, No. 4, pp 857-864, 1970.

38. LIGHTSTONE, L., S.I. OSAMUSALI and J.S. CHANG, "REGIME-3 Code for Prediction of Flow Regime Transition in a Two-Phase Manifold Flow", Proc. 13th Annual Can. Nucl. Society Simulation Symp., Chalk River, 1987.

39. CHANG, J.S., R. GIRARD, R. RAMAN and F.B.P. TRAN, "Measurement of Void Fraction in Vertical Gas-Liquid Two-Phase Flow by Ring-Type Capacitance Transducers", Mass Flow Measurement, T.R. Heidrick and R.M. Reimer, Eds., ASME Press, New York, FED-17, Vol. 1, pp 93-100, 1984.

40. CHANG, J.S., Y. ICHIKAWA and G.A. IRONS, "Flow Regime Characterization and Liquid Film Thickness Measurement in Horizontal Gas-Liquid Two-Phase Flow by an Ultrasonic Transmission Technique", Measurements in Polyphase Flow, T.R. Heidrick and B.R. Patel, Eds., ASME Press, New York, pp 7-12, 1982.

41. HEWITT, G.F. and D.N. ROBERTS, "Studies of Two-Phase Flow Patterns by Simultaneous X-Ray and Flash Photography", UKAEA Report No. AERE-M2159.

42. CHANG, J.S., J.C. CAMPEAU, S.I. OSAMUSALI, S.H. WANG and M.P. BUTLER, "Real Time Neutron Radiography for Visualization of Phase Distribution in Multiphase Flow", (To be Presented), Flow Visualization Conf., Beijing, China, 1988.

43. HUBBARD, M.G. and A.E. DUKLER, "The Characterization of Flow Regimes for Horizontal Two-Phase Flow: 1. Statistical Analysis of Wall Pressure Fluctuations", Proc. 1966 Heat Transfer and Fluid Mech. Inst., M.A. Saad and J.A. Miller, Eds., Stanford Univ. Press, pp 100-121, 1966.

44. JONES, O.C. and N. ZUBER, "The Interrelation Between Void Fraction Fluctuations and Flow Patterns in Two-Phase Flow", Vol.2, pp 273-306, 1975.

45. HEWITT, G.F., Measurement of Two-Phase Flow Parameters, Academic Press, London, 1978.

46. BARNERJEE, S. and R.T. LAHEY Jr., "Advances in Two-Phase Flow Instrumentation", Adv. Nuclear Sci. and Tech., Vol. 13, pp 227-414, 1981.

47. LIGHTSTONE, L. and J.S. CHANG, "Flow Regime Observations in Horizontal Gas-Liquid Two-Phase Dividing Flow in 'Tees' and 'Wyes' ", Proc. 33rd Canadian Chem. Eng. Conf., Vol. 1,pp 281-286, 1983.

48. CHANG, J.S., W. TOFILUK, T.A. MYINT, N. HAYASHI and K. BRODOWICZ, "Time-Averaged Particle Fraction and Flow Patterns in Gas-Powder Two-Phase Horizontal Flow", Multiphase Transport and Particulate Phenomena, Hemisphere Pub. Co., (In Press), 1988.

APPENDIX I

Calibration Curves

The various calibration curves for the void fraction and pressure drop measurements are documented in this appendix. The corresponding equilibrium liquid level for stratified flow has been calibrated as a function of the voltage, and a direct graphical look-up method is then used to obtain the void fraction. The void fraction calibration curves are presented separately for each geometry, namely, 5.08 cm i.d. pipe, annuli with inner-to-outer diameter ratios of 0.375, 0.500 and 0.625 in figures I.1 and I.2, I.3 and I.4, I.5 and I.6, I.7 and I.8, respectively. The pressure drop calibration curves for the annuli and rod bundle geometries are given in figures I.9 and I.10, respectively.

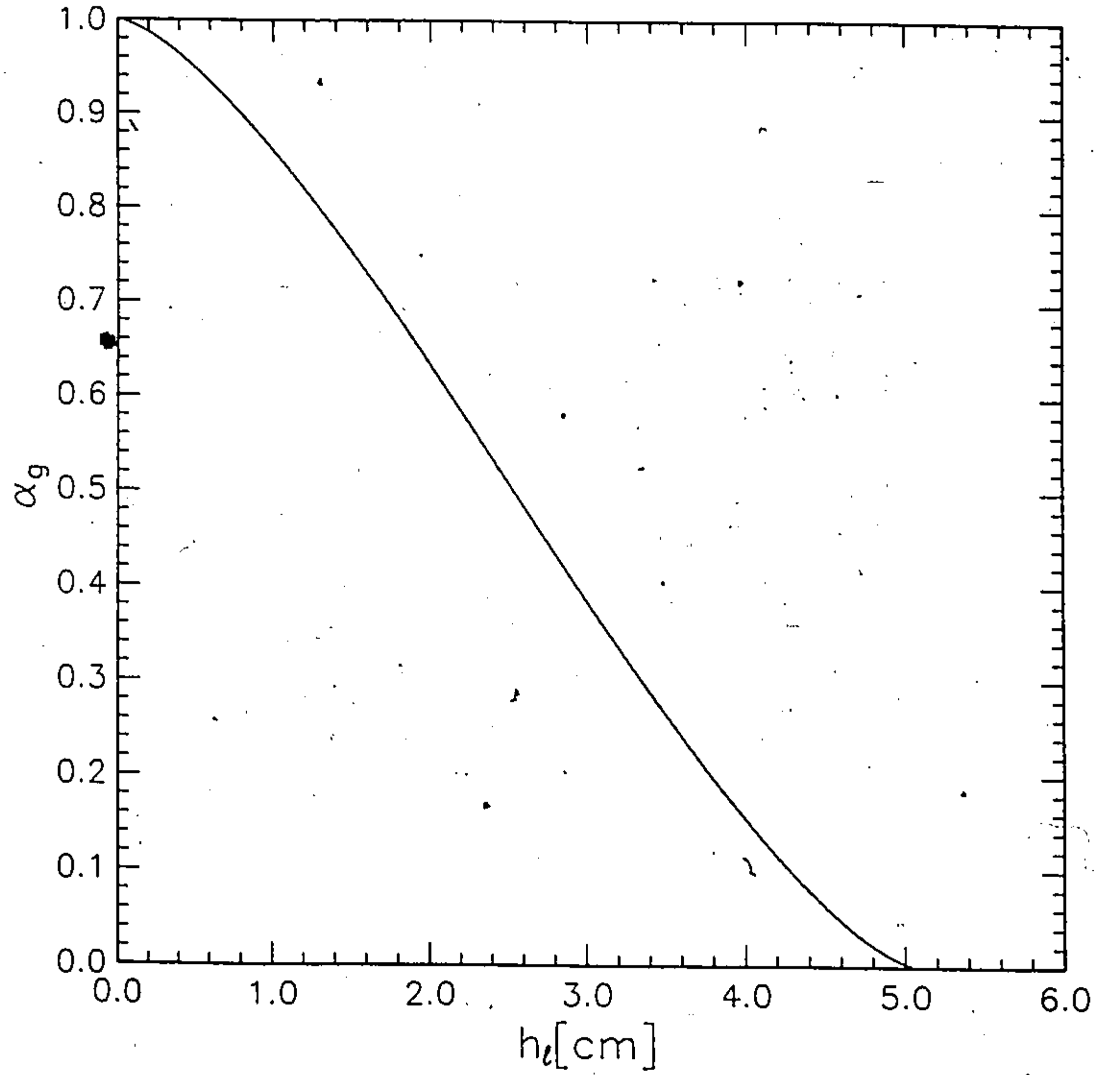

Figure I.1 Void Fraction for an Equilibrium Stratified Pipe Flow (5.08 cm i.d.).

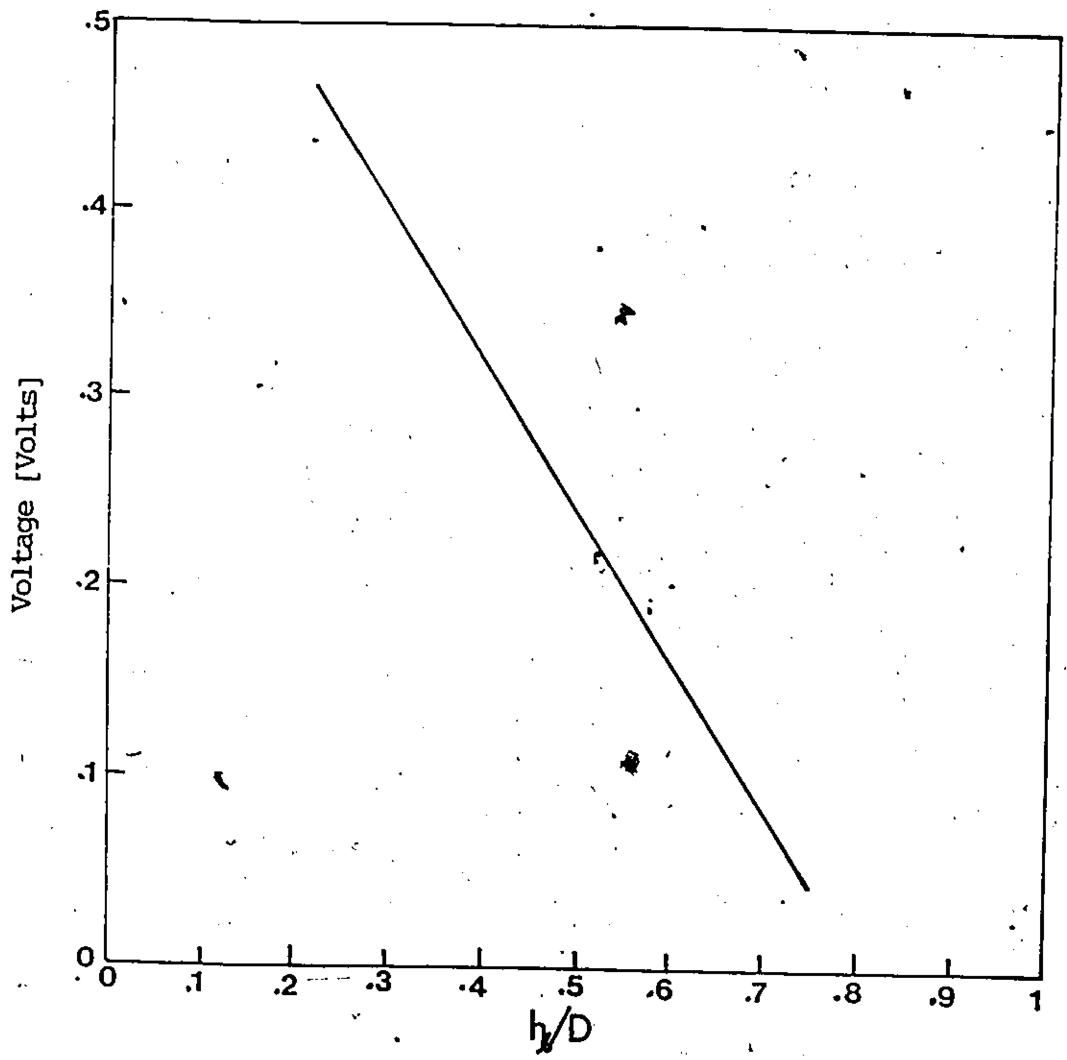

Figure I.2 Void Fraction Calibration Curve for a 5.08 cm i.d. Pipe.

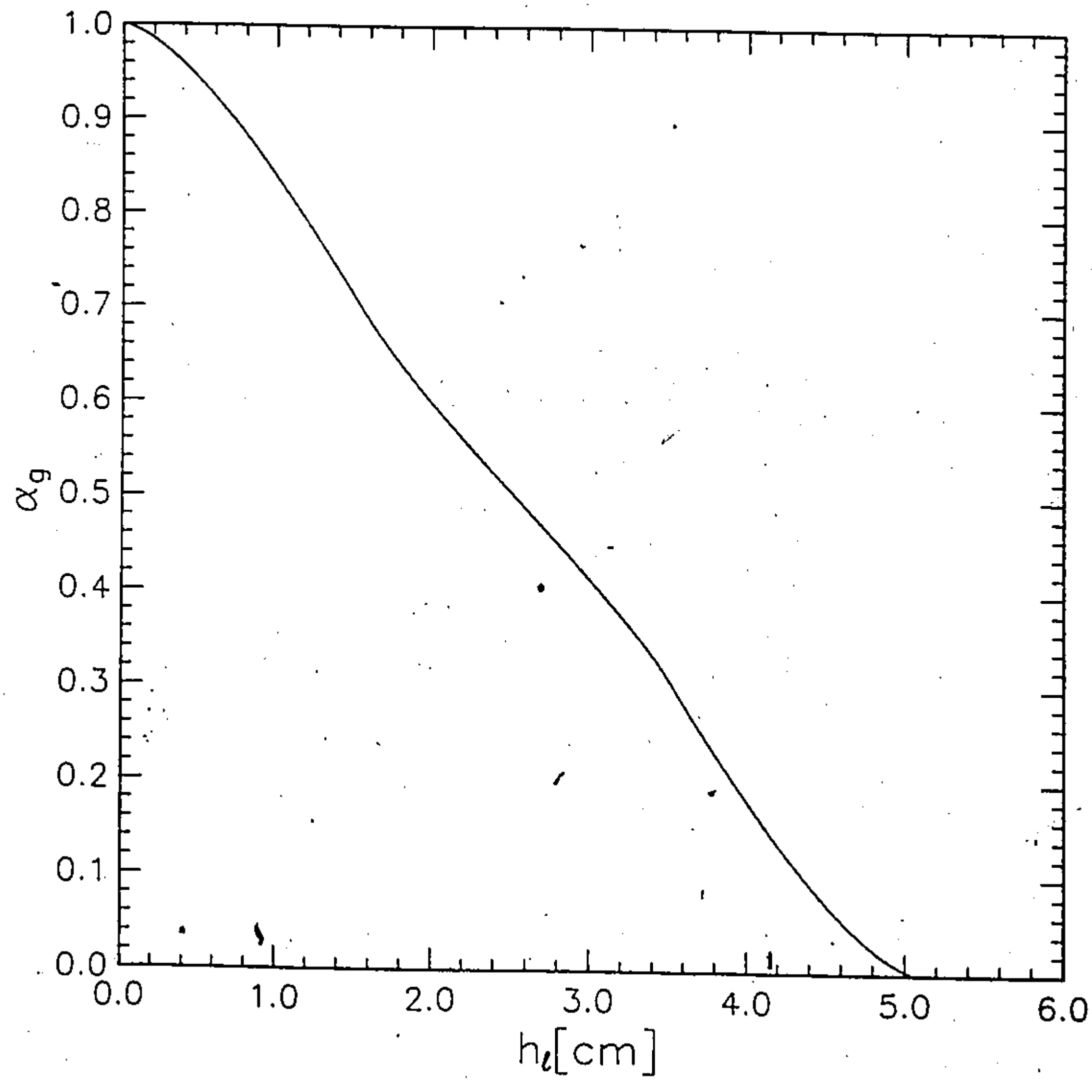

Figure I.3 Void Fraction for an Equilibrium Stratified Annulus Geometry of Inner-to-Outer Diamater Ratio, 0.375.

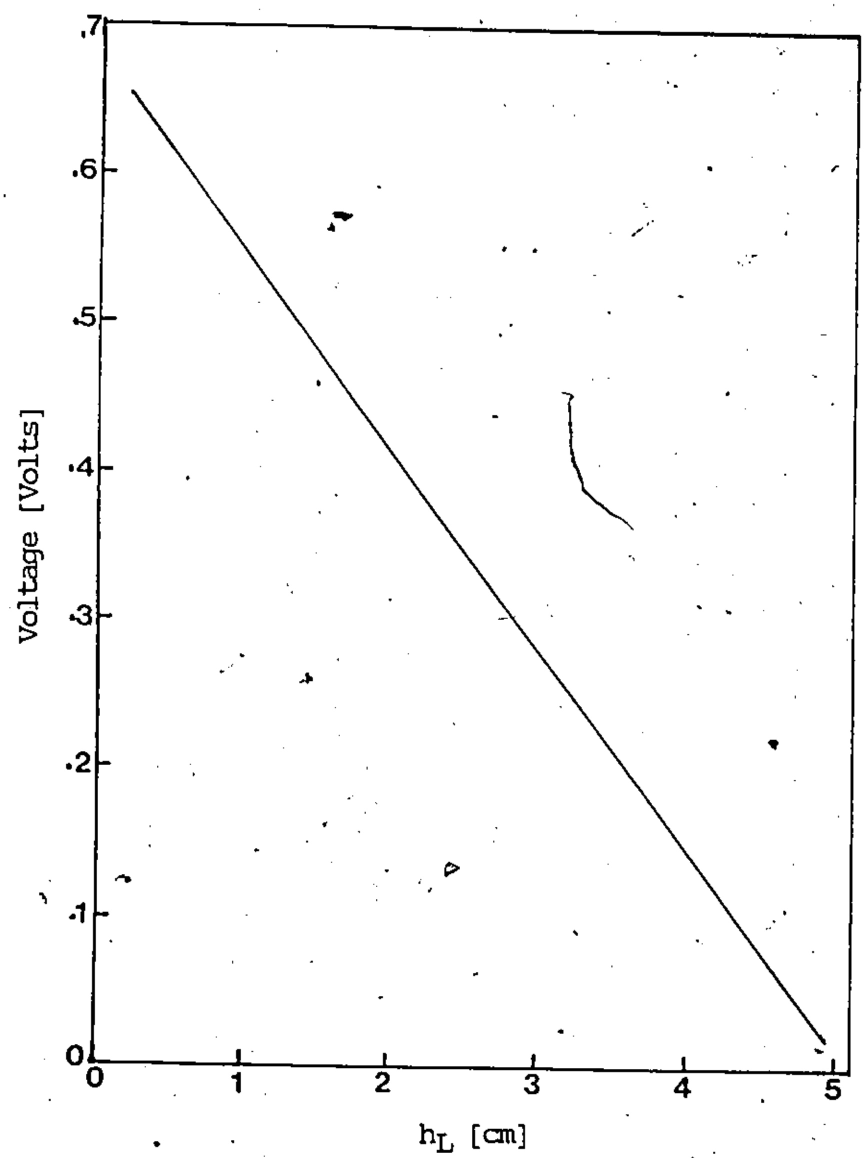

Figure I.4 Void Fraction Calibration Curve for Annulus Geometry of Inner-to-Outer Diameter Ratio, 0.375.

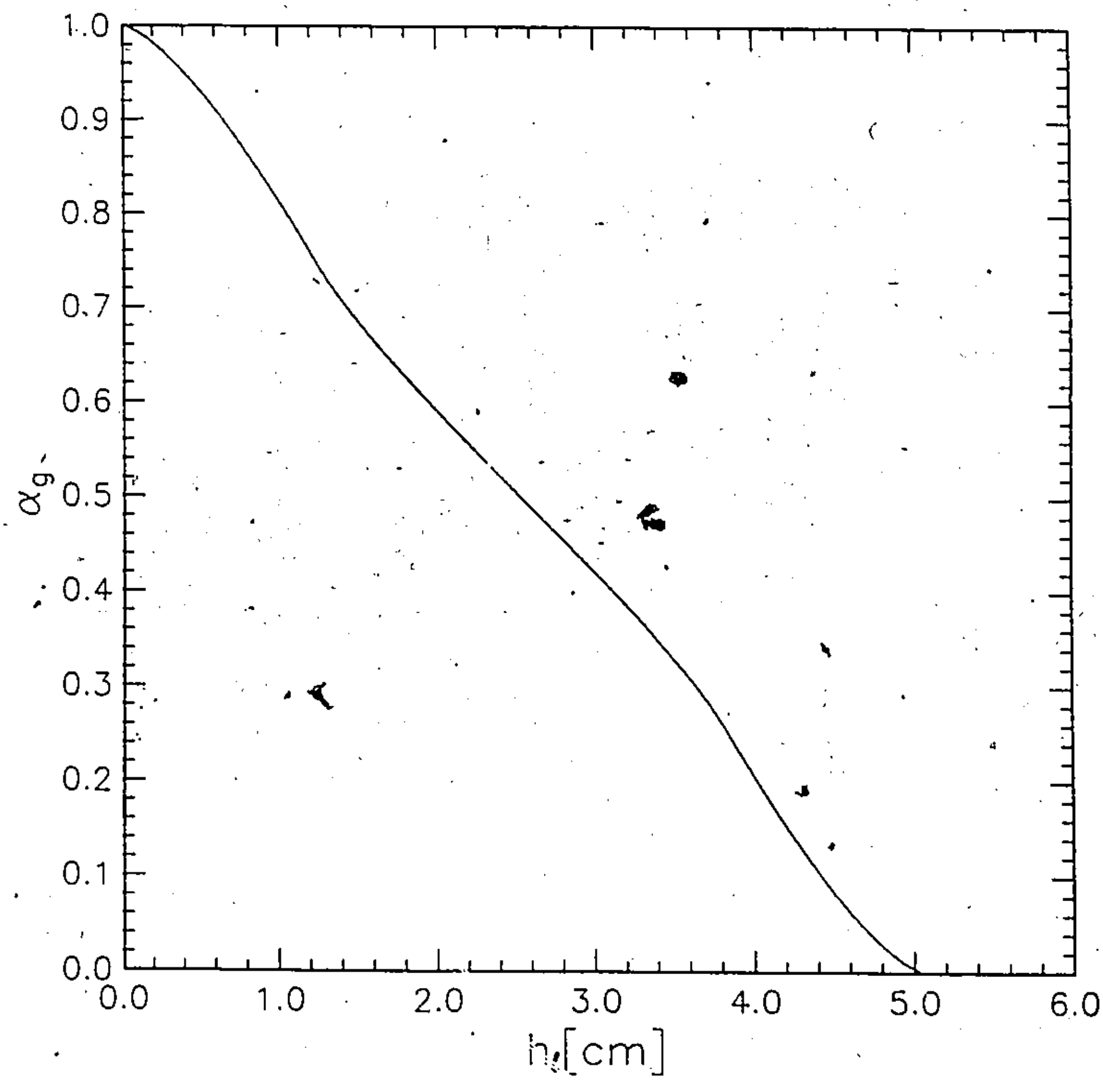

Figure I.5 Void Fraction for an Equilibrium Stratified Annulus Geometry of Inner-to-Outer Diameter Ratio, 0.500.

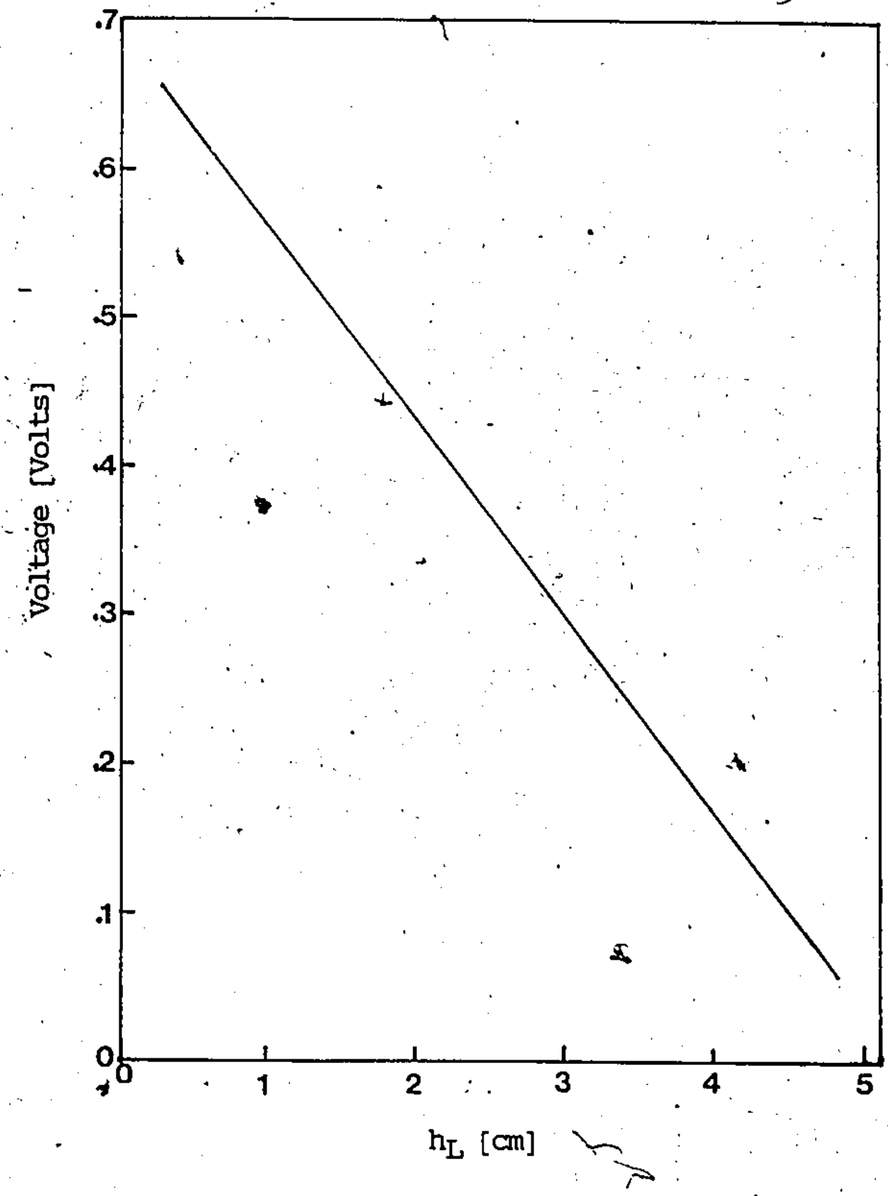

Figure I.6 Void Fraction Calibration Curve for Annulus Geometry of Inner-to-Outer Diameter Ratio, 0.500.

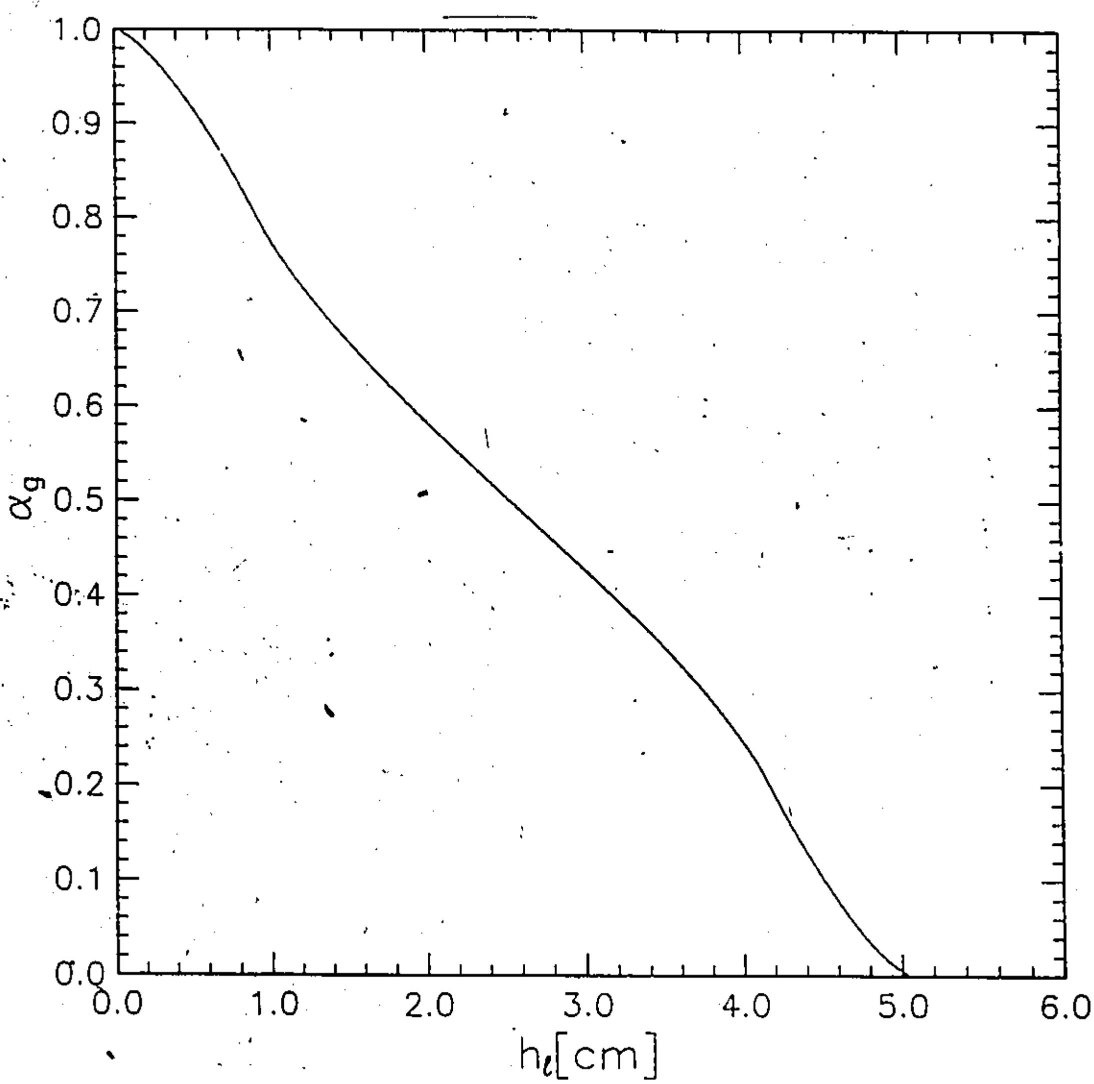

Figure I.7 **Void Fraction for an Equilibrium Stratified Annulus Geometry of Inner-to-Outer Diameter Ratio, 0.625.**

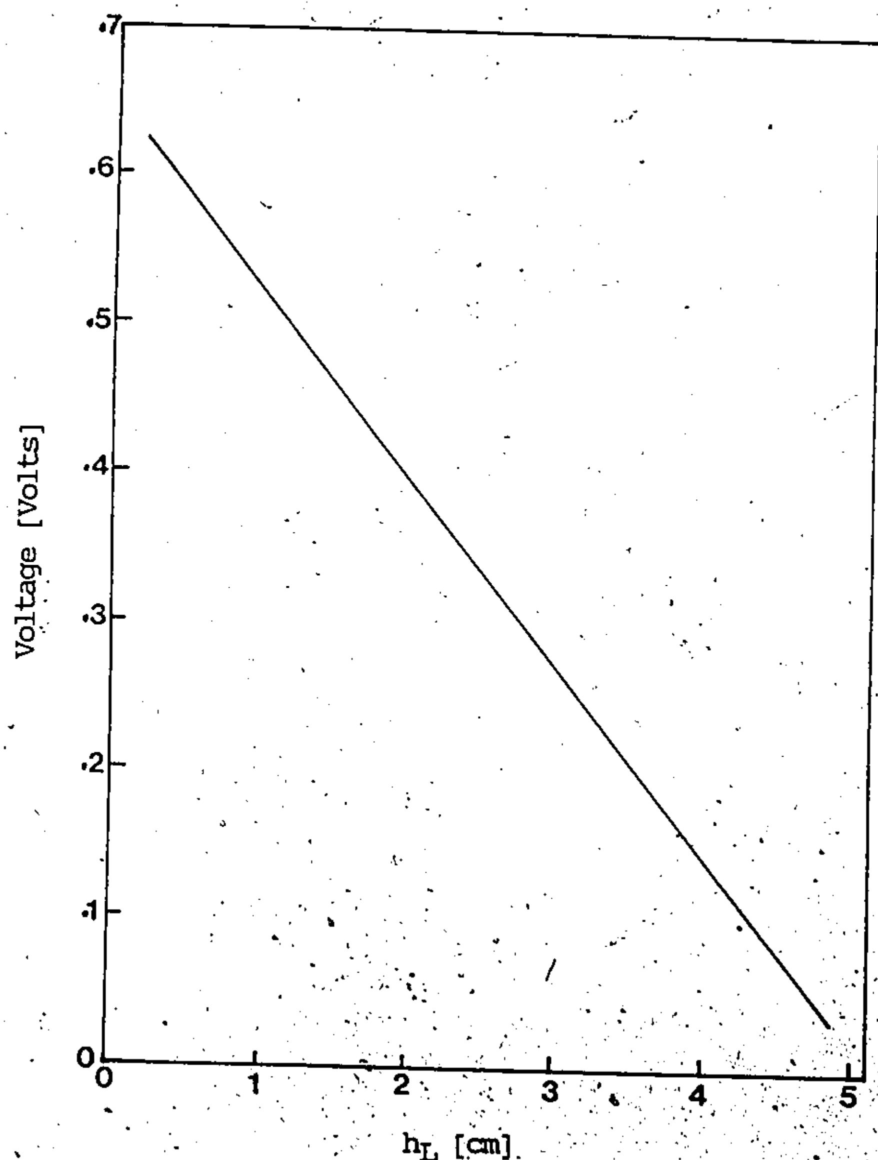

Figure I.8 Void Fraction Calibration Curve for Annulus Geometry of Inner-to-Outer Diameter Ratio, 0.625

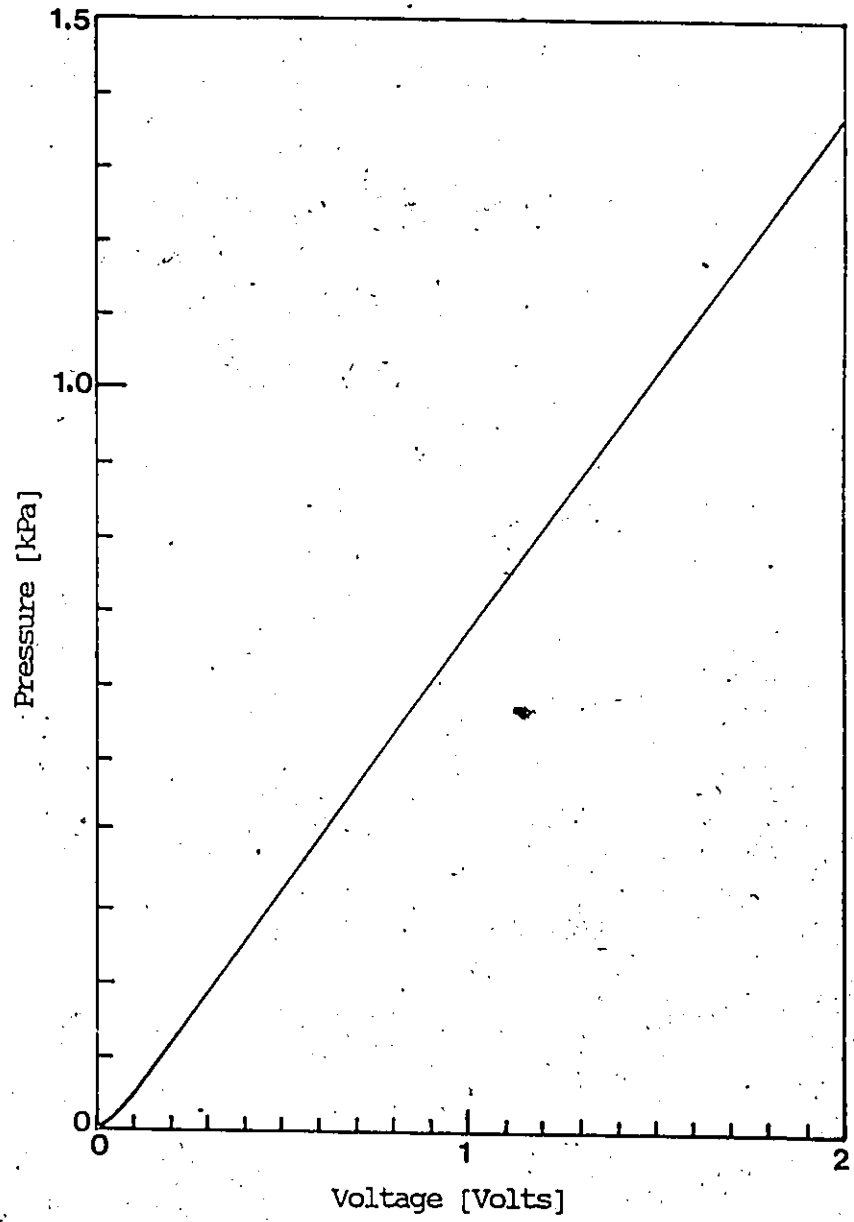

Figure 1.9 Pressure Drop Calibration Curve for the Annulus Flow Systems with a 1.38 kPa diaphragm.

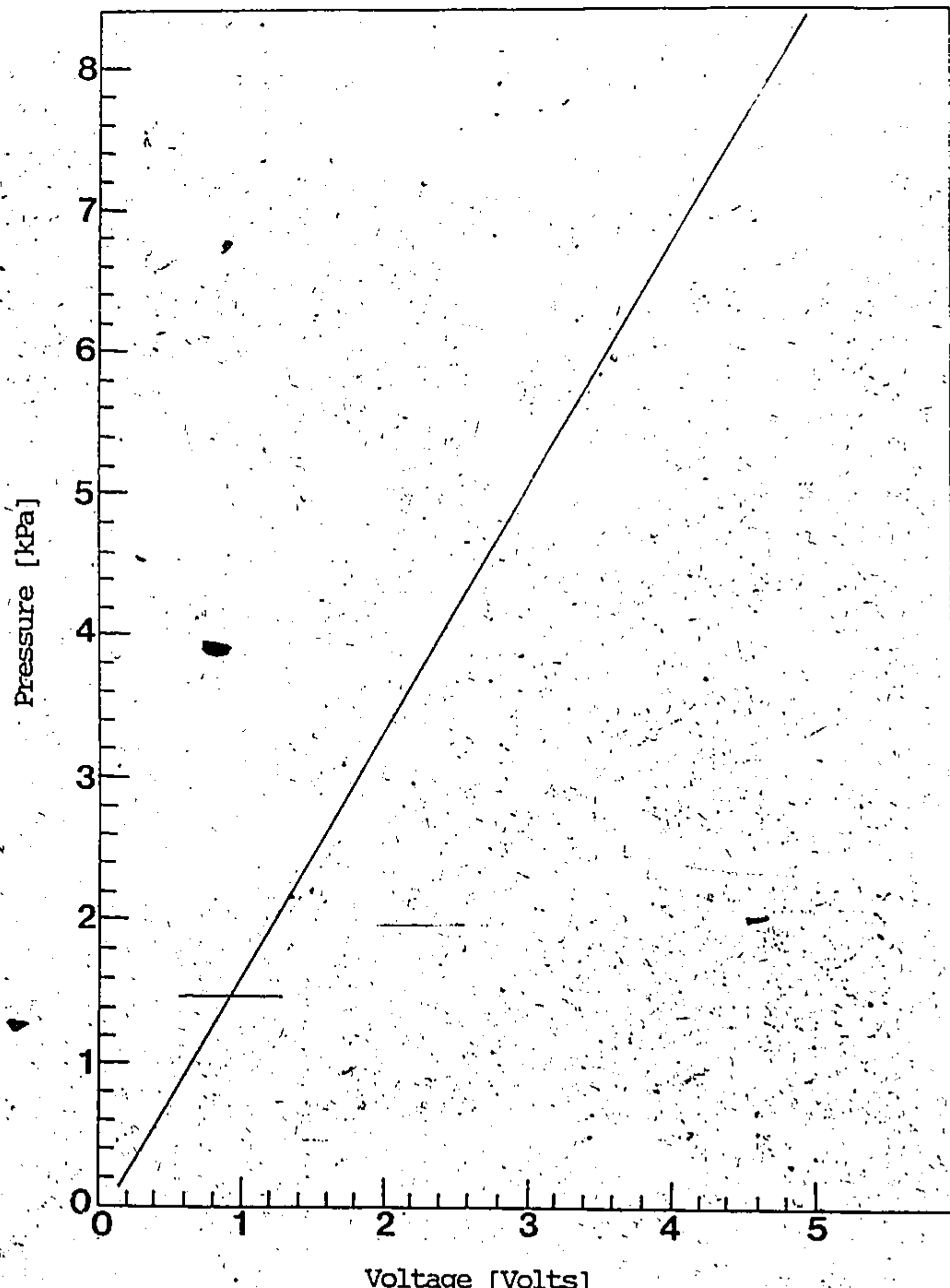

Figure 4.10 Pressure Drop Calibration Curve for the 37-Rod Bundle Flow System with an 8.62 kPa diaphragm.

APPENDIX II

Experimental Data

The measured and calculated experimental data are presented in this appendix. Further experimental time averaged void fraction results for various superficial liquid velocities, similar to those already discussed in the main text are also presented here. A typical result for flow pattern transitions in a split flow system at different junction angles is also given in this appendix.

Table II.1 Experimental Data for 5.08 cm i.d. Horizontal Pipe.

W_g (L/sec)	U_{gs} (m/sec)	Flow Pattern	α_g	File
Liquid Flow Rate = 0.105 L/sec, U_{ls} = 0.052 m/sec				
0.708	0.35	SS	0.65	TEST1
1.180	0.58	SS	0.65	TEST1
1.188	0.93	SS	0.65	T2
2.738	1.35	SS	0.66	SS1
3.493	1.72	SS	0.66	SS2
3.870	1.91	SS	0.68	SS3
4.909	2.42	SS	0.72	SS4
5.664	2.80	SS	0.75	SS5
6.136	3.03	SS	0.78	SS6
7.080	3.50	SS	0.81	SS7
7.552	3.73	SW	0.85	SW1
8.968	4.43	SW	0.87	SW2
9.912	4.89	SW	0.90	SW3
10.860	5.36	SW	0.94	SW4
Liquid Flow Rate = 0.167 L/sec, U_{ls} = 0.083 m/sec				
0.708	0.35	SS	0.56	-
1.180	0.58	SS	0.56	-
1.652	0.81	SS	0.56	-
2.360	1.16	SS	0.56	-
3.304	1.63	SS	0.56	-
4.248	2.10	SS	0.59	-
5.192	2.56	SS	0.67	-
6.136	3.03	SS	0.70	-
6.608	3.26	SS	0.75	-
7.080	3.49	SW	0.78	-
8.024	3.96	SW	0.80	SW5
8.968	4.42	SW	0.84	SW6
10.384	5.12	SW	0.91	SW7
Liquid Flow Rate = 0.278 L/sec, U_{ls} = 0.137 m/sec				
0.944	0.47	SS	0.39	-
1.888	0.93	SS	0.39	-
2.832	1.40	SS	0.40	-
3.776	1.86	SS	0.48	-
4.720	2.33	SS	0.56	-
5.192	2.56	SS	0.61	-
6.136	3.03	SS	0.66	-
6.608	3.26	SW	0.67	SW8
7.552	3.73	SW	0.76	SW9
8.496	4.19	SW	0.85	SW10
9.440	4.66	SW	0.88	SW11
10.860	5.36	SW	0.94	SW12

Table II.1 (Continued).

W_g (L/sec)	U_{gs} (m/sec)	Flow Pattern	α_g	File
Liquid Flow Rate = 0.389 L/sec, U_{ls} = 0.192 m/sec				
0.708	0.35	SS	0.29	–
1.180	0.58	SS	0.31	–
1.888	0.93	SS	0.32	–
2.832	1.40	SS	0.35	–
3.776	1.86	SS	0.51	–
4.248	2.10	SS	0.58	–
5.192	2.56	SS	0.59	–
5.664	2.80	SS	0.61	–
6.136	3.03	SW	0.66	–
6.608	3.26	SW	0.73	–
7.080	3.96	SL	0.96	SL1
8.024	3.96	SL	0.89	SL2
8.968	4.43	SW	0.99	SL3
9.912	4.89	SW	0.95	AN1
10.860	5.36	AN/WA	0.97	AN2
Liquid Flow Rate = 0.52 L/sec, U_{ls} = 0.257 m/sec				
0.708	0.35	SS	0.32	–
1.180	0.58	SS	0.34	–
1.935	0.95	SS	0.40	–
2.360	1.17	SS	0.48	–
2.832	1.40	SS	0.53	–
3.776	1.86	SS	0.58	–
4.720	2.33	SS	0.59	–
5.192	2.56	SW	0.62	–
5.758	2.84	SL	0.83	SL4
6.702	3.31	SL	0.90	SL5
7.552	3.73	SL	1.00	SL6
8.496	4.19	SL	1.00	SL7
9.440	4.66	AN/WA	1.00	AN3
10.860	5.36	AN/WA	1.00	AN4
Liquid Flow Rate = 0.60 L/sec, U_{ls} = 0.296 m/sec				
0.708	0.35	SS	0.29	–
1.180	0.58	SS	0.32	–
1.652	0.82	SS	0.37	–
2.360	1.17	SS	0.51	–
3.304	1.63	SS	0.54	–
3.965	1.96	SS/SW	0.54	–
4.720	2.33	SL	0.79	SL8
5.664	2.80	SL	1.00	SL9
6.608	3.26	SL	1.00	SL10
7.552	3.73	SL	1.00	–
8.968	4.43	SL	1.00	–
9.912	4.89	SL	1.00	–
10.860	5.36	SL/WA	1.00	–

Table II.1 (Continued).

W_g (L/sec)	U_{gs} (m/sec)	Flow Pattern	α_g	File
Liquid Flow Rate = 0.750 L/sec, U_{ls} = 0.370 m/sec				
0.708	0.35	SS	0.37	–
1.416	0.70	SS	0.40	–
2.360	1.17	SS	0.43	–
3.210	1.58	SL/PL	1.00	–
3.776	1.86	SL	1.00	SL14
4.720	2.33	SL	1.00	SL15
5.664	2.80	SL	1.00	SL16
6.702	3.31	SL	1.00	SL17
8.118	4.01	SL	1.00	SL18
8.968	4.43	SL	1.00	SL19
10.384	5.13	SL	1.00	SL20
Liquid Flow Rate = 0.900 L/sec, U_{ls} = 0.444 m/sec				
0.708	0.35	PL	0.38	PL2
1.086	0.54	PL	0.56	PL3
1.227	0.60	PL	0.72	PL4
1.794	0.89	PL	0.83	PL5
2.360	1.17	PL	0.81	PL6
3.304	1.63	SL	0.84	SL21
4.248	2.10	SL	0.93	SL22
5.664	2.80	SL	0.97	SL23
6.604	3.26	SL	1.00	SL24
7.552	3.73	SL	1.00	SL25
8.968	4.43	SL	1.00	SL26
9.912	4.89	SL	1.00	SL27
10.860	5.36	SL	1.00	SL28
Liquid Flow Rate = 1.055 L/sec, U_{ls} = 0.52 m/sec				
0.802	0.40	PL	0.61	PL7
1.227	0.61	PL	0.75	PL8
1.888	0.93	PL	0.79	PL9
2.738	1.35	PL	0.82	PL10
3.304	1.63	PL/SL	0.87	PL11
4.720	2.33	SL	0.96	SL29
5.664	2.80	SL	1.00	SL30
7.080	3.50	SL	1.00	SL31
8.024	3.96	SL	1.00	SL32
8.968	4.43	SL	1.00	SL33
9.914	4.89	SL	1.00	SL34
10.860	5.36	SL/AN	1.00	SL35

Table II.2 Experimental Data for Annulus Geometry of Inner-to-Outer Diameter Ratio of 0.375 (Pipe Diameter is 5.08 cm i.d., Rod Diameter is 1.905 cm)

W_g (L/sec)	U_{gs} (m/sec)	Flow Pattern	Void Fraction	Pressure Drop(kPa)	File
Liquid Flow Rate = 0.094 L/sec, U_{ls} = 0.054 m/sec					
1.038	0.60	SS	0.71	0.005	RUN1
1.416	0.81	SS	0.71	0.005	''
1.888	1.08	SS	0.71	0.005	''
2.832	1.63	SS	0.73	-0.010	SS1
4.248	2.44	SS	0.91	-0.015	SS2
5.192	2.98	SS	0.99	-0.010	SS3
6.230	3.58	SS	0.99	0.016	SS4
7.080	4.07	SS	0.99	0.019	SS5
8.024	4.61	SS	0.99	0.021	SS6
8.968	5.15	SW	1.00	0.026	SS7
9.912	5.69	SW	1.00	0.030	SS8
10.856	6.23	SW	1.00	0.036	SW1
Liquid Flow Rate = 0.111 L/sec, U_{ls} = 0.064 m/sec					
0.708	0.41	SS	0.64	0.005	-
1.180	0.68	SS	0.64	0.005	-
1.652	0.95	SS	0.64	0.005	-
2.360	1.36	SS	0.64	0.005	-
3.304	1.90	SS	0.64	0.005	-
4.719	2.71	SS	0.65	-0.015	-
5.758	3.31	SS	0.96	-0.005	SS9
6.608	3.79	SS	0.99	0.019	SS10
7.552	4.34	SS	1.00	-	-
8.496	4.88	SW	1.00	0.025	SW2
8.968	5.15	SW	1.00	0.028	SW3
9.912	5.69	SW	1.00	0.042	SW4
10.384	5.96	SW	1.00	0.041	SW5
10.856	6.23	SW	1.00	0.043	SW6

Table II.2 (Continued)

W_g (L/sec)	U_{gs} (m/sec)	Flow Pattern	Void Fraction	Pressure Drop (kPa)	File
Liquid Flow Rate = 0.161 L/sec, U_{ls} = 0.093 m/sec					
0.944	0.54	SS	0.53	0.005	-
1.888	1.08	SS	0.53	0.005	-
2.832	1.63	SS	0.53	0.005	-
3.776	2.17	SS	0.53	0.005	-
4.719	2.71	SS	0.53	0.00	-
5.192	2.98	SS	0.61	-0.020	-
5.662	3.25	SW	0.74	-0.010	-
6.136	3.52	SW	0.74	0.0	-
7.174	4.12	SW	0.74	0.020	SW7
8.024	4.61	SW	0.92	0.032	SW8
8.780	5.04	SW	0.97	0.044	SW9
9.534	5.47	SW	0.99	0.064	SW10
10.384	5.96	WA	1.00	0.063	AN1
11.328	6.50	WA	1.00	0.068	AN2
Liquid Flow Rate = 0.217 L/sec, U_{ls} = 0.125 m/sec					
0.944	0.54	SS	0.42	0.005	-
1.416	0.81	SS	0.42	0.005	-
1.888	1.08	SS	0.42	0.005	-
2.832	1.63	SS	0.42	0.005	-
3.776	2.17	SS	0.45	0.0	-
4.719	2.71	SS	0.45	0.015	-
5.192	2.98	SS	0.64	0.010	-
5.664	3.25	SW	0.67	0.021	-
6.136	3.52	SW	0.65	0.021	SW11
6.891	3.96	SW	0.69	0.025	SW12
7.600	4.36	SW	0.78	0.026	SW13
8.024	4.61	SW	0.86	0.032	SW14
8.968	5.15	SW	0.99	0.077	AN3
9.912	5.69	WA	0.99	0.099	AN4
10.384	5.96	WA	1.00	0.104	AN5
10.856	6.23	WA	1.00	0.118	AN6
11.328	6.50	WA	1.00	0.122	AN7

Table II.2 (Continued)

Liquid Flow Rate = 0.283 L/sec, U_{ls} = 0.163 m/sec					
W_g (L/sec)	U_{gs} (m/sec)	Flow Pattern	Void Fraction	Pressure Drop(kPa)	File
0.708	0.41	SS	0.30	0.005	–
1.652	0.95	SS	0.30	0.005	–
1.888	1.08	SS	0.30	0.005	–
2.832	1.63	SS	0.33	0.0	–
3.776	2.17	SS	0.42	0.0	–
4.719	2.71	SS	0.51	−0.015	–
5.664	3.25	SW	0.67	0.024	SW15
6.608	3.79	SW	0.90	0.031	SL1
7.552	4.34	SW	0.80	0.038	SL2
8.968	5.15	SW	0.97	0.09	AN8
9.912	5.69	WA	0.99	0.126	AN9
10.856	6.23	WA	1.00	0.142	AN10
Liquid Flow Rate = 0.400 L/sec, U_{ls} = 0.230 m/sec					
0.708	0.41	SS	0.14	0.005	–
0.944	0.54	SS	0.14	0.005	–
1.274	0.73	SS	0.18	0.005	–
1.652	0.95	SS	0.23	0.005	–
1.888	1.08	SS	0.25	0.005	–
2.360	1.36	SS	0.32	−0.010	–
2.832	1.63	PL	0.67	0.010	PL1
3.304	1.90	PL	0.73	0.014	PL2
3.776	2.17	SL	0.87	0.019	SL3
4.719	2.71	SL	0.93	0.025	SL4
5.664	3.25	SL	0.88	0.035	SL5
6.608	3.79	SL	0.87	0.049	SL6
7.552	4.34	SL	0.92	0.067	SL7
8.968	5.15	SL	0.96	0.107	SL8
9.912	5.69	WA	0.98	0.133	AN11
10.856	6.23	WA	0.99	0.171	AN12

Table II.2 (Continued)

W_g (L/sec)	U_{gs} (m/sec)	Flow Pattern	Void Fraction	Pressure Drop(kPa)	File
Liquid Flow Rate = 0.500 L/sec, U_{ls} = 0.288 m/sec					
0.944	0.54	PL	0.42	-	PL3
1.888	1.08	PL	0.83	0.032	PL4
2.832	1.63	PL	0.86	0.031	PL5
3.776	2.17	SL	0.86	0.025	SL9
4.719	2.71	SL	0.90	0.031	SL10
6.136	3.52	SL	0.90	0.044	SL11
7.080	4.07	SL	0.94	0.077	SL12
8.496	4.88	SL	0.96	0.130	SL13
9.912	5.69	WA	0.98	0.165	SL14
11.139	6.40	WA	0.99	0.174	AN13
Liquid Flow Rate = 0.622 L/sec, U_{ls} = 0.358 m/sec					
0.614	0.35	PL	0.41	0.025	PL6
1.038	0.60	PL	0.5[illegible]	0.036	PL7
1.416	0.81	PL	0.71	0.047	PL8
1.888	1.08	PL	0.73	0.035	PL9
2.832	1.63	PL	0.83	0.040	PL10
4.248	2.44	SL	0.86	0.035	SL15
5.664	3.25	SL	0.90	0.044	SL16
7.080	4.07	SL	0.92	0.070	SL17
8.496	4.88	SL	0.96	0.081	SL18
9.912	5.69	WA	0.97	0.144	SL19
11.328	6.50	WA	0.99	0.200	AN14
Liquid Flow Rate = 0.722 L/sec, U_{ls} = 0.416 m/sec					
0.708	0.41	PL	0.47	0.059	PL11
1.180	0.68	PL	0.61	0.069	PL12
1.794	1.03	PL	0.71	0.074	PL13
2.360	1.36	PL	0.78	0.049	PL14
3.304	1.90	SL	0.84	0.040	PL15
4.719	2.71	SL	0.86	0.034	SL20
5.664	3.25	SL	0.89	0.066	SL21
7.080	4.07	SL	0.93	0.049	SL22
8.024	4.61	SL	0.94	0.065	SL23
9.440	5.42	SL	0.96	0.097	SL24
10.856	6.23	WA	0.98	0.173	AN15

Table II.2 (Continued).

Liquid Flow Rate = 0.933 L/sec, U_{ls} = 0.538 m/sec					
W_g (L/sec)	U_{gs} (m/sec)	Flow Pattern	Void Fraction	Pressure Drop (kPa)	File
0.708	0.41	PL	0.28	0.117	PL16
1.274	0.73	PL	0.52	0.101	PL17
1.888	1.08	PL	0.67	0.096	PL18
2.832	1.63	PL	0.73	0.073	PL19
4.059	2.33	SL	0.81	0.073	SL25
5.192	2.98	SL	0.85	0.075	SL26
6.608	3.79	SL	0.90	0.061	SL27
8.024	4.61	SL	0.93	0.074	SL28
8.968	5.15	SL	0.96	0.087	SL29
10.384	5.96	SL	0.97	0.151	SL30
11.139	6.40	WA	0.97	0.166	AN16

Table II.3 Experimental Data for Annulus Geometry of Inner-to-Outer Diameter Ratio of 0.500 (Pipe Diameter = 5.08 cm i.d., Rod Diameter = 2.50 cm).

W_g (L/sec)	U_{gs} (m/sec)	Flow Pattern	Void Fraction	Pressure Drop(kPa)	File
Liquid Flow Rate = 0.10 L/sec, U_{ls} = 0.066 m/sec.					
0.708	0.47	SS	0.68	0.001	-
1.416	0.93	SS	0.68	0.001	-
1.888	1.24	SS	0.68	0.0	-
2.832	1.86	SS	0.65	-0.001	-
3.776	2.48	SS	0.69	-0.022	-
4.719	3.10	SS	0.80	-0.013	-
5.664	3.72	SS	0.86	0.020	-
6.608	4.34	SS	0.87	0.022	-
7.552	4.96	SS	0.96	0.034	PL1
8.024	5.27	SW	0.99	0.046	SW1
8.968	5.89	SW	1.00	0.133	SW2
9.912	6.51	SW	1.00	0.152	SW3
10.856	7.13	WA	1.00	0.168	SW4
Liquid Flow Rate = 0.155 L/sec, U_{ls} = 0.10 m/sec.					
0.708	0.47	SS	0.54	0.003	-
1.416	0.93	SS	0.54	0.003	-
1.888	1.24	SS	0.53	0.003	-
2.832	1.86	SS	0.54	0.002	-
3.776	2.48	SS	0.56	0.0	-
4.719	3.10	SS	0.65	0.015	-
5.664	3.72	SW	0.75	0.028	-
6.136	4.03	SW	0.75	0.031	-
7.080	4.65	SW	0.81	0.075	SW5
8.024	5.27	SW	0.98	0.147	SW6
8.968	5.89	WA	1.00	0.186	AN1
9.912	6.51	WA	1.00	0.210	AN2

Table II.3 (Continued)

W_g (L/sec)	U_{gs} (m/sec)	Flow Pattern	Void Fraction	Pressure Drop(kPa)	File
Liquid Flow Rate = 0.217 L/sec, U_{ls} = 0.142 m/sec.					
0.708	0.47	SS	0.42	0.007	–
1.416	0.93	SS	0.42	0.007	–
1.888	1.24	SS	0.42	0.006	–
2.832	1.86	SS	0.44	0.004	–
3.776	2.48	SS	0.53	-0.002	–
4.719	3.10	SW	0.68	0.00	–
5.664	3.72	SW	0.74	0.073	SW7
6.608	4.34	SW	0.77	0.082	SW8
7.552	4.96	SW	0.95	0.116	SW9
8.024	5.27	SL	0.96	0.168	SL1
9.062	5.95	WA	0.99	0.229	AN3
10.950	7.19	WA	1.00	0.282	AN4
Liquid Flow Rate = 0.278 L/sec, U_{ls} = 0.183 m/sec.					
0.708	0.47	SS	0.27	0.010	–
1.416	0.93	SS	0.27	0.010	–
1.888	1.24	SS	0.31	0.008	–
2.832	1.86	SS	0.43	0.006	–
3.776	2.48	SS	0.51	-0.015	–
4.719	3.10	SW	0.77	0.086	SL2
5.664	3.72	SL	0.94	0.090	SL3
6.608	4.34	SL	0.92	0.130	SL4
7.552	4.96	SL	0.96	0.164	SL5
8.496	5.58	SL	0.98	0.213	SL6
9.440	6.20	SL	0.99	0.280	AN5
10.384	6.82	WA	1.00	0.316	AN6
11.328	7.44	WA	1.00	0.345	AN7

Table II.3 (Continued).

Liquid Flow Rate = 0.339 L/sec, U_{ls} = 0.223 m/sec.					
W_g (L/sec)	U_{gs} (m/sec)	Flow Pattern	Void Fraction	Pressure Drop(kPa)	File
0.708	0.47	SS	0.37	0.027	-
1.558	0.93	SS	0.37	0.027	PL2
1.888	1.24	PL	0.51	0.032	PL3
2.832	1.86	PL	0.70	0.040	PL4
3.776	2.48	PL	0.92	0.066	PL5
4.719	3.10	SL	0.93	0.078	SL7
5.664	3.72	SL	0.94	0.120	SL8
6.608	4.34	SL	0.94	0.145	SL9
7.552	4.96	SL	0.96	0.167	SL10
8.496	5.58	SL	0.97	0.225	SL11
9.912	6.51	SL	0.99	0.319	SL12
10.856	7.13	WA	1.00	0.340	AN8
11.328	7.44	WA	1.00	0.369	AN9
Liquid Flow Rate = 0.433 L/sec, U_{ls} = 0.285 m/sec.					
1.416	0.93	PL	0.70	0.093	PL6
1.888	1.24	PL	0.82	0.096	PL7
2.832	1.86	PL	0.89	0.074	PL8
4.059	2.67	SL	0.89	0.076	SL13
4.719	3.10	SL	0.93	0.092	SL14
5.664	3.72	SL	0.91	0.139	SL15
6.608	4.34	SL	-	-	-
7.552	4.96	SL	0.95	0.162	SL16
8.496	5.58	SL	0.96	0.219	SL17
9.440	6.20	SL	0.97	0.298	AN10
10.384	6.82	SL	-	-	-
11.328	7.44	WA	0.99	0.369	AN11

Table II.3 (Continued).

W_g (L/sec)	U_{gs} (m/sec)	Flow Pattern	Void Fraction	Pressure Drop(kPa)	File
Liquid Flow Rate = 0.555 L/sec, U_{ls} = 0.365 m/sec.					
0.708	0.47	PL	0.57	0.099	PL9
1.416	0.93	PL	0.80	0.114	PL10
1.888	1.24	PL	0.81	0.124	PL11
2.832	1.86	PL	–	–	–
3.776	2.48	SL	0.87	0.082	SL18
4.719	3.10	SL	–	–	–
5.664	3.72	SL	0.92	0.105	SL19
6.608	4.34	SL	0.94	0.113	SL20
8.024	5.27	SL	0.96	0.175	SL21
8.968	5.89	SL	–	–	–
9.912	6.51	WA	0.97	0.307	AN12
11.328	7.44	WA	0.99	0.373	AN13
Liquid Flow Rate = 0.700 L/sec, U_{ls} = 0.460 m/sec.					
0.708	0.47	PL	0.54	0.159	PL12
1.180	0.78	PL	–	–	–
1.888	1.24	PL	0.81	0.140	PL13
2.832	1.86	PL	–	–	–
3.776	2.48	SL	0.89	0.117	SL22
4.719	3.10	SL	–	–	–
5.664	3.72	SL	0.91	0.089	SL23
6.608	4.34	SL	–	–	–
8.024	5.27	SL	0.95	0.158	SL24
8.968	5.89	SL	–	–	–
10.384	6.82	WA	0.98	0.363	AN14
11.328	7.44	WA	–	–	–
Liquid Flow Rate = 0.890 L/sec, U_{ls} = 0.584 m/sec.					
0.708	0.47	PL	0.38	0.183	PL14
1.416	0.93	PL	0.68	0.217	PL15
1.888	1.24	PL	0.70	0.166	PL16
3.021	1.98	PL	0.84	0.132	PL17
4.248	2.79	SL	0.82	0.129	SL25
5.192	3.41	SL	–	–	–
6.136	4.03	SL	0.89	0.135	SL26
7.080	4.65	SL	0.93	0.168	SL27
8.496	5.58	SL	0.95	0.169	SL28
9.440	6.20	SL	–	–	–
10.384	6.82	SL	–	–	–
11.328	7.44	WA	–	–	–

Table II.4 Experimental Data for Annulus Geometry of Inner-to-Outer Diameter Ratio of 0.625 (Pipe Diameter = 5.08 cm i.d., Rod Diameter = 3.175 cm).

W_g (L/sec)	U_{gs} (m/sec)	Flow Pattern	Void Fraction	Pressure Drop(kPa)	File
Liquid Flow Rate = 0.009 L/sec, U_{ls} = 0.072 m/sec.					
0.472	0.38	SS	0.63	0.0	–
2.360	1.91	SS	0.63	0.0	–
2.832	2.29	SS	0.65	0.0	–
3.304	2.67	SS	0.68	-0.018	–
3.776	3.06	SS	0.70	-0.015	–
4.248	3.44	SS	0.79	0.0	–
4.719	3.82	SW	0.80	0.020	SW1
5.192	4.20	SW	0.80	0.022	SW2
5.662	4.58	SW	0.79	0.024	SW3
6 136	4.97	SW	0.79	0.028	SW4
6.608	5.35	SW	0.83	0.047	SW5
7.080	5.73	WA	0.98	0.075	AN1
7.552	6.11	WA	1.00	0.074	AN2
8.496	6.88	WA	1.00	0.084	AN3
9.912	8.02	WA	1.00	0.111	AN4
Liquid Flow Rate = 0.111 L/sec, U_{ls} = 0.09 m/sec.					
0.472	0.38	SS	0.56	0.0	SS1
2.360	1.91	SS	0.56	0.0	–
2.832	2.29	SS	0.57	0.0	–
3.776	3.06	SS	0.65	-0.015	–
4.106	3.32	SW	0.74	-0.006	–
4.248	3.44	SW	0.75	0.020	SW6
4.719	3.82	SW	0.74	0.024	SW7
5.192	4.20	SW	0.75	0.027	SW8
6.136	4.97	SW	0.78	0.036	SW9
6.608	5.35	SW	0.81	0.055	SW10
7.080	5.73	WA	0.95	0.077	AN5
7.552	6.11	WA	0.99	0.104	SL1
8.024	6.49	WA	1.00	0.117	AN6
8.968	7.26	WA	1.00	0.129	AN7
10.384	8.40	WA	1.00	0.162	AN8

Table II.4 (Continued).

W_g (L/sec)	U_{gs} (m/sec)	Flow Pattern	Void Fraction	Pressure Drop(kPa)	File
Liquid Flow Rate = 0.139 L/sec, U_{ls} = 0.112 m/sec.					
0.472	0.38	SS	0.48	0.0	-
1.888	1.53	SS	0.48	0.0	-
2.360	1.91	SS	0.50	0.0	-
2.832	2.29	SS	0.51	0.0	-
3.304	2.67	SS	0.58	0.0	-
3.776	3.06	SS	0.73	-0.01	-
4.059	3.29	SW	0.72	0.0	-
4.248	3.44	SW	0.72	0.024	SW11
4.719	3.82	SW	0.73	0.028	SW12
5.192	4.20	SW	0.74	0.032	SW13
5.665	4.58	SW	0.75	0.037	SW14
6.325	5.12	SW	0.81	0.059	SW15
6.608	5.35	SW	0.88	0.067	SW16
7.363	5.96	WA	0.98	0.086	AN9
8.496	6.88	WA	1.00	0.149	AN10
9.912	8.02	WA	1.00	0.174	AN11
Liquid Flow Rate = 0.178 L/sec, U_{ls} = 0.144 m/sec.					
1.888	1.53	SS	0.43	0.015	-
2.832	2.29	SS	0.48	0.017	-
3.304	2.67	SS	0.56	0.009	-
3.587	2.90	SW	0.68	0.006	-
3.870	3.13	SW	0.68	0.014	SW17
4.248	3.44	SW	0.69	0.039	SW13
4.719	3.82	SW	0.73	0.047	SW18
5.003	4.05	SW	0.74	0.047	SW19
5.664	4.58	SW	0.80	0.059	SW20
6.136	4.97	SW	0.89	0.070	SL1
6.608	5.35	SW	0.94	0.095	SL2
7.080	5.73	SW	0.97	0.098	SL3
7.552	6.11	WA	0.98	0.124	SL4
8.213	6.65	WA	0.99	0.153	AN12
8.968	7.26	WA	1.00	0.174	AN13
9.912	8.02	WA	1.00	-	AN14

Table II.4 (Continued).

W_g (L/sec)	U_{gs} (m/sec)	Flow Pattern	Void Fraction	Pressure Drop(kPa)	File
Liquid Flow Rate = 0.222 L/sec, U_{ls} = 0.180 m/sec.					
0.472	0.38	SS	0.37	0.006	-
2.360	1.91	SS	0.37	0.006	-
2.832	2.29	SS	0.51	-0.010	SW21
3.304	2.67	SW	0.65	-	SW22
3.776	3.06	SW	0.76	0.034	SL5
4.248	3.44	SL	0.86	0.040	SL6
4.719	3.82	SL	0.89	0.037	SL7
5.664	4.58	SL	0.90	0.073	SL8
6.608	5.35	SL	0.95	0.111	SL9
7.552	6.11	SL	0.98	0.120	SL10
8.496	6.88	WA	0.99	0.179	AN15
9.440	7.64	WA	1.00	0.215	AN16
10.384	8.40	WA	1.00	0.235	AN17
Liquid Flow Rate = 0.255 L/sec, U_{ls} = 0.208 m/sec.					
0.614	0.57	PL	0.33	0.013	PL1
0.708	0.76	PL	0.43	0.010	PL2
0.944	1.15	PL	0.60	0.015	PL3
1.416	1.53	PL	0.57	0.023	PL4
1.888	1.91	PL	0.72	-	PL5
2.360	2.29	SL	0.80	0.017	PL6
2.832	3.06	SL	0.90	0.029	SL11
3.776	3.82	SL	0.91	0.036	SL12
4.719	4.58	SL	0.92	0.081	SL13
5.664	5.35	SL	0.96	0.098	SL14
7.552	6.11	SL	0.98	0.124	SL15
8.496	6.88	WA	0.99	0.198	AN18
9.440	7.64	WA	0.99	0.209	AN19
10.384	8.40	WA	1.00	0.237	AN20

Table II.4 (Continued).

W_g (L/sec)	U_{gs} (m/sec)	Flow Pattern	Void Fraction	Pressure Drop(kPa)	File
Liquid Flow Rate = 0.333 L/sec, U_{ls} = 0.270 m/sec.					
0.708	0.57	PL	0.61	0.030	PL7
1.180	0.96	PL	0.79	0.029	PL8
1.652	1.34	PL	0.84	0.031	PL9
2.360	1.91	SL	0.91	0.028	SL16
3.304	2.67	SL	0.90	0.028	SL17
4.248	3.44	SL	0.91	0.029	SL18
5.192	4.20	SL	0.90	0.083	SL19
6.136	4.97	SL	0.94	0.090	SL20
7.080	5.73	SL	0.96	0.113	SL21
8.024	6.49	SL	0.97	0.156	AN21
9.440	7.64	WA	0.99	0.241	AN22
10.384	8.40	WA	1.00	0.256	AN23
Liquid Flow Rate = 0.444 L/sec, U_{ls} = 0.360 m/sec.					
0.708	0.57	PL	0.69	0.061	PL10
1.416	1.15	PL	0.84	0.057	PL11
1.888	1.53	PL	0.87	0.036	PL12
2.360	1.91	SL	0.89	0.025	SL22
3.304	2.67	SL	0.89	0.027	SL23
4.719	3.82	SL	0.88	0.067	SL24
5.664	4.58	SL	0.93	0.061	SL25
6.608	5.35	SL	0.95	0.102	SL26
7.552	6.11	SL	0.96	0.140	AN24
8.496	6.88	SL	0.97	0.228	AN25
9.440	7.64	WA	0.99	0.243	AN26
10.384	8.40	WA	1.00	0.268	AN27

Table II.4 (Continued).

Wg (L/sec)	Ugs (m/sec)	Flow Pattern	Void Fraction	Pressure Drop(kPa)	File
Liquid Flow Rate = 0.611 L/sec, U_{ls} = 0.494 m/sec.					
0.472	0.38	PL	0.48	0.102	PL13
0.944	0.76	PL	0.65	0.109	PL14
1.888	1.53	PL	0.84	0.047	PL15
2.832	2.29	SL	0.84	0.042	SL27
3.776	3.06	SL	–	–	–
4.719	3.82	SL	–	–	–
6.136	4.97	SL	–	–	–
7.080	5.73	SL	–	–	–
8.024	6.49	SL	–	–	–
8.968	7.26	WA	0.98	0.216	AN28
9.912	7.64	WA	0.99	0.266	AN29
Liquid Flow Rate = 0.822 L/sec, U_{ls} = 0.665 m/sec.					
0.472	0.38	PL	–	–	–
0.944	0.76	PL	–	–	–
1.888	1.53	PL	–	–	–
2.832	2.29	SL	–	–	–
3.776	3.06	SL	–	–	–
4.719	3.82	SL	–	–	–
5.664	4.59	SL	–	–	–
7.080	5.73	SL	–	–	–
8.024	6.49	SL	–	–	–
8.496	6.88	WA	–	–	–
9.440	7.64	WA	–	–	–
10.384	8.40	WA	–	–	–

Table II.5 Experimental Data for the 37-Rod Bundle Geometry
(Pipe i.d. = 10.16 cm, Rod Diameter = 1.27 cm).

Liquid Flow Rate = 0.111 L/sec, U_{ls} = 0.032 m/sec.

W_g (L/sec)	U_{gs} (m/sec)	Flow Pattern	Void Fraction	Presure Drop(kPa)	File
0.472	0.14	SS	0.92	0.184	-
1.416	0.41	SS	0.92	0.184	-
2.360	0.69	SS	0.92	0.184	-
3.304	0.97	SS	0.92	0.184	-
4.248	1.24	SS	0.92	0.167	-
5.192	1.52	SS	0.92	0.167	-
6.136	1.79	SS	0.92	0.131	-
7.080	2.07	SS	0.92	0.114	-
8.024	2.35	SS	0.94	0.149	-
8.968	2.63	SS	0.94	0.149	-
9.912	2.90	SS	0.94	0.078	-
11.328	3.31	SW	0.96	0.078	-

Liquid Flow Rate = 0.222 L/sec, U_{ls} = 0.064 m/sec.

W_g (L/sec)	U_{gs} (m/sec)	Flow Pattern	Void Fraction	Presure Drop(kPa)	File
0.472	0.14	SS	0.84	0.096	-
1.146	0.41	SS	0.83	0.096	-
2.360	0.69	SS	0.83	0.114	-
3.304	0.97	SS	0.83	0.114	-
4.248	1.24	SS	0.83	0.096	-
5.192	1.52	SS	0.84	0.096	-
6.136	1.79	SS	0.86	0.096	-
7.080	2.07	SS	0.86	0.096	-
8.024	2.35	SS	0.86	0.096	-
8.968	2.63	SS	0.86	0.096	-
9.912	2.90	SW	0.88	0.096	-
11.328	3.31	SW	0.92	0.149	-

Table II.5 (Continued).

Liquid Flow Rate = 0.333 L/sec, U_{ls} = 0.097 m/sec.					
W_g (L/sec)	U_{gs} (m/sec)	Flow Pattern	Void Fraction	Presure Drop(kPa)	File
0.472	0.14	SS	0.70	0.184	–
1.416	0.41	SS	0.72	0.184	–
2.360	0.69	SS	0.74	0.184	–
3.304	0.97	SS	0.74	0.184	–
4.248	1.24	SS	0.76	0.202	–
5.192	1.52	SS	0.78	0.202	–
6.136	1.79	SS	0.78	0.202	–
7.080	2.07	SS	0.78	0.202	–
8.024	2.35	SW	0.72	0.219	SS1
8.968	2.63	SW	0.72	0.184	SW1
9.912	2.90	SW	0.80	0.202	SW2
11.328	3.31	SW	0.82	0.219	SW3
Liquid Flow Rate = 0.444 L/sec, U_{ls} = 0.129 m/sec.					
W_g (L/sec)	U_{gs} (m/sec)	Flow Pattern	Void Fraction	Presure Drop(kPa)	File
0.472	0.14	SS	0.54	0.361	–
1.416	0.41	PL	0.54	0.343	–
2.360	0.69	PL	0.75	0.325	–
3.304	0.97	PL	0.76	0.325	–
4.248	1.24	PL	0.76	0.325	–
5.192	1.52	SL	0.75	0.219	SL1
6.136	1.79	SL	0.75	0.237	SL2
7.080	2.07	SL	0.76	0.219	SL3
8.024	2.35	SW	0.80	0.219	–
8.968	2.63	SW	0.80	0.237	–
9.912	2.90	SW	0.82	0.237	–
11.328	3.31	SL	0.82	0.219	SL4

Table II.5 (Continued).

Liquid Flow Rate = 0.555 L/sec, U_{ls} = 0.161 m/sec.					
W_g (L/sec)	U_{gs} (m/sec)	Flow Pattern	Void Fraction	Pressure Drop(kPa)	File
0.519	0.15	PL	0.61	0.219	PL1
1.416	0.41	PL	0.52	0.202	PL2
2.360	0.69	PL	0.61	0.219	PL3
3.304	0.97	PL	0.52	0.219	PL4
4.248	1.24	PL	0.60	0.219	PL5
5.192	1.52	SL	0.76	0.237	SL5
6.136	1.79	SL	0.72	0.237	SL6
7.080	2.07	SL	0.75	0.255	SL7
8.024	2.35	SL	0.76	0.255	SL8
8.968	2.63	SL	0.54	0.237	SL9
9.912	2.90	SL	0.56	0.237	SL10
11.328	3.31	SL	0.62	0.237	SL11
Liquid Flow Rate = 0.666 L/sec, U_{ls} = 0.193 m/sec.					
W_g (L/sec)	U_{gs} (m/sec)	Flow Pattern	Void Fraction	Pressure Drop(kPa)	File
0.472	0.14	PL	0.22	0.202	PL6
1.416	0.41	PL	0.21	0.202	PL7
2.360	0.69	PL	0.29	0.219	PL8
3.304	0.97	PL	0.30	0.219	PL9
4.248	1.24	SL	0.42	0.219	SL12
5.192	1.52	SL	0.52	0.237	SL13
6.136	1.79	SL	0.52	0.272	SL14
7.080	2.07	SL	0.60	0.272	SL15
8.024	2.35	SL	0.52	0.272	SL16
8.968	2.63	SL	0.56	0.272	SL17
9.912	2.90	SL	0.54	0.272	SL18
11.328	3.31	SL	0.80	0.290	SL19

Table II.5 (Continued).

Liquid Flow Rate = 0.777 L/sec, U_{ls} = 0.225 m/sec.					
W_g (L/sec)	U_{gs} (m/sec)	Flow Pattern	Void Fraction	Pressure Drop(kPa)	File
0.472	0.14	PL	0.22	0.202	PL10
1.416	0.41	PL	0.29	0.219	PL11
2.360	0.69	PL	0.48	0.219	PL12
3.304	0.97	PL	0.62	0.219	PL13
4.248	1.24	SL	0.72	0.237	PL14
5.192	1.52	SL	0.73	0.255	SL20
6.136	1.79	SL	0.72	0.272	SL21
7.080	2.07	SL	0.76	0.290	SL22
8.024	2.35	SL	0.79	0.290	SL23
8.968	2.63	SL	0.76	0.290	SL24
9.912	2.90	SL	0.79	0.308	SL25
11.328	3.31	SL	0.77	0.308	SL26
Liquid Flow Rate = 0.944 L/sec, U_{ls} = 0.274 m/sec.					
W_g (L/sec)	U_{gs} (m/sec)	Flow Pattern	Void Fraction	Pressure Drop(kPa)	File
0.472	0.14	EB	0.11	0.237	EB1
0.944	0.28	EB	0.16	0.237	EB2
1.888	0.55	PL	0.35	0.255	PL15
2.832	0.83	PL	0.48	0.272	PL16
3.776	1.10	SL	0.65	0.290	PL17
4.719	1.38	SL	0.68	0.255	SL27
5.664	1.66	SL	0.69	0.272	SL28
6.608	1.93	SL	0.70	0.290	SL29
7.552	2.21	SL	0.72	0.308	SL30
8.496	2.48	SL	0.76	0.308	SL31
9.440	2.76	SL	0.75	0.290	SL32
10.384	3.04	WA	0.74	0.325	SL33
11.328	3.31	WA	0.75	0.325	AN1

Table II.5 (Continued).

Liquid Flow Rate = 1.110 L/sec, U_{ls} = 0.322 m/sec.					
W_g (L/sec)	U_{gs} (m/sec)	Flow Pattern	Void Fraction	Pressure Drop(kPa)	File
0.472	0.14	EB	0.08	0.219	EB3
1.416	0.41	EB	0.15	0.237	EB4
2.360	0.69	EB	0.24	0.255	EB5
3.306	0.97	PL	0.30	0.255	PL18
4.248	1.24	PL	0.54	0.272	SL34
5.192	1.52	SL	0.60	0.290	SL35
6.136	1.79	SL	0.61	0.290	SL36
7.080	2.07	SL	0.62	0.290	SL37
8.024	2.35	SL	0.67	0.308	SL38
8.968	2.63	SL	0.66	0.308	SL39
9.912	2.90	WA	0.68	0.343	SL40
11.328	3.31	WA	0.66	0.325	AN2

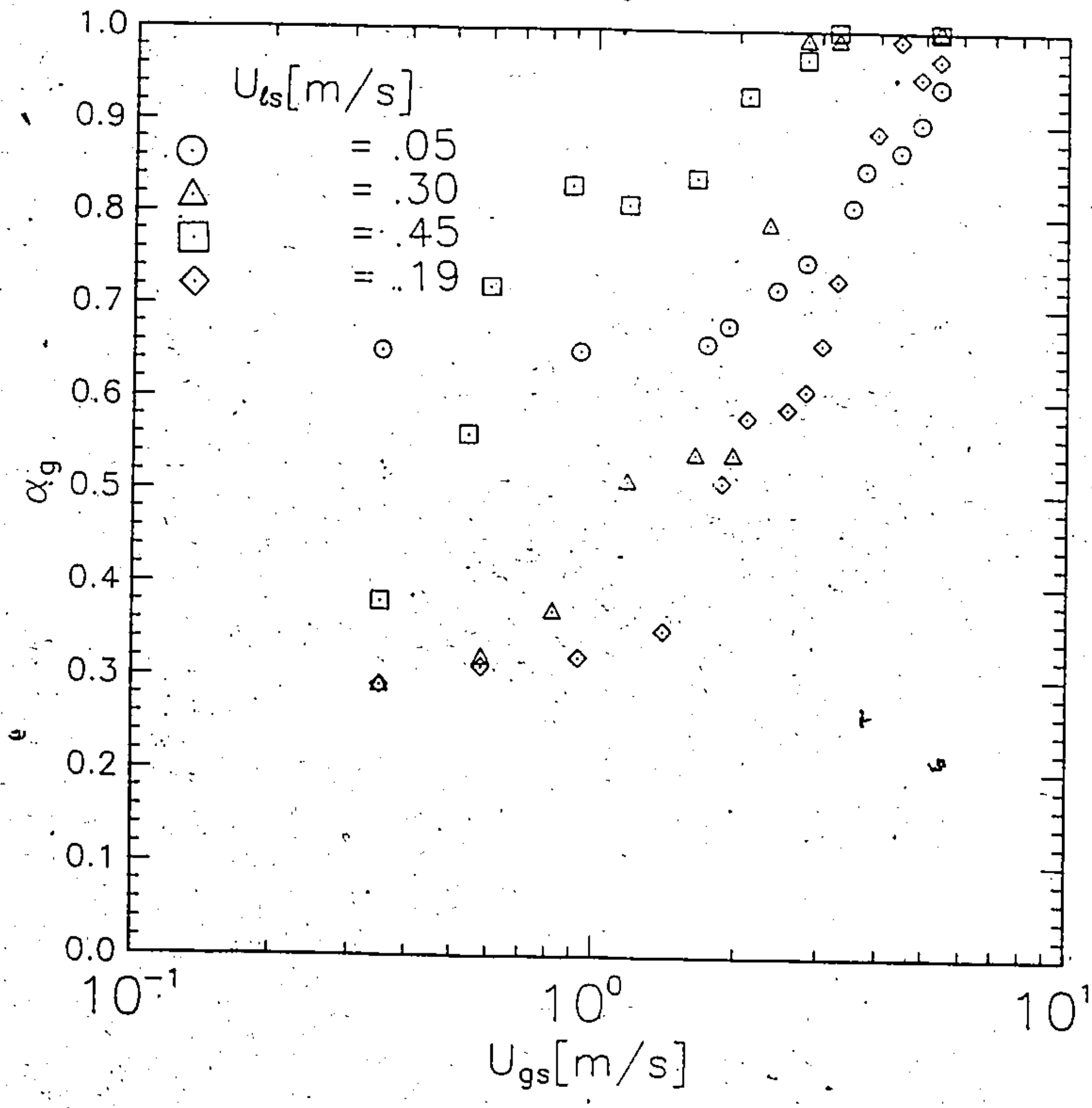

Figure II.1 Time Averaged Void Fraction as a Function of Superficial Velocities for a 5.08 cm i.d., Pipe.

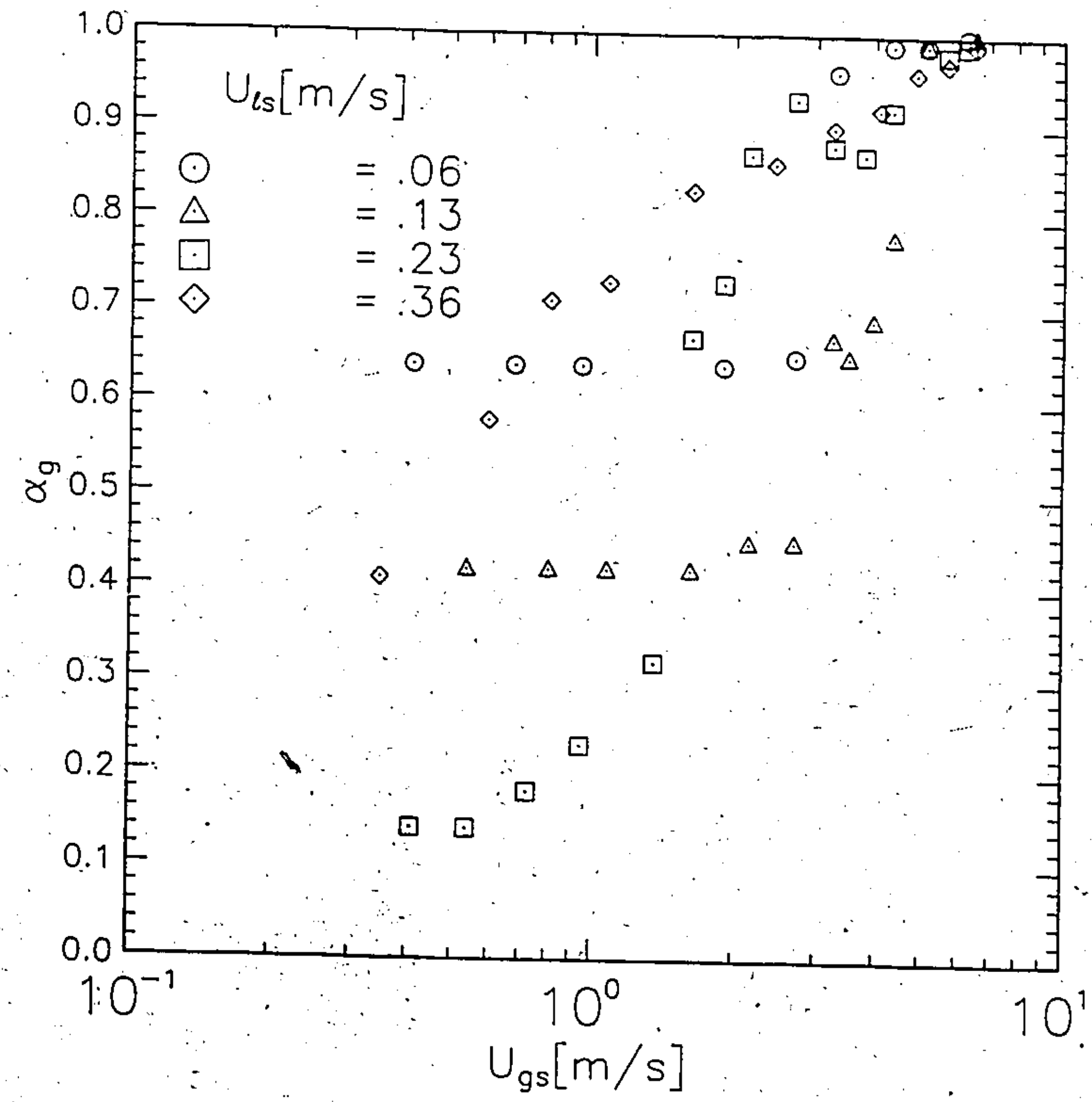

Figure II.2 Time Averaged Void Fraction as a Function of Superficial Velocities for Annulus Geometry of Inner-to-Outer Diameter Ratio, 0.500.

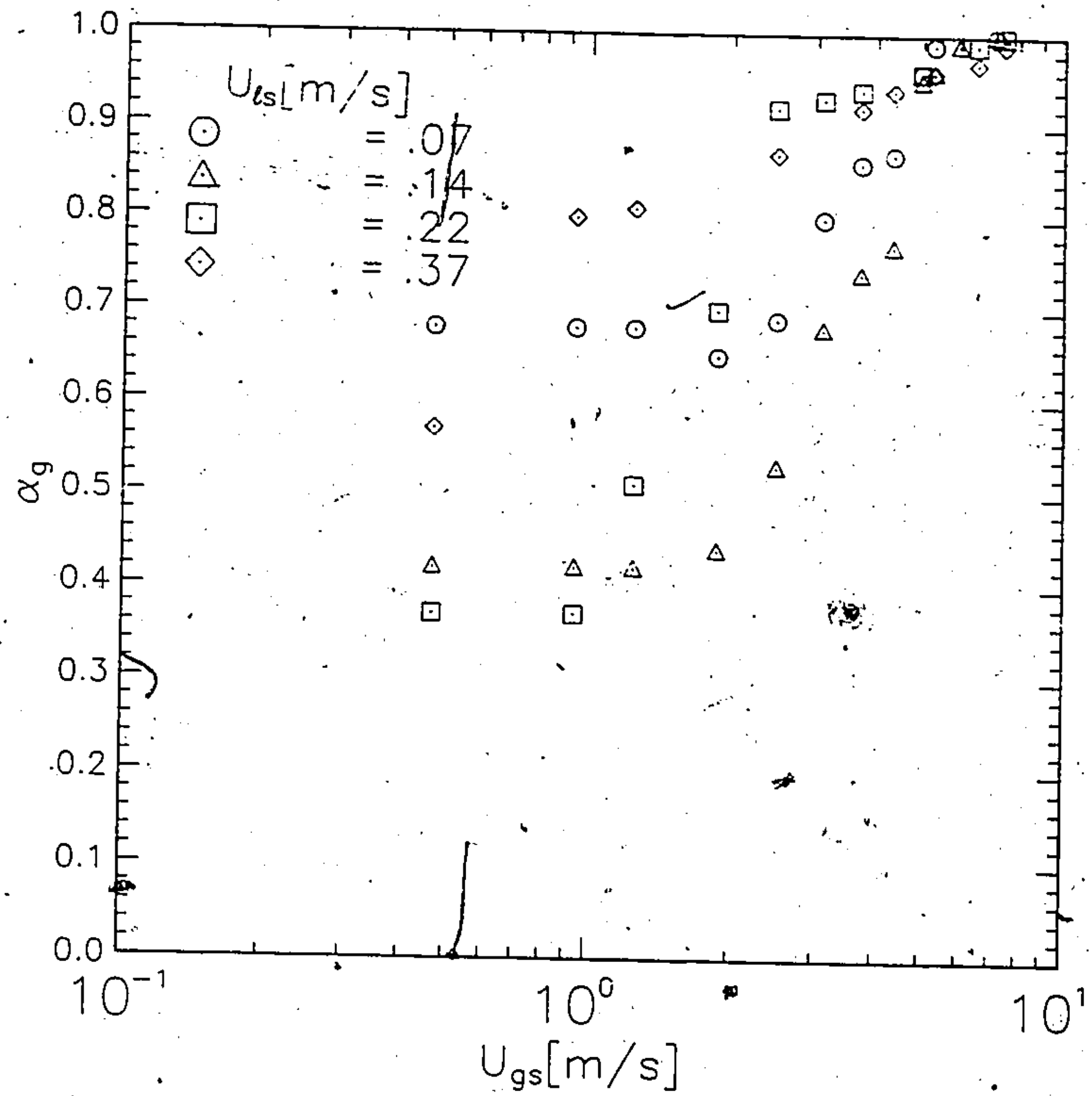

Figure II.3 Time Averaged Void Fraction as a Function of Superficial Velocities for Annulus Geometry of Inner-to-Outer Diameter Ratio, 0.625.

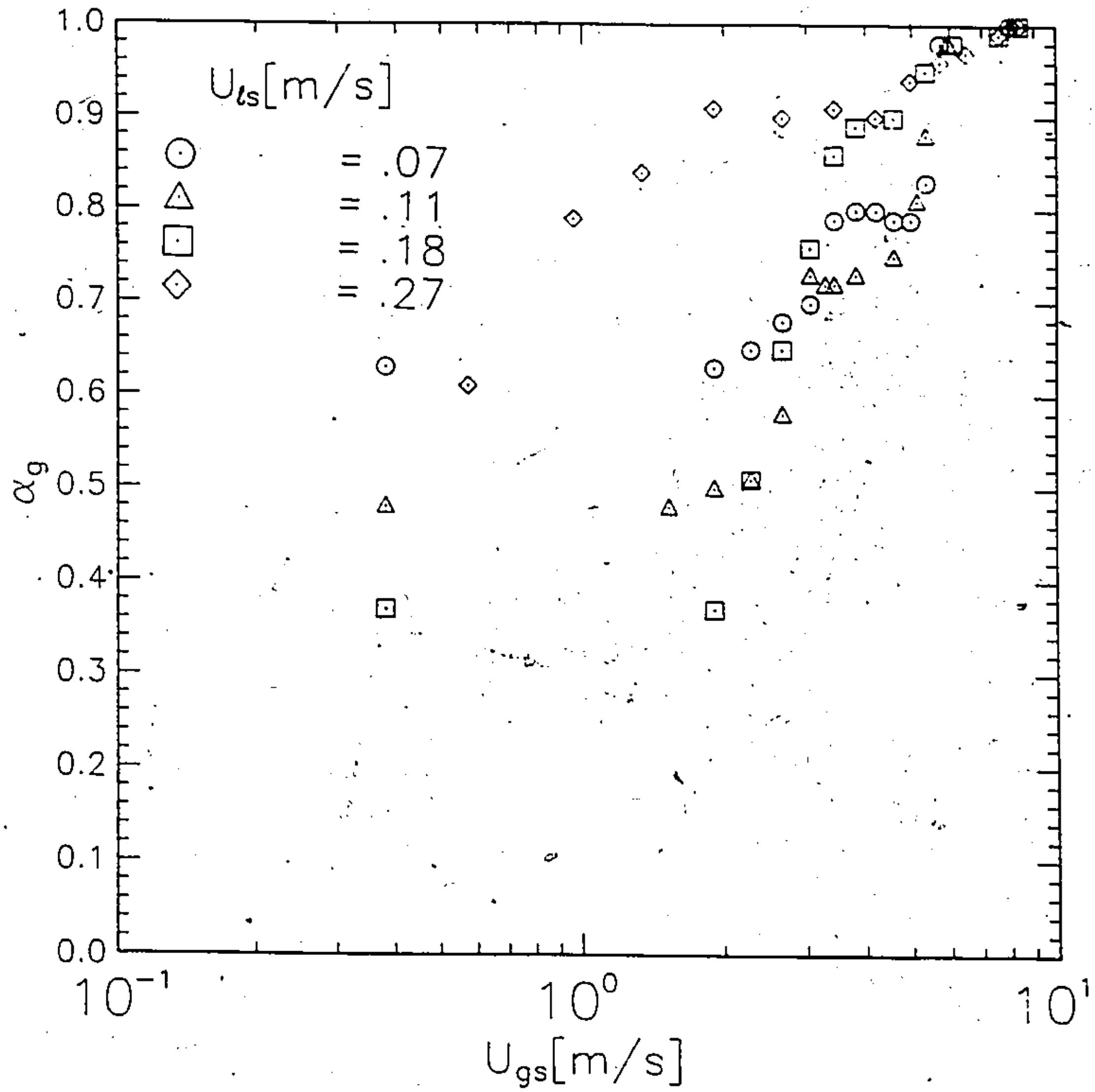

Figure II.4 Time Average Void Fraction as a Function of Superficial Velocities for Annulus Geometry of Inner-to-Outer Diameter Ratio, 0.625.

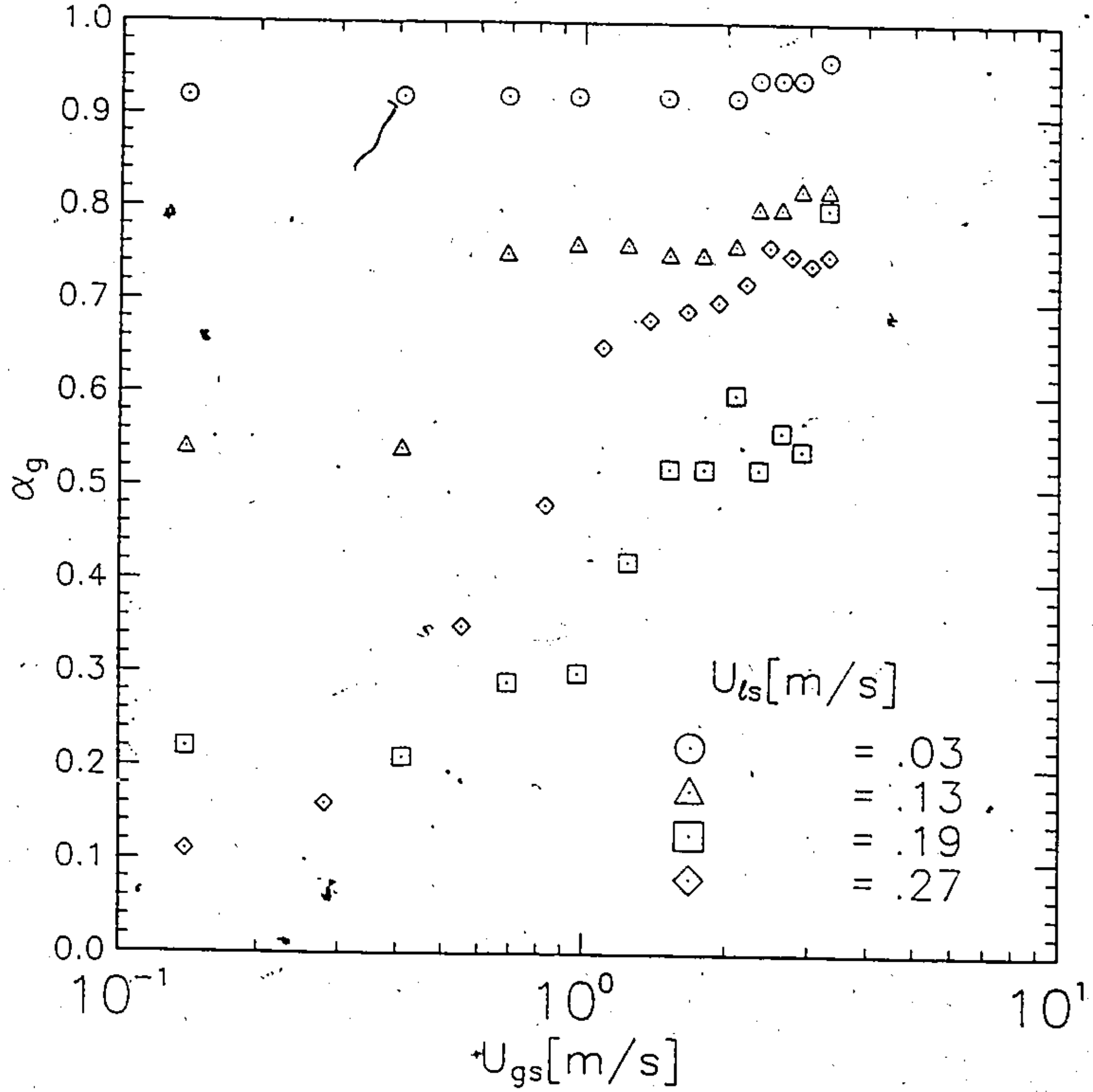

Figure II.5 Time Averaged Void Fraction as a Function of Superficial Velocities for the 37-Rod Bundle Geometry (Paper i.d. = 10.16 cm, Rod Diameter = 1.27 cm).

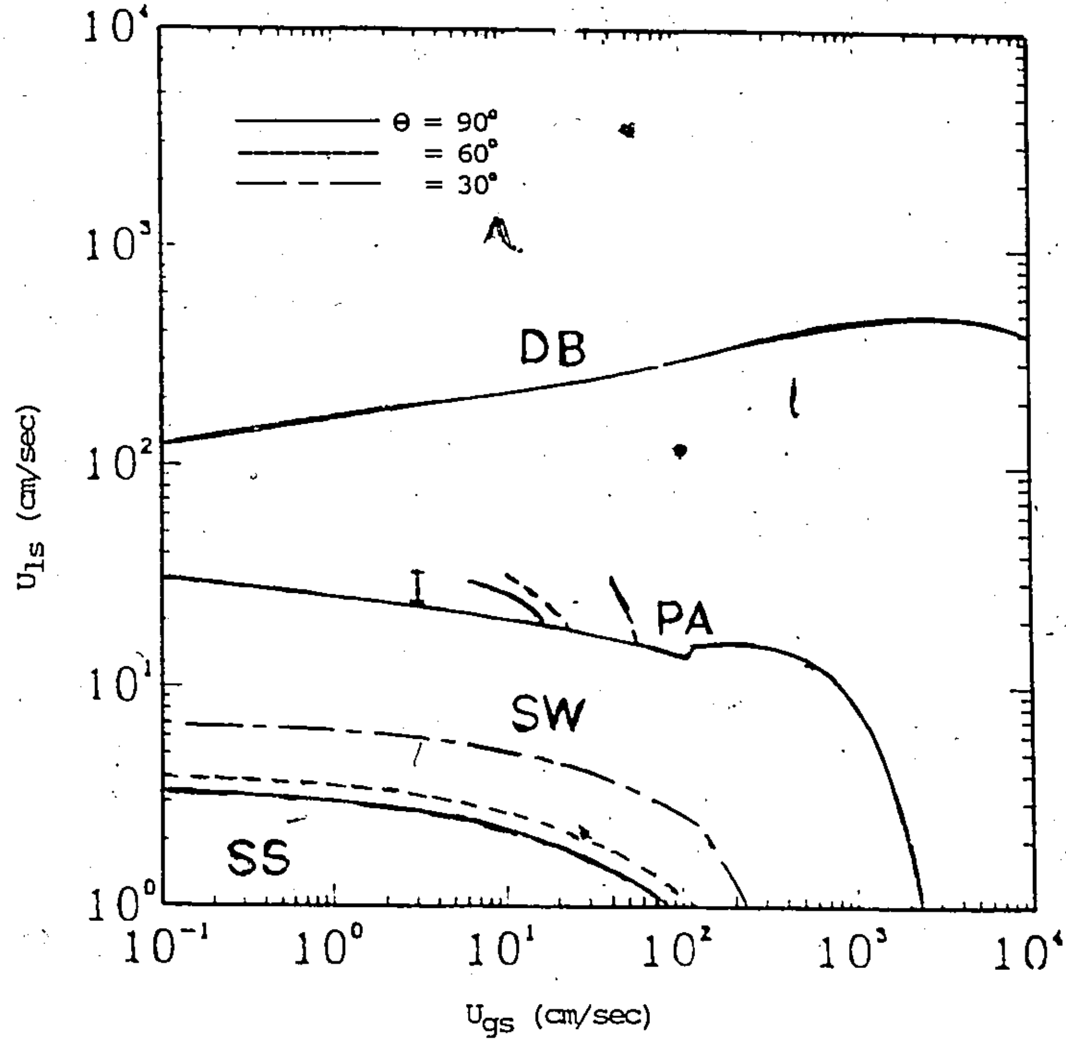

Figure II.6 Predicted Flow Pattern Transitions for Flow Split Systems at Various Junction angles (Paper Diameter = 5.08 cm i.d.).

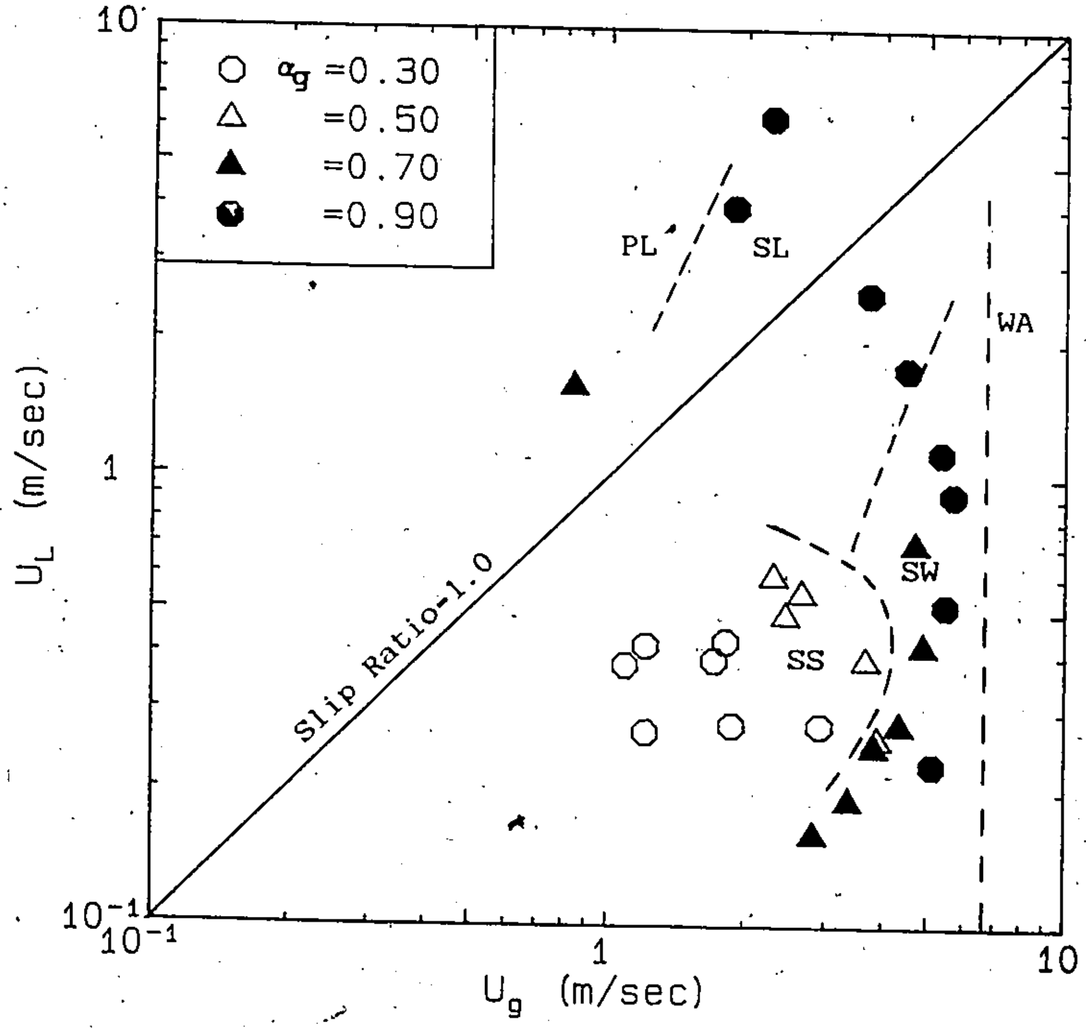

Figure II.7 Time Averaged Void Fraction as a Function of Local Phase Velocities for a 5.08 i.d. Pipe.

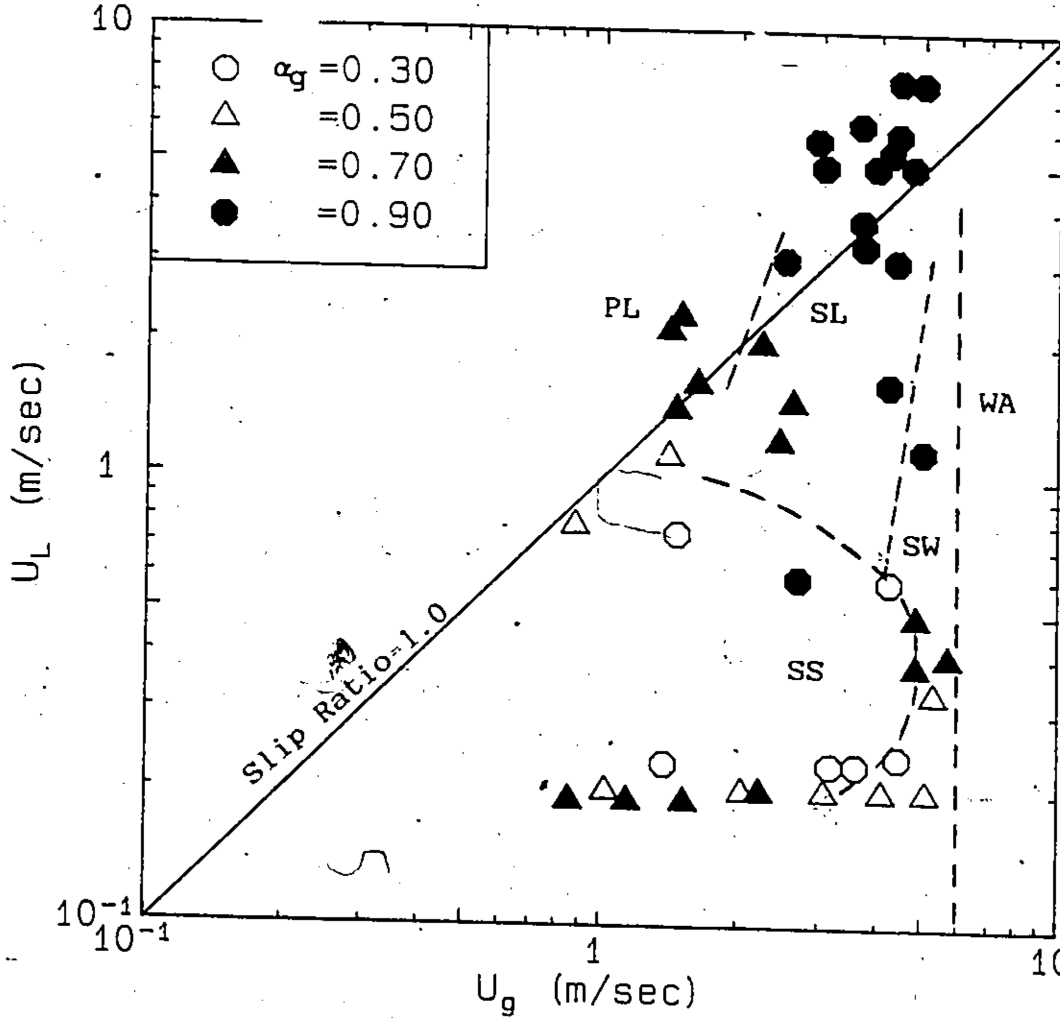

Figure II.8 Time Averaged Void Fraction as a Function of Local Phase Velocities for Annulus Geometry of Inner-to-Outer Diameter Ratio, 0.375.

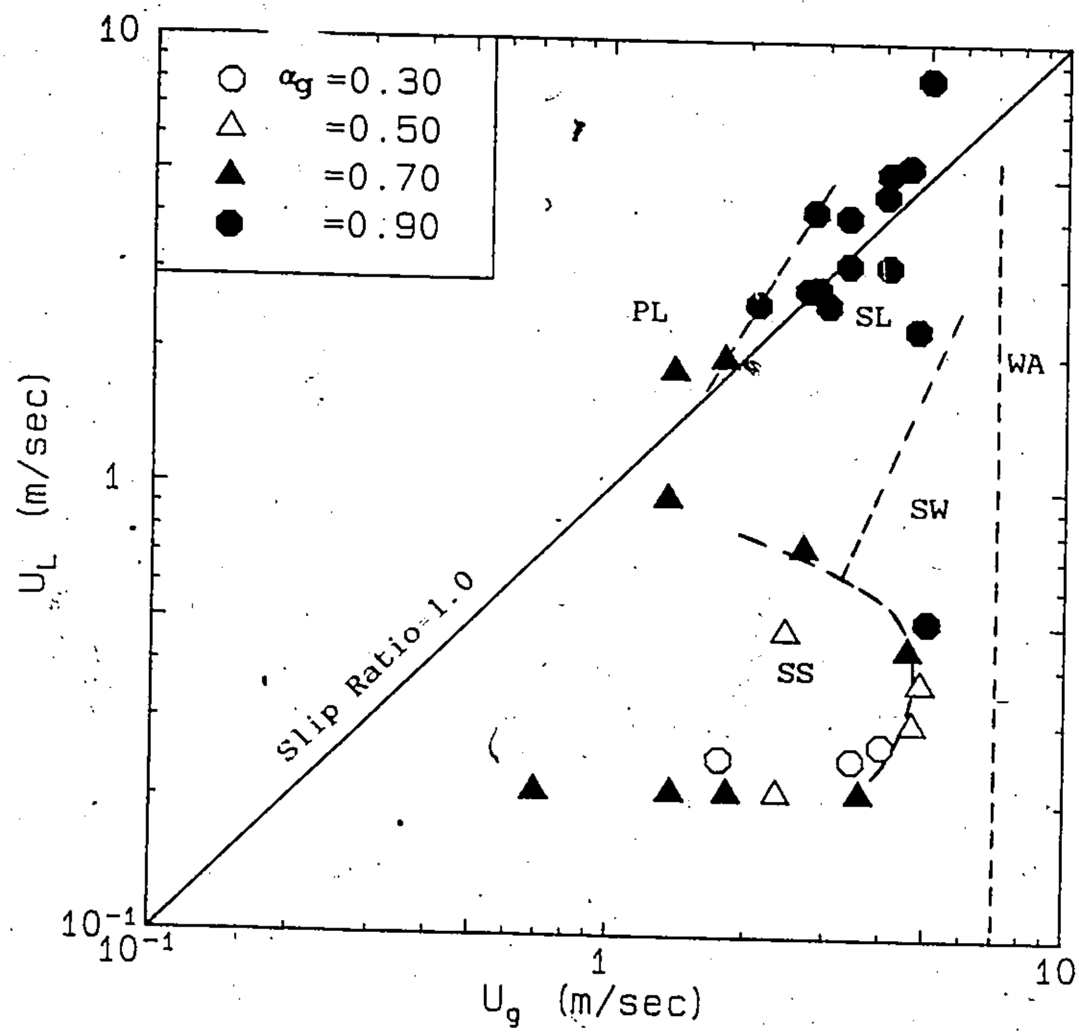

Figure II.9 Time Averaged Void Fraction as a Function of Local Phase Velocities for Annulus Geometry of Inner-to-Outer Diameter Ratio, 0.500.

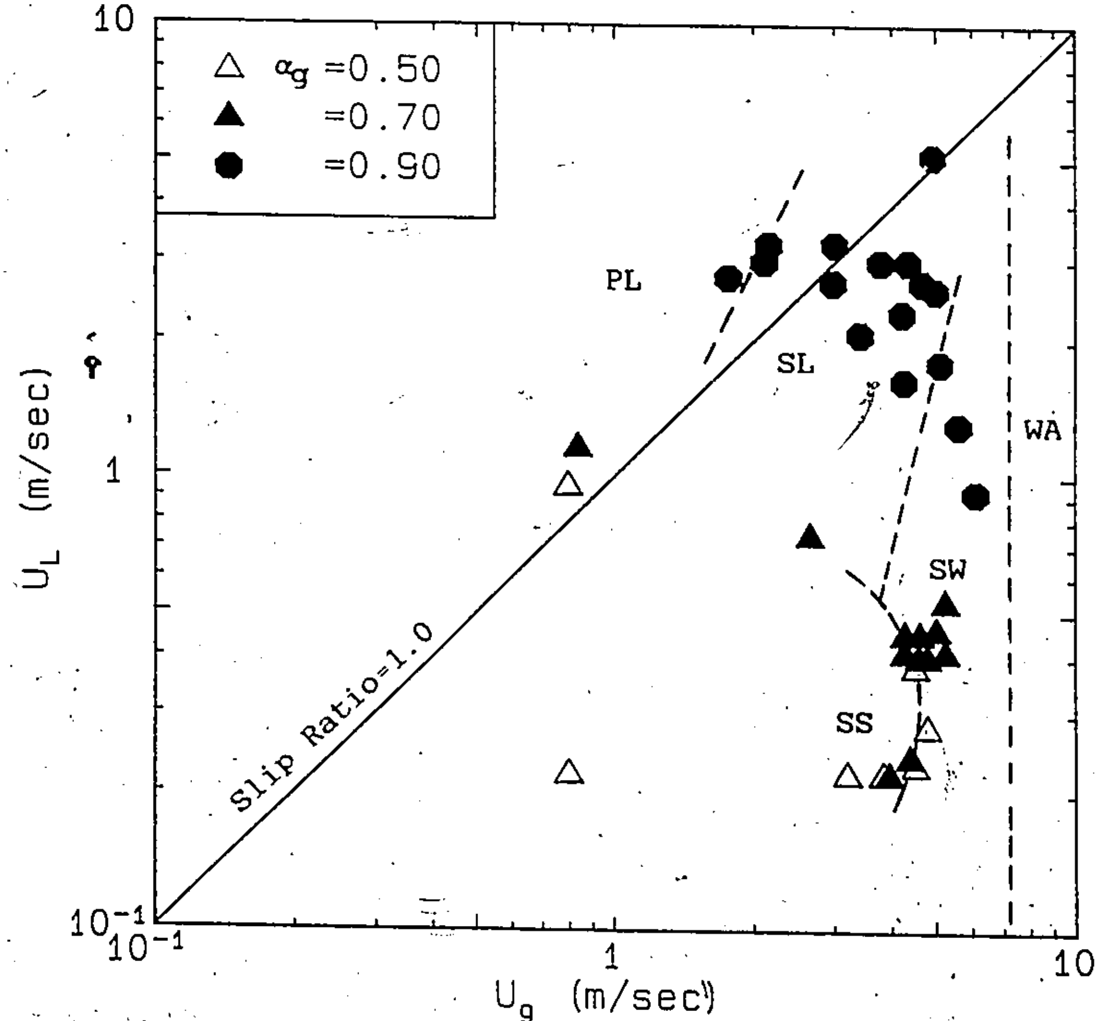

Figure II.10 Time Averaged Void Fraction as a Function of Local Phase Velocities for Annulus Geometry of Inner-to-Outer Diameter Ratio, 0.625.

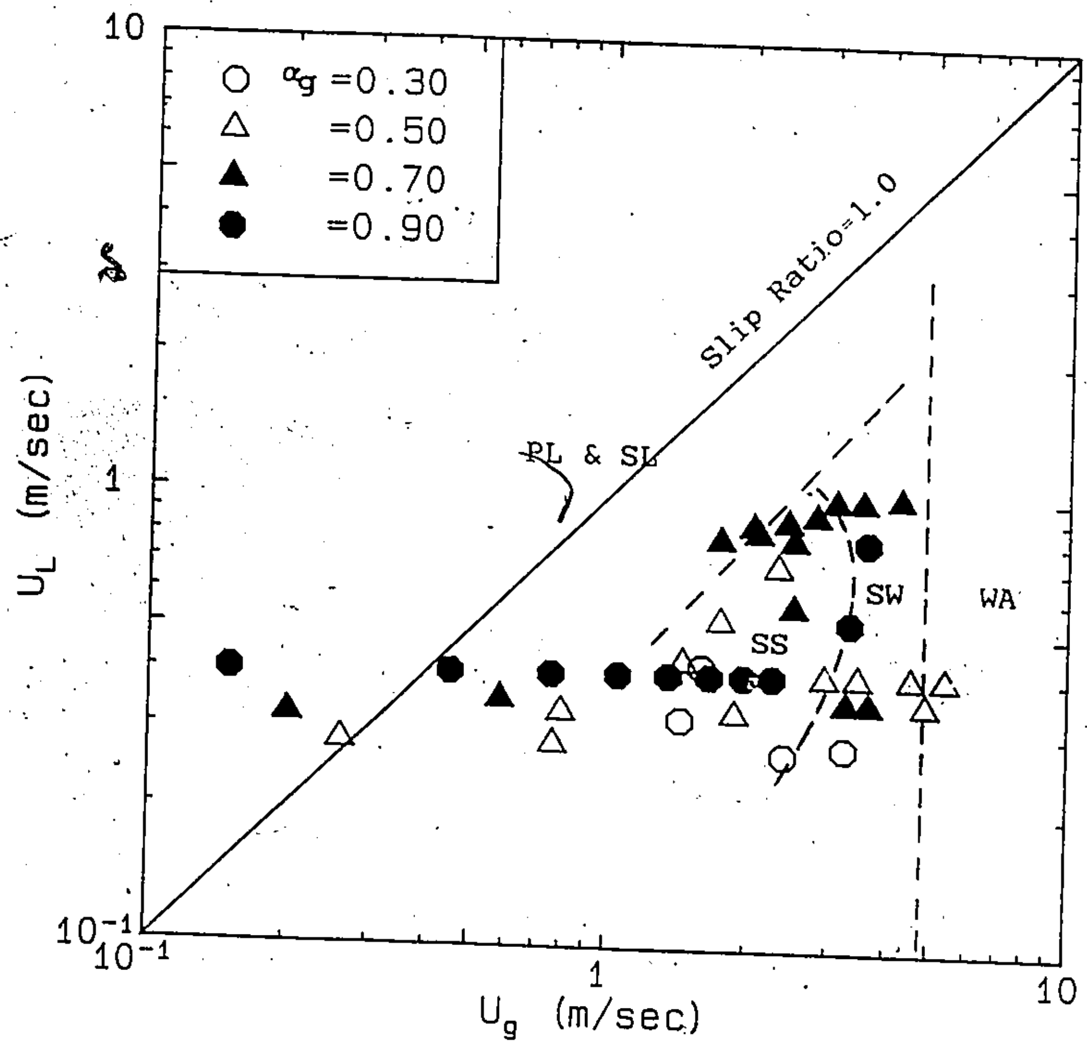

Figure II.11 Time Averaged Void Fraction as a Function of Local Phase Velocities for the 37-Rod Bundle Geometry (Pipe i.d. = 10.16 cm, Rod Diameter = 1.27 cm).

APPENDIX III

Computer Programs Listing

APPENDIX III

COMPUTER PROGRAMS LISTING

```
      PROGRAM REGIM
      DATA DENSL/1.0/,DENSG/0.001185/,VISCL/0.01/
      DATA VISCG/0.155/,D/5.08/,EPS/0.0001/,G/981.0/
      OPEN (3,FILE='PIPE1.DAT',STATUS='NEW')
      REWIND 3
      Z=99999
* PROGRAM REGIME DETERMINES THE FLOW REGIME TRANSITIONS
* FOR AIR/WATER TWO-PHASE FLOW IN A HORIZONTAL PIPE.
*
* GEOMETRICAL DATA
      PI=4.0*ATAN(1.0)
      A=PI*(D**2)/4.0
      S=PI*D
      SIGMA=72.0
   50 CONTINUE
*
* CALCULATION OF SS TO SW TRANSITION
*
      PRINT*,'ENTER A 1 TO DETERMINE THE SS TO SW TRANSITION'
      READ*,IWANT
      IF(IWANT.NE.1)GO TO 300
      PRINT*,'ENTER VALUE OF SHELTERING COEFFICIENT'
      READ*,SJ
      PRINT 1000
      DO 200 I=1,99
      K=0
      K1=0
      H=FLOAT(I)*D/100.0
      CALL SHAPE(H,AL,AG,SL,SG,SI,D)
      UL=2.00
      JL=2
      JG=2
  100 UL1=UL
      UG2=4.0*VISCL*(DENSL-DENSG)*G/(SJ*DENSG*UL)
      UG=SQRT(UG2)
      CALL SPEED(AL,AG,SL,SG,SI,UL,UG,RL,RG,JL,JG)
      DIFF=ABS(1.0-UL/UL1)
      K=K+1
      IF(K.GT.1000)GO TO 200
      CALL LAMTURB(RL,RG,JL,JG,ICHANG,K1)
  175 IF(ICHANG.EQ.1)GO TO 100
      IF(DIFF.GT.EPS)GO TO 100
      ULS=UL*AL/A
```

```
      UGS=UG*AG/A
      VOID=AG/A
      DIMH=H/D
      DIMSI=SI/D
      WRITE(3,*)UGS,ULS
  200 PRINT 1500,ULS,UGS,JL,JG,H,VOID
      WRITE(3,*)Z,Z
*
*   CALCULATION OF SS TO I TRANSITION
  300 PRINT*,'ENTER A 1 TO DETERMINE THE SS TO I TRANSITION'
      READ*,IWANT
      IF(IWANT.NE.1)GO TO 880
      PRINT 1000
      DO 500 J=1,99
      KK=0
      K1=0
      H=FLOAT(J)*D/100.0
      JL=2
      JG=2
      CALL SHAPE(H,AL,AG,SL,SG,SI,D)
      C2=1.0-H/D
      UL=2.0
      DADH=D*SQRT(1.0-(2.0*H/D-1.0)**2)
      UG=C2*SQRT(2.0*(DENSL-DENSG)*G*AG/(DENSG*DADH))
  350 UL1=UL
      CALL SPEED(AL,AG,SL,SG,SI,UL,UG,RL,RG,JL,JG)
      DIFF=ABS(1.0-UL/UL1)
      KK=KK+1
      IF(KK.GT.1000)GO TO 500
      CALL LAMTURB(RL,RG,JL,JG,ICHANG,K1)
      IF(ICHANG.EQ.1)GO TO 350
      IF(DIFF.GT.EPS)GO TO 350
      ULS=UL*AL/A
      UGS=UG*AG/A
      VOID=AG/A
      WRITE(3,*)UGS,ULS
  500 PRINT 1500,ULS,UGS,JL,JG,H,VOID
      WRITE(3,*)Z,Z
*
* CALCULATION OF SS TO I TRANSITION ALLOWING FOR SURFACE TENSION
* IN SMALL DIAMETER PIPES
*
  880 PRINT*,'ENTER A 1 TO DETERMINE THE S TO I TRANSITION'
      PRINT*,'DUE TO CAPILLARITY FORCE IN SMALL PIPES'
      READ*,IWANT
      IF(IWANT.NE.1)GO TO 153
      PRINT 1000
      THETA=SIGMA/(DENSL*G*(1.0-PI/4.0))
      HG=PI*SQRT(THETA)/4.0
      IF(HG.LE.D)GO TO 525
      HG=PI*D/4.0
```

```
  525 CONTINUE
      H=D-HG
      CALL SHAPE(H,AL,AG,SL,SG,SI,D)
      DGAS=10.0
      DO 700 J=1,99
      KS=0
      K1=0
      JG=2
      JL=2
      UL=2.0
      UG=DGAS*FLOAT(J)
  550 UL1=UL
      CALL SPEED(AL,AG,SL,SG,SI,UL,UG,RL,RG,JL,JG)
      DIFF=ABS(1.0-UL/UL1)
      KS=KS+1
      IF(KS.GT.1000)GO TO 700
      CALL LAMTURB(RL,RG,JL,JG,ICHANG,K1)
      IF(ICHANG.EQ.1)GO TO 550
      IF(DIFF.GT.EPS)GO TO 550
      ULS=UL*AL/A
      UGS=UG*AG/A
      VOID=AG/A
      WRITE(3,*)UGS,ULS
  700 PRINT 1500,ULS,UGS,JL,JG,H,VOID
      WRITE(3,*)Z,Z
  153 CONTINUE
*
*   CALCULATION OF I TO DB TRANSITION
      PRINT*,'ENTER A 1 TO DETERMINE THE I TO DB TRANSITION'
      READ*,IWANT
      IF(IWANT.NE.1)GO TO 888
      PRINT 1000
      DO 353 J=1,99
      H=FLOAT(J)*D/100.0
      CALL SHAPE(H,AL,AG,SL,SG,SI,D)
      KK=0
      JL=2
      JG=2
      XL=0.2
      CL=0.046
      UG=0.2
      DL=(4.0*AL/(SL*VISCL))**XL
      EXP=1.0/(2.0-XL)
      UL=(4.0*G*AG*(DENSL-DENSG)*DL/(SI*CL*DENSL))**EXP
  453 UG1=UG
      CALL SPEEDG(AL,AG,SL,SG,SI,UL,UG,RL,RG,JL,JG)
      DIFF=ABS(1.0-UG/UG1)
      KK=KK+1
      IF(KK.GT.1000)GO TO 353
      CALL LAMTURB(RL,RG,JL,JG,ICHANG,K1)
      IF(ICHANG.EQ.1)GO TO 453
```

```
      IF(DIFF.GT.EPS)GO TO 453
      ULS=UL*AL/A
      UGS=UG*AG/A
      VOID=AG/A
      WRITE(3,*)UGS,ULS
  353 PRINT 1500,ULS,UGS,JL,JG,H,VOID
      WRITE(3,*)Z,Z
*
* CALCULATION OF I TO A TRANSITION
  888 PRINT*,'ENTER A 1 TO DETERMINE THE I TO A TRANSITION'
      READ*,IWANT
      IF(IWANT.NE.1)GO TO 850
      PRINT 1000
      H=0.50*D
      CALL SHAPE(H,AL,AG,SL,SG,SI,D)
      UG=450.0
      DO 800 J=1,99
      KA=0
      K1=0
      JG=2
      JL=2
      UL=2.0
  750 UL1=UL
      CALL SPEED(AL,AG,SL,SG,SI,UL,UG,RL,RG,JL,JG)
      DIFF=ABS(1.0-UL/UL1)
      KA=KA+1
      IF(KA.GT.1000)GO TO 800
      CALL LAMTURB(RL,RG,JL,JG,ICHANG,K1)
      IF(ICHANG.EQ.1)GO TO 750
      IF(DIFF.GT.EPS)GO TO 750
      ULS=UL*AL/A
      UGS=UG*AG/A
      VOID=AG/A
      UG=1000.0*FLOAT(J)
      WRITE(3,*)UGS,ULS
  800 PRINT 1500,ULS,UGS,JL,JG,H,VOID
      WRITE(3,*)Z,Z
  850 CONTINUE
*
* FORMAT STATEMENTS
 1000 FORMAT(/,4X,'ULS',5X,'UGS',5X,'JL',3X,'JG',4X,'H',4X,'VOID',/)
 1500 FORMAT(2X,F6.1,2X,F8.1,4X,I1,4X,I1,2X,F5.2,2X,F4.2)
 2000 FORMAT(2X,7(F6.1,2X))
      REWIND 3
      STOP
      END
*
* SUBROUTINES
*
      SUBROUTINE SHAPE(HT,AAL,AAG,SSL,SSG,SSI,DD)
*
```

```
* SUBROUTINE SHAPE CALCULATES THE GEOMETRIC
* CONFIGURATION IN THE TUBE BASED ON WATER LEVEL
*
      PY=4.0*ATAN(1.0)
      AA=PY*(DD**2)/4.0
      SS=PY*DD
      ARG=(2.0*HT/DD)-1.0
      AAL=(PY-ACOS(ARG)+ARG*SQRT(1.0-ARG**2))*(DD**2)/4.0
      AAG=AA-AAL
      SSL=(PY-ACOS(ARG))*DD
      SSG=SS-SSL
      SSI=DD*SQRT(1.0-ARG**2)
      RETURN
      END
*
*
*
      SUBROUTINE SPEED(AAL,AAG,SSL,SSG,SSI,UUL,UUG,REL,REG,JJL,JJG)
      DIMENSION C(2),X(2)
      DATA ROHL/1.0/,ROHG/0.001185/,VISL/0.01/,VISG/0.155/
      DATA (C(I),I=1,2)/16.0,0.046/
      DATA (X(I),I=1,2)/1.0,0.2/
*
* SUBROUTINE SPEED CALCULATES THE WATER SPEED WITH
* GAS SPEED AND GEOMETRIC PARAMETERS GIVEN
*
* ITERATE
*
      HDG=4.0*AAG/(SSG+SSI)
      REG=HDG*UUG/VISG
      HDL=4.0*AAL/SSL
      REL=HDL*UUL/VISL
      T1=ROHG*C(JJG)*SSG*AAL*(REL**X(JJL))
      T2=ROHL*C(JJL)*SSL*AAG*(REG**X(JJG))
      T3=SSI*(1.0+AAG/AAL)/SSG
      UUL2=(T1/T2)*(1.0+T3)*(UUG**2)
      UUL=SQRT(UUL2)
      RETURN
      END
*
      SUBROUTINE SPEEDG(AAL,AAG,SSL,SSG,SSI,UUL,UUG,REL,REG,JJL,JJG)
      DIMENSION C(2),X(2)
      DATA ROHL/1.0/,ROHG/0.001185/,VISL/0.01/,VISG/0.155/
      DATA (C(I),I=1,2)/16.0,0.046/
      DATA (X(I),I=1,2)/1.0,0.2/
*
* SUBROUTINE SPEEDG CALCULATES THE GAS SPEED WITH
* THE LIQUID SPEED AND GEOMETRIC PARAMETERS GIVEN
*
* ITERATE
*
```

```
      HDG=4.0*AAG/(SSG+SSI)
      REG=HDG*UUG/VISG
      HDL=4.0*AAL/SSL
      REL=HDL*UUL/VISL
      T1=ROHG*C(JJG)*SSG*AAL*(REL**X(JJL))
      T2=ROHL*C(JJL)*SSL*AAG*(REG**X(JJG))
      T3=SSI*(1.0+AAG/AAL)/SSG
      UUG2=(UUL**2)/((T1/T2)*(1.0+T3))
      UUG=SQRT(UUG2)
      RETURN
      END
*
      SUBROUTINE LAMTURB(REL,REG,JJL,JJG,IGHANGE,KK1)
*
* SUBROUTINE LAMTURB DETERMINES WHETHER THE TWO
* FLUIDS ARE IN LAMINAR OR TURBULENT FLOW AND
* ADJUSTS THE FRICTION FACTORS ACCORDINGLY.
*
*
*
      JGOLD=JJG
      IF(REG.GT.2000.0)JJG=2
      IF(REG.LE.2000.0)JJG=1
      IF(JGOLD.NE.JJG)ICHANGE=1
      KK1=KK1+1
      RETURN
      END
*
*
*
      SUBROUTINE SPEEDL(AAL,AAG,SSL,SSG,SSI,UUL,UUG,REL,REG,JJL,JJG)
      DIMENSION C(2),X(2)
      DATA ROHL/1.0/,ROHG/0.0012/,VISL/0.01/,VISG/0.15/
      DATA C/16.0,0.046/,X/1.0,0.2/
*
* SUBROUTINE SPEEDL CALCULATES GAS SPEED WITH
* LIQUID LEVEL AND SPEED GIVEN
*
      HDG=4.0*AAG/(SSG+SSI)
      HDL=4.0*AAL/SSL
      REL=HDL*UUL/VISL
      FL=C(JJL)/(REL**X(JJL))
      F1=SSL*AAG/(AAL*SSG)
      F2=SSI*(1.0+AAG/AAL)/SSG
      TAUL=FL*ROHL*(UUL**2)/2.0
      F3=TAUL*F1
      IT=0
*
* ITERATE
*
 6200 REG=HDG*UUG/VISG
```

```
      FG=C(JJG)/(REG**X(JJG))
      TAUI=FG*ROHG*((UUG-UUL)**2)/2.0
      UUG2=(F3-TAUI*F2)*2.0/(FG*ROHG)
      IF(UUG2.GT.0.0.AND.UUG2.LT.10000000.0)GO TO 6500
      PRINT*,UUG2
      PRINT*,'ERROR IN SPEEDL'
      GO TO 7000
6500  IT=IT+1
      UUG1=SQRT(UUG2)
      ERROR=ABS(1.0-UUG/UUG1)
      UUG=UUG1
      IF(IT.GT.1000)GO TO 7000
      IF(ERROR.GT.0.001)GO TO 6200
7000  CONTINUE
      RETURN
      END
```

APPENDIX III (continued)

```
      PROGRAM BNDL37
      DIMENSION TTA(37),R(37),TITA(37)
      DATA (R(I),I=1,37)/1.49,1.49,1.49,1.49,1.49,1.49,2.88,2.88
     -,2.88,2.88,2.88,2.88,2.88,2.88,2.88,2.88,2.88,2.88,4.33,4.
     -33,4.33,4.33,4.33,4.33,4.33,4.33,4.33,4.33,4.33,4.33,4.33,
     -4.33,4.33,4.33,4.33,4.33,0.0/
      DATA (TTA(I),I=1,37)/0.0,12.0,24.0,36.0,48.0,60.0,3.0,9.0,
     -15.0,21.0,27.0,33.0,39.0,45.0,51.0,57.0,63.0,69.0,0.0,4.0,
     -8.0,12.0,16.0,20.0,24.0,28.0,32.0,36.0,40.0,44.0,48.0,52.0
     -,56.0,60.0,64.0,68.0,0.0/
      DATA DENSL/1.0/,DENSG/0.001185/,VISCL/0.01/,VISCG/0.155/
      DATA D/10.16/,DR/1.27/,NN/37/,EPS/1.0E-4/,G/981.0/,RT/0.0/
      OPEN (3,FILE='DATA1.DAT',STATUS='NEW')
      REWIND 3
      Z=99999
      RN=FLOAT(NN)
* PROGRAM BNDL37 DETERMINES THE TWO-PHASE FLOW REGIME TRANSITIONS
* IN A HORIZONTAL ROD BUNDLE GEOMETRY.
*
* GEOMETRICAL DATA
      PI=ATAN(1.0)*4.0
      A=PI*((D**2)-RN*(DR**2))/4.0
      S1=PI*(D+RN*DR)
      SIGMA=72.0
      ROT=RT*PI/36.0
      DO 112 I=1,37
      TITA(I)=PI*TTA(I)/36.0
      TITA(I)=TITA(I)+ROT
  112 CONTINUE
      DH=D/100.0
   50 CONTINUE
*
* CALCULATION OF SS TO SW TRANSITION
*
      PRINT*,'ENTER A 1 TO DETERMINE THE SS TO SW TRANSITION'
      READ*,IWANT
      IF(IWANT.NE.1)GO TO 300
      PRINT*,'ENTER VALUE OF SHELTERING COEFFICIENT'
      READ*,SJ
      PRINT 1000
      DO 200 I=1,99
      H=FLOAT(I)*DH
      CALL SHAPE(H,AL,AG,SL,SG,SI,D,DR,R,TITA,RN)
      K=0
      JL=2
      JG=2
      UL=2.0
  100 UL1=UL
```

```
      UG2=4.0*VISCL*(DENSL-DENSG)*G/(SJ*DENSG*UL)
      UG=SQRT(UG2)
      CALL SPEED(AL,AG,SL,SG,SI,UL,UG,RL,RG,JL,JG)
      DIFF=ABS(1.0-UL/UL1)
      K=K+1
      IF(K.GT.1000)GO TO 200
      CALL LAMTURB(RL,RG,JL,JG,ICHANG,K1)
      IF(ICHANG.EQ.1)GO TO 100
      IF(DIFF.GT.EPS)GO TO 100
      ULS=UL*AL/A
      UGS=UG*AG/A
      VOID=AG/A
      DIMH=H/D
      DIMSI=SI/D
      WRITE(3,*)UGS,ULS
  200 PRINT 1500,ULS,UGS,JL,JG,H,VOID
      WRITE(3,*)Z,Z
*
* CALCULATION OF SS TO I TRANSITION
  300 PRINT*,'ENTER A 1 TO DETERMINE THE SS TO I TRANSITION'
      READ*,IWANT
      IF(IWANT.NE.1)GO TO 880
      PRINT 1000
      ALL=0.0
      DO 500 I=1,99
      H=FLOAT(I)*DH
      CALL SHAPE(H,AL,AG,SL,SG,SI,D,DR,R,TITA,RN)
      KK=0
      JL=2
      JG=2
      C2=1.0-H/D
      DADH=ABS((AL-ALL)/DH)
      ALL=AL
      UG=C2*SQRT((DENSL-DENSG)*G*AG/(DENSG*DADH))
      UL=0.01
  350 UL1=UL
      CALL SPEED(AL,AG,SL,SG,SI,UL,UG,RL,RG,JL,JG)
      DIFF=ABS(1.0-UL/UL1)
      KK=KK+1
      IF(KK.GT.1000)GO TO 500
      CALL LAMTURB(RL,RG,JL,JG,ICHANG,K1)
      IF(ICHANG.EQ.1)GO TO 350
      IF(DIFF.GT.EPS)GO TO 350
      ULS=UL*AL/A
      UGS=UG*AG/A
      VOID=AG/A
      DIMH=H/D
      DIMSG=SG/S1
      WRITE(3,*)UGS,ULS
  500 PRINT 1500,ULS,UGS,JL,JG,H,VOID
      WRITE(3,*)Z,Z
```

```
*
*
* CALCULATION OF I TO DB TRANSITION
 880 PRINT*,'ENTER A 1 TO DETERMINE THE I TO DB TRANSITION'
     READ*,IWANT
     IF(IWANT.NE.1)GO TO 888
     PRINT 1000
     DO 433 I=1,99
     H=FLOAT(I)*DH
     CALL SHAPE(H,AL,AG,SL,SG,SI,D,DR,R,TITA,RN)
     KK=0
     JL=2
     JG=2
     XL=0.2
     CL=0.046
     UG=0.1
     DL=(4.0*AL/(SL*VISCL))**XL
     EXP=1.0/(2.0-XL)
     UL=(4.0*G*AG*(DENSL-DENSG)*DL/(SI*CL*DENSL))**EXP
 400 UG1=UG
     CALL SPEEDG(AL,AG,SL,SG,SI,UL,UG,RL,RG,JL,JG)
     DIFF=ABS(1.0-UG/UG1)
     KK=KK+1
     IF(KK.GT.1000)GO TO 433
     CALL LAMTURB(RL,RG,JL,JG,ICHANG,K1)
     IF(ICHANG.EQ.1)GO TO 400
     IF(DIFF.GT.EPS)GO TO 400
     ULS=UL*AL/A
     UGS=UG*AG/A
     VOID=AG/A
     WRITE(3,*)UGS,ULS
 433 PRINT 1500,ULS,UGS,JL,JG,H,VOID
     WRITE(3,*)Z,Z
*
* CALCULATION OF I TO A TRANSITION
*
 888 PRINT*,'ENTER A 1 TO DETERMINE THE I TO A TRANSITION'
     READ*,IWANT
     IF(IWANT.NE.1)GO TO 850
     PRINT 1000
     H=0.50*D
     CALL SHAPE(H,AL,AG,SL,SG,SI,D,DR,R,TITA,RN)
     UG=600.0
     DO 800 I=1,99
     KA=0
     JG=2
     JL=2
     UL=2.0
 750 UL1=UL
     CALL SPEED(AL,AG,SL,SG,SI,UL,UG,RL,RG,JL,JG)
     DIFF=ABS(1.0-UL/UL1)
     KA=KA+1
```

```
      IF(KA.GT.1000)GO TO 800
      CALL LAMTURB(RL,RG,JL,JG,ICHANG,K1)
      IF(ICHANG.EQ.1)GO TO 750
      IF(DIFF.GT.EPS)GO TO 750
      ULS=UL*AL/A
      UGS=UG*AG/A
      VOID=AG/A
      UG=1000.0*FLOAT(I)
      WRITE(3,*)UGS,ULS
  800 PRINT 1500,ULS,UGS,JL,JG,H,VOID
      WRITE(3,*)Z,Z
  850 PRINT*,'ENTER A 1 TO RUN AGAIN'
      READ*,IRUN
      IF(IRUN.EQ.1)GO TO 50
*
* FORMAT STATEMENTS
 1000 FORMAT(/,4X,'ULS',5X,'UGS',5X,'JL',3X,'JG',4X,'H',4X,'VOID',/)
 1500 FORMAT(2X,F8.3,2X,F9.2,4X,I1,4X,I1,2X,F6.3,2X,F6.3)
 2000 FORMAT(2X,7(F6.1,2X))
      REWIND 3
      STOP
      END
*
* SUBROUTINES
*
      SUBROUTINE SHAPE(HT,AAL,AAG,SSL,SSG,SSI,DD,DDR,R,TTA,RN)
      DIMENSION BDL(37),BDH(37),ARL(37),ARG(37),PL(37)
      DIMENSION TTA(37),BAY(37),PG(37),PPI(37),R(37)
*
* SUBROUTINE SHAPE CALCULATES THE GEOMETRIC
* CONFIGURATION IN THE ROD BUNDLE BASED ON WATER LEVEL
*
      PY=4.0*ATAN(1.0)
      RAY=(2.0*HT/DD)-1.0
      AAG1=(ACOS(RAY)-RAY*SQRT(1.0-(RAY**2)))*(DD**2)/4.0
      AAL1=(PY-ACOS(RAY)+RAY*SQRT(1.0-(RAY**2)))*(DD**2)/4.0
      SSG1=DD*ACOS(RAY)
      SSL1=(PY-ACOS(RAY))*DD
      SSI1=DD*SQRT(1.0-(RAY**2))
      AREAL=0.0
      AREAG=0.0
      SUMPL=0.0
      SUMPG=0.0
      SUMPI=0.0
      DO 17 I=1,37
      BAY(I)=((2.0*HT)-DD-(2.0*R(I)*SIN(TTA(I))))/DDR
      BDL(I)=(DD-DDR+(2.0*R(I)*SIN(TTA(I))))/2.0
      BDH(I)=(DD+DDR+(2.0*R(I)*SIN(TTA(I))))/2.0
      IF(HT.LE. BDL(I))THEN
      ARL(I)=0.0
      ARG(I)=PY*(DDR**2)/4.0
```

```
      PL(I)=0.0
      PG(I)=PY*DDR
      PPI(I)=0.0
      END IF
      IF(HT.GE.BDH(I))THEN
      ARL(I)=PY*(DDR**2)/4.0
      ARG(I)=0.0
      PL(I)=PY*DDR
      PG(I)=0.0
      PPI(I)=0.0
      END IF
      IF(HT.GT.BDL(I).AND.HT.LT.BDH(I))THEN
      ARL(I)=(PY-ACOS(BAY(I))+BAY(I)*SQRT(1.0-
     (BAY(I)**2)))*(DDR**2)/4.0
      ARG(I)=(ACOS(BAY(I))-BAY(I)*SQRT(1.0-(BAY(I)**2)))*(DDR**2)/4.0
      PL(I)=(PY-ACOS(BAY(I)))*DDR
      PG(I)=DDR*ACOS(BAY(I))
      PPI(I)=DDR*SQRT(1.0-(BAY(I)**2))
      END IF
      AREAL=AREAL+ARL(I)
      AREAG=AREAG+ARG(I)
      SUMPL=SUMPL+PL(I)
      SUMPG=SUMPG+PG(I)
      SUMPI=SUMPI+PPI(I)
   17 CONTINUE
      AAL=AAL1-AREAL
      AAG=AAG1-AREAG
      SSL=SSL1+SUMPL
      SSG=SSG1+SUMPG
      SSI=SSI1-SUMPI
      RETURN
      END
*
      SUBROUTINE SPEED(AAL,AAG,SSL,SSG,SSI,UUL,UUG,REL,REG,JJL,JJG)
      DIMENSION C(2),X(2)
      DATA ROHL/1.0/,ROHG/0.001185/,VISL/0.01/,VISG/0.155/
      DATA (C(I),I=1,2)/16.0,0.046/
      DATA (X(I),I=1,2)/1.0,0.2/
*
* SUBROUTINE SPEED CALCULATES THE WATER SPEED WITH
* GAS SPEED AND GEOMETRIC PARAMETERS GIVEN
*
* ITERATE
*
      HDG=4.0*AAG/(SSG+SSI)
      REG=HDG*UUG/VISG
      HDL=4.0*AAL/SSL
      REL=HDL*UUL/VISL
      T1=C(JJG)*ROHG*SSG*AAL*(REL**X(JJL))
      T2=C(JJL)*ROHL*SSL*AAG*(REG**X(JJG))
      T3=SSI*(1.0+AAG/AAL)/SSG
```

```
      UUL2=(T1/T2)*(1.0+T3)*(UUG**2)
      UUL=SQRT(UUL2)
      RETURN
      END
*
*
      SUBROUTINE SPEEDG(AAL,AAG,SSL,SSG,SSI,UUL,UUG,REL,REG,JJL,JJG)
      DIMENSION C(2),X(2)
      DATA ROHL/1.0/,ROHG/0.001185/,VISL/0.01/,VISG/0.155/
      DATA (C(I),I=1,2)/16.0,0.046/
      DATA (X(I),I=1,2)/1.0,0.2/
*
* SUBROUTINE SPEEDG CALCULATES THE GAS SPEED WITH
* WATER SPEED AND GEOMETRIC PARAMETERS GIVEN
*
* ITERATE
*
      HDG=4.0*AAG/(SSG+SSI)
      REG=HDG*UUG/VISG
      HDL=4.0*AAL/SSL
      REL=HDL*UUL/VISL
      T1=C(JJG)*ROHG*SSG*AAL*(REL**X(JJL))
      T2=C(JJL)*ROHL*SSL*AAG*(REG**X(JJG))
      T3=SSI*(1.0+AAG/AAL)/SSG
      UUG2=(UUL**2)/((T1/T2)*(1.0+T3))
      UUG=SQRT(UUG2)
      RETURN
      END
*
*
*
      SUBROUTINE LAMTURB(REL,REG,JJL,JJG,ICHANGE,KK1)
*
* SUBROUTINE LAMTURB DETERMINES WHETHER THE TWO
* FLUIDS ARE IN LAMINAR OR TURBULENT FLOW AND
* ADJUSTS THE FRICTION FACTORS ACCORDINGLY
*
      JGOLD=JJG
      IF(REG.GT.2000.0)JJG=2
      IF(REG.LE.2000.0)JJG=1
      IF(JGOLD.NE.JJG)ICHANGE=1
      RETURN
      END
```

APPENDIX III (continued)

```
      PROGRAM ANULUS
      DATA DENSL/1.0/,DENSG/0.001185/,VISCL/0.01/
      DATA VISCG/0.155/,D/5.08/,EPS/0.0001/,G/981.0/
      DATA RSTA/0.625/
      OPEN (3,FILE='ANULUS3.DAT',STATUS='NEW')
      REWIND 3
      Z=99999
* PROGRAM ANULUS DETERMINES THE FLOW REGIME TRANSITIONS
* FOR AIR/WATER TWO-PHASE FLOW IN A HORIZONTAL ANNULUS
* FLOW GEOMETRY
*
* GEOMETRICAL DATA
      PI=4.0*ATAN(1.0)
      A=PI*(D**2)*(1.0-(RSTA**2))/4.0
      S=PI*D*(1.0+RSTA)
      BD1=D*(1.0-RSTA)/2.0
      BD2=D*(1.0+RSTA)/2.0
      SIGMA=72.0
   50 CONTINUE
*
* CALCULATION OF SS TO SW TRANSITION
*
      PRINT*,'ENTER A 1 TO DETERMINE THE SS TO SW TRANSITION'
      READ*,IWANT
      IF(IWANT.NE.1)GO TO 300
      PRINT*,'ENTER VALUE OF SHELTERING COEFFICIENT'
      READ*,SJ
      PRINT 1000
      DO 200 I=1,99
      K=0
      K1=0
      H=FLOAT(I)*D/100.0
      IF(H.LE.BD1)THEN
      CALL SHAPE1(H,AL,AG,SL,SG,SI,D,RSTA,DADH)
      END IF
      IF(H.GT.BD1.AND.H.LT.BD2)THEN
      CALL SHAPE2(H,AL,AG,SL,SG,SI,D,RSTA,DADH)
      END IF
      IF(H.GE.BD2)THEN
      CALL SHAPE3(H,AL,AG,SL,SG,SI,D,RSTA,DADH)
      END IF
      UL=2.00
      JL=2
      JG=2
  100 UL1=UL
      UG2=4.0*VISCL*(DENSL-DENSG)*G/(SJ*DENSG*UL)
      UG=SQRT(UG2)
      CALL SPEED(AL,AG,SL,SG,SI,UL,UG,RL,RG,JL,JG)
```

```
      DIFF=ABS(1.0-UL/UL1)
      K=K+1
      IF(K.GT.1000)GO TO 200
      CALL LAMTURB(RL,RG,JL,JG,ICHANG,K1)
  175 IF(ICHANG.EQ.1)GO TO 100
      IF(DIFF.GT.EPS)GO TO 100
      ULS=UL*AL/A
      UGS=UG*AG/A
      VOID=AG/A
      WRITE(3,*)UGS,ULS
  200 PRINT 1500,ULS,UGS,JL,JG,H,VOID
      WRITE(3,*)Z,Z
*
* CALCULATION OF SS TO I TRANSITION
  300 PRINT*,'ENTER A 1 TO DETERMINE THE SS TO I TRANSITION'
      READ*,IWANT
      IF(IWANT.NE.1)GO TO 880
      PRINT 1000
      DO 500 J=1,199
      KK=0
      K1=0
      H=FLOAT(J)*D/200.0
      JL=2
      JG=2
      IF(H.LE.BD1)THEN
      CALL SHAPE1(H,AL,AG,SL,SG,SI,D,RSTA,DADH)
      END IF
      IF(H.GT.BD1.AND.H.LT.BD2)THEN
      CALL SHAPE2(H,AL,AG,SL,SG,SI,D,RSTA,DADH)
      END IF
      IF(H.GE.BD2)THEN
      CALL SHAPE3(H,AL,AG,SL,SG,SI,D,RSTA,DADH)
      END IF
      C2=1.0-H/D
      UG=C2*SQRT(2.0*(DENSL-DENSG)*G*AG/(DENSG*DADH))
      UL=2.0
  350 UL1=UL
      CALL SPEED(AL,AG,SL,SG,SI,UL,UG,RL,RG,JL,JG)
      DIFF=ABS(1.0-UL/UL1)
      KK=KK+1
      IF(KK.GT.1000)GO TO 500
      CALL LAMTURB(RL,RG,JL,JG,ICHANG,K1)
  400 IF(ICHANG.EQ.1)GO TO 350
      IF(DIFF.GT.EPS)GO TO 350
      ULS=UL*AL/A
      UGS=UG*AG/A
      VOID=AG/A
      WRITE(3,*)UGS,ULS
  500 PRINT 1500,ULS,UGS,JL,JG,H,VOID
      WRITE(3,*)Z,Z
*
```

```
* CALCULATION OF I TO DB TRANSITION
      PRINT*,'ENTER A 1 TO DETERMINE THE I TO DB TRANSITION'
      READ*,IWANT
      IF(IWANT.NE.1)GO TO 866
      PRINT 1000
      DO 440 J=1,99
      H=FLOAT(J)*D/100.0
      IF(H.LE.BD1)CALL SHAPE1(H,AL,AG,SL,SG,SI,D,RSTA,DADH)
      IF(H.GT.BD1.AND.H.LT.BD2)THEN
      CALL SHAPE2(H,AL,AG,SL,SG,SI,D,RSTA,DADH)
      END IF
      IF(H.GE.BD2)CALL SHAPE3(H,AL,AG,SL,SG,SI,D,RSTA,DADH)
      KK=0
      JL=2
      JG=2
      XL=0.2
      CL=0.046
      UG=0.2
      DL=(4.0*AL/(SL*VISCL))**XL
      EXP=1.0/(2.0-XL)
      UL=(4.0*G*AG*(DENSL-DENSG)*DL/(SI*CL*DENSL))**EXP
  444 UG1=UG
      CALL SPEEDG(AL,AG,SL,SG,SI,UL,UG,RL,RG,JL,JG)
      DIFF=ABS(1.0-UG/UG1)
      KK=KK+1
      IF(KK.GT.1000)GO TO 440
      CALL LAMTURB(RL,RG,JL,JG,ICHANG,K1)
      IF(ICHANG.EQ.1)GO TO 444
      IF(DIFF.GT.EPS)GO TO 444
      ULS=UL*AL/A
      UGS=UG*AG/A
      VOID=AG/A
      WRITE(3,*)UGS,ULS
  440 PRINT 1500,ULS,UGS,JL,JG,H,VOID
      WRITE(3,*)Z,Z
  866 CONTINUE
*
* CALCULATION OF I TO A TRANSITION
      PRINT*,'ENTER A 1 TO DETERMINE THE I TO A TRANSITION'
      READ*,IWANT
      IF(IWANT.NE.1)GO TO 850
      PRINT 1000
      DGAS=10.0
      H=0.5*D
      IF(H.LE.BD1)THEN
      CALL SHAPE1(H,AL,AG,SL,SG,SI,D,RSTA,DADH)
      END IF
      IF(H.GT.BD1.AND.H.LT.BD2)THEN
      CALL SHAPE2(H,AL,AG,SL,SG,SI,D,RSTA,DADH)
      END IF
      IF(H.GT.BD2)THEN
```

```
      CALL SHAPE3(H,AL,AG,SL,SG,SI,D,RSTA,DADH)
      END IF
      UG=450.0
      DO 800 J=1,99
      KA=0
      K1=0
      JG=2
      JL=2
      UL=2.0
  750 UL1=UL
      CALL SPEED(AL,AG,SL,SG,SI,UL,UG,RL,RG,JL,JG)
      DIFF=ABS(1.0-UL/UL1)
      KA=KA+1
      IF(KA.GT.1000)GO TO 800
      CALL LAMTURB(RL,RG,JL,JG,ICHANG,K1)
  775 IF(ICHANG.EQ.1)GO TO 750
      IF(DIFF.GT.EPS)GO TO 750
      ULS=UL*AL/A
      UGS=UG*AG/A
      VOID=AG/A
      UG=100.0*DGAS*FLOAT(J)
      WRITE(3,*)UGS,ULS
  800 PRINT 1500,ULS,UGS,JL,JG,H,VOID
      WRITE(3,*)Z,Z
  850 CONTINUE
*
* FORMAT STATEMENTS
 1000 FORMAT(/,4X,'ULS',5X,'UGS',5X,'JL',3X,'JG',4X,'H',4X,'VOID',/)
 1500 FORMAT(2X,F6.1,2X,F8.1,4X,I1,4X,I1,2X,F4.2,2X,F4.2)
 2000 FORMAT(2X,7(F6.1,2X))
      REWIND 3
      STOP
      END
*
* SUBROUTINES
*
      SUBROUTINE SPEED(AAL,AAG,SSL,SSG,SSI,UUL,UUG,REL,REG,JJL,JJG)
      DIMENSION C(2),X(2)
      DATA ROHL/1.0/,ROHG/0.001185/,VISL/0.01/,VISG/0.155/
      DATA (C(I),I=1,2)/16.0,0.046/
      DATA (X(I),I=1,2)/1.0,0.2/
*
* SUBROUTINE SPEED CALCULATES THE WATER SPEED WITH
* GAS SPEED AND GEOMETRIC PARAMETERS GIVEN
*
* ITERATE
*
      HDG=4.0*AAG/(SSG+SSI)
      REG=HDG*UUG/VISG
      HDL=4.0*AAL/SSL
      REL=HDL*UUL/VISL
```

```
      T1=ROHG*C(JJG)*SSG*AAL*(REL**X(JJL))
      T2=ROHL*C(JJL)*SSL*AAG*(REG**X(JJG))
      T3=SSI*(1.0+AAG/AAL)/SSG
      UUL2=(T1/T2)*(1.0+T3)*(UUG**2)
      UUL=SQRT(UUL2)
      RETURN
      END
*
*
*
      SUBROUTINE LAMTURB(REL,REG,JJL,JJG,ICHANGE,KK1)
*
* SUBROUTINE LAMTURB DETERMINES WHETHER THE TWO
* FLUIDS ARE IN LAMINAR OR TURBULENT FLOW AND
* ADJUST THE FRICTION FACTORS ACCORDINGLY
*
*
*
      JGOLD=JJG
      IF(REG.GT.2000.0)JJG=2
      IF(REG.LE.2000.0)JJG=1
      IF(JGOLD.NE.JJG)ICHANGE=1
      KK1=KK1+1
      RETURN
      END
*
*
*
      SUBROUTINE SPEEDL(AAL,AAG,SSL,SSG,SSI,UUL,UUG,REL,REG,JJL,JJG)
      DIMENSION C(2),X(2)
      DATA ROHL/1.0/,ROHG/0.0012/,VISL/0.01/,VISG/0.15/
      DATA C/16.0,0.046/,X/1.0,0.2/
*
* SUBROUTINE SPEEDL CALCULATES GAS SPEED WITH
* LIQUID LEVEL AND SPEED GIVEN
*
      HDG=4.0*AAG/(SSG+SSI)
      HDL=4.0*AAL/SSL
      REL=HDL*UUL/VISL
      FL=C(JJL)/(REL**X(JJL))
      F1=SSL*AAG/(AAL*SSG)
      F2=SSI*(1.0+AAG/AAL)/SSG
      TAUL=FL*ROHL*(UUL**2)/2.0
      F3=TAUL*F1
      IT=0
*
* ITERATE
*
 6200 REG=HDG*UUG/VISG
      FG=C(JJG)/(REG**X(JJG))
```

```
      TAUI=FG*ROHG*((UUG-UUL)**2)/2.0
      UUG2=(F3-TAUI*F2)*2.0/(FG*ROHG)
      IF(UUG2.GT.0.0.AND.UUG2.LT.10000000.0)GO TO 6500
      PRINT*,UUG2
      PRINT*,'ERROR IN SPEEDL'
      GO TO 7000
 6500 IT=IT+1
      UUG1=SQRT(UUG2)
      ERROR=ABS(1.0-UUG/UUG1)
      UUG=UUG1
      IF(IT.GT.1000)GO TO 7000
      IF(ERROR.GT.0.001)GO TO 6200
 7000 CONTINUE
      RETURN
      END
*
*
      SUBROUTINE SHAPE1(HT,AAL,AAG,SSL,SSG,SSI,DD,RSTAR,DADHL)
*
      PY=4.0*ATAN(1.0)
      AA=PY*(DD**2)*(1.0-(RSTAR**2))/4.0
      SS=PY*DD*(1.0+RSTAR)
      ARG=1.0-(2.0*HT/DD)
      SSL=DD*ACOS(ARG)
      SSI=DD*SQRT(1.0-(ARG**2))
      SSG=SS-SSL
      AAL=DD*(SSL-(SSI*ARG))/4.0
      AAG=AA-AAL
      DADHL=DD*SQRT(1.0-(ARG**2))
      RETURN
      END
*
*
      SUBROUTINE SHAPE2(HT,AAL,AAG,SSL,SSG,SSI,DD,RSTAR,DADHL)
      PY=4.0*ATAN(1.0)
      AA=PY*(DD**2)*(1.0-(RSTAR**2))/4.0
      SS=PY*DD*(1.0+RSTAR)
      ARG=1.0-(2.0*HT/DD)
      SSL=DD*(ACOS(ARG)+RSTAR*ACOS(ARG/RSTAR))
      SSI=DD*(SQRT(1.0-ARG**2)-SQRT(RSTAR**2-ARG**2))
      SSG=SS-SSL
      AAL=(DD**2)*(ACOS(ARG)-(RSTAR**2)*ACOS(ARG/RSTAR)-SSI*ARG/DD
     +)/4.0
      AAG=AA-AAL
      DADHL=DD*(SQRT(1.0-(ARG**2))-SQRT(RSTAR**2-ARG**2))
      RETURN
      END
*
*
      SUBROUTINE SHAPE3(HT,AAL,AAG,SSL,SSG,SSI,DD,RSTAR,DADHL)
*
```

```
      PY=4.0*ATAN(1.0)
      AA=PY*(DD**2)*(1.0-(RSTAR**2))/4.0
      SS=PY*DD*(1.0+RSTAR)
      ARG=(2.0*HT/DD)-1.0
      SSG=DD*ACOS(ARG)
      SSI=DD*SQRT(1.0-(ARG**2))
      SSL=SS-SSG
      AAG=DD*(SSG-(SSI*ARG))/4.0
      AAL=AA-AAG
      DADHL=DD*SQRT(1.0-(ARG**2))
      RETURN
      END
*
*
      SUBROUTINE SPEEDG(AAL,AAG,SSL,SSG,SSI,UUL,UUG,REL,REG,JJL,JJG)
      DIMENSION C(2),X(2)
      DATA ROHL/1.0/,ROHG/0.001185/,VISL/0.01/,VISG/0.155/
      DATA (C(I),I=1,2)/16.0,0.046/
      DATA (X(I),I=1,2)/1.0,0.2/
      HDG=4.0*AAG/(SSG+SSI)
      REG=HDG*UUG/VISG
      HDL=4.0*AAL/SSL
      REL=HDL*UUL/VISL
      T1=ROHG*C(JJG)*SSG*AAL*(REL**X(JJL))
      T2=ROHL*C(JJL)*SSL*AAG*(REG**X(JJG))
      T3=SSI*(1.0+AAG/AAL)/SSG
      UUG2=(UUL**2)/((T1/T2)*(1.0+T3))
      UUG=SQRT(UUG2)
      RETURN
      END
```